Elucidación de las Especies Activas en la Reacción de Dehidroaromatización de Metano a Aromáticos sobre Sistemas Mo-M/Zeolita: Efecto de la Activación y de la Adición de un Segundo Metal

Elucidation of Active Species in the Dehydroaromatization Reaction of Methane to Aromatics on Mo-M/Zeolite Systems: Effect of Activation and Second Metal Addition

Memoria presentada para optar al grado de Doctor por la Universidad de Sevilla.

Fdo. Ángeles López Martín

DIRECTORES

Fdo: Alfonso Caballero Martínez **Fdo: Gerardo Colón Ibáñez**

Sevilla, febrero de 2022.

INDEX

Chapter 1. Introduction

1.1. Energy context and utilization of natural gas

Today, the environmental problems associated with fossil fuels and the importance of managing energy reserves are highly topical. The development of new energy technologies is therefore crucial from a socio-political and environmental point of view. However, the production and consumption of oil is still the base for the current economic system as is show in **Figure 1**. Thus, sectors such as transportation, manufacture of goods, or plastics and rubber industries, are highly dependent on oil as a raw material.[1] Despite the relevancy of the research and development of renewable energy, reality indicates that most technologies based on renewable energy are at a very early stage of development, making it difficult to implement them within a realistic time frame. This makes it necessary to improve existing industrial processes based on oil sources.

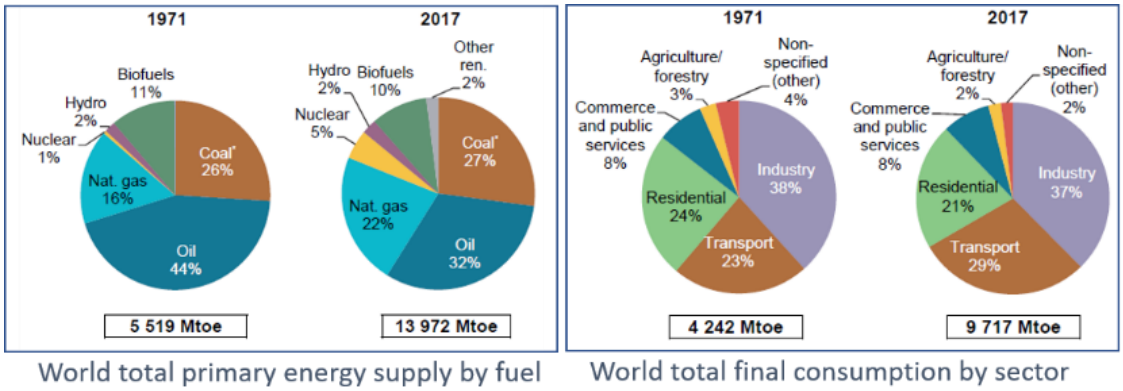

Figure 1. World energy supply by fuel and energy consumption by sector.

Natural gas could be considered a cleaner fossil energy and a feedstock for chemicals due to the possibility to convert it catalytically into liquid fuels or useful chemicals. World consumption of natural gas is projected to increase from 120 trillion cubic feet in 2012 to 203 trillion cubic feet in 2040. This makes natural gas the energy source with the largest increase in the world and remaining a key fuel in the electric power sector and in the industrial sector.[2] Shale gas is a form of natural gas (mostly methane), found underground in shale rock. Recently, a significant number of shale gas deposits have

been discovered in continental North America. The 'shale gas revolution' in the United States created an oversupply of liquefied natural gas and downward pressure on gas prices across the globe. The combination of horizontal drilling, high-pressure fracturing, multiple fracturing stages, and more efficient working fluids, has opened up vast reservoirs of shale gas. At the same time, methane hydrates, found in the sediments of the ocean floors, are estimated to represent twice the amount of carbon in all other known fossil fuel reserves making it the most important source of hydrocarbons in the long term.[3,4] This rapid increase of proven natural gas reserves in the last few years, the fluctuating prices and progressively depleted reserves of crude oil have attracted great attention over natural gas.

Natural gas is a mixture of gaseous hydrocarbons with varying quantities of nonhydrocarbons, which normally are considered impurities. Its composition varies depending on the deposit from which it is extracted, it is mainly composed of methane in amounts that are usually between 85-96%. It can be found in fossil deposits and also be obtained through decomposition processes of organic residues.

Much of the methane is usually located in remote areas, far from industrial complexes, burning more than 5.3 trillion cubic feet of flare gas in the world every year due to transportation of methane over a long distance not being economically viable. Therefore, there is an urge to convert methane to a product, chemical or fuel, that could be easily transported (gas to liquids processes, *GTL*), such as olefins, aromatics, etc. However, methane is one of the most thermodynamically stable forms in which carbon can be widely found with a binding energy of 435 KJ / mol, making its activation a challenge. The molecule of methane has perfect tetrahedral symmetry with four equivalent C−H bonds and, therefore, lacks a net dipole moment. The absence of this dipole moment and a rather small polarizability imply that methane activation would proceed through the abstraction of a hydrogen atom yielding a methyl group, either a radical, a cation, or an anion depending on the catalytic system. Such process requires high temperatures and the use of oxidation agents. For this reason, catalysis plays an important role in most processes for methane conversion. The transformation of

methane into hydrocarbons of higher molecular weight and higher added value began to be studied from the second half of the 20th century and nowadays, some of them are applied in industry. These processes can be classified into direct and indirect routes, as shown in **Figure 2**:

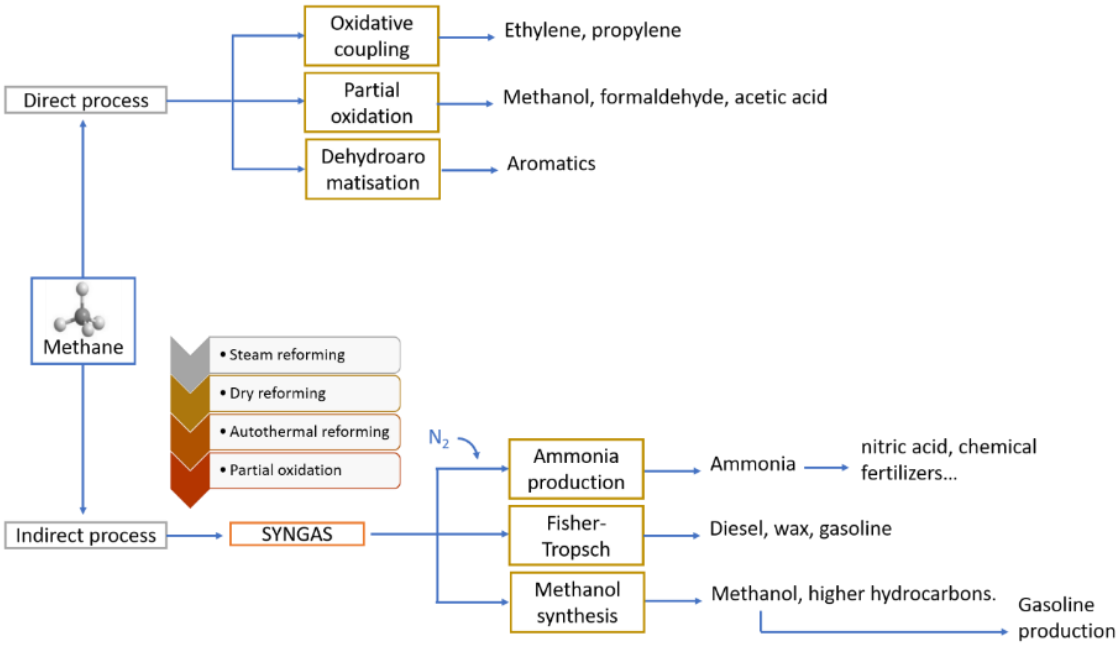

Figure 2. Classification scheme of direct and indirect process for methane transformation.

Today, almost all commercial processes for large scale natural gas conversion involve synthesis gas (*syngas*), a mixture of molecular hydrogen and carbon monoxide, requiring more than one chemical reaction step. The most important products produced on a large scale through this indirect process are ammonia and methanol, but also diesel fuel, gasoline, dimethyl ether, paraffins, higher alcohols, etc. The processes used for *syngas* production are steam methane reforming, dry reforming, partial oxidation and autothermal reforming, and a combination of steam methane reforming and partial oxidation:

However, analysis of the economics of these processes reveals that 60% or more of the capital cost of GTL plants is associated with the production of *syngas*. Consequently, the development of technologies involving direct conversion of methane into the desired

products is a goal [3]. This challenge has led to an intense research on catalyst development within this area, avoiding the generation of *syngas* with the consequent reduction in costs. On the other hand, since methane is a very stable molecule, its reactions show high activation energy values. Moreover, obtained products are often much more active than methane and easily react, leading to low selectivity of the desired products and to small product yields making progressing to a commercial stage difficult. Some direct processes are: [5,6,7]

- *Thermal and catalytic pyrolysis of methane.* This process produces hydrogen and elemental carbon through methane pyrolisis:

  $$CH_4 \rightarrow 2\,H_2 + C$$

  This reaction can be thermal non-catalytic or catalytic and serves as an alternative to SMR and provides CO_2 free H_2. Non-catalytic pyrolysis is challenging below 1200 °C while the catalytic approach has the potential to lower the temperature required for the decomposition of methane from more than 1000 °C to less than 700 °C.

- *Oxidative coupling of methane* (*OCM*). This reaction has been explored since the 80s as a potential route for synthesis of C2 hydrocarbons directly from methane. It is carried out at elevated temperatures and O_2 presence, where methane reacts over a catalyst to form C_2H_6 as a primary product and C_2H_4 as a secondary product.

  $$2\,CH_4 + {}^1/_2\,O_2 \rightarrow C_2H_6 + H_2O$$
  $$C_2H_6 + {}^1/_2\,O_2 \rightarrow C_2H_4 + H_2O$$

  However, this reaction has some drawbacks: on the one hand, both methane and ethylene can be converted to carbon dioxide, on the other hand, the C2 yield is limited to approximately 25%, so despite the existing work at *OCM*, this technology has not yet been commercialized.

- *Partial oxidation of methane to methanol* and formaldehyde. Under mild conditions (< 250 °C) is a global challenge inspired by an enzyme, the methane monooxygenase (*MMO*), founded in methanotrophic bacteria which is capable of carrying out this reaction. The active site of this enzyme has been elucidated as bis(μ-oxo)diiron complexes and as bis(μ-oxo)dicopper complexes, and the discovery of an analogous inorganic catalyst for his industrial implementation is the aim of the study. These efforts have led to a transition metal-exchanged zeolites, like Fe/ZSM-5 or Cu/ZSM-5, however, the two major problems of theses metal-loaded zeolites are low yield to methanol and batch system which would be challenging to extend to an industrial scale.

- *Methane dehydroaromatization* (*MDA*). In this reaction methane is converted in the absence of O_2 into aromatics, ethylene and hydrogen, with the advantage of preventing irreversible overoxidation to CO_2 or H_2O. This reaction is the aim of the study in this work, and it will be widely discussed above.

1.2. Aromatic hydrocarbons production

Aromatic hydrocarbons such as benzene, toluene and xylene (so called as *BTX*) play an essential role in the petrochemical and fine chemical industries, providing a basic building block for a wide variety of products, such as plastics, resins, solvents, and pharmaceuticals. Traditionally, *BTX* aromatics are obtained mainly by catalytic cracking and catalytic reforming processes of petroleum. Aromatics plants are generally situated within refineries or petrochemical complexes, reflecting the interconnection between the feedstocks for these processes.

Benzene is the most widely used aromatic in industrial processes, with a global market expected to surpass 46 million metric tons by 2020. This is due to the growing demand from various industries that use benzene derivatives in their manufacturing processes.[8] Most production today comes from the following three routes:

- *Cracking of oil products* from crude oil distillation, like naphtha (C5- C10) or gas oil (C14-C20) fractions, breaking the larger molecules into smaller ones.

- *Catalytic reforming of naphtha*, obtaining molecules with the same number of carbon atoms but with different structures. It uses platinum/alumina catalysts to obtain benzene, and other aromatics.

- *Disproportionation of toluene,* which is a product from the reforming of naphtha with a lower demand. However, it can be converted to dimethylbenzene and benzene using a catalyst.

Ethylbenzene is the main derivate of benzene, being used in the synthetic rubber industry to manufacture resins and latex derived from styrene, which are mainly used in the automotive industry. Therefore, ethylbenzene can be considered as the main driver of the benzene market. Other benzene derivates are cumene, cyclohexane and nitrobenzene, used for the manufacture of protective coatings, nylon fibers and detergents.

In the case of other aromatics, toluene is commonly used as organic solvent, for paint thinner. However, its largest industrial use is in the production of benzene and xylene. On the other hand, P-xylene is used to produce the polyester PET, for clothing, fibres, plastic bottles, film and the production of other plastic products. Hence, the demand in the market for p-xylene being highly correlated with the demand for PET.[9]

1.3. Zeolites in catalysis

As described in the previous section, limited fossil fuels and global warming alerted the scientific community to move towards greener design processes. On this matter, catalysis offers green chemistry advantages.[10] Catalysts are essential for the reduction of air and water pollution and thereby contribute to reducing the emissions of products

that are harmful to human health and the environment. Also, it plays an important role in society and its well-being. Without catalysis the manufacture of many materials and foodstuffs would not be possible. The worldwide annual demand for catalysts was estimated to be 850,000 tons in 2007 and was projected to increase by 3.5-4 % annually through 2012.[11] Some examples involving catalysts are:

- *Fuels and energy uses*, as an example, the Fluid Catalytic Cracking (FCC), a process developed in 1942 which produces gasoline as well as heating oil, fuel oil, propane, butane, and chemical feedstocks. Over half the world's gasoline is currently produced using this process.

- *Emissions control*, for example CO, NO_x and hydrocarbon emissions from automobiles, sulphur based emissions in the combustion of fuels or emissions from the world's coal fired power plants.

- *Polymer production* of adhesives, coatings, foams, and packaging materials, textile and industrial fibres, etc.

- *The pharmaceutical industry*, for instance, William Knowles in the 1970s found that rhodium bonded to chiral phosphine ligands could perform asymmetric catalytic hydrogenation. The method was soon developed for the commercial production of the anti-Parkinson drug.[12]

- *The food industry* uses enzymes in brewing, dairy processing, in oil and fat production, for the preparation of meat or fish products or for baking specialties.

Summarizing, it is estimated that most of the chemical processes (85–90 %) involve at least one catalytic step. [10]

In heterogeneous catalysis, the active sites and their coordination environment and electronic structure are the most important factors that affect the performance of the

catalysts. To obtain a high degree of metal dispersion, a solid with adequate surface area is used as a support for an active component that is dispersed as very small particles, with dimensions of 1 to 20 nm, often referred to as nanoparticles. Some typical supports are for example Al_2O_3, SiO_2, TiO_2, CeO_2 and zeolite. But only a small fraction of these nanoparticles, located at apices, edges, steps, and corners are exposed to reactant.[13,14]

Advances in characterization and synthesis methods are allowing us to understand and control the variables that affects the performance of a catalysts in a reaction, considering that surface structure and electronic properties can change greatly in this size range. An example is the activity dependence of the size in Au nanoparticles, being active at ambient conditions for the oxidation of CO to CO_2 only in the range of 2 to 3 nm.[15]

Support design is also critical, and advanced catalysts have been designed in the forms of nanocrystalline and nanoporous materials, tailoring the pore structures to provide for ultrahigh surface areas and product selectivity. This knowledge, the recent approaches to nanoparticle synthesis, and the increasing need for greener chemical manufacturing processes is contributing to the design and development of new catalysts. Also, due to the change in the structure and composition of the systems under reaction conditions, it is important to characterize catalysts *in operando* leading to develop these types of characterisation techniques.

Zeolites are crystalline aluminosilicates consisting of SiO_4 and AlO_4^- tetrahedra, which are inner linked through oxygen atoms to give a three-dimensional network through which long channels and cavities, also called cages, are developed with diameters of molecular dimensions (0.3 to 1.4 nm). Many zeolites are known, some of them of natural origin, but the majority synthesized. Petroleum refining and basic petrochemistry are based in the use of zeolites, some examples are the industrial use in fluid catalytic cracking (FCC) of heavy petroleum distillates producing more gasoline with a higher-octane rate. The synthesis of ethylbenzene, precursor of styrene and polystyrene, is also based on zeolites, the disproportionation of toluene into benzene and xylenes and also

the isomerization of xylenes to produce *para*- xylene, the chemical precursor for terephthalic acid, precursor to the polyester PET.[16]

By April 2021, 253 zeolite framework types had been identified.[17] Zeolites can be classified according to different criteria, the most used concerns the dimensions of the pore apertures. The diameter of the channels is determined by the number of tetrahedra that form it, which are a denominated number of member rings (MR). Based on that, zeolites can be classified as:

- *Small pore zeolites,* like chabazite, with channels formed by 8 member rings and pore diameters of 3 to 4.5 Å.
- *Medium pore zeolites*, like MCM-22, with channels consisting of 10 member rings and pore diameters of 4.5 to 6 Å.
- *Large pore zeolites*, like mordenite, with channels consisting of 12 member rings and pore diameters of 6 to 8 Å.
- *Extra-large pore zeolites*, like UTD-1, with channels formed by 14 member rings and pore diameters up to 10 Å. [18]

The inner pore structure depends on the composition, the zeolite type, and the cations. The latter is another aspect of zeolites to describe, zeolites have extraframework cations to compensate for the excess negative charge from the AlO_4^-. They are exchangeable by other cations or by a proton. In the case of the latter, the zeolite is exchanged with an ammonium ion, usually NH_4NO_3, and performing a thermal dissociation in which it decomposes, obtaining the acid-zeolite form. This allows the production of protonic zeolites, which are very strong solid Brönsted acids. The Brönsted acid strength is related to the Si/Al ratio which cannot be lower than one. However, each acid site becomes a somewhat *weaker* Brönsted site as the population of protons increases, in this way the acid strength of Brönsted acid sites can be modulated through isomorphic substitution. [19] [20] Lewis acidity in a zeolite generally results from aluminum which is not tetrahedrally bound in the framework. It is usually much weaker in zeolites than Brönsted acidity. Extra-framework aluminum is often an artifact of the synthesis process but, also, can be

created by purpose steaming a zeolite to remove Al from the framework. This process is used to increase the Si/Al ratio of zeolite-Y for cracking catalysts.

Besides the acidity of the Brönsted sites mentioned before, this 3D network gives the zeolite some interesting properties, like a high surface area and therefore a high adsorption capacity, the possibility of being used as a molecular sieve, or as a shape-selective molecule. Zeolites, with their precise pore dimensions, can discriminate reagents and products by size and shape if they present significant differences, which will influence diffusivity through channels. [21]

Currently, the techniques for the preparation of zeolites involve the use of templates or organic structure directing agents (SDA), which have allowed the preparation of several new zeolites with different structures by guiding the formation and controlling the size of zeolite channels, cavities, etc. Zeolites are prepared by hydrothermal crystallization at 100-200°C in basic medium in order to facilitate the dissolution of silicon precursors, and using cationic templates that are decomposed and eliminated by washing or burning.[22]

In recent years, techniques to adapt the nature and properties of zeolites have been studied and developed. To do this, two strategies can be tried: one is to try to obtain the zeolite with the desired properties by modifying its synthesis procedure, and the other is to try to modify the properties with post-synthesis treatments. Some examples are the incorporation of different heteroelements into zeolites, the reduction of the zeolite crystal size or the generation of intracrystalline mesoporosity.

The replacement of framework atoms in a crystalline compound such as a zeolite is also called isomorphic substitution. In that, the type of crystal does not change but other properties of the zeolite can be tuned such as the nature and catalytic function of the formed Brönsted and Lewis acid sites. For this, the critical difference for isomorphic substitution is assumed to be 15% for the radii of the ions, and the difference in electronegativity values is 0.4 a.u. on the Pauling scale. Following these criteria, zeolites

can be isomorphically substituted by Be^{+}, Zn^{2+}, B^{3+}, Al^{3+}, Ga^{3+}, Fe^{3+}, Ge^{4+}, Ti^{4+}, Sn^{4+} among others.[23]

Another example of the variation of the zeolites and their properties is the reduction of the crystal size at nanometric scale or the design of layered zeolites. For the former, the objective is decreasing the use of expensive SDA and seed-assisted crystallization of zeolite nanocrystals seems to be a good solution. For the latter the design of layered zeolites, has been successfully applied for MFI, BEA, and SAPO-34.[24,25,26]

The way to introduce mesoporosity to the crystal structure has also been studied in recent years. One option is to use hard templates, such as carbon particles, that are trapped in the synthesis but are subsequently removed by burning, thus forming pores.[27] Some examples of mesoporous zeolites prepared by this method are MFI, MWT, BEA. Another option to achieve mesoporous zeolites is using different post-synthesis modifications such as dealumination, performed by steaming or mineral acid treatment, or desilication in alkaline medium.[28,29]

Some of these processes could help us overcome some of the drawbacks found when carrying out our work. As an example, the introduction of porosity helps reduce the limitations of mass transport, shortening the access of reactive molecules to sites assets and the output of products from zeolite channels. The possibility of adjusting the different properties of the zeolite would allow its optimization for specific uses, having a key role in the green and sustainable chemistry of the future.[30].

1.5. Methane Dehydroaromatization (*MDA*)

1.5.1. Generalities

MDA involves the selective conversion of methane to a mixture of aromatics, predominantly benzene but also naphthalene and toluene, and hydrogen. This process is as follows:

$$6CH_4(g) \rightarrow C_6H_6\,(g) + 9H_2\,(g) \quad ;$$

$$\Delta G_r^\circ = +433\,KJ/mol\,;\ \Delta H_r^\circ = +532\,KJ/mol$$

Along with this reaction, these others occur:

$$2CH_4 \leftrightarrow C_2H_6 + H_2$$

$$2CH_4 \leftrightarrow C_2H_4 + 2H_2$$

Methane dehydroaromatization is an extremely unfavorable reaction thermodynamically,[3,35,31] leading to very low equilibrium conversions and benzene yields. For that reason, high temperature is required to obtain a significant benzene production.[32,33] Moreover, within this high temperature the formation of coke is thermodynamically favoured. This limitation makes necessary to develop catalysts showing increasing methane reactivity by activating the carbon-hydrogen bonds and, at the same time decreasing the carbon formation.

In 1993, Wang *et al.*[34] reported that methane could be converted to benzene and hydrogen using Mo/ZSM-5 as catalyst. Since then, many different catalytic systems have been studied and applied to *MDA*. Regarding the metallic phase, a better performance has been observed using Mo, W, Fe, V, Cr and Re. On the other side, concerning the supports, a lot of variety of inorganic oxides like SiO_2, Al_2O_3 or TiO_2, or also zeolites like ZSM-5, ZSM-8, ZSM-11, SAPO, MCM-41 or MCM-22 have been considered. However, Mo/H-ZSM-5 system is still the catalyst that has showed the best results in terms of conversion and selectivity for *MDA* reaction and, therefore, the most studied.

The large number of studies carried out in these years have allowed us to obtain a wide knowledge of both this catalyst and the aromatization process itself. This fact has let reaching a certain consensus in the scientific community regarding some important aspects: [35]

- Mo-based systems are usually significantly more active and selective as compared to other transition metals.

- Mo/H-ZSM-5 catalysts contain highly dispersed Mo(VI)-oxo centers, which are reduced or carburized under the reaction conditions generating the active Mo-sites.
- The Brönsted acidity of the zeolite plays a critical role in the catalytic activity, l
- eading to catalyst deactivation when there is an excess of Brönsted acid sites.
- Zeolite shape selectivity is critical for *MDA* performance. Only zeolite topologies with pore sizes of about 5.5 Å demonstrate high benzene selectivity.
- There are different stages during the *MDA* reaction: induction, quasi-steady-state production of benzene, and deactivation.

All these aspects and processes will be discussed in more depth over the following sections.

1.5.2. Reaction mechanism

After many studies on *MDA* reaction, a consensus on the mechanism of reaction that takes place has not yet been reached. Different mechanisms have been proposed for this reaction: the mechanism via CH_3• was one of the early hypotheses [36] In this mechanism the free radicals dimerize and dehydrogenate to form ethane and ethylene. Subsequently, ethylene aromatized to benzene with the aid of the available protons of H-ZSM-5 zeolite. It can be seen in the following equations:

$$CH_4 \rightarrow CH_3^{\bullet} + H^{\bullet}$$
$$2\ CH_3^{\bullet} \rightarrow C_2H_4 + H_2$$
$$3\ C_2H_4 \rightarrow C_6H_6 + 3\ H_2$$

Later, bifunctional mechanism was suggested for the mechanism of methane dehydroaromatization over Mo/zeolite. This mechanism has been widely accepted in the recent literature studies.[37,38] According to this, methane activation occurs at the Mo active site to form ethane, ethylene or acetylene intermediates. This is the so-called *induction period* in which the maximum conversion of the reaction occurs. After that,

conversion decreases due to carbon deposition that is taking place. It is during the induction period when Mo^{6+} ions are reduced, forming a metal carbide, the structure of which is the subject of much discussion (Mo_2C or MoO_xC_y, among others). Based on this mechanism, some studies suggest that metal carbide is the *active site* where methane reacts to ethylene. Thus, by surface migration or by diffusion in the gas phase, ethylene reaches the Brönsted acid sites of the zeolite, where the reaction intermediates are oligomerized, cyclized and aromatized, forming benzene and other aromatic compounds. A scheme of this mechanism is shown in the next figure:

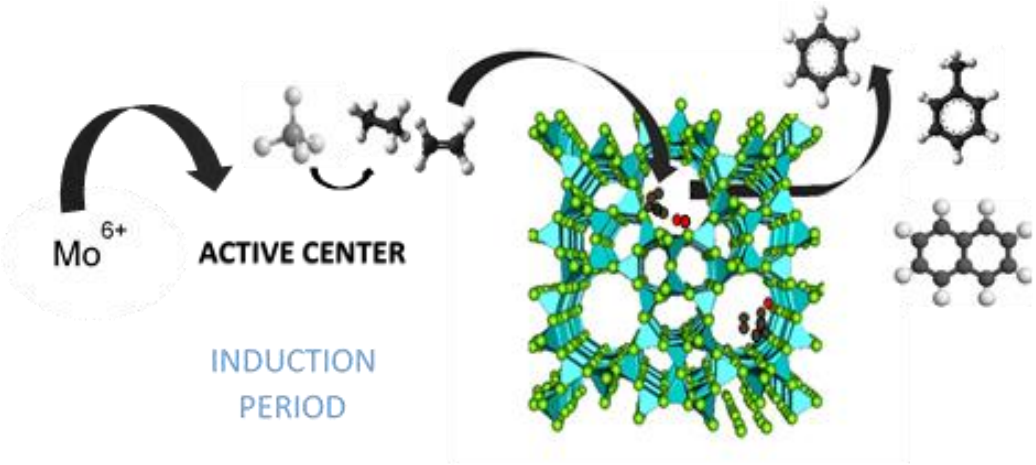

Figure 3. Scheme of the bifunctional mechanism by two steps

Recently, a new mechanism for the *MDA* reaction was proposed showing certain similarities with the reaction mechanism proposed for the methanol to hydrocarbons reaction. In this way, methane is activated on the Mo active sites, producing reactive radicals or C2 species that react with linear polyaromatic species trapped in the pores of ZSM-5 zeolite. These compounds are the called "*hydrocarbon pool*" and it is of great importance for the *MDA* reaction. Thus, according to this mechanism, benzene would be produced from secondary reactions of these compounds with the initial products of CH_4 activation.[39,40] However, many details about this hypothesis are still unknown, such as the condensed aromatics species that could be formed in the micropores of ZSM-5 zeolite.

On this basis, it is clear that the aromatization process of methane is very complex, and there are still many doubts about the reaction mechanism. Furthermore, the rapid deactivation and high reaction temperatures make it difficult to determine the species formed in each of the stages. Also, depending on the catalyst used, the species can be very diverse, suggesting different mechanisms. The possibility of several mechanisms in the process cannot be ruled out either, all of which makes the determination of the reaction mechanism and the active species a challenge for the field of catalysis, as well as of great importance.

1.5.3 Role of acid sites and shape selectivity

As Wang *et al.* demonstrated, by loading Mo species on zeolite supports *MDA* activity improves markedly. The zeolite Brönsted acid sites (*BAS*) have a very important role in the reaction, they serve as anchor points for molybdenum species inside or outside the pores. Some of the formed Mo species are also believed to be the active centers for the reaction. Therefore, the quantity of *BAS*, as well as its location and distribution are important factors to consider and that may be modulated if needed.[41]

Xu *et al.* characterized the interaction between ammonium heptamolybdate and NH_4-ZSM-5 zeolite at different stages of catalyst preparation, concluding that by calcining at a suitable temperature, molybdenum species interact with Brönsted acid sites, migrating to channels of the zeolite. Furthermore, they showed that there is a strong interaction between the Mo species and the Al frame, leading to the extraction of the Al frame.[42, 43]

Using 'H MAS NMR *in-situ* spectroscopy to study proton species on Mo/H-ZSM-5, Bao *et al.* observed that the Mo species are kept in contact with the Al framework through two oxygen bridges. In addition, they observed that Brönsted acid sites attracted Mo species, that migrated to the channels anchoring themselves in the aluminum sites by an oxygen bridge. Hence, their studies supported that bifunctional catalytic mechanism for *MDA*

would take place in this reaction.[44] Moreover, they argued that catalyst synthesis methods would have a high influence in the introduction of surface metal oxide species into the zeolite channel.

Ichikawa *et al*. showed that from infrared spectroscopy measurements, they observed that the SiO_2/Al_2O_3 ratio, hence the Brönsted acid sites, influences the formation rate of benzene. The highest benzene formation and minimum coke formation for Mo/H-ZSM-5 were obtained with a SiO_2/Al_2O_3 ratio of 40.[45]

However, other catalysts with supports without Brönsted acidity have also been studied. An example can be found in Kosinov *et al.* study of Silicalite-1-based catalysts. In this paper authors show that studied catalysts were indeed active, highlighting that Brönsted acidity is not required. They proposed a mono-functional mechanism for the *MDA* reaction and non-bifunctional mechanism.[41, 46, 47]

Another aspect to consider for zeolite-based catalysts, is that the open frame structure of the channel in the catalyst exhibits shape selectivity and will affect the species of products formed. As above mentioned, reaction selectivity control by zeolite pore shape has been widely applied in heterogeneous catalysis to promote preferential production of desired products.

In this sense, Zhang *et al.* correlated the catalytic performance with the structure of the zeolites. It was concluded that the zeolites that presented a higher selectivity to benzene were those whose pore size was close to the dynamic size of benzene (5.9 Å), making them good supports for catalysts for the *MDA* reaction.[48]

Therefore, H-ZSM-5 zeolite-based catalysts have been frequently used in *MDA* reactions due to their adjustable Brönsted acid sites, intermediate microporous channel dimensions, and high hydrothermal stability. ZSM-5 exhibits MFI topology, the structure

of MFI zeolite contains two types of intersecting channels, both formed by 10-membered silicate rings, characterizing this material as a medium-pore zeolite. One channel type is straight and has a nearly circular opening with dimensions 5.3 x 5.6 Å along [010], while the other one is sinusoidal and has an elliptical opening with dimensions 5.1 x 5.5 Å along [100]. Such dimensions would make this zeolite a good support for *MDA* reaction. The Si/Al ratio may vary depending on the needs.

Zeolite MCM-22 consists of a structure of two independent channel systems. One is sinusoidal and is delimited by 10-membered rings with dimensions 4.1 x 5.1 Å and the other is formed by large 3D cavities delimited by 12-membered rings, although these are only accessible through 10-membered rings. The dimensions of these supercavities are 7.1 x 7.1 x 18.2 Å and their 4.0 x 5.5 Å side openings.[49]

Bao *et al.* compared catalysts Mo/H-ZSM-5 and Mo/H-MCM-22 for *MDA* reaction. The latter showed better catalytic performance with higher selectivity to benzene, and a longer useful life due to better tolerance of carbonaceous deposits.[50] The higher selectivity to benzene in these catalysts compared to the ZSM-5 catalysts may be due to the presence of the 12-ring supercages. On the one hand MCM-22 can accommodate more transition metal ions, on the other hand, the presence of these supercavities also avoids the blockage of the channels by coke, for which reason the catalyst takes longer to deactivate.

As described in the section, the modification of the topology of the zeolites is possible in different ways, either by modifying synthesis or with post-synthetic treatments of the zeolite. This allows different properties to be adjusted for use as a catalyst for this reaction.

1.5.4. Species on Mo/H-ZSM-5

During these years, many of the *MDA* studies have been directed to the identification of the active phase, as well as the study of the evolution of the species throughout the

reaction in the main system, the catalyst Mo/H-ZSM-5. Below are some of the most relevant results obtained by the main researchers throughout the last few decades.

Solymosi *et al.* studied the activity and the presence of different species by X-ray photoelectron spectroscopy with the systems Mo/H-ZSM-5 and Mo_2C/ZSM-5 but also the unsupported molybdenum species. They showed that the MoO_3 and MoO_2 interact with methane, reducing and forming new species as well as coke deposits. These molybdenum species are transformed into carbides during the reaction with methane at high temperature and suggested that Mo_2C provides the active site for the formation of ethylene from methane, which would convert to benzene and other aromatics in the acid sites of the zeolite. Mo_2C would thus be considered the active species.[38,51–53]

Lunsford *et al.* also characterized the Mo/H-ZSM-5 catalyst by X-ray photoelectron spectroscopy, obtaining similar results as Solymosi. Thus, during the initial induction period, methane would reduce MoO_3 to Mo_2C, being that carbidic molybdenum species the active centers for the activation of methane. However, they specified that since preforming Mo_2C on the catalyst, without coke deposition, did not eliminate the induction period, the clean Mo_2C surface could be too reactive to form higher hydrocarbons. Therefore, they proposed a coke-modified Mo_2C surface as the actual active species in the formation of ethylene as a reaction intermediate.[54,55]

Howe *et al.* study Mo/H-ZSM-5 catalysts for *MDA* reaction by using Fourier-transform infrared spectroscopy, ^{27}Al and ^{29}Si NMR. They obtained evidences of molybdenum migration into the zeolite pores during catalyst calcination at high temperatures, reacting with Brönsted acid sites to remove aluminium from the lattice and generate an aluminium molybdate phase. They also performed extended X-ray absorption fine structure spectroscopy (EXAFS) and they confirmed that calcination produces highly dispersed oxo-molybdenum or molybdate species which are converted to a molybdenum carbide phase under reaction conditions.[56]

Ichikawa *et al*. characterized the active phase and studied the mechanism of *MDA*. For this, they used Mo K-edge Extended X-ray absorption fine structure spectroscopy (EXAFS), TG/DTA/MASS and Fourier-transform infrared spectroscopy techniques (FTIR). These results revealed that the zeolite supported Mo oxide are highly dispersed in the internal channels of H-ZSM-5. It is endothermically converted to molybdenum carbide (Mo_2C) cluster under methane, which initiates the methane aromatization at 600-750 °C. Furthermore, it was demonstrated that there is a close correlation between the benzene formation and the Brönsted acidity of Mo/H-ZSM-5 catalyst.[57]

Iglesia *et al*. prepared a series of Mo/H-ZSM-5 catalysts with different loading by the solid-state reaction method and, using a variety of characterization technologies, including XANES, ^{27}Al MAS NMR, Raman spectroscopy, TPO and TPR, studied the location of Mo species and their modification during the preparation process. They found that, at 350 °C, the MoO_x migrated to the surface. However, when calcined at a higher temperature, between 500 and 700 °C, MoO_x would migrate to the zeolite channels. There, they react at the *BAS*s forming water and $(MoO_2(OH))^+$ species, which can condense with one another to form $(Mo_2O_5)^{+2}$ dimers or can also react with a second Brönsted acid site to form a $(MoO_2)^{+2}$ cation bridging two framework oxygens and water. In addition, they indicated that condensation of bridging OH groups leads to extraction of Al ions from the framework, with the subsequent formation of water and the disappearance of two Brönsted acid sites. They proposed that $(Mo_2O_5)^{+2}$ species are reduced to the active MoC_x species during the initial stages of the reaction (groups of about 0.6 nm in diameter and that would contain approximately 10 Mo atoms). However, they demonstrated that when there is an excess of Mo, the MoO_x species are lost as MoO_3 oligomers by sublimation, or instead, it can form $Al_2(MoO_4)_3$ by extraction of framework aluminium. [3,58–60,]

Ma *et al.* and Liu *et al*. reported that Mo ions interact with the zeolite lattice migrating into the internal channels where they react with the *BAS* preferentially. There, Mo ions are attached to the zeolite framework near aluminium ions via oxygen bond. When this kind of interaction is very strong, aluminium associated species can be formed, extracting aluminium from the lattice and decreasing the crystallinity in the zeolite. They

also investigated Mo/H-ZSM-5 by electron paramagnetic resonance spectroscopy (EPR) and found two kinds of Mo species located at different positions. The first Mo species is located on the external surface. These species consist on polynuclear entities and can be octahedrally-coordinated MoO_3 crystallites as well as MoO_x in square-pyramidal coordination. The second kind is closely associated with Al ions in the zeolite channels, in two different locations, it is mononuclear and migrates inside the channels during the calcination. They also indicated that there are differences in the reducibility of the different species. While those on the external surface are fully reduced to Mo_2C during the induction period, species inside the channels are only partially reduced into MoO_xC_y. They suggested that both Mo species play a key role in methane dehydroaromatization. [3,61–64,]

Nagai *et al.* studied the active species of Mo carbides and carbonaceous carbon of Mo catalysts using mass spectroscopy, X-ray diffraction, and diffuse reflectance FTIR, among others. They identified three different carbides and two types of carbonaceous carbons: α-Mo_2C_{1-x}, β-Mo_2C and η-Mo_3C_2, pyrolytic carbon and graphitic carbon. They showed that the CH_4 conversion on the oxidized catalyst had an induction period for the activation of MoO_3 to β-Mo_2C and that benzene was formed less on η-Mo_3C_2 than at the other carbide species.[65]

Bao *et al.* synthesized Mo/H-ZSM-5 catalysts by solid state reaction and was studied by NH_3-TPD and ^1H MAS NMR. They found that Mo species were widely dispersed on both, the inner and outer surface of the ZSM-5 zeolite. Inside the channels, molybdenum species were found that formed $[Mo_5O_{12}]^{6+}$ type units, which interacted with the zeolite *BAS*s. On the outer surface they showed the presence of a different molybdenum that they called “molybdenum oxide crystallites”, with a size of less than 3 nm. Both types of molybdenum species were converted to MoO_xC_y, Mo_2C on the outer surface and $[Mo_5O_xC_y]^{n+}$ inside the channels during the first stage of the reaction. Bao et al. claimed that these were the active catalytic centers for methane conversion. Specifically, they suggested that benzene was mainly formed in the $[Mo_5O_xC_y]^{n+}$, this was due to the fact that the species located inside the channels were not capable of aggregate and sublimate, maintaining catalytic activity.[66 ,3]

On the other side, Zaikovskii *et al.* described a different situation concerning the active Mo species. Using high-resolution transmission electron microscopy (HRTEM), they showed that, during the reaction, molybdenum carbide (Mo_2C) is formed on the ZSM-5 surface, with a particle size of 2-15 nm. It was also shown how the carbon deposits were formed both on the surface of Mo_2C particles and on the zeolite surface. They also demonstrated that molybdenum-containing clusters with sizes of 1 nm were formed in the ZSM-5 channels, proposing that these molybdenum-containing clusters would be the active centers for the *MDA* reaction.[67,68]

Wachs *et al.* determined the identity and anchoring sites of the initial Mo structures present at the catalyst as an isolated oxide species with a single Mo atom on aluminium sites in the zeolite framework and on silicon sites on the zeolite external surface. They proposed that in the course of the reaction, the initial isolated Mo oxide species agglomerate and convert into carbide Mo nanoparticles (MoC_x or MoC_xO_y). This process was reversible being as it was possible to restore it by a treatment with oxygen.[69]

Beale *et al.* studied the evolution of Mo species and their location using high-resolution fluorescence detection XANES, and XRD, among others. The results indicated that after calcination most of the species present are isolated Mo-oxo species, attached to the zeolite framework at the straight channels. They showed how through the reaction, Mo was first partially carburized to metastable MoC_xO_y species which were responsible for C2 and C3 formation. Further carburization led to the detaching from the zeolite and aggregating, forming $Mo_{1.6}C_3$ clusters. The results reflected that this was the moment when benzene production was at its maximum. After that, the $Mo_{1.6}C_3$ clusters grew on the outer zeolite surface which appeared to be the primary cause of catalyst deactivation.[70,71]

Gascón *et al.* found that the Mo precursor state and the aluminium distribution do not play a decisive role in the final performance. At the beginning of the reaction, the Mo oxide was converted to Mo (oxy-)carbide, and they described how the isolation of Mo oxo units and their location within the zeolite channels were the factors that seem to be

crucial in the development of efficient catalysts.[72,73] They also studied the active site using ^{13}C NMR after precarburizing Mo/H-ZSM-5 with carbon monoxide and observed two types of Mo (oxy-)carbidic molecular species in addition to Mo_2C nanoparticles. Furthermore, they found that the carbon from the preformed carbide was incorporated into the main products of the *MDA* reaction, pointing to a dynamic active site.[74] In agreement to Beale and others, they proposed an oxidation state between 4+ and 6+ for Mo species and explained that Mo (oxy-)carbidic species no longer transform during the induction period. This would imply that the build-up of a hydrocarbon pool is necessary for the catalyst to achieve maximum activity.[75] To obtain more information about the viability of this mechanism, they performed a computational study showing that the exposure of Mo/H-ZSM-5 to the *MDA* conditions yields a range of reduced sites including mono- and binuclear Mo-oxo and Mo carbide complexes. These sites can catalyse the reaction via two alternative reaction channels, namely, the C–C coupling (ethylene) and the hydrocarbon-pool propagation mechanisms. Their results showed that the binuclear Mo carbide species that operate through the hydrocarbon pool mechanism are the most effective species.[76]

Results shown by Gascón were corroborated by Hensen *et al*. They combined a pulse reaction technique with isotope labelling of methane and found *MDA* is shown to be governed by a hydrocarbon pool mechanism in which benzene is derived from secondary reactions of confined polyaromatic carbon species with the initial products of methane activation.[39]

1.5.5. Deactivation and regeneration

To date, rapid deactivation of catalysts in the *MDA* reaction remains the main drawback that hinders the final industrial application of this reaction.[3,32,77,78] There are several factors to consider and that influence deactivation of the catalyst.[79] Active sites are known to be easily covered with carbon deposits during the reaction, deactivating the zeolite, which can even lead to channel blockage. This may be due to the presence of an excess of Brönsted acid sites, causing condensation reactions between aromatic rings to

continue beyond naphthalene, causing coke deposition. There is no consensus on the nature of these deactivation coke deposits, but according to the literature there are different types of carbons formed during the reaction that will affect the reaction: coke could be associated with active Mo sites or with Brönsted acid sites, it could be a carbide or pre-graphite carbon. Another factor to consider that can also lead to deactivation of the catalyst is the dealumination of the zeolite produced during the reaction, which would lead to the loss of the zeolite structure. Finally, it is indicated that given the high temperature at which the reaction is carried out, the sintering of the active phase is another factor to be considered. [60,80]

Despite not reaching a consensus on this issue, modulation of certain parameters has been proposed to avoid, or at least slow down, the deactivation of the systems. On the one hand, modulation of the amount, distribution and strength of the accessible Brönsted acid centers in the zeolite is of interest, so as to avoid the formation of coke that covers the active sites or blocks the channels. On the other hand, the improvement in the diffusion in the zeolite can also benefit this task. Both approaches are usually related and the modification of one can lead to the variation of the other, so you have to be cautious and study the different properties well.

The study and understanding of systems as well as the understanding of reaction is the only way to overcome this barrier, and that is why many research groups focus their work on this task. Below are some of the studies and results obtained related to deactivation, mainly of the Mo/H-ZSM-5 catalyst, as well as their regeneration, or their proposals to slow down the deactivation.

Lunsford *et al*. distinguished three types of carbon by using X-ray photoelectron spectroscopy (XPS). These include carbide carbon in Mo_2C (C *1s* 282.7 eV), carbon in pre-graphite carbonaceous deposits (sp-type, C *1s* 283.2 eV) and carbon in carbonaceous deposits with graphite structure (C_{1s} 284.6 eV). They explained that pre-graphite deposits are formed on the external surface of the zeolite, whereas graphite is formed

in the zeolite channels. [78] These results were corroborated by Bao et al. who also showed how the amount of the sp-type carbon increases during the reaction, until it gradually covers both the zeolite surface and Mo_2C phase. Thus, it is considered responsible for the deactivation of Mo catalysts.[3,50]

Ismagilov et al. determined that during the reaction carbonaceous deposits were formed as graphite layers on the surface of Mo_2C nanoparticles that were >2 nm in size, and as friable layers and disordered structure on the external surface of the zeolite. According to the energy dispersive X-Ray (EDX), X-ray diffraction analysis (XRD), and differential thermal analysis (DTA) results they obtained, they confirmed that the content of the carbonaceous deposits and the extent of their condensation increases with the time on stream, methane concentration in the feed, temperature and feed flow rate.[68]

Liu *et al*. also investigated the carbonaceous deposits on Mo/H-MCM-22 finding two types of coke: the first type located near the Brönsted acid sites, inert and what they pointed as the cause of catalyst deactivation, and the second type associated with Mo species which are reactive towards H_2, also forming ethylene and benzene.[81] However, they repeated the same analysis on Mo/H-ZSM-5 catalysts obtaining different results. They characterised the nature of deposited carbon on this last catalyst using several techniques including XPS, thermo gravimetric analysis (TGA), differential thermal analysis (DTA) and high-resolution transmission electron microscopy (HRTEM). Their results confirmed that the sp^2/sp^3 bonding ratio of coke species increases during the reaction, suggesting that the deposition of heavier aromatic-type carbon is the main reason for catalyst deactivation.[82]

Hensen *et al*. studied the deactivation of Mo/H-ZSM-5 catalysts using X-ray photoelectron spectroscopy (XPS), Raman spectroscopy, thermo gravimetric analysis (TGA), and TEM characterisation techniques. They found two types of carbon deposition which denominated as “hard” and “soft”. This distinction was related to the location of coke species inside the pores and on the external surface, respectively. They also found

during this study that MoO_3 species act as an active oxidation catalyst, reducing the combustion temperature of a certain fraction of coke.[40]

At present, Beale *et al*. carried out different studies in which some of the factors mentioned in the literature as possible causes of the deactivation of the catalysts during the reaction were discarded. In their initial work, they suggested dealumination during reaction was minimal and that deactivation was due to carbon deposition which occurs in the zeolite outer surface.[70] Subsequently, they studied Mo/H-ZSM-5 catalysts after reacting for different periods of time. They used for their study the quasielastic neutron scattering technique (QENS) and the results of this work indicated that the diffusion of methane in the samples did not appear strongly affected by the presence of the deposited coke, suggesting the access to the pore network is not significantly held back by the reaction coke.[83] In another later study, they observed that $Mo_{1.6}C_3$ clusters grow on the outer zeolite surface, which appears to be the primary cause of catalyst deactivation. They finally concluded that the deactivation was not only due to a decrease in the amount of active Mo available on the surface but also due to a loss in shape-selectivity which leads to an increased carbon deposition at the outer shell of the zeolite crystals and eventually to pore blockage.[71]

Despite the studies carried out by the different research groups on the factors that influence the deactivation of the catalysts during the *MDA* reaction, and considering the speed with which it takes place, the importance of the regeneration of the catalysts becomes evident. Recent studies in this field include, for example, the use of O_2 and H_2, the use of cyclic regenerators that allow obtaining a stable and continuous benzene production, etc. Some of these examples are shown below:

Zhang *et al*. compared the O_2 and the H_2 regeneration of Mo/H-ZSM-5 systems, concluding that under oxidative and high temperature conditions Mo is found as MoO_3 which is easily sublimable. Also, they found that this specie easily reacted with the framework aluminium of the zeolite to form inactive $Al_2(MoO_4)_3$. They concluded that the regeneration of coked Mo/H-ZSM-5 has to be performed in a reductive

environment, demonstrating a full recovery of the benzene formation activity of Mo/H-ZSM-5 at its working temperatures using H_2 for regeneration.[84]

Hensen *et al.* investigated the structural and textural stability of H-ZSM-5 as a function of the Mo loading in air at high temperature (550–700 °C). They found differences in the behaviour of catalysts with low Mo load (1–2 wt% Mo), and catalysts with higher Mo load. For the first case, the catalysts presented a high stability making them suitable candidates for isothermal (700 °C) reaction - air regeneration protocol of methane dehydroaromatization. However, at higher loading, catalysts rapidly lost their initial activity due to the irreversible damage to the zeolite framework, as a result of the aluminium molybdate formation after reaction of mobile MoO_3 species with framework Al.[85]

Kim *et al*. also studied a series of Mo/H-ZSM-5 catalysts with different Mo loadings and applied reaction-regeneration cycles under both oxidative and reductive regeneration conditions, also using different temperatures for it. Their results revealed that, for 5%Mo/H-ZSM-5 the most active of their catalyst, reductive regeneration required a temperature higher than 700 °C for coke removal, which resulted in thermal degradation of the catalyst. However, oxidative regeneration at 450 °C is the most efficient for maintaining catalytic activity and stability, while at higher temperatures of 550–850 °C, irreversible deactivation was observed. They observed that the selective recovery of Brönsted acid sites near Mo sites, as opposed to the isolated acid sites were sufficient to restore the catalytic activity in terms of benzene formation. [86]

1.5.6. Approaches to improve MDA

Many studies have been devoted to the optimization of the MDA reaction system. Some of the strategies followed by the different research groups have been the creation of mesopores in zeolite, the reduction of the size of its crystals, the co-feeding of other gases with methane to reduce the formation of coke, as well as the creation of new catalysts, the “chemical looping” or the use of different types of reactors.

However, carbon formation seems inevitable, but the experimental findings show this can be kinetically limited using H_2, oxidants, CO_2 or steam in the CH_4 feed. [31] On the ZSM-5 catalysts, various approaches have been attempted:
Iglesia *et al.* showed that the stability of MoC_x/H-ZSM-5 catalysts can be improved by adding CO_2 to CH_4 feeds at low concentrations. They explained the improvement as a result of the H_2 formed by CO_2–CH_4 reactions.[87]

Liu and co-workers also found that H_2 can be added to the feed, finding that it minimizes carbon formation, particularly on the Bronsted acid sites of the zeolite.[88]

The addition of O_2 or NO also has also been studied during these years. Au el al. used these gases as oxidant and their results showed there was an optimum, below which presumably coke is not oxidized sufficiently rapidly, and above which oxidation of the active Mo carbide decreases the activity.[89]

Another method used to try to avoid deactivation of the catalyst was used by Lin et al. They showed that by hydrothermal post-synthesis treatment in NaOH solution, a commercial zeolite could be restructured, modifying the microporous structure and the acidity. The process stabilized the framework with high crystallinity and prevented the creation of substantial extra pores. Consequently, the restructured Mo/H-ZSM-5 catalyst showed significant improvement in both catalytic durability and selectivity to aromatics in the methane dehydroaromatization reaction.[90]

Over the last few years, many researchers have developed new catalysts with the aim of finding a more robust one, which allows its use in industry for the MDA reaction. Some of them are based on zeolites and some are not:

Yung *et al*. used Ag–Ga/H-ZSM-5 catalyst for co-aromatization of methane and propylene at 400 °C. Their results showed an excellent catalytic performance, which they

explained was due to a better dispersion of Ag and Ga on the zeolite surface and moderate amount of strong Brönsted and Lewis surface acid sites. They also suggested the existence of a synergetic effect where methane was activated and converted into aromatics with the help of a coexisting olefin. However, benzene was not the major product.[91]

Veser *et al.* studied the nature of the active species in Fe/H-ZSM-5 catalysts prepared by different methods. They showed that coking is reduced with increasing Fe dispersion and that atomically dispersed Fe^{2+} inside the zeolite micropores constitutes the selective species for *MDA* reaction. However, the presence of Brönsted acid sites in the zeolite results in continued coke formation.[92]

Xiaoguang Guo *et al.* studied another type of catalyst, like the Fe©SiO_2 which showed excellent stability, methane conversion, and aromatic selectively in MDA reaction. Neither coking nor deactivation happened in a test of 60 h.[93]

Li *et a*l. studied GaN nanowires, which were first studied for direct conversion of methane into benzene and molecular hydrogen under ultraviolet illumination. During this work, they observed that GaN exhibited high activity toward methane C−H bond activation. In a second study they analyzed the thermal catalytic activity of GaN. This was a commercial catalyst consisted of GaN powders with a wurtzite crystal structure. Their results showed a superior stability and reactivity for converting light alkanes, including methane into benzene with high selectivity. The catalyst was also highly robust and was used repeatedly without noticeable deactivation.[94,95]

The fixed bed reactor has disadvantages in terms of industrial use; however, it remains the most widely used reactor for the study of the methane aromatization reaction. Adopting a type of reactor that enables an instantaneous regeneration of coked Mo/H-ZSM-5 catalyst or selectively removing hydrogen for shifting the chemical equilibrium to the products side are some of the strategies studied. Like this, one of the strategies followed to improve thermodynamic limitation is through the method that combines MDA with chemical loop. Xu et al. developed this strategy by coupling *MDA* reaction

with chemical looping to achieve reactive separation of H_2 from the *MDA* products by using a Fe_3O_4/FeO redox pair. Their results indicated that the yield of aromatics was significantly increased.[96]

Regarding the use of different reactors, the application of membrane reactor, fluidized bed reactors, or even plasma reactor are some examples:

Kjølseth *et al*. integrated an electrochemical $BaZrO_3$-based membrane in the reactor which exhibited proton and oxide ions conductivity. Their results demonstrated high aromatic yields and a better stability of the catalyst reducing the coke production rate.[97]

Xu *et al*. proposed a two beds type of circulating fluidized bed reactor system for industrial application of the *MDA* reaction. In this system, one catalyst bed serves as CH_4 convertor and the other as catalyst regenerator, and under operation catalyst particles are continuously circulated between the two beds to realize continuous regeneration of coked catalyst and hence ensure the simultaneous realization of industrially required continuous operation and high catalyst activity.[84]

Kim *et al.* decreased the reaction temperature by using a dielectric barrier discharge (*DBD*) plasma-catalyst hybrid system. When the plasma was applied to the Mo/H-ZSM-5 catalytic reactor, methane was converted at much lower temperatures than the conventional process. They showed as the benzene selectivity could be improved by enhancing the interaction between plasma and catalyst, and the catalyst deactivation was effectively prevented when H_2 gas was mixed with the reaction feed.[98]

Some research demonstrated that by incorporating an additional metal ion into the Mo/H-ZSM-5 system, catalytic activity could be enhanced. These are some examples:

Xu *et al*. doped several metal species, like Fe, Cu, Co, Mn, on Mo/H-ZSM-5 catalyst finding that catalytic performances and stability were promoted when the catalyst was doped with Fe due to the generation of carbon nanotubes induced by iron species. They explained these carbon nanotubes could suppress the formation of surface coke.[99]

Scurrell *et al*. doped Pt and Sn on Mo/H-ZSM-5 catalyst for methane aromatization. Their catalytic results of Pt−Mo/HZSM-5 catalyst showed an increase of methane conversion and a reduction of coke deposition. This last phenomenon happened as well when they doped the catalysts with a low load of tin. Furthermore, they co-impregnated the Mo/H-ZSM-5 catalyst with Pt and Sn finding that these catalysts exhibited higher selectivity to aromatic and lower selectivity to carbon deposition. They observed that the order of impregnation affected to the catalytic results and the structural and electronic properties of the catalyst.[100]

Martinez *et al.* exchanged H^+ in H-ZSM-5 with alkali (Na^+, Cs^+) and alkaline-earth (Ca^{2+}, Mg^{2+}) cations in order to modulate both strength and density of Brönsted acid sites. They found that partially exchanging H^+ with Na^+ reduced the density of Brönsted acid sites showing lower coke formation and higher aromatics selectivity.[101]

Currently, Hensen and co-workers have studied other types of strategies to improve the *MDA* efficiency, such as introducing O_2 pulses into methane feeding or performing the reaction at high pressure. In the first strategy they observed that a periodic supply of short pulses of oxygen into the methane feed led to doubling of the benzene yield, decreasing the rate of coke formation four times. Their results showed how the rapid cycling between the oxidic and carbidic forms of molybdenum did not affect the catalyst framework, and neither is molybdenum lost by sublimation. They explained these facts were due to the stabilization of molybdenum-oxo complexes on cation-exchange sites of the zeolite. [102] Using the second strategy, Hensen *et al*. showed that catalyst productivity can be improved by nearly an order of magnitude by raising the reaction pressure to 15 bar, demonstrating that performing the *MDA* reaction at elevated pressure leads to an increased rate of surface species hydrogenation, lower overall coke selectivity, and higher methane conversion capacity. Their results showed that the improvement of the catalytic performance at increased pressure is independent of the Mo loading, reaction temperature and methane space velocity. Operando XAS results evidenced that, although the Mo-oxide precursor is reduced easier under elevated pressure, the structure of the active sites during the actual reaction is independent of pressure. They explained this improvement in the performance as the result of a faster

coke hydrogenation at high pressure, which resulted in a lower coke selectivity and better utilization of the zeolite micropore space. [103]

These have been some of the studies carried out to improve the results obtained by performing the *MDA* reaction. As we have seen, different strategies have been developed; however, despite all the studies carried out, the low efficiency and the deactivation of carbon deposits continue to prevent this reaction from being commercialized.

1.6. Aim of this work

The main objective of this thesis is to understand the guiding principles of Mo/zeolite catalyst systems in the aromatization reaction of methane. Through the catalytic study and the characterization of these, it is intended to expand the knowledge of the active species in the reaction, the processes involved in the rapid deactivation of the catalyst, etc. This study would facilitate the development of new, more efficient catalysts that would allow the reaction to be commercialized. To achieve this, several partial objectives have been met:

1. Investigate the effect of preparing Mo/ZSM-5 catalyst with different loadings on the structure and catalytic performance for methane dehydroaromatization in order to optimize the system and obtain the best performance for the studied reaction (**Chapter 3**).

2. Study the nature of the active species in the Mo/zeolite catalyst as well as their influence on the deactivation mechanism (**Chapter 3, 4 and 7**).

3. A deep understanding of the effect of the addition of rhenium as a promoter of the classic Mo/zeolite system on the structure and activity performance for *MDA* reaction is also a subject of this work. (**Chapter 5 and 7**).

4. Understand the effect of different H_2 pretreatment conditions on the structure and activity of molybdenum catalysts (**Chapter 6**).

5. Finally. the optimization of *MDA* reaction variables such as gas composition, space velocity, dilution of the catalyst in SiC, etc.

1.7. References

1. International Energy Agency. World energy balances: An Overview. *J. Chem. Inf. Model.* **53**, 1689–1699 (2019).
2. Energy information administration of US Department of Energy. International energy outlook 2016-Natural gas. *Int. energy outlook 2016* **2016**, 37–60 (2016).
3. Ma, S., Guo, X., Zhao, L., Scott, S. & Bao, X. Recent progress in methane dehydroaromatization: From laboratory curiosities to promising technology. *J. Energy Chem.* **22**, 1–20 (2013).
4. Middleton, R. S., Gupta, R., Hyman, J. D. & Viswanathan, H. S. The shale gas revolution: Barriers, sustainability, and emerging opportunities. *Appl. Energy* **199**, 88–95 (2017).
5. Holmen, A. Direct conversion of methane to fuels and chemicals. *Catal. Today* **142**, 2–8 (2009).
6. Lunsford, J. H. Catalytic conversion of methane to more useful chemicals and fuels: a challenge for the 21st century. *Catal. Today* **63**, 165–174 (2000).
7. Alvarez-Galvan, M. C. *et al.* Direct methane conversion routes to chemicals and fuels. *Catal. Today* **171**, 15–23 (2011).
8. Benzene Market By Feedstock, Derivative Type 2020- TechSci Research. Available at: https://www.techsciresearch.com/report/global-benzenemarket-forecast-and-opportunities-2020/198.html. (Accessed: 15th April 2020)
9. Chen, A. *et al. Production of BTX from Ethane*. (2015).
10. Rodríguez-Padrón, D., Puente-Santiago, A. R., Balu, A. M., Muñoz-Batista, M. J. &

Luque, R. Environmental Catalysis: Present and Future. *ChemCatChem* **11**, 18–38 (2019).

11. Acmite Market Intelligence. *World Catalyst Market*. (2011).

12. Knowles, W. S. Asymmetric Hydrogenations. *Angew. Chem. Int. Ed.* **41**, 1998–2007 (2002).

13. Li, X., Huang, Y. & Liu, B. Catalyst: Single-Atom Catalysis: Directing the Way toward the Nature of Catalysis. *Chem* **5**, 2733–2735 (2019).

14. Bell, A. T. The Impact of Nanoscience in Heterogeneous Catalysis. *Science.* **299**, 1688–1691 (2003).

15. Valden, M., Lai, X. & Goodman, D. W. Onset of catalytic activity of gold clusters on titania with the appearance of nonmetallic properties. *Science.* **281**, 1647–1650 (1998).

16. Jens Weitkamp. Zeolites and catalysis. *Solid State Ionics* **131**, 175–188 (2000).

17. Zeolite Framework Type Codes. Available at: http://www.iza-structure.org/IZA-SC_FTC.htm. (Accessed: 15th April 2020)

18. *Zeolites in Industrial Separation and Catalysis*. (Wiley-VCH, 2010).

19. Sheldon, R. A., Arends, I. W. C. E. & Hanefeld, U. *Green Chemistry and Catalysis*. *Wiley-VCH* (2007).

20. Hagen, J. *Industrial Catalysis- A Practical Approach*. *Wiley-VCH* (Wiley-VCH, 2006).

21. Corma, A. State of the art and future challenges of zeolites as catalysts. *J. Catal.* **216**, 298–312 (2003).

22. Busca, G. *Zeolites and Other Structurally Microporous Solids as Acid–Base Materials*. *Heterogeneous Catalytic Materials, Elsevier.* **1**, (2014).

23. Shamzhy, M., Opanasenko, M., Concepción, P. & Martínez, A. New trends in tailoring active sites in zeolite-based catalysts. *Chem. Soc. Rev.* **48**, 1095–1149 (2019).

24. Petushkov, A., Yoon, S. & Larsen, S. C. Synthesis of hierarchical nanocrystalline

ZSM-5 with controlled particle size and mesoporosity. *Microporous Mesoporous Mater.* **137**, 92–100 (2011).

25. Taniguchi, T., Nakasaka, Y., Yoneta, K., Tago, T. & Masuda, T. Size-controlled synthesis of MFI metallosilicate and their catalytic performance on acetone to olefins reaction. *Microporous Mesoporous Mater.* **224**, 68–74 (2016).

26. Roth, W. J., Nachtigall, P., Morris, R. E. & Čejka, J. Two-dimensional zeolites: Current status and perspectives. *Chem. Rev.* **114**, 4807–4837 (2014).

27. Wei, X. & Smirniotis, P. G. Synthesis and characterization of mesoporous ZSM-12 by using carbon particles. *Microporous Mesoporous Mater.* **89**, 170–178 (2006).

28. Valtchev, V., Majano, G., Mintova, S. & Pérez-Ramírez, J. Tailored crystalline microporous materials by post-synthesis modification. *Chem. Soc. Rev.* **42**, 263–290 (2013).

29. Verboekend, D. & Pérez-Ramírez, J. Design of hierarchical zeolite catalysts by desilication. *Catal. Sci. Technol.* **1**, 879–890 (2011).

30. Busca, G. Microporous and Mesoporous Materials Acidity and basicity of zeolites : A fundamental approach. *Microporous Mesoporous Mater.* **254**, 3–16 (2017).

31. Spivey, J. J. & Hutchings, G. Catalytic aromatization of methane. *Chem. Soc. Rev.* **43**, 792–803 (2014).

32. Ismagilov, Z. R., Matus, E. V. & Tsikoza, L. T. Direct conversion of methane on Mo/ZSM-5 catalysts to produce benzene and hydrogen: Achievements and perspectives. *Energy Environ. Sci.* **1**, 526–541 (2008).

33. Vollmer, I., Yarulina, I., Kapteijn, F. & Gascon, J. Progress in Developing a Structure-Activity Relationship for the Direct Aromatization of Methane. *ChemCatChem* **11**, 39–52 (2019).

34. Wang, L. *et al.* Dehydrogenation and aromatization of methane under non-oxidizing conditions. *Catal. Letters* **21**, 35–41 (1993).

35. Kosinov, N. & Hensen, E. J. M. Reactivity, Selectivity, and Stability of Zeolite-Based Catalysts for Methane Dehydroaromatization. *Adv. Mater.* **32**, (2020).

36. Chen, L. Y., Lin, L., Xu, Z., Li, X. & Zhang, T. Dehydro-oligomerization of methane to ethylene and aromatics over molybdenum/HZSM-5 catalyst. *Journal of Catalysis* **157**, 190–200 (1995).

37. Xu, Y., Liu, S., Guo, X., Wang, L. & Xie, M. Methane activation without using oxidants over Mo/HZSM-5 zeolite catalysts. *Catal. Letters* **30**, 135–149 (1994).

38. Solymosi, F., Cserényi, J., Szöke, A., Bánsági, T. & Oszkó, A. Aromatization of methane over supported and unsupported Mo-based catalysts. *J. Catal.* **165**, 150–161 (1997).

39. Kosinov, N. *et al.* Confined Carbon Mediating Dehydroaromatization of Methane over Mo/ZSM-5. *Angew. Chemie Int. Ed.* **57**, 1016–1020 (2018).

40. Kosinov, N. *et al.* Structure and Evolution of Confined Carbon Species during Methane Dehydroaromatization over Mo/ZSM-5. *ACS Catal.* **8**, 8459–8467 (2018).

41. Kosinov, N. *et al.* Methane Dehydroaromatization by Mo/HZSM-5: Mono- or Bifunctional Catalysis? *ACS Catal.* **7**, 520–529 (2017).

42. Xu, Y. & Lin, L. Recent advances in methane dehydro-aromatization over transition metal ion-modified zeolite catalysts under non-oxidative conditions. *Appl. Catal. A Gen.* **188**, 53–67 (1999).

43. Liu, W., Xu, Y., Liu, S. & Guo, X. Dehydrogenation and aromatization of CH_4 in the absence of O_2 on Mo/HZSM-5. *Chinese J. Catal.* **17**, 99–100 (1996).

44. Ma, D. *et al.* In situ 1H MAS NMR spectroscopic observation of proton species on a Mo-modified HZSM-5 zeolite catalyst for the dehydroaromatization of methane. *Angew. Chemie - Int. Ed.* **39**, 2928–2931 (2000).

45. Liu, S., Wang, L., Ohnishi, R. & Ichikawa, M. Bifunctional catalysis of Mo/HZSM-5 in the dehydroaromatization of methane to benzene and naphthalene XAFS/TG/DTA/ MASS/FTIR characterization and supporting effects. *J. Catal.* **181**, 175–188 (1999).

46. Vollmer, I., Abou-Hamad, E., Gascon, J. & Kapteijn, F. Aromatization of Ethylene –

Main Intermediate for MDA? *ChemCatChem* **12**, 544–549 (2020).

47. Agote-Arán, M. *et al.* Implications of the Molybdenum Coordination Environment in MFI Zeolites on Methane Dehydroaromatisation Performance. *ChemCatChem* **12**, 294–304 (2020).

48. Zhang, C. L. *et al.* Aromatization of methane in the absence of oxygen over Mo-based catalysts supported on different types of zeolites. *Catal. Letters* **56**, 207–213 (1998).

49. Leonowicz, M. E., Lawton, J. A., Lawton, S. L. & Rubin, M. K. MCM-22: A Molecular Sieve with Two Independent Multidimensional Channel Systems. *Science.* **264**, 1910–1913 (1994).

50. Ma, D. *et al.* Mo/HMCM-22 catalysts for methane dehydroaromatization: A multinuclear MAS NMR study. *J. Phys. Chem. B* **105**, 1786–1793 (2001).

51. Solymosi, F., Erdöhelyi, A. & Szöke, A. Dehydrogenation of methane on supported molybdenum oxides. Formation of benzene from methane. *Catal. Letters* **32**, 43–53 (1995).

52. Solymosi, F., Szöke, A. & Cserényi, J. Conversion of methane to benzene over Mo_2C and Mo_2C/ZSM-5 catalysts. *Catal. Letters* **39**, 157–161 (1996).

53. Szöke, A. & Solymosi, F. Selective oxidation of methane to benzene over K_2MoO_4/ZSM-5 catalysts. *Appl. Catal. A Gen.* **142**, 361–374 (1996).

54. Wang, D., Lunsford, J. H. & Rosynek, M. P. Characterization of a Mo/ZSM-5 catalyst for the conversion of methane to benzene. *J. Catal.* **169**, 347–358 (1997).

55. Wang, D., Lunsford, J. H. & Rosynek, M. P. Catalytic conversion of methane to benzene over Mo/ZSM-5. *Top. Catal.* **3**, 289–297 (1996).

56. Zhang, J., Long, M. A. & Howe, R. F. Molybdenum ZSM-5 zeolite catalysts for the conversion of methane to benzene. **44**, (1998).

57. Liu, S., Wang, L., Ohnishi, R. & Ichikawa, M. Bifunctional Catalysis of Mo/HZSM-5 in the Dehydroaromatization of Methane to Benzene and Naphthalene XAFS/TG/DTA/ MASS/FTIR Characterization and Supporting Effects. *J. Catal.* **181**,

175–188 (1999).

58. Borry, R. W., Kim, Y. H., Huffsmith, A., Reimer, J. A. & Iglesia, E. Structure and density of Mo and acid sites in Mo-exchanged H-ZSM5 catalysts for nonoxidative methane conversion. *J. Phys. Chem. B* **103**, 5787–5796 (1999).

59. Wei Li, George D. Meitzner, Richard W. Borry III, and E. I. Raman and X-Ray Absorption Studies of Mo Species in Mo/H-ZSM5 Catalysts for Non-Oxidative CH_4 Reactions. *J. Catal.* **191**, 373–383 (2000).

60. Ding, W., Li, S., Meitzner, G. D. & Iglesia, E. Methane conversion to aromatics on Mo/H-ZSM5: structure of molybdenum species in working catalysts. *J. Phys. Chem. B* **105**, 506–513 (2001).

61. Ma, D. *et al.* Towards guest - Zeolite interactions: An NMR spectroscopic approach. *Chem. - A Eur. J.* **8**, 4557–4561 (2002).

62. Liu, H., Bao, X. & Xu, Y. Methane dehydroaromatization under nonoxidative conditions over Mo/HZSM-5 catalysts : Identification and preparation of the Mo active species. **239**, 441–450 (2006).

63. Liu, H., Shen, W., Bao, X. & Xu, Y. Methane dehydroaromatization over Mo / HZSM-5 catalysts : The reactivity of MoC_x species formed from MoO_x associated and non-associated Brönsted acid sites. **295**, 79–88 (2005).

64. Ma, D., Shu, Y., Bao, X. & Xu, Y. Methane dehydro-aromatization under nonoxidative conditions over Mo/HZSM-5 catalysts: EPR study of the Mo species on/in the HZSM-5 zeolite. *J. Catal.* **189**, 314–325 (2000).

65. Nagai, M., Nishibayashi, T. & Omi, S. Molybdenum carbides and carbonaceous carbons on Mo / Al-FSM16 for methane conversion. **253**, 101–112 (2003).

66. Li, B. *et al.* Structure and acidity of Mo/ZSM-5 synthesized by solid state reaction for methane dehydrogenation and aromatization. *Microporous Mesoporous Mater.* **88**, 244–253 (2006).

67. Zaikovskii, V. I. *et al.* Properties and deactivation of the active sites of an MoZSM-5 catalyst for methane dehydroaromatization: Electron microscopic and EPR

studies. *Kinet. Catal.* **47**, 389–394 (2006).

68. Matus, E. V. *et al.* Study of methane dehydroaromatization on impregnated Mo/ZSM-5 catalysts and characterization of nanostructured molybdenum phases and carbonaceous deposits. *Ind. Eng. Chem. Res.* **46**, 4063–4074 (2007).

69. Jie Gao, Yiteng Zheng, Jih-Mirn Jehng, Y. T. & Israel E. Wachs, S. G. P. Identification of molybdenum oxide nanostructures on zeolites for natural gas conversion. *Science.* **348**, (2015).

70. Lezcano-González, I. *et al.* Molybdenum Speciation and its Impact on Catalytic Activity during Methane Dehydroaromatization in Zeolite ZSM-5 as Revealed by Operando X-Ray Methods. *Angew. Chemie - Int. Ed.* **55**, 5215–5219 (2016).

71. Agote-Arán, M. *et al.* Determination of Molybdenum Species Evolution during Non-Oxidative Dehydroaromatization of Methane and its Implications for Catalytic Performance. *ChemCatChem* **11**, 473–480 (2019).

72. Vollmer, I. *et al.* Relevance of the Mo-precursor state in H-ZSM-5 for methane dehydroaromatization. *Catal. Sci. Technol.* **8**, 916–922 (2018).

73. Vollmer, I. *et al.* Applied Catalysis A , General Quantifying the impact of dispersion , acidity and porosity of Mo / HZSM-5 on the performance in methane dehydroaromatization. *Appl. Catal. A, Gen.* **574**, 144–150 (2019).

74. Vollmer, I. *et al.* On the dynamic nature of Mo sites for methane dehydroaromatization. *Chem. Sci.* **9**, 4801–4807 (2018).

75. Vollmer, I. *et al.* A site-sensitive quasi-in situ strategy to characterize Mo/HZSM-5 during activation. *J. Catal.* **370**, 321–331 (2019).

76. Li, G., Vollmer, I., Liu, C., Gascon, J. & Pidko, E. A. Structure and Reactivity of the Mo/ZSM - 5 Dehydroaromatization Catalyst: An Operando Computational Study. *ACS Catal.* **9**, 8731–8737 (2019).

77. Tang, P., Zhu, Q., Wu, Z. & Ma, D. Methane activation: The past and future. *Energy Environ. Sci.* **7**, 2580–2591 (2014).

78. Weckhuysen, B. M., Rosynek, M. P. & Lunsford, J. H. Characterization of surface

carbon formed during the conversion of methane to benzene over Mo/H-ZSM-5 catalysts. *Catal. Letters* **52**, 31–36 (1998).

79. Zheng, H. *et al.* Methane dehydroaromatization over Mo/HZSM-5: A study of catalytic process. *Catal. Letters* **111**, 111–114 (2006).

80. Tempelman, C. H. L. & Hensen, E. J. M. On the deactivation of Mo/HZSM-5 in the methane dehydroaromatization reaction. *Appl. Catal. B Environ.* **176**–**177**, 731–739 (2015).

81. Liu, H. *et al.* The chemical nature of carbonaceous deposits and their role in methane dehydro-aromatization on Mo/MCM-22 catalysts. *Appl. Catal. A Gen.* **236**, 263–280 (2002).

82. Liu, B. S., Jiang, L., Sun, H. & Au, C. T. XPS, XAES, and TG/DTA characterization of deposited carbon in methane dehydroaromatization over Ga-Mo/ZSM-5 catalyst. *Appl. Surf. Sci.* **253**, 5092–5100 (2007).

83. Silverwood, I. P., Arán, M. A., González, I. L., Kroner, A. & Beale, A. M. QENS study of methane diffusion in Mo/H-ZSM-5 used for the methane dehydroaromatisation reaction. *AIP Conf. Proc.* **1969**, (2018).

84. Xu, Y., Song, Y. & Zhang, Z. G. A binder-free fluidizable Mo/HZSM-5 catalyst for non-oxidative methane dehydroaromatization in a dual circulating fluidized bed reactor system. *Catal. Today* **279**, 115–123 (2017).

85. Kosinov, N. *et al.* Stable Mo/HZSM-5 methane dehydroaromatization catalysts optimized for high-temperature calcination-regeneration. *J. Catal.* **346**, 125–133 (2017).

86. Han, S. J. *et al.* Non-oxidative dehydroaromatization of methane over Mo/H-ZSM-5 catalysts: A detailed analysis of the reaction-regeneration cycle. *Appl. Catal. B Environ.* **241**, 305–318 (2019).

87. Lacheen, H. S. & Iglesia, E. Stability, structure, and oxidation state of Mo/H-ZSM-5 catalysts during reactions of CH_4 and CH_4-CO_2 mixtures. *J. Catal.* **230**, 173–185 (2005).

88. Zheng Liu, Michael A. Nutt, and E. I. The effects of CO_2, CO and H_2 co-reactants on methane reactions catalyzed by Mo/H-ZSM-5. *Catal. Letters* **81**, (2002).

89. Tan, P. L., Leung, Y. L., Lai, S. Y. & Au, C. T. Methane aromatization over 2 wt% Mo/HZSM-5 in the presence of O_2 and NO. *Catal. Letters* **78**, 251–258 (2002).

90. Song, Y., Sun, C., Shen, W. & Lin, L. Hydrothermal post-synthesis of HZSM-5 zeolite to enhance the coke-resistance of Mo/HZSM-5 catalyst for methane dehydroaromatization. *Catal. Letters* **109**, 21–24 (2006).

91. He, P., Gatip, R., Yung, M., Zeng, H. & Song, H. Co-aromatization of olefin and methane over Ag-Ga/ZSM-5 catalyst at low temperature. *Appl. Catal. B Environ.* **211**, 275–288 (2017).

92. Lai, Y. & Veser, G. The nature of the selective species in Fe-HZSM-5 for non-oxidative methane dehydroaromatization. *Catal. Sci. Technol.* **6**, 5440–5452 (2016).

93. Guo, X. *et al.* Direct, nonoxidative conversion of methane to ethylene, aromatics, and hydrogen. *Science.* **344**, 616–619 (2014).

94. Li, L., Fan, S., Mu, X., Mi, Z. & Li, C. J. Photoinduced conversion of methane into benzene over GaN nanowires. *J. Am. Chem. Soc.* **136**, 7793–7796 (2014).

95. Li, L. *et al.* Thermal non-oxidative aromatization of light alkanes catalyzed by gallium nitride. *Angew. Chemie - Int. Ed.* **53**, 14106–14109 (2014).

96. Brady, C., Murphy, B. & Xu, B. Enhanced Methane Dehydroaromatization via Coupling with Chemical Looping. *ACS Catal.* **7**, 3924–3928 (2017).

97. Morejudo, S. H. *et al.* Direct conversion of methane to aromatics in a catalytic co-ionic membrane reactor. *Science.* **353**, 563–566 (2016).

98. Park, S. *et al.* Plasma-Assisted Non-Oxidative Conversion of Methane over Mo/HZSM-5 Catalyst in DBD Reactor. *Top. Catal.* **60**, 735–742 (2017).

99. Xu, Y., Wang, J., Suzuki, Y. & Zhang, Z. G. Improving effect of Fe additive on the catalytic stability of Mo/HZSM-5 in the methane dehydroaromatization. *Catal. Today* **185**, 41–46 (2012).

100. Tshabalala, T. E., Coville, N. J., Anderson, J. . & Scurrell, M. S. Dehydroaromatization of methane over Sn–Pt modified Mo/H-ZSM-5 zeolite catalysts: Effect of preparation method. *Appl. Catal. A Gen.* **485503**, 218–226 (2015).

101. Martínez, A. & Peris, E. Non-oxidative methane dehydroaromatization on Mo/HZSM-5 catalysts: Tuning the acidic and catalytic properties through partial exchange of zeolite protons with alkali and alkaline-earth cations. *Appl. Catal. A Gen.* **515**, 32–44 (2016).

102. Kosinov, N., Coumans, F. J. A. G., Uslamin, E., Kapteijn, F. & Hensen, E. J. M. Selective Coke Combustion by Oxygen Pulsing During Mo/ZSM-5-Catalyzed Methane Dehydroaromatization. *Angew. Chemie - Int. Ed.* **55**, 15086–15090 (2016).

103. Kosinov, N. *et al.* Reversible Nature of Coke Formation on Mo/ZSM-5 Methane Dehydroaromatization Catalysts. *Angew. Chemie - Int. Ed.* **58**, 7068–7072 (2019).

Chapter 2. Catalyst synthesis and experimental techniques

In this chapter the experimental techniques used during the development of this thesis have been defined. The equipment used for the characterization of the samples, as well as the experimental setups used to determine the catalytic activity, are also briefly detailed. The choice of these techniques is due, on the one hand, to the intention of providing valuable information on the physical-chemical, structural, textural and morphological properties of the samples, and on the other hand, to the availability of them in our facilities or in other accessible centers.

2.1. Catalyst preparation

2.1.1. ZSM-5 based catalyst

Commercial ZSM-5 (SiO_2/Al_2O_3=23, Alfa Aesar) was also used as support for the catalysts. The commercial ZSM-5 was first calcined at 550 °C for 3 h in order to have its protonated form (HZSM-5).

For methane dehydroaromatization, molybdenum was loaded onto the HZSM-5: the dried zeolite was impregnated with a solution containing the stoichiometric amounts ammonium heptamolybdate tetrahydrate (Aldrich) in water and kept under stirring for 20 hours. After that, water was eliminated in a rotary evaporator. After impregnation, the samples were dried for 4 h, and calcined in air at 550 °C for 3 h, at a rate of 5°C /min. The impregnation procedure is equivalent for other metals we use for *MDA* reaction, like rhenium and also for different types of zeolites.

2.1.2. MCM-22 based catalysts.

MCM-22 was obtained by hydrothermal sythesis, the classic method or microwave assisted. The classic method consists of PTFE-lined stainless-steel reactors of 170 mL that can be introduced inside a heater at the required temperature. The second method consists of a set of hydrothermal reactors of smaller size which rotate and are heated using microwave radiation whith internal agitation in each reactor (Milestone EthosEZ Microwave). For the preparation, the following compounds were used: hexamethylenimine (HMI, 99 %, Aldrich), silicic acid ($SiO_2 \cdot H_2O$, 100-200 mesh, Sigma-Aldrich), sodium aluminate ($NaAlO_2 \cdot 2H_2O$, Al_2O_3: 50-56 % Na_2O: 37-45 %, Sigma-Aldrich), sodium hydroxide (NaOH, Merck), and deionized water. Typically, the relation for the synthesis mixtures were SiO_2/Al_2O_3= 30, Na/SiO_2= 0.18, HMI/SiO_2=0.35 and H_2O/SiO_2=19.5. The general procedure consists on dissolving the sodium hydroxide and the sodium aluminate in deionized water. To this solution, the amount of silicic acid and hexamethyleneimine were added, and the resulting mixture was stirred until it was

visibly homogeneous. After this, the resulting gels were introduced in the hydrothermal reactor and crystallization of the dry gel was carried out at 155 °C, for different periods of time depending on the version of the method used and under the autogenous pressure. After quenching the autoclaves in cold water to room temperature, the samples were filtered, washed, dried at 110 °C overnight and calcined in air at 550 °C for 8 h, at a rate of 2 °C/min.

The calcined samples were ion-exchanged in a 1 M NH_4NO_3 solution for 12 h, and after washed and filtered. This procedure was repeated three times. After drying overnight at 110 °C, the solids were calcined at 550 °C for 3 h in air to finally obtain the H-form zeolite.

Molybdenum was supported on the zeolite by means of the impregnation method described before, obtaining catalysts of different metal loads supported on MCM-22.

2.2. Characterization techniques.

2.2.1. Nitrogen physisorption.

Surface area and pore structure are properties of key importance for any catalyst or support material. Gas adsorption measures are widely used for the characterization of a wide variety of porous solids, such as oxides, carbons, zeolites or organic polymers.

At physisorption, a gas interacts with a solid surface by a van der Waals bond, weaker than a typical chemical bond. The formation of many layers of adsorbed molecules which is achieved due to the van der Waals interactions between adsorbed molecules is not much different from the van der Waals interaction between the molecules and the surface. The amount of gas adsorbed at a given temperature for a relative gas pressure depends on different factors such as specific surface, porosity, etc, and it can be represented as a graph called adsorption isotherm.

The IUPAC classification of adsorption isotherms is illustrated in **Figure 1**. The six types of isotherm (IUPAC classification) are characteristic of adsorbents that are microporous (type I), nonporous or macroporous (types II, III, and VI), or mesoporous (types IV and V).

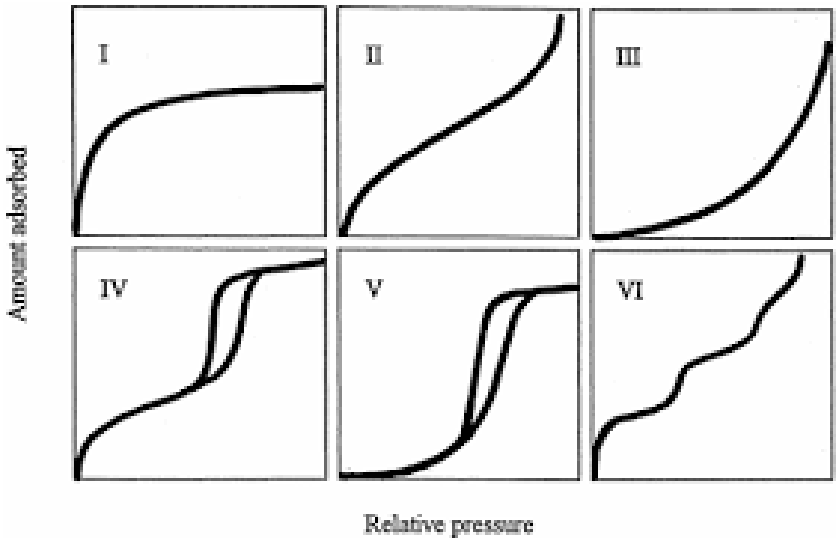

Figure 1. The IUPAC classification of adsorption isotherms for gas.

Several mathematical models have been developed to describe the equilibrium adsorption capacity of adsorbents. Among the most common is the Brunauer, Emmet y Teller (BET), it is based on the Langmuir model and extended to multilayers adsorption allowing the determination of the specific surface of a solid.[1,2]

$$\frac{P}{V_{ads}(P_0-P)} = \frac{1}{V_m C} + \frac{C-1}{V_m C} \cdot \frac{P}{P_0} \qquad \text{(Eq. 1)}$$

Where P is the partial pressure of the adsorbed gas, P_0 the vapor pressure of the gas, V_m the adsorbed gas volume when a monolayer is created, C is a constant, and V_{ads} the adsorbed gas volume at a pressure P.

If it is represented $\frac{P}{V_{ads}(P_0-P)}$ vs $\frac{P}{P_0}$ a straight line will be obtained, with a slope and an intercept that will allow V_m and C to be obtained. Using the value of V_m the specific surface BET can be obtained using this equation:

$$S_{BET} = \left[\frac{V_m}{M \cdot g}\right] \cdot N_A \cdot \sigma \qquad \text{(Eq. 2.)}$$

Where, as we said before, V_m the adsorbed gas volume when a monolayer is created, M is the molar volume of the gas, g is the weight of the sample, N_A is Avogadro number and σ is the area occupied by an adsorbate molecule in the monolayer. [3]

The pore size distribution consists of expressing the pore volume versus the pore size to which it is ascribed. It is not a direct measure, but the consequence of applying complex mathematical models. The most widely used mathematical model is the BJH (Barrett, Joyner y Halenda), it is based on an analysis of the condensation and capillary phenomena of the condensed phase. It is a modification of the Kelvin equation which predicts the pressure at which adsorptive will be spontaneously condensed and evaporate in a cylindrical pore of a given size. [4]

$$ln\left(\frac{P}{P_0}\right) = -\left(\frac{2\gamma v cos\theta}{RTr_m}\right) \qquad \text{(Eq. 3.)}$$

Where P^* is the critic condensation pressure, P_0 the vapor pressure of the gas, γ the *surface* tension, v the molar volume of the condensate, Θ the contact angle between the solid and the condensate (*Θ=0 for nitrogen, cos 0=1)*, and r_m the radius of curvature of the condensate.

The value of r_m will be the corresponding pore radius at which capillary condensation takes place for relative pressure P/P_0 and is termed the Kelvin radius. Since there is already some liquid adsorbed on the wall of the pore before the capillary condensation takes place, the true radius r should be r_m plus τ, where τ is the thickness of liquid adsorbed. Replacing r_m with (r - τ) the pore radius can be found:

$$r = \frac{2\gamma v}{RTLn\left(\frac{P}{P_0}\right)} + \tau \qquad \text{(Eq. 4.)}$$

To calculate the surface area, pore size and pore volume of each catalyst a Micromeritics Tristar instrument was used. For this technique a known mass of sample, was placed in a tube of known volume and heated under vacuum. Then it was cooled in liquid nitrogen and a known amount of nitrogen gas was introduced. The pressure was measured, and the sequence was repeated with successive pulses of nitrogen. As the volume of the system, the temperature and the amount of gas added with each pulse was known, the expected pressure in the absence of any adsorption was able to be calculated. Due to the difference between the calculated pressure and the observed pressure at each point the amount of nitrogen adsorbed was determined.

2.2.2. X-ray powder diffraction.

X-ray diffraction methods are based on the phenomenon of wave interferences. It is used to identify crystalline phases inside catalysts by means of lattice structural parameters, and to obtain an indication of particle size.

X-ray beams incident on a crystalline solid will be diffracted by the crystallographic planes, the deflected waves will not be in phase except when the following relationship is satisfied:

$$n\lambda = 2d \sin \Theta; \text{ n=1, 2, 3...} \qquad \text{(Eq.5.)}$$

this equation is called Bragg's Law, where λ is the wavelength of the X-rays, d is the distance between two lattice planes, Θ is the angle between the incoming X-rays and the normal to the reflecting lattice plane, n is an integer called the order of the reflection.

This law relates the wavelength of electromagnetic radiation to the diffraction angle and the lattice spacing in a crystalline sample. Knowing the spacing of crystallographic planes by diffraction methods, we can determine the crystal structure of materials. These

diffracted X-rays are then detected, processed and counted. By scanning the sample through a range of 2θ angles, all possible diffraction directions of the lattice should be attained due to the random orientation of the powdered material. [5]

In the present work, XRD patterns of the studied catalysts were obtained by using a Siemens D-501 diffractometer with Ni filter and graphite monochromator and using the Cu *Kα* radiation.

2.2.3. Thermogravimetric analysis

Thermogravimetric analysis (TGA) is a technique for measuring changes in the sample mass while the sample temperature is changing. The result of TGA measurements is a thermogravimetric curve that can be presented in either integral or differential form. DTG curves allow one to better identify individual mass loss steps.[6]

TGA is mainly used for understanding certain thermal events such as absorption, adsorption, desorption, vaporization, sublimation, decomposition, oxidation, and reduction. It is also possible to study the kinetics of chemical reactions under various conditions using this technique.[7]

A TGA consists of a sample pan that is supported by a precision balance, and which resides in a furnace where the sample can be heated or cooled during the experiment. The mass of the sample is monitored during the experiment and a purge gas flows over the sample.

Our samples were analyzed by a TA Instruments Q600 TGA/DSC instrument. For this purpose, certain amount of sample was placed in an alumina crucible which was heated to 800 °C under air flow.

2.2.4. Transmission electron microscopy and scanning transmission electron microscopy

Electron microscopy is a very versatile technique, working through different modes and combining with another spectroscopic techniques it lets us obtain physical and chemical information of our samples: structure, chemical composition, etc.

The transmission electron microscope (TEM) operates on the same basic principles as the light microscope but uses electrons instead of light, having a better resolution due to the smaller wavelength of electrons.

There are two ways of working: conventional transmission electron microscopy (TEM) and scanning electron transmission microscopy (STEM). For the first one, a high energy beam of electrons is directed using electromagnetic lenses and incises over a thin sample. The image is formed when after the interaction, the beam crosses the objective lens below the sample, obtaining the output wave that contains information on the structure of the sample. This wave propagates through the objective lens to the posterior focal plane, where the diffraction diagram is obtained, and then to the image plane, where the image is obtained. The electrons are elastically or inelastically scattered as they penetrate the sample. Either the transmitted electrons or the scattered electrons can be imaged, known as dark-field and bright-field imaging, respectively. For the second way of working, the STEM, the electron beam is focused into a very small spot which is scanned over the sample and passes through it. This electron beam interacts with the thin sample and the transmitted beam is collected by a detector, depending on the angular range of intensity to be collected.

The image is the distribution map of the signal intensity in the XY plane. These are the different types of detector:

- Bright-field detector (BF): small angles (<0-10 mrad). These images are similar to the bright-field images obtained using TEM.

- Annular dark-field detector (ADF): larger angles (10-50 mrad).
- High-angle annular dark-field detector (HAADF): Angles > 50mrad. The electrons diffracted at a high angle come from the Rutherford diffraction phenomenon and pass very close to the nucleus of the atoms. Its intensity and the contrast generated in the image is sensitive to the atomic number, Z. This is also known as Z-contrast imaging and it enhances contrast, especially at lower atomic numbers, compared to TEM.

Atomic-resolution mapping of the individual elements in a material can be achieved using either electron energy-loss spectroscopy (EELS) or energy-dispersive X-ray spectroscopy (EDS), both are spectroscopic techniques associated with transmission electron microscopes.

In the present work we have used energy-dispersive X-ray spectroscopy. This technique is based on the relaxation of the atoms of the sample after a previous interaction with the incident beam: it excites an internal electron of an atom, which leaves a hole that is occupied by an electron of a higher energy level, emitting a photon of energy ΔE that will be characteristic of the element in question, allowing the identification of this. [8]

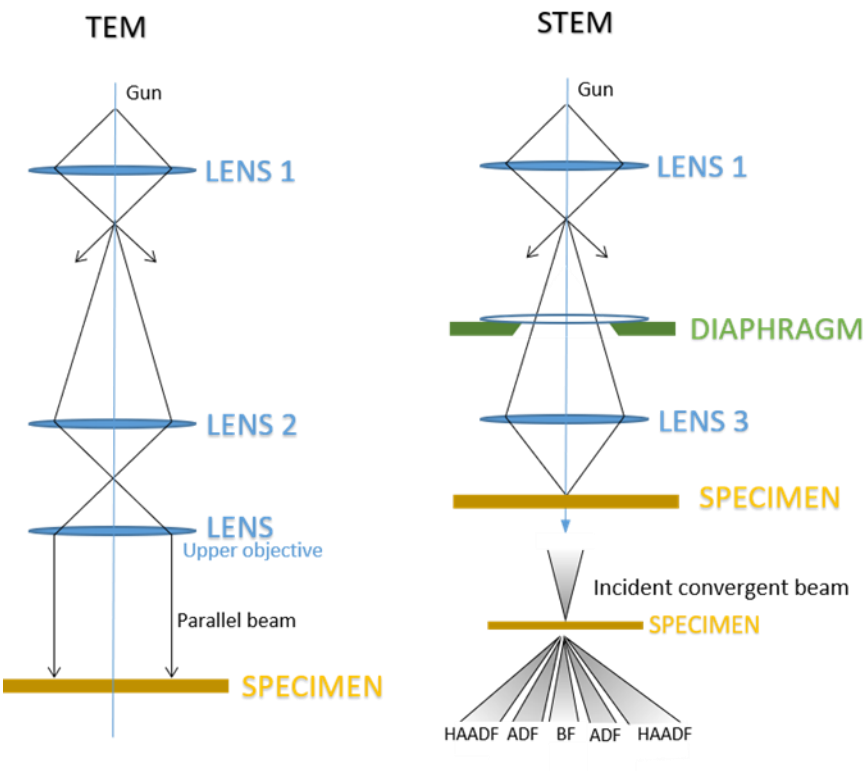

Figure 2. Scheme of two ways of working: conventional transmission electron microscopy (TEM) and scanning electron transmission microscopy (STEM).

Transmission electron microscopy (TEM) was performed by using a JEOL 2100Plus microscope. We also used a TALOS (FEGTEM, 200 KV), which obtained images of transmitted electrons by scanning the beam (STEM) and, also, it allows information to be visually displayed on the chemical composition of the sample (HAADF detector). It is equipped with an X-ray detector to perform elemental composition analysis obtaining sample composition maps. Samples were prepared by dipping a carbon grid into the powder sample.

2.2.5. Temperature-programmed reduction

Temperature-programmed reduction (TPR) is a useful tool for the characterization of metal oxides. The TPR method provides qualitative and quantitative information on the reducibility of the oxide's surface, as well as the heterogeneity of the reducible surface.

A reducing gas mixture (typically hydrogen diluted in argon, but in our case also methane diluted in helium) flows over the sample, which is placed in a fixed-bed reactor while the temperature is increased according to a linear temperature programme. The difference between the inlet and outlet concentration of the gas stream is measured using a thermal conductivity detector and/or a mass spectrometer. The resulting TPR profile contains qualitative information on the oxidation state of the reducible species present, but the technique is intrinsically quantitative and the information obtained is of a kinetic nature and can be correlated with catalytic behaviour. Like this, it is possible to determine the energetic nature of catalysts and to identify the temperature required to activate the metallic phase.[9]

Commercial patterns are used for calibration, converting the TCD signal into active gas concentration and integrating the area under the concentration vs time graph. Knowing the stoichiometry of the reduction reaction, it is easy to determine the consumed hydrogen.

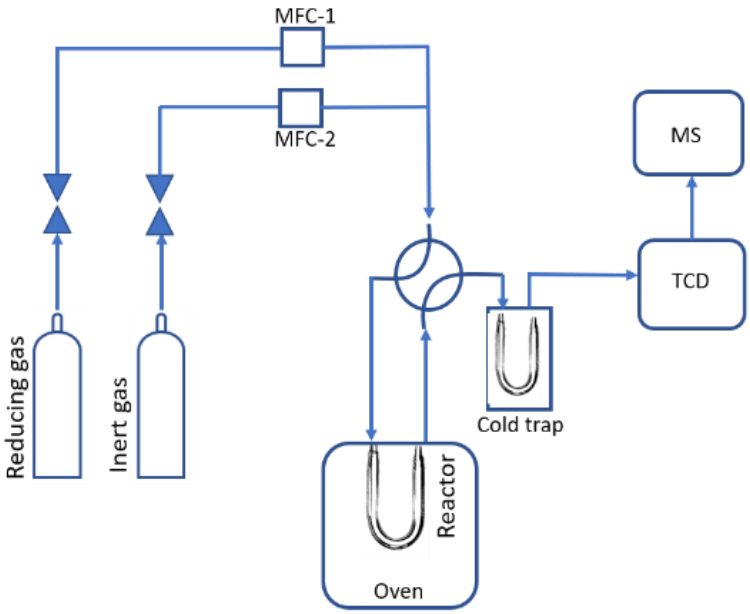

Figure 3. Simplified representation of the TPR setup.

In our case, TPR analysis were carried out using a Quantachrome Chemstar instrument equipped with a thermal conductivity detector and mass spectrometer. About 35 mg of catalyst was first heated to 150 °C in an inert flow of argon at 30 mL/min for 60 min

previous to each experiment for water desorption. The experimental conditions were chosen to fulfil the resolution conditions.

2.2.6. Diffuse reflectance UV-vis spectroscopy

UV-visible spectroscopy is based on the electronic absorption of electromagnetic radiation when it interacts with matter in the wavelength range between 190 nm and 800 nm. For powder samples, the diffuse reflectance measure is used because in powders of randomly oriented particles part of the incident light goes back at all angles into the hemisphere of provenance of the light. The phenomenon resulting from the reflection, refraction, diffraction, and absorption by particles oriented in all directions is called diffuse reflection, in contrast with regular reflection from a plane phase boundary.

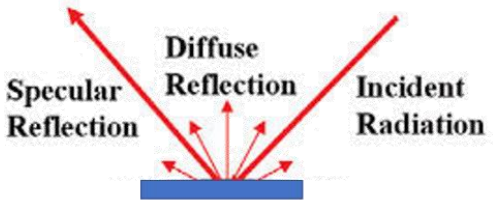

Figure 4. Projection of the spectrometer beam into the sample where it is reflected, scattered and transmitted through the sample material.

The ultraviolet-visible spectroscopy by diffuse reflectance (UV-Vis DRS) provides information on the environment of the metallic and organic species present in the material, as long as they present transitions between molecular levels separated by energies of the order of the region UV and / or visible from electromagnetic radiation.[8]

In a UV-Vis DRS spectrum, the ratio of the light scattered from an infinitely thick layer and the scattered light from an ideal non-absorbing reference sample is measured as a function of the wavelength. The resulting spectrum is usually obtained as a percentage

of reflectance against the wavelength, establishing as 100 % of reflectance that was obtained for the non-absorbing reference sample.

The studies of diffuse reflectance spectra in this work were obtained on a UV–vis scanning spectrophotometer Agilent Cary 300, equipped with an integrating sphere, using Spectralon® as reference material and ZSM-5 as background. UV-vis spectra were performed in the diffuse reflectance mode (*R*) and transformed to a magnitude proportional to the extinction coefficient (*K*) through the Kubelka-Munk function, F(R∞). For the sake of comparison, all spectra were arbitrary normalized in intensity to 1.

2.2.7. Raman spectroscopy

Raman spectroscopy is a technique based on inelastic monochromatic light scattering in the visible, near infrared, or near ultraviolet range, and it is a powerful tool for determining chemical species.

It exploits the existence of Stokes and Anti-Stokes scattering to examine molecular structure: when a laser falls upon the sample, most of it is scattered elastically (Rayleigh scattering), but a small amount of light is scattered inelastically, and therefore has a change in its frequency. That is, the electronic cloud of the molecule is excited and goes into a virtual excited state. To return to the ground state it emits a photon, however, since the dispersion is inelastic, energy has been lost or gained, and the molecule does not return to the same state, but goes into a rotational or vibrational other than the initial one. The difference in energy between these states is what modifies the frequency of the emitted photon and is characteristic of the chemical nature and the physical state of the sample. This is typically measured as the change in the wavenumber from the incident light source.

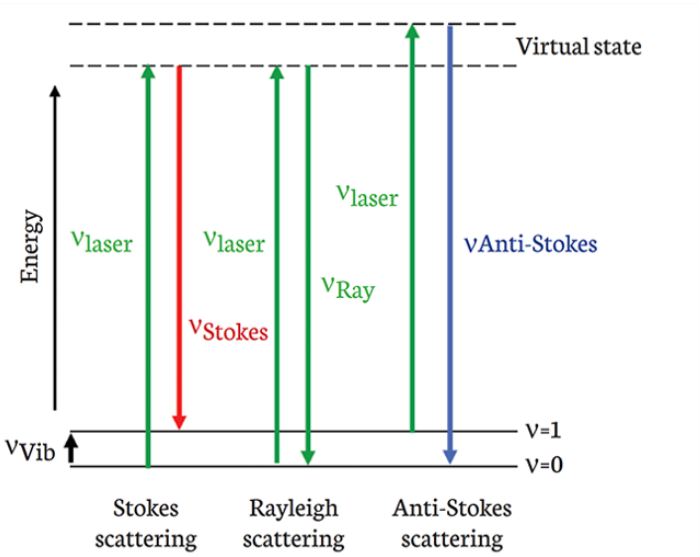

Figure 5. Vibrational energy-level diagram showing the states involved in Raman scattering phenomenon.

Raman spectroscopy requires a change in polarizability and allows obtaining complementary spectral information on homonuclear molecules. This is a measure of the deformability of a bond in an electric field and depends on how easy it is for the electrons in the bond to be displaced, inducing a temporary dipole. [10]

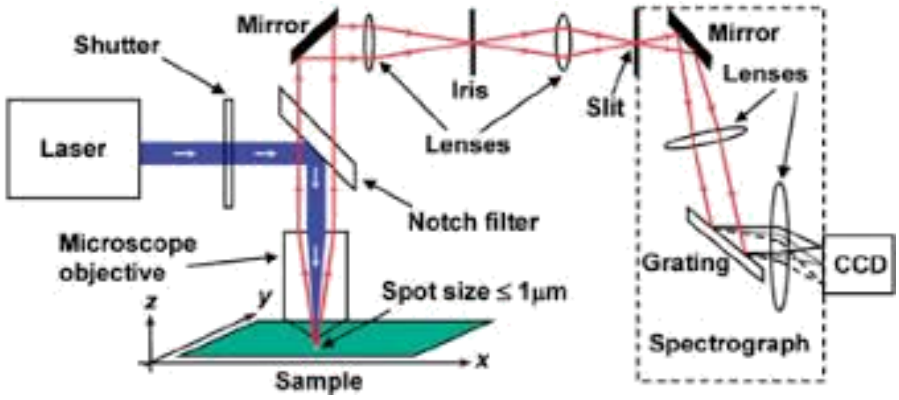

Figure 6. Scheme of operation of a Raman equipment.

Micro-Raman measurements were performed using a LabRAM Jobin Yvon spectrometer equipped with a microscope. Laser radiation (λ = 532 nm) was used as excitation source

at 5 mW. All measurements were recorded under the same conditions (2s of integration time and 30 accumulations) using a 100x magnification objective and a 125 mm pinhole.

2.2.8. Inductively coupled plasma atomic emission spectroscopy (ICP-OES)

Inductively coupled plasma atomic emission spectroscopy is a spectral method used to quantitatively determine the elemental composition of samples at trace and ultra-trace levels.

ICP-AES works by the emission of photons from analytes that are brought to an excited state by the use of high-energy plasma. The sample, in liquid form, it is transported to the nebulizer system using a peristaltic pump where it is transformed into an aerosol thanks to the action of argon gas. This aerosol is led to the ionization zone consisting of a plasma in which temperatures of up to 7000 °C can be reached. The plasma source is induced when passing argon gas through an alternating electric field that is created by an inductively couple coil. The atoms are ionized or excited and emit radiation of a wavelength that is characteristic of each element in order to return to their ground state. The radiation is separated according to its wavelength and a detector measures the intensity of each radiation, obtaining like this the concentration of each element in the sample.[11]

The elemental determination of the samples was performed using a SPECTRO SectroBLUE spectrometer equipped with a CCD detector. Previously, the samples were digested in an EthosOne Microwave, firstly using a mixture of acids and heating at 240 °C, and then in boric acid at 220 °C to end the digestion.

2.2.9. X-ray photoelectron spectroscopy

XPS is based on the photoelectric effect and it provides information on the elemental composition, oxidation state and, in favourable cases, on the dispersion or chemical

environment. When a sample is irradiated with X-ray, an electron can be ejected. This happens if the energy of the X-ray is bigger than the binding energy of the electron. The kinetic energy of the ejected electron will follow this equation:

$$E_k = h\nu - E_b - \varphi \qquad \text{(Eq. 6.)}$$

Where E_k is the kinetic energy of the photoelectron, h is Planck's constant, ν is the frequency of the exciting radiation, E_b is the binding energy of the photoelectron with respect to the Fermi level of the sample and φ is the work function of the spectrometer.

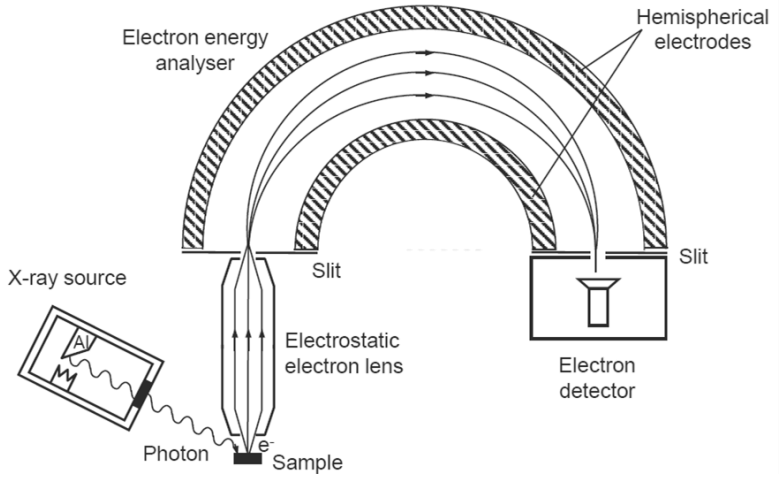

Figure7. Scheme of an XPS spectrometer.

By measuring the number of ejected electrons (intensity) and the kinetic energy, a xps spectrum is obtained, and it provides information about elemental composition of the sample, oxidation state, dispersion of the element and chemical environment. The change of this in the sample produces a chemical shift, which consists of a change in binding energy of a core electron of an element. To remove or to add electronic charge as a result of changes in bonding will alter the shielding: the withdrawal of valence electron charge produces an increase in binding energy (oxidation), and the addition a decrease in binding energy.

Photoelectrons do not travel far in solids due to interactions with atoms resulting in inelastic scattering. The number of photoelectrons that reach a surface are described by the Beer-Lambert law:

$$N = N_0 e^{-x/\lambda \sin\Theta} \qquad \text{(Eq. 7.)}$$

Where λ is the inelastic mean free path (IMPF, average distance that an electron with a given energy travels between successive inelastic collisions), N_0 and N are the number of electrons before and after passage through the sample, x is the thickness of sample and Θ is the angle between the surface and the plane of acceptance of the electron optics.

With a path length of one λ, 63 % of all electrons are scattered and no longer contribute to the peak in the XPS spectrum. Sampling Depth is defined as the depth from which 95% of all photoelectrons are scattered by the time they reach the surface (3λ). Most λs are in the range of 1 – 3.5 nm for Al $K\alpha$ radiation, so the sampling depth (3λ) for XPS under these conditions is 3-10 nm

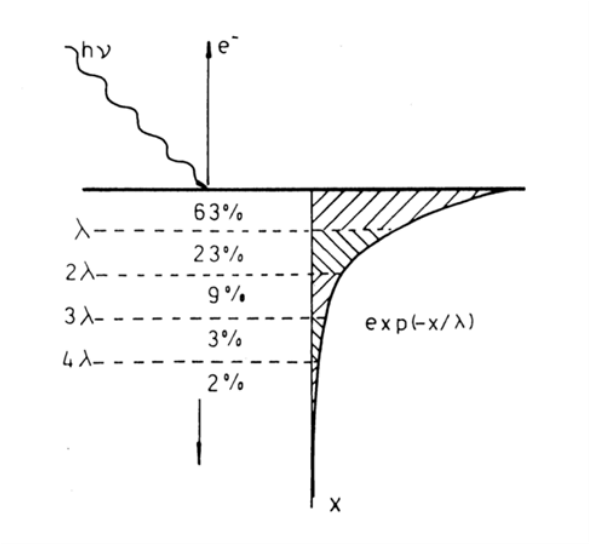

Figure 8. Probability of emitted electron reaches the surface and being analysed.

XPS data was recorded on pellets which were outgassed in the prechamber of the instrument at room temperature up to a pressure below $2 \cdot 10^{-8}$ torr to remove chemisorbed water from their surfaces. Spectra were recorded using a Leybold-Heraeus LHS-10 spectrometer, working with constant pass energy of 50 eV. The spectrometer main chamber, working at a pressure $<2 \cdot 10^{-9}$ Torr, is equipped with an EA-200 MCD hemispherical electron analyser with a dual X-ray source working with Al $K\alpha$ (hv= 1486.6

eV) at 120 W and 30 mA. Si *2p* and C *1s* signal (103.0 and 284.6 eV respectively) were used as internal energy reference depending on the experiments.

2.2.10. Ammonia adsorption microcalorimetry

The study of adsorption calorimetry allows the determination of the number, strength, and force distribution of acid / base sites in solids and is useful in predicting the effect of these parameters on catalytic properties.

This technique measures the heats of adsorption of a base probe molecule. In order to measure the acid sites of our samples we used ammonia as our probe molecule. It is one of the most used in calorimetry since it is extremely basic and also small, so its diffusion is hardly affected by the porous structure.

The disadvantage of using ammonia is that it adsorbs very strongly even in the weakest acid sites, so its interactions with the acid sites are relatively nonspecific.

In the adsorption microcalorimetry technique, the sample is kept at a constant temperature while a known volume of ammonia is adsorbed on its surface, and a heat flux detector emits a signal proportional to the amount of heat transferred per unit of time that it is collected and integrated. Adsorption takes place by repeatedly sending small aliquots of gas over the sample, which has been previously degassed, until saturation ranges are reached. The calorimetric data is generally displayed as a plot of enthalpy of adsorption versus coverage.[12,13]

Ammonia adsorption microcalorimetry measurements were performed with a Tian-Calvet heat flow microcalorimeter (Setaram), equipped with a volumetric vacuum line. Each sample (ca. 0.1 g, 40-80 mesh) was thermally pretreated at 80 °C for 12 h under vacuum (5 mPa). Ammonia adsorption was carried out by admitting successive doses of the probe gas and measuring the equilibrium pressure relative to each adsorbed amount by means of a differential pressure gauge (Datameritics) up to a final equilibrium pressure of about 133 Pa. The thermal effect corresponding to the adsorption of each

dose was simultaneously recorded. The adsorption temperature was kept at 80 °C, in order to limit physisorption. After overnight outgassing at the same temperature, a re-adsorption run was carried out, in order to distinguish the acid sites weak enough to be made free through the outgassing step. The adsorption and calorimetric isotherms were obtained from each adsorption (and re-adsorption) experiment. Combining the two sets of data, a plot of the differential heat of adsorption, Q_{diff}, as a function of the adsorbed amount was drawn, which gives information on the strength distribution of the adsorbing sites.

2.3. Catalytic activity study

The catalysts were tested in a fixed-bed stainless steel tube reactor with 0.1g of catalyst diluted in the same quantity of SiC (Sigma Aldrich) and located between two quartz wool plugs. Methane dehydroaromatization reaction was performed under CH_4/N_2 (85:15) with a flow of 5 mL/min, at 700 °C with a 10 °C temperature ramp. Obtained products were analyzed by using online GC (Agilent, 7890B) equipped with 3 channels for separate analyses of light gases (HAYESEP Q precolumn, MolSieve 5Å column, thermal conductivity detector, TCD), light hydrocarbons (GS-GASPRO column, flame ionization detector, FID) and aromatics (HP-88, flame ionization detector, FID).

The methane conversion (X_{CH_4}), selectivity ($S_{C_6H_6}$, etc) and yield ($Y_{C_6H_6}$, etc) for the different products obtained were calculated using *Equations* 10 to 12.

$$X_{CH_4}(\%) = \frac{[CH_4]_i - [CH_4]_t}{[CH_4]_i} \times 100 \quad \text{(Eq. 10.)},$$

where $[CH_4]_i$ are the methane mol at the reactor inlet, and $[CH_4]_t$ the methane mol at the reactor outlet at a time *t*.

$$S_{C_6H_6}(\%) = \frac{[C_6H_6]_t \times 6}{\sum([product_i]_t \times n_i)} \times 100 \quad \text{(Eq. 11)},$$

where $[C_6H_6]_t$ are the benzene mol at a time *t*, n_i the stoichiometric factor of the product *i* and $[product_i]_t$ the products mol at a time *t.*

$$Y_{C_6H_6}(\text{mmol}/g_{cat}) = \sum([C_6H_6]_t \times C) \quad \text{(Eq. 12)},$$

Where *C* is a constant where it is included different factors as the loop volume, time of each GC analysis and methane flow.

2.4. References

1. Brunauer, B. S. & Emmett, P. H. in Multimolecular. **60**, 309–319 (1938).
2. Harkins, W. D. & Jura, G. Surfaces of Solids. XIII. A Vapor Adsorption Method for the Determination of the Area of a Solid without the Assumption of a Molecular Area, and the Areas Occupied by Nitrogen and Other Molecules on the Surface of a Solid. *J. Am. Chem. Soc.* **66**, 1366–1373 (1944).
3. Union, I., Pure, O. F. & Chemistry, A. International Union of Pure Commission on Colloid and Surface Chemistry Including Catalysis * Reporting Physisorption Data for Gas / Solid Systems with Special Reference to the Determination of Surface Area and Porosity. **57**, 603–619 (1985).
4. Barrett, E. P., Joyner, L. G. & Halenda, P. P. The Determination of Pore Volume and Area Distributions in Porous Substances. I. Computations from Nitrogen Isotherms. *J. Am. Chem. Soc.* **73**, 373–380 (1951).
5. Methods, X. D. *X-ray Diffraction Methods*. (2008).
6. Vyazovkin, S. Thermogravimetric Analysis: Characterisation of Materials. *Charact. Mater.* 344–362 (2012).
7. Loganathan, S., Valapa, R. B., Mishra, R. K., Pugazhenthi, G. & Thomas, S. *Thermogravimetric Analysis for Characterization of Nanomaterials*. *Thermal and Rheological Measurement Techniques for Nanomaterials Characterization* **3**, (Elsevier Inc., 2017).
8. Niemantsverdriet, J. W. (Eindhoven U. of T., Catalysis, S. I. of, 2, D. D., Eindhoven,

5612 AZ & Netherlands)., T. *Spectroscopy in Catalysis*. (2007 WILEY-VCH Verlag GmbH & Co. KGaA, Weinheim).

9. Malet, P. & Caballero, A. The selection of experimental conditions in temperature-programmed reduction experiments. *J. Chem. Soc. Faraday Trans. 1 Phys. Chem. Condens. Phases* **84**, 2369–2375 (1988).

10. Nakamoto, K. & Brown, C. W. *Introductory Raman Spectroscopy*. (Elsevier, 2003).

11. Agrawal, A. *et al. Physical Methods in Chemistry and Nano Science*.

12. Solinas, V. & Ferino, I. Microcalorimetric characterisation of acid-basic catalysts. *Catal. Today* **41**, 179–189 (1998).

13. Auroux, A. Microcalorimetry methods to study the acidity and reactivity of zeolites, pillared clays and mesoporous materials. *Top. Catal.* **19**, 205–213 (2002).

Chapter 3. Physico-chemical characterization of Mo/H-ZSM-5 systems for *MDA* reaction.

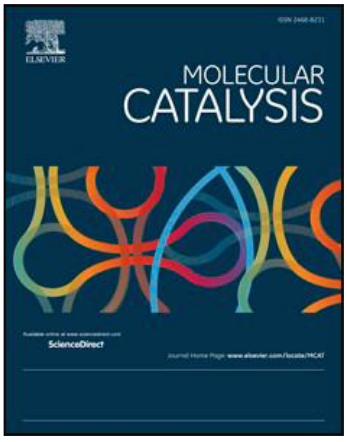

A. López-Martín, A. Caballero, G. Colón

"Structural and surface considerations on Mo/ZSM-5 systems for methane dehydroaromatization reaction"

Molecular Catalysis, 486, 110787, 2020

We have prepared a series of Mo/H-ZSM-5 systems with different metal loading following the method described in the previous chapter. The obtained catalysts were widely structural and surface characterized. As Mo content increases, the surface feature of the support is affected especially its mesoporosity. The enormous complexity of Mo species present in the studied system is noted. *In-situ* characterization by XPS reveals different reduction and carburization behaviour depending on the Mo content.

3.1. Introduction

As it was explained in **Chapter 1**, recent developments in natural gas production technology have led to lower prices for methane and renewed interest in converting methane to higher value products such as aromatic compounds.[1–3] In recent years, extensive research has been carried out on the transformation of methane to valuable chemicals, such as benzene, through the direct methane aromatization reaction. Up to now and due to its superior performance, Mo based catalytic systems supported on zeolites, particularly ZSM-5, remains the most investigated *MDA* catalyst.[4] Although it is feasible, this *MDA* reaction brings many problems, mainly due to poor inactivation and conversion processes. Therefore, a deeper understanding of these systems is required.

We can start building a description of the different parts that form this catalytic system.

In relation to ZSM-5, it is constituted by a three-dimensional ordering with two 10-membered ring channel systems. This zeolite is formed by straight channels running parallel to [010] with pore diameter 5.3 x 5.6 Å and interconnected to these, sinusoidal channels parallel to [100] of 5.1 x 5.5 Å diameter (**Figure 1**). ZSM-5 also possesses unusual catalytic properties and have high thermal stability.[5,6] In fact, the MFI zeolite framework type is one of the most robust open silica structures due to the absence of Si−O−Si bond angles less than 140°. Such high stability allows the use of ZSM-5 in processes such as the *MDA* reaction in which high temperatures are required.[7]

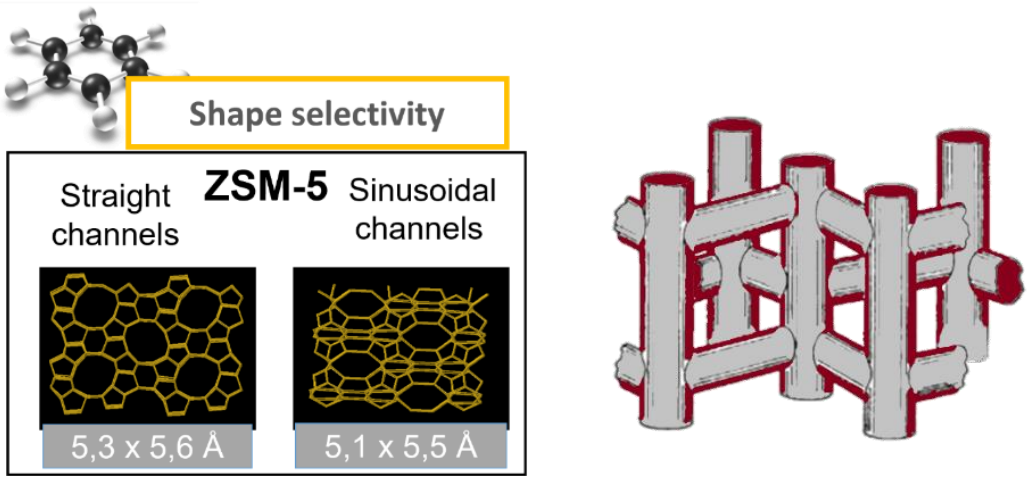

Figure 1. Framework structure (left) and channel intersection (right) of the ZM-5 zeolite.

If the kinetic diameter of the molecules involved in *MDA* is observed, the largest would be that of the aromatics, approximately 5.85 Å. It is a diameter greater than the size of the ZSM-5 channels, however we know that these products diffuse through this zeolite. This is because the pore diameters indicated are only approximations obtained for empty zeolites. Instead, zeolite structures are flexible and if there are small molecules inside, the channel system can expand or deform depending on the shape of the occluded molecule.

The Mo/H-ZSM-5 catalysts discussed in this chapter are generally prepared by impregnation with an aqueous solution containing $(NH_4)_6Mo_7O_{24}$, as in our case. Molybdenum is therefore in the form of an ion, which, being large, remains on the surface of the zeolite. It is by increasing the temperature that the molybdenum species migrate to the pore channels of the zeolite and become anchored.[8] Thus, during calcination process, which is carried out at temperatures between 500 °C and 700 °C with low heating ramps, it is possible to achieve a good dispersion of molybdenum species. If, on the other hand, the temperature is raised rapidly, the structure of the zeolite can be damaged and Al can be extracted, forming Al_2MoO_4 and hampering the catalytic activity of these systems.[9]

The reported results during these last years on the existing molybdenum species in the Mo/H-ZSM-5 catalytic systems remain a subject of intense debate. In this sense, the exact nature of the Mo-oxo precursor in the catalysts will depend on several parameters to take into account at the time of synthesis, such as the preparation method, the Si/Al ratio and the Mo loading. According to the bibliography, after catalyst calcination Mo is found in the oxidation states of 6+ and 5+, the latter forming aluminium molybdate. Some of the Mo-oxo intermediates observed are $(MoO_2)^{2+}$ and $MoO_2(OH)^+$ monomers and $(Mo_2O_5)^{2+}$ dimers (**Figure 2**). The species can stabilize on two proximate BAS but also on silanols. On the external surface larger Mo(VI)-oxo oligomers have also been detected. According to previous publications, if the Si/Al ratio or the Mo content is increased, the formation of dimers is favoured. If, on the other hand, the Si/Al ratio or the Mo content is reduced, the formation of $(MoO_2)^{2+}$ monomers is favored.[10–12]

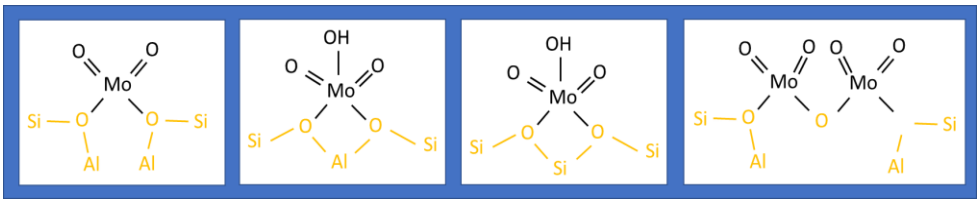

Figure 2. Schematic of proposed molecular Mo-oxo species adsorbed in ZSM-5 structure.

Moreover, these precursor molybdenum species can be found in different positions in the ZSM-5 structure, both at the surface or inside the porous structure. In the case that Mo species were inside the channels, they could also be found in straight channels, sinusoidal channels or at the intersection of both.

Thus, we have to highlight the great complexity of the catalyst systems frequently used in the *MDA* reaction. Therefore, the first stage of our work will be to characterize and understand, as far as possible, the systems from which we start. A detailed knowledge of the catalytic system will require the analysis of its physicochemical, textural and structural properties, combining different characterization techniques. By correlating this information with the performance of the catalyst, a better understanding of the processes that are carried out in this reaction and a more efficient future design of catalysts will be possible.

In this chapter, the physico-chemical characterization of the Mo/H-ZSM-5 systems has been carried out using different techniques such as XRD, TPR and TEM, in addition to the *in-situ* XPS during the catalyst reduction and carburization process. For this, different molybdenum systems supported in commercial ZSM-5 have been synthesized following the protocol detailed in **Chapter 2.**

3.2. Catalysts characterization and performance

3.2.1. Catalytic activity

Figure 3 shows the time-on-stream reaction for a series of Mo/H-ZSM-5 systems, formed by 1, 2, 4, 8 and 10 wt% of Mo supported on the zeolite.

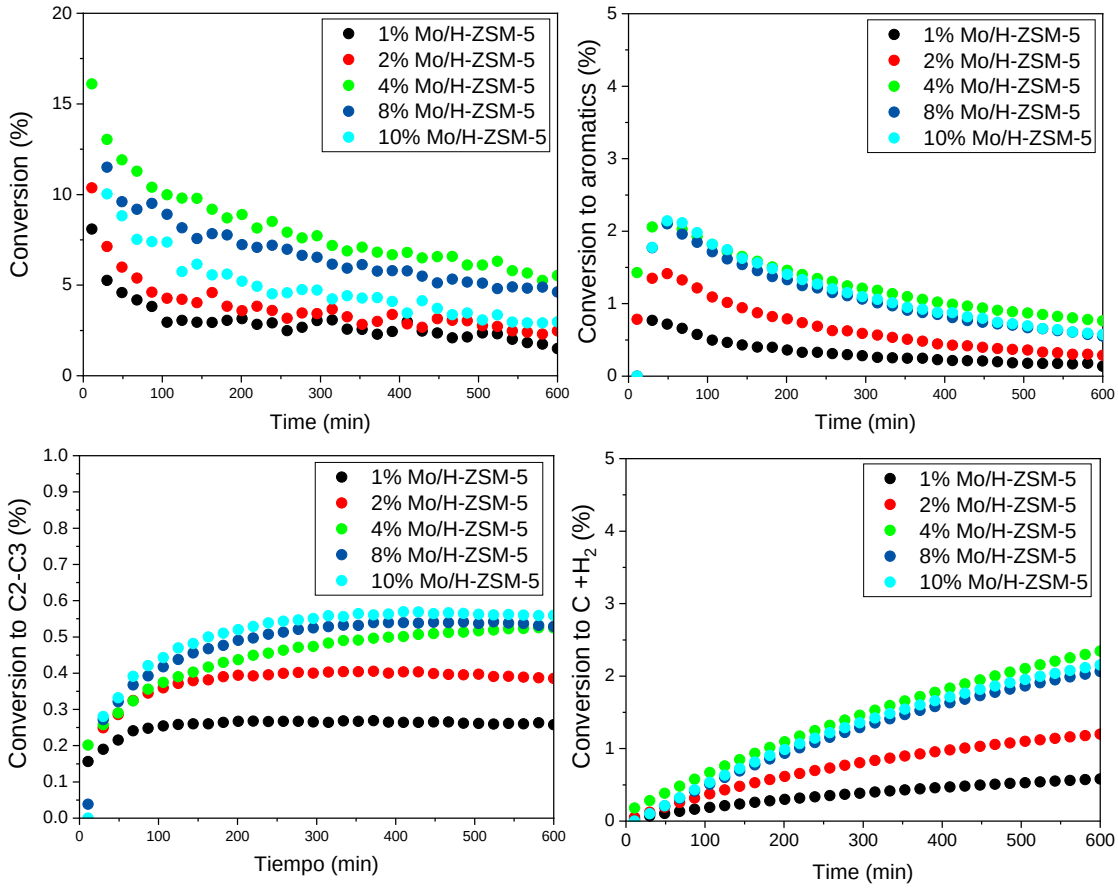

Figure 3. Conversion plots for different Mo/H- ZSM-5 catalysts during methane aromatization reaction.

As a general trend, methane conversion progressively decays with reaction time, indicating a clear catalyst deactivation with it. In fact, the obtained values of methane conversion at 700°C lies between 15% for 4%Mo and 5% for 1%Mo, showing a rapid and progressive decay. This feature is in agreement with most of the reported values in the literature.[4]

Among the studied systems, 4 wt% molybdenum loading attained the maximum CH_4 conversion rate. When the content of supported Mo exceeds that value, the catalytic performance quickly decreases. The main hydrocarbon product observed was benzene, being naphthalene the main aromatic side product. Thus, achieved selectivities for aromatic compounds are ca 80 % in all cases. It can be stated that the lower aromatic conversion in the other systems can be related to a higher occurrence of intermediate products such as ethylene, ethane or propene (**Figure 3**).

At the same time to aromatization reaction, important CH_4 cracking is taking place with continuous conversion to H_2 (**Figure 3**). Thus, the continuous coke formation during the reaction would lead to the progressive catalyst deactivation. If we consider the yield for desired compounds the 4%Mo/H-ZSM-5 gave a significantly higher amount of benzene after ca. 12 hours of reaction (**Figure 4**). Thus, the selectivity to aromatics was 80 % for 4%Mo/H-ZSM-5 sample. Contrary to benzene and aromatics formation, ethylene is continuously formed along the whole reaction time (**Figure 4**). Thus, it can be said that the deactivation of catalysts affects specifically to the aromatic production. This fact was already described and was explained by considering the progressive blocking of the porous structure and the accessibility to Brönsted acid sites by coke deposition during the reaction[13] In accordance with the bifunctional mechanism, at this point the formed C_2 and C_3 products (ethane/ethylene, propane/propene) cannot proceed its polymerization to bigger C-compounds.

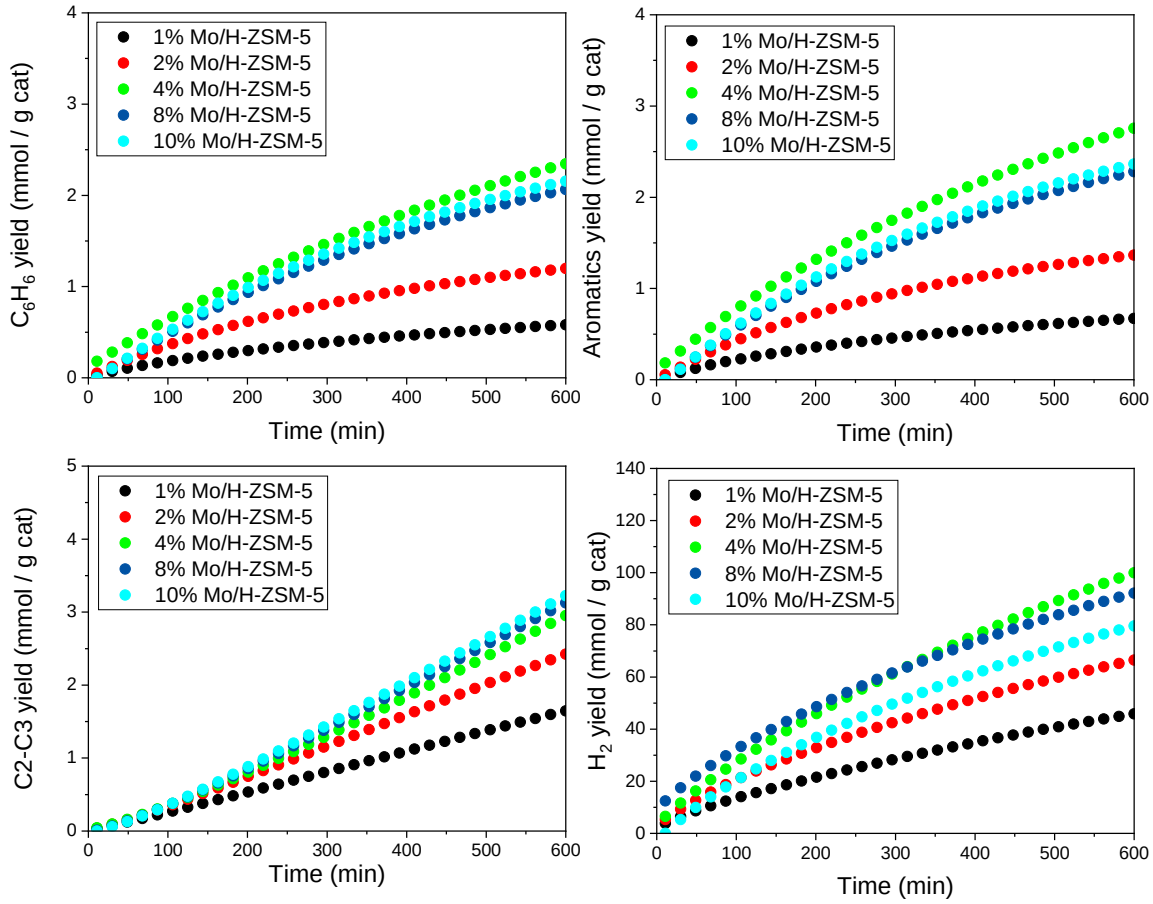

Figure 4. Product yields for different Mo/H- ZSM-5 catalysts during methane aromatization reaction.

3.2.2. Surface area measurements

The BET surface area of Mo/H-ZSM-5 systems was measured to determine the changes in the surface area of former ZSM-5 upon Mo deposition and after reaction. All catalysts showed type IV isotherms with a clear hysteresis loop, indicating the presence of micro- and mesoporosity (**Figure 5. (left)**):

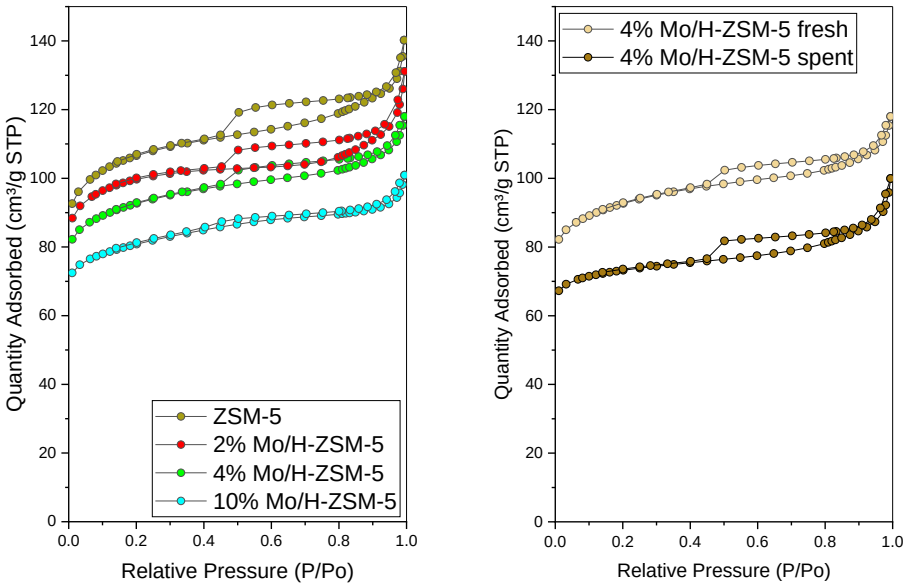

Figure 5. Adsorption-desorption isotherms for different Mo/H-ZSM-5 catalysts *(left);* Comparison of adsorption-desorption isotherms for 4%Mo/H-ZSM-5 fresh and spent catalysts *(right).*

In **Table 1** we summarize the BET surface areas of selected Mo/H-ZSM-5 systems. After Mo deposition, it can be evidenced that the hysteresis loop progressively disappeared as Mo loading increases, denoting that mesopores are highly affected by metal deposition while microporosity remains almost unaltered for low Mo content and slightly diminished for Mo loading higher than 2% (**Table 1**). Moreover, after reaction the coke deposition strongly affects to the surface area and porosity of the catalyst. Thus, for spent 4%Mo sample ca. 20 % of the total BET surface area is lost after reaction, being this diminution more drastic for mesopores. In **Figure 5** (*right*) it can be seen the noticeable modification of the adsorption-desorption isotherms as well as hysteresis feature. Thus, for spent 4 % Mo sample ca. 20 % of the total BET surface area is lost after reaction, being this diminution more drastic for mesopores which decreases at 50 % (**Table 1**). We may say that, in principle such textural collapse would be in part the responsible of the catalytic activity deactivation.

Catalyst	Surface Area (m^2/g)		Pore Volume (cm^3/g)	
	Total	Micro*	Total	Micro*
H-ZSM-5	361	267	0.20	0.12
2%Mo	336	265	0.18	0.12
4%Mo	313	236	0.17	0.11
4%Mo spent	245	207	0.14	0.10
10%Mo	272	209	0.15	0.10

*S_{micro} and V_{micro} were calculated using t-plot method.

Table 1. Textural properties of the different samples

3.2.3. X-ray diffraction

The XRD of fresh samples are shown in **Figure 6**.

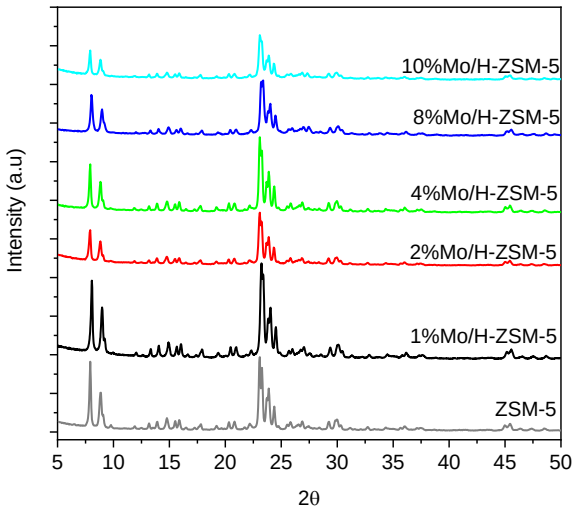

Figure 6. XRD patterns for Mo/H-ZSM-5 catalysts.

All catalysts exhibit diffraction peaks that can be ascribed to ZSM-5. Although the former diffraction patterns are preserved, the gradual reduction in the intensity of typical diffraction peaks of H-ZSM-5 with Mo loading would confirm that metal incorporation and diffusion through the zeolite pores causes indeed some losses in the crystallinity.[14] Moreover, since no evidence of MoO_x can be found it can be inferred that Mo clusters

are well dispersed on the zeolite channels even at higher loadings.[15] After reaction, catalysts suffers a great change in the surface features due to the formation of metal carbide and coke deposition. In this sense, it has been reported that remarkable deposition of coke as well as Mo species sintering and detaching from zeolite structure would be the responsible of the catalyst deactivation.[16]

3.2.4. Transmission electron microscopy

In the images obtained by TEM of fresh samples, it is difficult to distinguish the presence of Mo species, especially in 4%Mo/H-ZSM-5 (**Figure 7**). After reaction, all samples show noticeable clusters that could be ascribed to metal carbide formed during reaction.

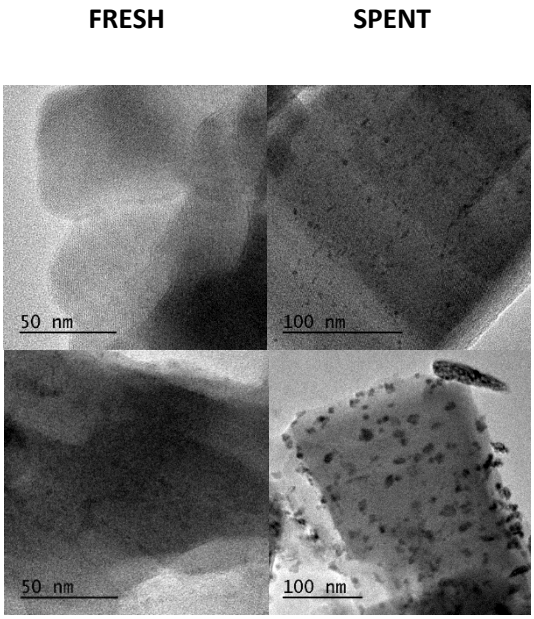

Figure 7. TEM images for 4%Mo/H-ZSM-5 *(top)* and 10%Mo/H-ZSM-5 *(bottom)* fresh and spent catalysts.

3.2.5. Thermogravimetric analysis

As pointed out before, the formation of coke that could be in principle associated to the catalyst deactivation can be studied by thermogravimetric analysis of spent carburized samples at different times. As reported in the literature, different weight loss regions can be identified in the range from 100 °C to 800 °C. By observing the DTG plots (**Figure 8** (*left*)), three weight loss steps can be clearly identified. The first weight loss below 220

°C would correspond to the physi- and chemisorbed water evolution, as corroborated from TPD experiment (**Figure 8** (*right*))**.**

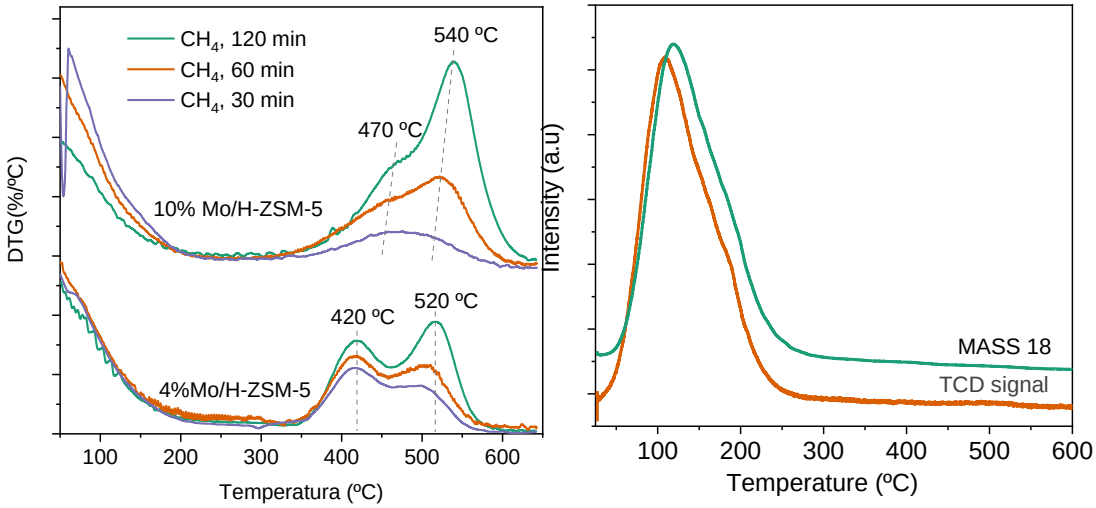

Figure 8. Thermogravimetric analysis of different 4 and 10%Mo/H-ZSM-5 catalysts after 30, 60 and 120 min reaction *(left),* TPD experiment of 4%Mo/H-ZSM-5 sample *(right).*

Above this temperature, we may expect the decomposition of metal carbide and coke. This second process occurs at temperature above 300 °C and involves two clear stages at around 450 °C and 550 °C that can be ascribed indistinctly to the elimination of coke and the decomposition of metal carbide. If we follow the evolution of the different contributions to the weight loss with the reaction time, it is evident that the process a higher temperature (ca. 530 °C) become more noticeable as reaction time increases (**Figure 8** (*left*)). Therefore, we may infer that carbide decomposition would occur at lower temperature after which coke combustion would take place.

3.2.6. Raman and UV-vis spectroscopy

It has been reported that *"bulk"* MoO_3 shows Raman bands located at 822 and 998 cm^{-1} and weaker bands around 300 cm^{-1}, corresponding to the antisymmetric stretching mode of Mo–O–Mo, the stretching mode of Mo=O, and the bending mode of Mo=O bonds in bulk MoO_3 crystallites, respectively.[17] In **Figure 9** *(left)* we show the Raman spectra for different Mo/H-ZSM-5 samples.

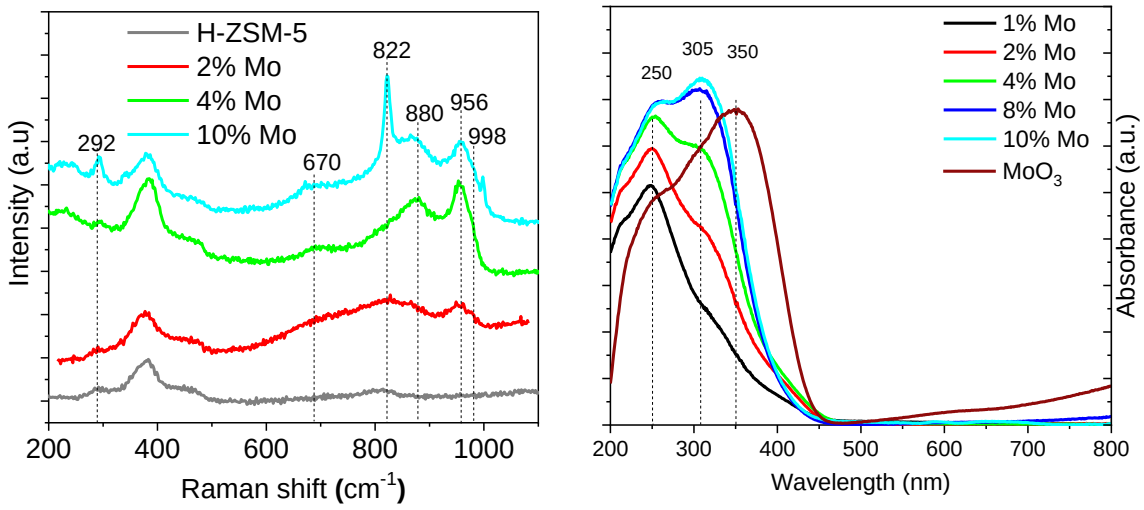

Figure 9. Raman *(left)* and diffuse reflectance UV-vis spectra *(right)* for different Mo/H-ZSM-5 catalysts.

In our case, 10%Mo/H-ZSM-5 sample exhibits the characteristics bands of MoO_3, showing intense bands at 822, 956 and a small shoulder at 998 cm^{-1}. The relative intensities of 822 and 998 cm^{-1} bands would indicate that the number of bridging Mo–O–Mo bonds are relative in higher extent than terminal Mo=O bonds. Moreover, the occurrence of 956 cm^{-1} would also denote the presence of polymeric molybdate species.[18,19] This later band is predominantly present in 2%Mo and 4%Mo/H-ZSM-5 samples, for which Mo-O-Mo stretching mode and terminal Mo=O are almost disappeared.

From Raman results, it can be assessed the existence of small clusters or oligomers of MoO_3 at lower loading levels (below 10 wt%), while observable *"bulk"* crystal phase of MoO_3 would only emerge at significantly higher loading levels (10 wt% or above).

Complementary, we have also performed the diffuse reflectance spectra of the studied samples (**Figure 9** (*right*)). For low Mo-loading catalysts, only a single ligand-to-metal charge transfer (*LMCT*) transition of the O *2p* to Mo *3d* orbital is observed at 240-300 nm, becoming more pronounced at higher molybdenum loading. Moreover, for 4%Mo and 10%Mo/H-ZSM-5 samples a *LMCT* tiny transition at around 400 nm arises,

characteristic to crystalline MoO_3 nanoparticles, indicating that crystalline MoO_3-like nanoparticles are residually present in this sample. If we observe the calculated band-gap energies for different Mo-loadings, the corresponding edge energy value (*Eg*) for the 1%Mo/H-ZSM5 is located at 4.2 eV, which unambiguously falls into the range of isolated MoO_x. However, as Mo-content arises the *Eg* value shifts toward lower energies (ca. 3.4 eV) assigned to oligomeric MoO_4-MoO_6 clusters.

3.2.7. Temperature-programmed reduction

TPR was performed on fresh catalysts in order to distinguish the different Mo species in the samples and its degree of reducibility. H_2-TPR of fresh Mo/H-ZSM-5 samples are shown in **Figure 10**.

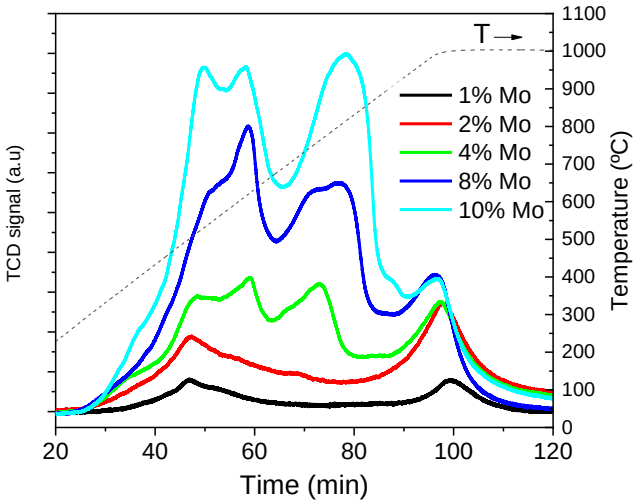

Figure 10. TPR profiles for the Mo/H-ZSM-5 catalysts.

We can see how all catalysts exhibit a similar reduction trend and two reduction processes located at around 500 - 800 °C and 1000 °C.

From the amount of H_2 consumed and assuming the complete Mo reduction at the end of the experiment, we can estimate the Mo contents for all catalysts (**Table 2**). From these values, it can be said that a good agreement is achieved between nominal and estimated ones. As example, the chemical analysis for 4%Mo sample obtained from ICP-OES gives a Mo content of 4.2 wt%, stating the correctness of the TPR estimation.

Catalyst	Consumed H_2 (µmol/g $_{cat}$)	wt% Mo
1%Mo/H-ZSM-5	0.22	0.70
2%Mo/H-ZSM-5	0.54	1.72
4%Mo/H-ZSM-5	1.09	3.48
8%Mo/H-ZSM-5	1.95	6.25
10%Mo/H- ZSM-5	2.74	8.76

Table 2. Calculated Mo content from TPR H_2 consumption (assuming complete Mo reduction).

In order to complete the information about the Mo evolution during reaction, we have performed carburization and subsequent oxidation experiments by means of CH_4-TPR + TPO for 4%Mo and 10%Mo catalysts (**Figure 11**).

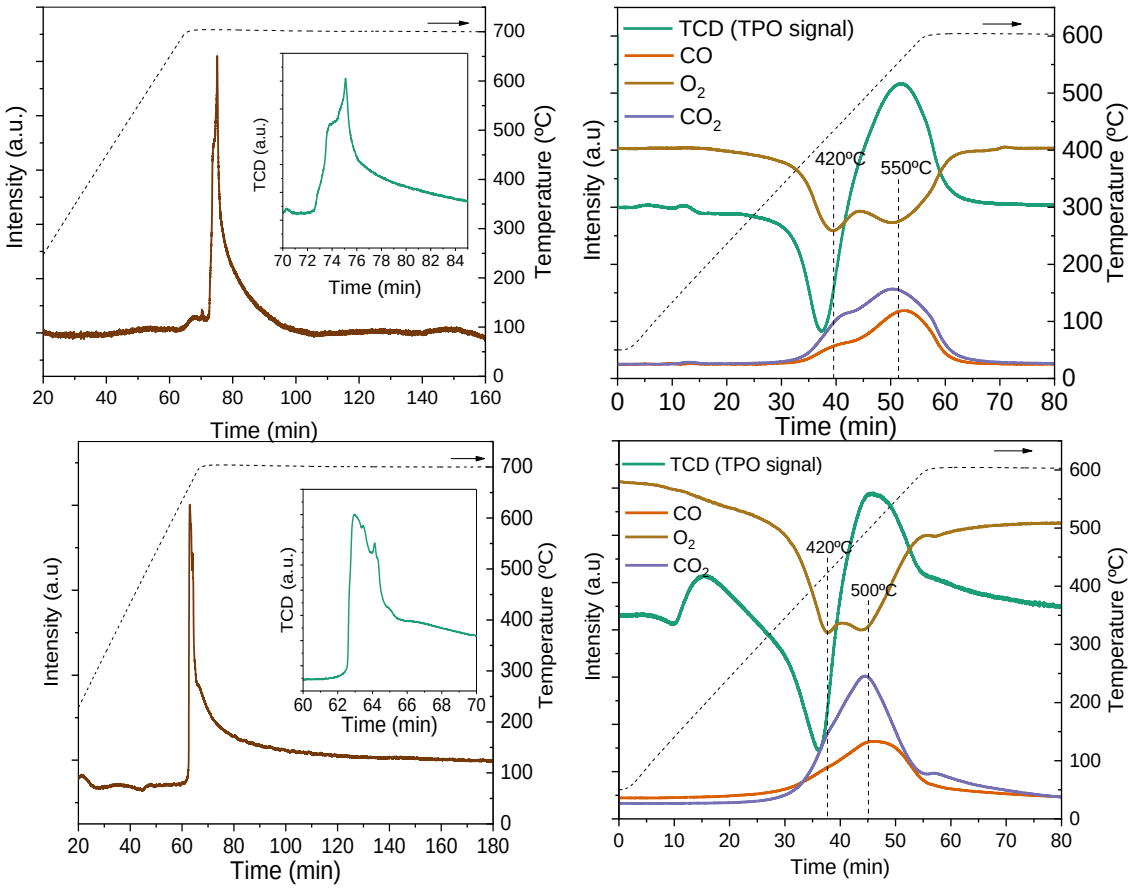

Figure 11. TPR profiles under CH_4 stream (left) and subsequent TPO profile (right) for 4%Mo (up) and 10%Mo catalysts (bottom).

By following the CH_4 consumption, it is possible to distinguish two clear processes in the proximities of 700 °C. These two processes would correspond to the metal carbide formation and the subsequent methane cracking that is taking place abruptly at this first stage of the reaction. After this sharp initial CH_4 consumption, a long tailed event which progresses along the reaction time is observed. During this second period, the CH_4 is converted into aromatics.

By observing the subsequent TPO experiment, we are also able to differentiate two clear oxidation processes at ca 420 °C and 550 °C. As O_2 is consumed, CO and CO_2 are evolved denoting the combustion of either metal carbide and deposited coke formed during reaction. This double process agrees with the previous DTG curves of spent catalyst. It is worthy to mention that first O_2 consumption is accompanied by a smaller CO-CO_2 evolution. Therefore, we may infer that this first step at 420 °C would be associated to metal carbide decomposition as well as Mo oxidation. Then, coke combustion would proceed at temperatures higher than 550 °C leading to a wide O_2 consumption curve and the simultaneous production of CO/CO_2. By comparing the profiles for 4%Mo and 10%Mo catalysts, it is possible to infer that for 4% Mo coke combustion is notably prominent and wider with respect to 10%Mo. This could be explained by considering the different reactivity of these two catalysts that would form different types of coke.

3.2.8. X-ray photoelectron spectroscopy

To complete the physico-chemical characterization of the calcined systems, a study was carried out using XPS. **Figure 12** shows the analysis of fresh samples. After *in-situ* calcination at 500 °C under O_2, Mo $3d_{5/2}$ level shows a binding energy around 233.5 eV for all samples which are assigned to Mo^{6+}.[20] From the quantification of the Mo content at the surface, we may notice that the amount of Mo appears higher with respect to the nominal values. Furthermore, it can be noticed that as Mo loading increases, surface is progressively enriched with Mo metal clusters.

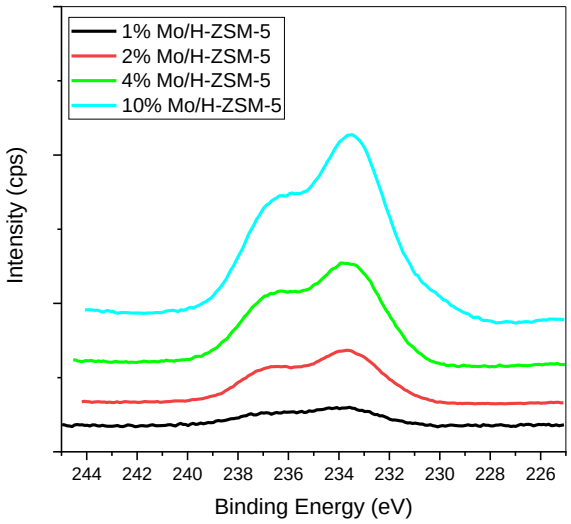

Figure 12. XPS Mo *3d* level for different Mo/H-ZSM-5 catalysts.

3.2.8.1. In-situ reduction

Thermal treatments were achieved in a cell directly attached to the XPS main chamber, allowing treatment while in contact with a mixture of gases emulating the TPR experiments. *In-situ* XPS reduction and carburization treatments have been recorded in the same XPS instrument. The evolution of Mo-sites upon reduction at different temperatures is depicted in **Figure 13**. It is worthy to note that in the case of 1%Mo and 10%Mo samples complete reduction of Mo sites takes place at higher temperature. In both samples, a mixture of oxidic and metallic Mo species can be found at 550 °C, being the oxidic fraction predominant. This could indicate that Mo species are more difficult to be reduced, probably due to different reasons in each case. Thus, for 1%Mo/H-ZSM-5 the low Mo content would favour the Mo position at inner positions in the ZSM-5 and/or with a higher interaction with the support. In the case of 10%Mo/H-ZSM-5, the occurrence of higher Mo clusters would lead to less reduction degree at this moderate temperature. In any case, it can be inferred that the whole fraction of Mo-sites is completely reduced at 700 °C.

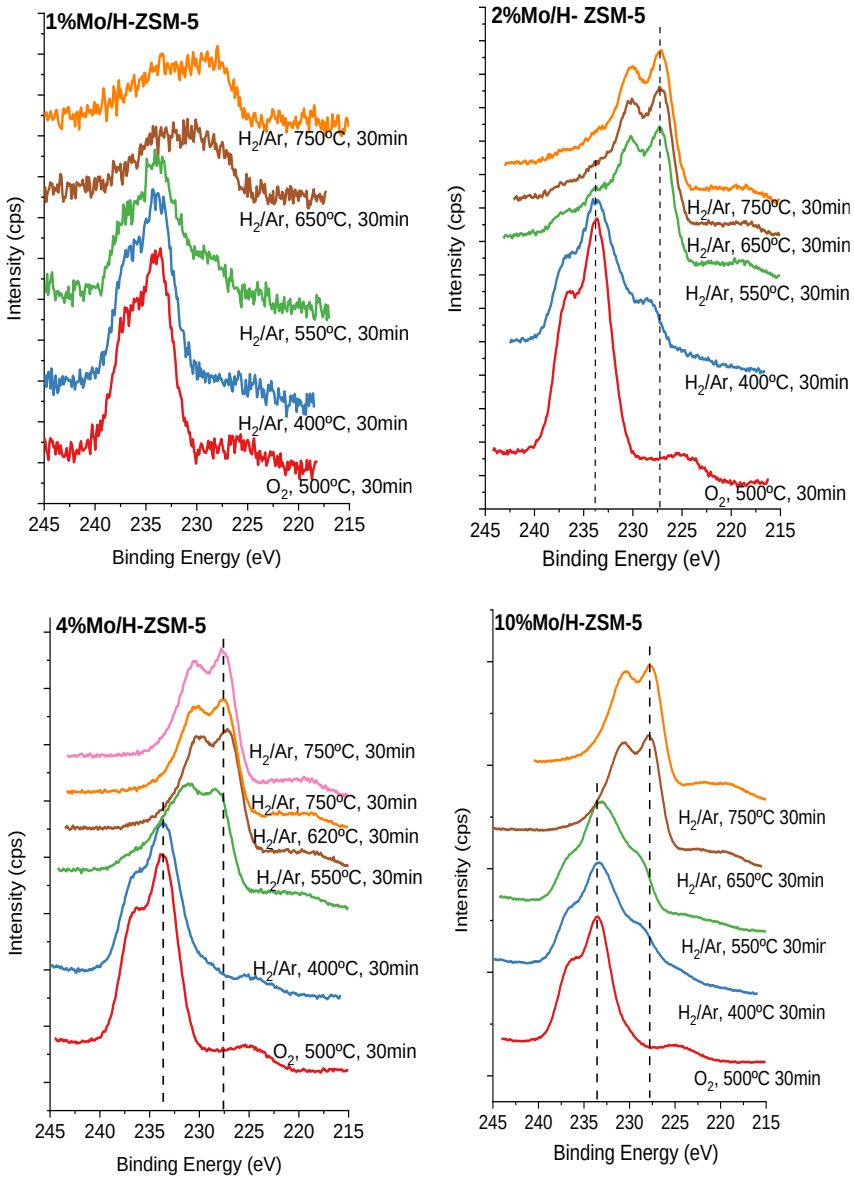

Figure 13. XPS evolution of Mo *3d* under *in-situ* reduction at different temperatures.

In all cases, the initial Mo *3d* peak at 233.5 eV assigned to Mo^{6+} shifts toward lower binding energy upon reduction at temperatures above 550 °C. The new doublet peak located at ca. 227 eV has been associated to Mo^{0}.[21]

3.2.8.2. In-situ carburization

By XPS analysis, we have also followed the evolution of molybdenum and carbon during carburization process (**Figure 14 and 15**):

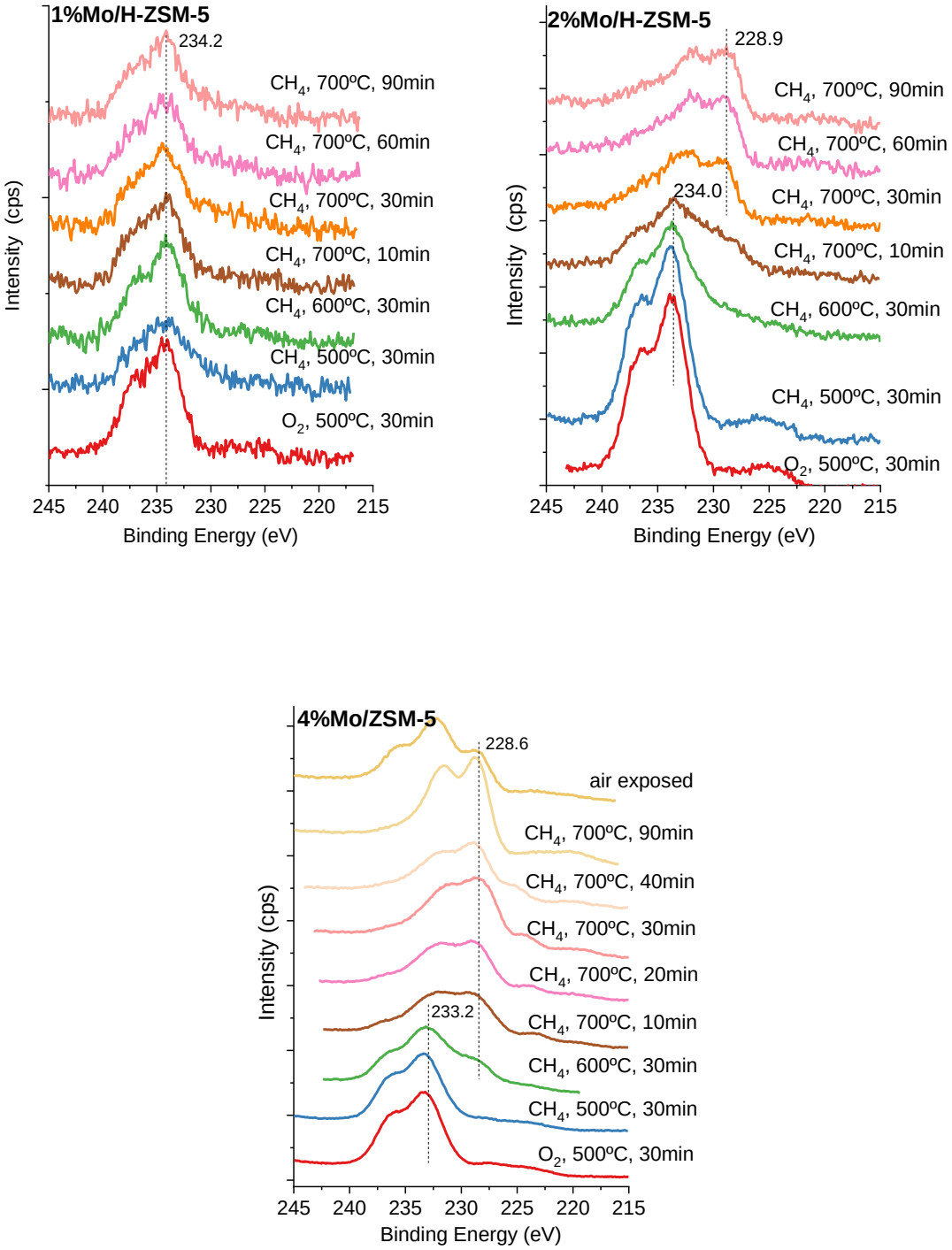

Figure 14. XPS evolution with time of *Mo 3d* under *in-situ* reaction with CH_4 at 700 °C.

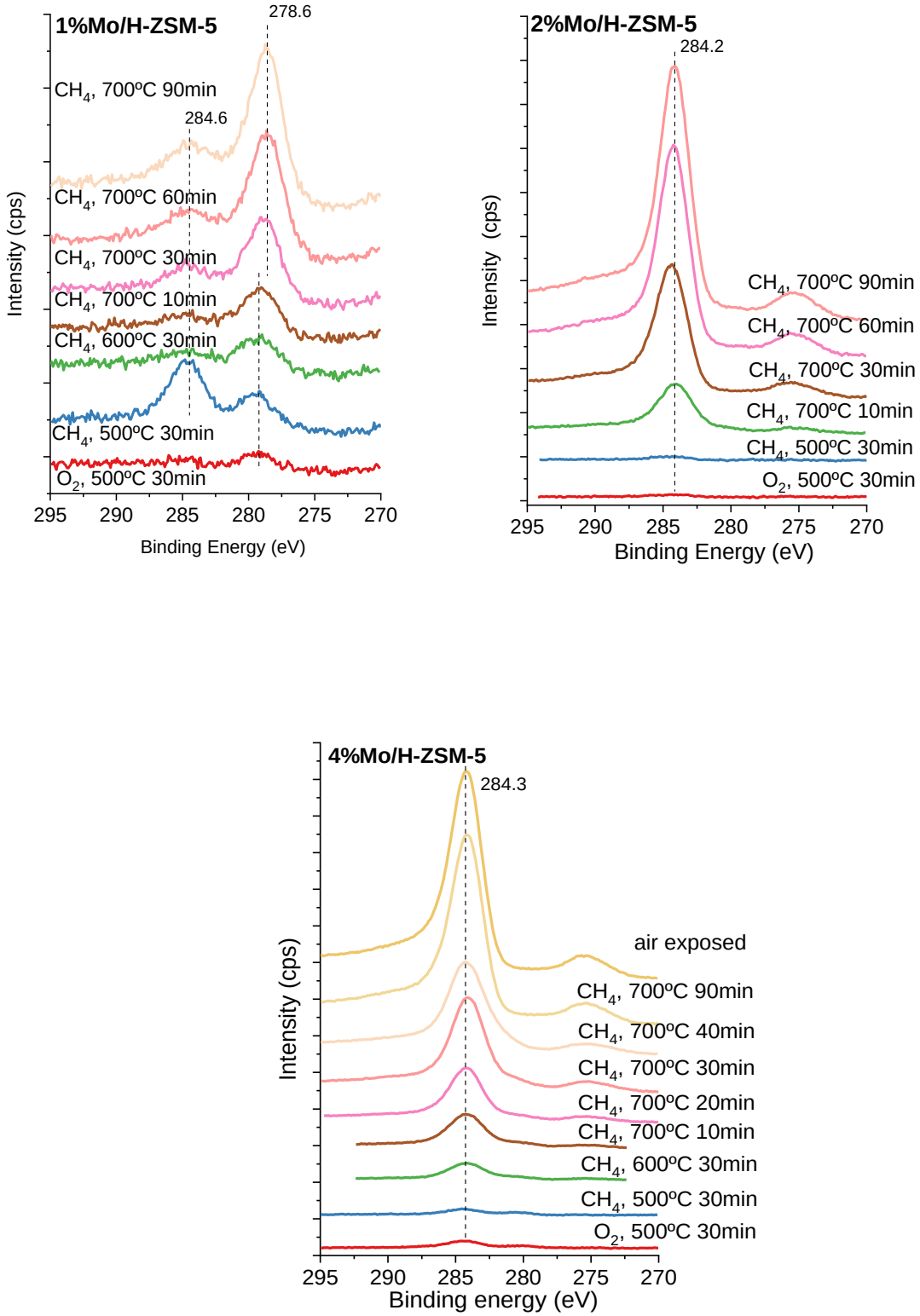

Figure 15. XPS evolution with time *C 1s* under *in-situ* reaction with CH_4 at 700 °C.

From the observation of the Mo *3d* signals, we could envisage the formation of molybdenum carbide that would be accomplished at temperature higher than 600 °C.

This is in accordance with CH_4-TPR, in which the CH_4 consumption is taking place at ca 700 °C. New XPS band at ca. 228 eV is observed for 2%Mo and 4%Mo samples. This binding energy has been assigned in the literature to Mo^{2+} in the Mo_2C.[22] It is worthy to note that for lower Mo content systems, the appearance of Mo-carbide band seems to be delayed at higher temperature. Thus, for Mo loadings higher than 4% the band assigned to carbide species located at 228 eV is present after CH_4 treatment at 600 °C.

However, the formation of Mo-carbide cannot be clearly detected from the C *1s* band. It has been reported that the carbidic carbon shows a XPS band at around 282 eV.[23] Since CH_4 cracking process and coke formation would happen close to carburization, C *1s* from carbide species would strongly overlap with the graphitic carbon peak at 284.6 eV. Nevertheless, the shift of the big C *1s* peak towards lower BE region could serve as an indication for significant Mo_2C formation. The amount of carbon after carburization treatment significantly increases, denoting the high degree of carbon deposition (**Table 4**):

Mo/H-ZSM-5	O_2 @ 500°C, 30 min				
	Mo	C	Si	Al	O
1wt%	1.39	0,06	46,81	4.03	47.71
2wt%	4.53	0.28	43.99	4.84	46.35
4wt%	9.95	1.30	41.77	5.23	41.75
Mo/H-ZSM-5	CH_4 @ 700°C, 90 min				
	Mo	C	Si	Al	O
1wt%	0.47	3.08	47.34	3.59	45.51
2wt%	1.61	25.16	37.58	3.62	32.03
4wt%	9.01	22.35	35.78	2.82	30.04

Table 4. Surface chemical composition from XPS (wt%).

The presence of an intense C *1s* peak is observed even after few minutes of carburization. The formation of carbon during this process strongly affects to the surface

features of the catalysts. As previously stated, coke deposition produces an important diminution of zeolite mesoporosity. The decrease in accessibility to the Brönsted acid sites of micropores has been reported as the responsible of the rapid deactivation of the systems.[13] Furthermore, from the quantitative analysis of carburized samples, it can be noted that the amount of surface Mo drastically decays specially for 1%Mo and 2%Mo/H-ZSM-5. This fact would be probably associated with the formation of graphitic carbon that could cover Mo sites.

3.3. Conclusions

We have prepared a series of Mo/H-ZSM-5 systems by impregnation method with different metal loadings. In all cases, Mo species present high dispersion and were not detected by XRD even at high loading. The TPR study clearly reveals the great complexity of Mo species present, especially as loading increases. Indeed, *in-situ* reduction and carburization analysis by XPS also denotes the different behaviour of catalysts by metal loading. Thus, the formation of Mo-carbide would take place at different temperatures conditioned by the metal content. This clearly points out the different nature and reactivity of metal species, denoting the great complexity of the Mo/H-ZSM-5 systems indicated in the introduction to this chapter. The optimum performance has been attained for 4% metal loading, yielding to ca. 2 $mmol_{benzene}/g_{cat}$ at the end of the reaction. We have correlated the important deactivation observed to the coke formation by means of CH_4 cracking being more pronounced for most active systems.

3.4. References

1. Spivey, J. J., Hutchings, G. Catalytic aromatization of methane. *Chem. Soc. Rev.* **43**, 792–803 (2014).

2. Jang, W. J., Shim, J. O., Kim, H. M., Yoo, S. Y., Roh, H. S. A review on dry reforming of methane in aspect of catalytic properties. *Catal. Today* **324**, 15–26 (2019).

3. Fujita, K. I. Development and application of new iridium catalysts for efficient dehydrogenative reactions of organic molecules. *Bull. Chem. Soc. Jpn.* **92**, 344–

351 (2019).

4. Galadima, A., Muraza, O. Advances in Catalyst Design for the Conversion of Methane to Aromatics: A Critical Review. *Catal. Surv. from Asia* **23**, 149–170 (2019).

5. Olson, D. H., Kokotailo, G. T., Lawton, S. L. Crystal Structure and Structure-Related Properties of ZSM-5. *J. Phys. Chem.* **85**, 2238–2243 (1981).

6. Meier, W. M., Olson, D. H., Kokotailo, G. T., Lawton, S. L. Structure of synthetic zeolite ZSM-5. *Nature* **272**, 437–438 (1978).

7. Hoff, T. C., Thilakaratne, R., Gardner, D. W., Brown, R. C., Tessonnier, J. P. Thermal Stability of Aluminum-Rich ZSM-5 Zeolites and Consequences on Aromatization Reactions. *J. Phys. Chem. C* **120**, 20103–20113 (2016).

8. Ma, D. *et al.* MAS NMR, ESR and TPD studies of Mo/HZSM-5 catalysts: Evidence for the migration of molybdenum species into the zeolitic channels. *Catal. Letters* **66**, 155–160 (2000).

9. Tan, P. L., Leung, Y. L., Lai, S. Y., Au, C. T. The effect of calcination temperature on the catalytic performance of 2 wt.% Mo/HZSM-5 in methane aromatization. *Appl. Catal. A Gen.* **228**, 115–125 (2002).

10. Jie Gao, Yiteng Zheng, Jih-Mirn Jehng, Y. T., Israel E. Wachs, S. G. P. Identification of molybdenum oxide nanostructures on zeolites for natural gas conversion. *Science.* **348**, (2015).

11. Vollmer, I. *et al.* Relevance of the Mo-precursor state in H-ZSM-5 for methane dehydroaromatization. *Catal. Sci. Technol.* **8**, 916–922 (2018).

12. Tessonnier, J. P., Louis, B., Rigolet, S., Ledoux, M. J., Pham-Huu, C. Methane dehydro-aromatization on Mo/ZSM-5: About the hidden role of Brønsted acid sites. *Appl. Catal. A Gen.* **336**, 79–88 (2008).

13. Tempelman, C. H. L., Hensen, E. J. M. On the deactivation of Mo/HZSM-5 in the methane dehydroaromatization reaction. *Appl. Catal. B Environ.* **176–177**, 731–739 (2015).

14. Hu, J. *et al.* Effect of the particle size of MoO3on the catalytic activity of Mo/ZSM-5 in methane non-oxidative aromatization. *New J. Chem.* **39**, 5459–5469 (2015).

15. S. Rajagopal, H.J. Marini, J. A. Ma., R. M. Silica-Alumina-Supported Acidic Molybdenum Catalysts- TPR and XRD Characterization. *J. Catal.* **147**, 417–428 (1994).

16. Lezcano-González, I. *et al.* Molybdenum Speciation and its Impact on Catalytic Activity during Methane Dehydroaromatization in Zeolite ZSM-5 as Revealed by Operando X-Ray Methods. *Angew. Chemie - Int. Ed.* **55**, 5215–5219 (2016).

17. Windom, B. C., Sawyer, W. G., Hahn, D. W. A raman spectroscopic study of MoS_2 and MoO_3: Applications to tribological systems. *Tribol. Lett.* **42**, 301–310 (2011).

18. Liu, B. *et al.* Methanol-to-hydrocarbons conversion over MoO_3 /H-ZSM-5 catalysts prepared *via* lower temperature calcination: a route to tailor the distribution and evolution of promoter Mo species, and their corresponding catalytic properties. *Chem. Sci.* **6**, 5152–5163 (2015).

19. Wei Li, George D. Meitzner, Richard W. Borry III, E. I. Raman and X-Ray Absorption Studies of Mo Species in Mo/H-ZSM5 Catalysts for Non-Oxidative CH_4 Reactions. *J. Catal.* **191**, 373–383 (2000).

20. Choi, J. G., Thompson, L. T. XPS study of as-prepared and reduced molybdenum oxides. *Appl. Surf. Sci.* **93**, 143–149 (1996).

21. Xia, T., Li, Q., Liu, X., Meng, J., Cao, X. Morphology-controllable synthesis and characterization of single-crystal molybdenum trioxide. *J. Phys. Chem. B* **110**, 2006–2012 (2006).

22. Oshikawa, K., Nagai, M., Omi, S. Characterization of molybdenum carbides for methane reforming by TPR, XRD, and XPS. *J. Phys. Chem. B* **105**, 9124–9131 (2001).

23. Mir, R. A., Sharma, P., Pandey, O. P. Thermal and structural studies of carbon coated Mo_2C synthesized via in-situ single step reduction-carburization. *Sci. Rep.* **7**, 1–12 (2017).

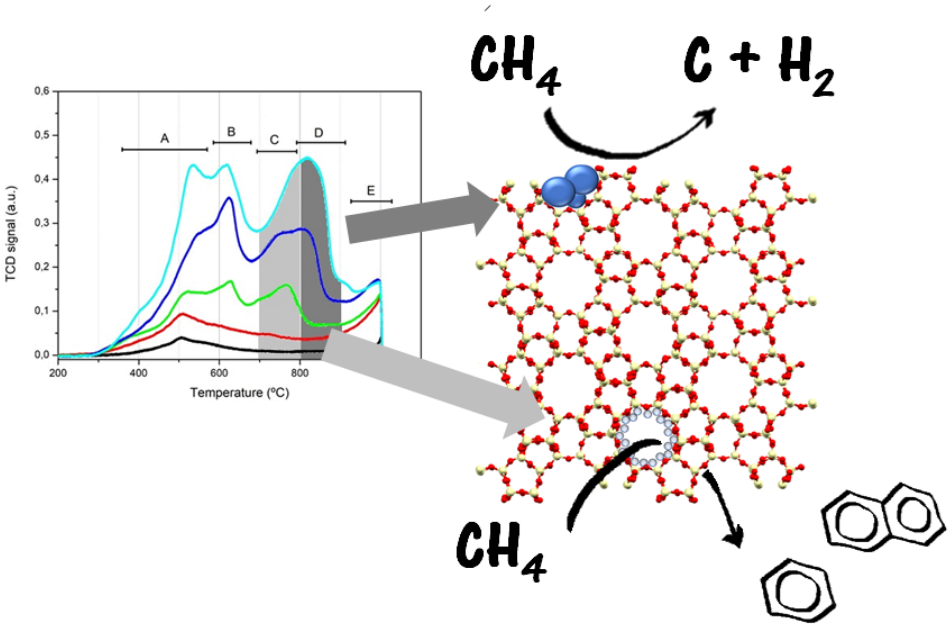

Chapter 4. Acid treatment of Mo/ZSM-5 catalysts: Study of the Mo phases and the performance in the MDA reaction.

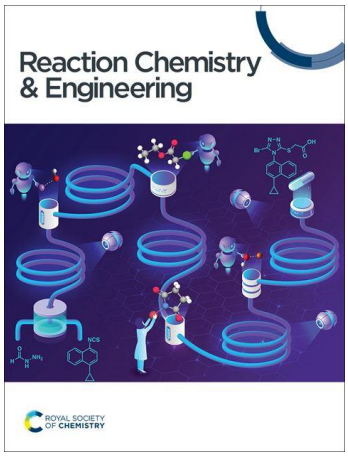

Á. López-Martín, F. Platero, G. Colón, A. Caballero

"*Elucidating the nature of Mo species on ZSM-5 and its role in the methane aromatization reaction*"

Reaction Chemistry & Engineering, 6, 1265-1276, 2021

In this chapter some of the catalysts that have been previously described above have been subjected to a post- synthesis treatment with sulfuric acid. With the combination of chemical (TPR), spectroscopic (XPS), HAADF and other techniques have allowed us to identify the different Mo precursors stabilized in the calcined ZSM-5 support, their nature (monomers, dimers and bulk Mo oxides), location in the zeolite framework (external surface or micropores), and the partial segregation of aluminum during the preparation of catalysts. The role of each Mo phase promoting or hindering the transformation of methane in aromatics has been also clarified.

4.1. Introduction.

As above anticipating, many of reported previous studies have been devoted to the mechanism of the *MDA* reaction. All of them discussed about the role of different factors such as the preparation method, the catalyst pretreatment, the loading and dispersion of metal active site or the acidity of the zeolite support.[1–7] These variables seem to determine important features such as the dispersion of molybdenum precursors, its location in the internal microporous structure of zeolite or the external surface, and/or the geometry of these precursors.[8–12]

There is a general consensus that under reaction conditions, typically pure methane at a temperature around 700 °C, the Mo(VI)-oxo centers are reduced or carburized generating a metal carbide phase, which is accepted as the active phase.[13,14] Thus, all these issues are essential to establish the role played by each specific phase in the *MDA* reaction, from highly active phases to merely inactive or spectator phases, or even phases that could hinder the catalytic performance of the system. In this sense, the role of these aspects concerning the nature and amount of coke, that would block the zeolite micropores and the access to the active phase, turns crucial and determines the *MDA* reaction mechanism.[11,12,15–21] As mentioned above, there is a general agreement that the more important molybdenum phase is a highly dispersed one, located inside the micropores of the zeolite, which under reaction conditions generates small molybdenum (oxy)-carbide entities. However, active phases for methane aromatization as well as the reaction mechanism have not yet been completely understood. Several of them have been proposed in the literature and was previously described in **Chapter 1.**[22]

This chapter delves deeper into the understanding of the catalytic series described in the previous section. We already discussed in **Chapter 3 on** how the catalytic performance decreased when the Mo load was higher than 4%. In addition, mesopores were affected and the presence of MoO_3 bulk phases were observed at metallic loading up to 10 wt%. On this basis, it is not strange to think that removing this excess of molybdenum could have some effect on the *MDA* reaction. To eliminate these Mo phases that hinder the aromatization we submit the catalyst to acid treatment in order

to leach as possible the non-active Mo species. Thus, for this sake we used two different concentrations of sulfuric acid and applied them to 10%Mo/H-ZSM-5. The two new catalysts obtained were fully characterized and their catalytic performance was measured to compare them with the rest of the catalysts of this series. To obtain a better understanding of our systems and observe the changes caused by the acid treatment some HAADF-STEM studies have been carried out. Like this, the partial and selective elimination of the phases, together with the new results obtained by HAADF, and the XPS and TPR results described extensively in the previous chapter, have allowed us to identify the nature of the stabilized Mo phases in the calcined catalyst, their location in ZSM-5, as well as the role of each phase, either promoting or hindering the methane aromatization reaction.

4.2. Catalysts characterization and performance

The **Figure 1** depicts the TPR profiles obtained for the original samples (2, 4 and 10%Mo/H-ZSM-5). Thus, as the metal loading increases, it can be noticed the formation of different molybdenum oxides species reducing at different temperatures. In order to discuss in detail, we have named the observed TPR reduction peaks from *A* to *E* (**Figure 1**). As we mentioned in **Chapter 3**, essentially two main reduction processes are present in the low loaded catalyst (2%Mo), whose maximum temperature peaks are around 510 °C and 1000 °C, denoted as processes *A* and *E*, respectively.

Besides these main reduction processes, minor amounts of Mo reducing at temperatures between these two main reduction processes can be also observed This fact clearly evidences the high heterogeneity of the chemical states of molybdenum supported on zeolite. These new intermediate reducing processes much more clearly appear in the higher Mo loading samples. Thus, the 4%Mo sample shows at least two additional reducing processes peaked at 615 °C and 755 °C (*B* and *C in* **Figure 1**), while the catalyst with the higher Mo loading (10%Mo) presents another new reducing peak around 825 °C (process *D* in **Figure 1**).

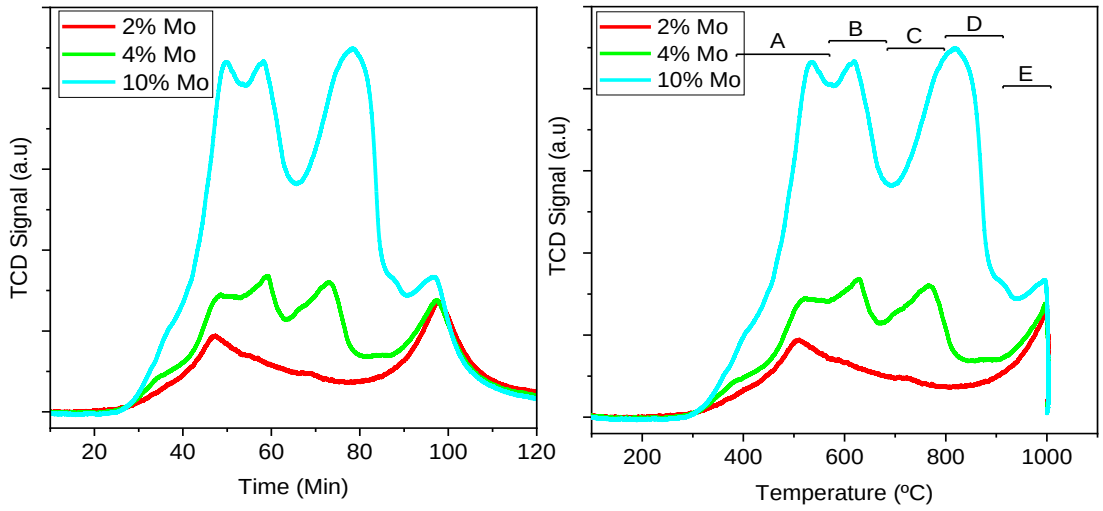

Figure 1. TPR profiles of Mo/H-ZSM-5 catalysts up to 1000 °C.

These new reducing processes are better appreciated in the next figure in which we represent the difference profile for 4%Mo and 10%Mo catalysts.

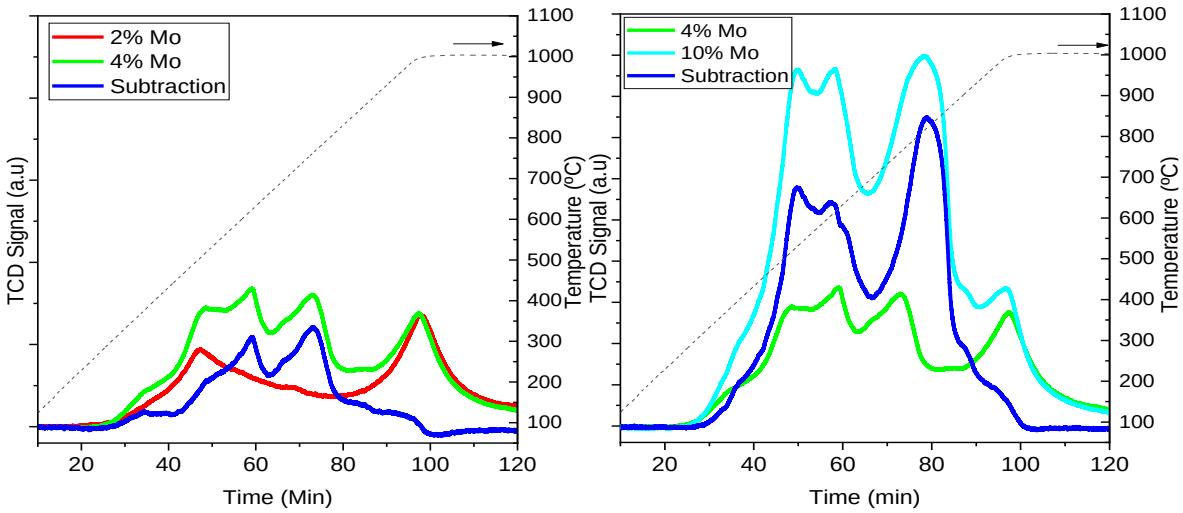

Figure 2. Profiles obtained by subtraction of TPRs of Mo/H-ZSM-5 catalysts.

In these graphs, the profiles obtained by subtracting the different TPRs clearly show the formation of these new Mo species by increasing the Mo loading of the catalysts.
Therefore, as a summary, in a rough approximation at least 5 different molybdenum reducing processes can be detected in the Mo/H-ZSM-5 catalysts, which gradually appear when the Mo loading in the zeolite increases from 2% to 10%.

That said, it is important to point out that these reduction processes can come from different Mo species present in the catalysts, as well as from different stages of reduction from the original Mo^{6+} to Mo^{0}. Moreover, as stated above, these identified peaks, as five main reduction processes, are accompanied with other minority processes reducing at intermediate temperatures. This is a clear indication of the great chemical complexity of these catalytic systems. Taking into account this circumstance, we have decided not to proceed with a deconvolution analysis of the TPR profiles, and just made a qualitative study of these five main processes.

The study of the catalytic performance of these catalysts in the methane aromatization to benzene was shown in the previous chapter. We observed that the maximum activity is reached for the 4% Mo/H-ZSM-5 catalyst (**Figure 3**). Specifically, as referenced in **Table 1**, after 5 hours in stream the figures for the 4%Mo/H-ZSM-5 catalyst show 7.6 % total conversion and 71.7 % of selectivity to aromatics, being significantly lower for the other samples, which drop down when the Mo loading deviates from 4 wt%.

Catalyst	H_2 Consumed (µmol/mg)	Wt. % Mo	Methane conversion (%)	Aromaticsselectivity (%)	BET area ($m^2.g^{-1}$)	Mo reduction processes
ZSM-5	--	--	1.3	0.0	361	--
2% Mo	0.54	1.7	3.4	59.2	336	A+E
4% Mo	1.09	3.5	7.6	71.7	313	A+B+C+E
10% Mo	2.74	8.8	4.6	66.4	272	A+B+C+D+E
10% Mo H_2SO_4 0.1M	1.71	5.5	6.9	71.0	272	A*+*B+C+*D+E
10% Mo H_2SO_4 0.5M	1.40	4.5	4.5	65.8	274	A*+B*+C*+D*+E

Table 1. Mo content (from TPR, assuming complete Mo reduction), methane conversion and aromatics selectivity after 5 hours in stream, BET and detected Mo species. (**species partially or totally eliminated*)

Thus, in a first and quick assessment, the correlation of the catalytic performances with the reducing processes depicted in **Figure 1** would indicate that one or both of the new reduction processes appearing in the 4%Mo system, identified as *B* and *C*, could be related with the higher performance for the aromatization of methane. On the contrary, the process *D*, appearing in the 10%Mo catalyst would have a detrimental effect for the *MDA* reaction.

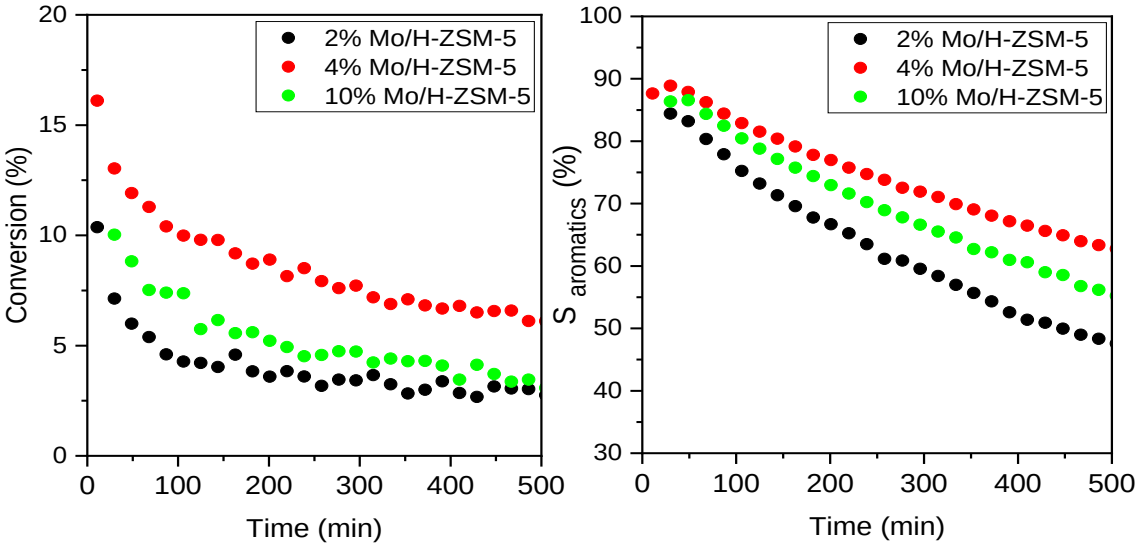

Figure 3. Conversion of methane and aromatics selectivity of Mo/H-ZSM-5 catalysts.

In order to delve into the origin of these different Mo reducing processes and their role in the catalytic performance, the high loaded 10%Mo/H-ZSM-5 catalyst was subjected to two different acid treatments. It is known that these treatments partially leach the Mo precursors from the surface of the ZSM-5 support, especially those with the weaker interaction with support.[23]

After these acid treatments, the samples were washed with water until neutral pH and no noticeable changes in the acidity of the zeolite support have been observed in these acid-treated catalysts. Thus, after a soft treatment with sulfuric acid 0.1 M we obtain the TPR outlined in **Figure 4** (*left panel*). We include also the former TPR of 10%Mo/H-ZSM-5 sample as well as the line obtained by subtracting both TPRs. The evaluation of the hydrogen consumption during the TPRs demonstrates that about 38 % of Mo species have been eliminated by this soft acid treatment, resulting now in a catalyst with a nominal loading of 5.5 % Mo (**Table 1**).

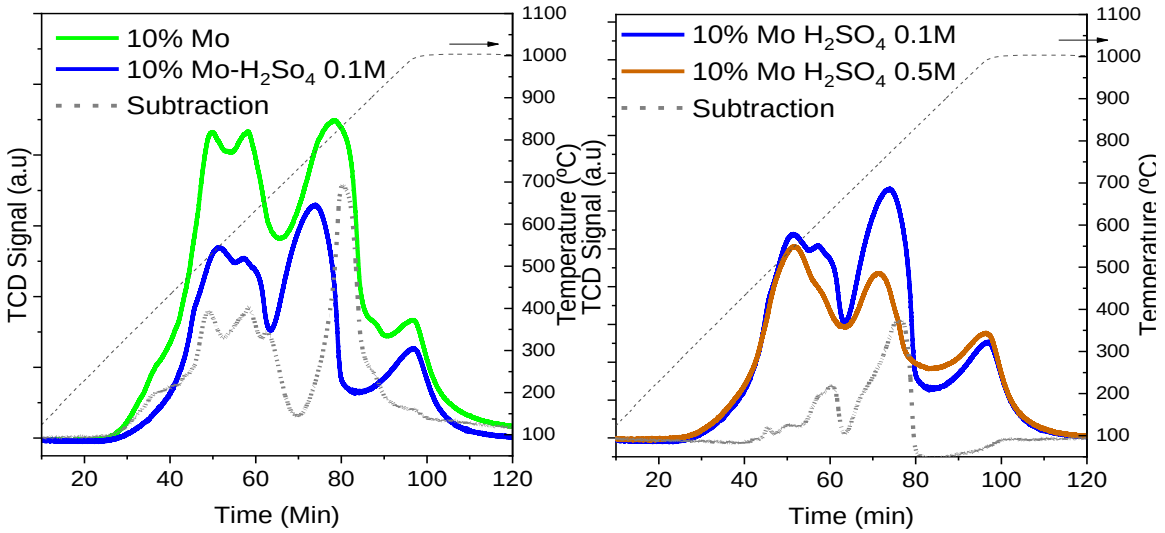

Figure 4. TPR profiles of 10%Mo/H-ZSM-5catalysts before and after H_2SO_4 acid treatments.

By analyzing the profile obtained by subtracting both TPR lines (*left panel* in **Figure 4**), it is clear that the species eliminated by this soft acid treatment are mainly those reducing

in the interval 350-700 °C (*A* and *B*) and between 800 and 900 °C (*D*). However, the species *C* and *E* are not severely affected by this treatment. On the other hand, the stronger acid treatment with sulfuric acid 0.5 M induces a drastic modification of the TPR profile (*right panel in* **Figure 4**). It can be noticed an important diminution of the reduction process centered at 750 °C (mainly the *C* species) and to a less extent the *B*-named process (peak at ca. 600 °C). Moreover, it is worthy to note that according to the total amount of hydrogen consumed in this TPR, the nominal Mo loading is only slightly affected with respect to the catalyst submitted to soft acid treatment, now being 4.5 wt% Mo (**Table 1**).

This selective extraction of Mo species is especially relevant in view of the catalytic activities measured for both treated catalysts. As shown in **Figure 5**, the 10%Mo/H-ZSM-5 catalyst after the soft acid treatment improved the activity and selectivity to aromatics, now close to that of original 4%Mo sample. On the contrary, the hard acid treatment with 0.5 M sulfuric acid leads to a system with a very poor catalytic performance, both in terms of activity and selectivity, in spite of the similar Mo content as the 4%Mo catalyst (**Table 1**).

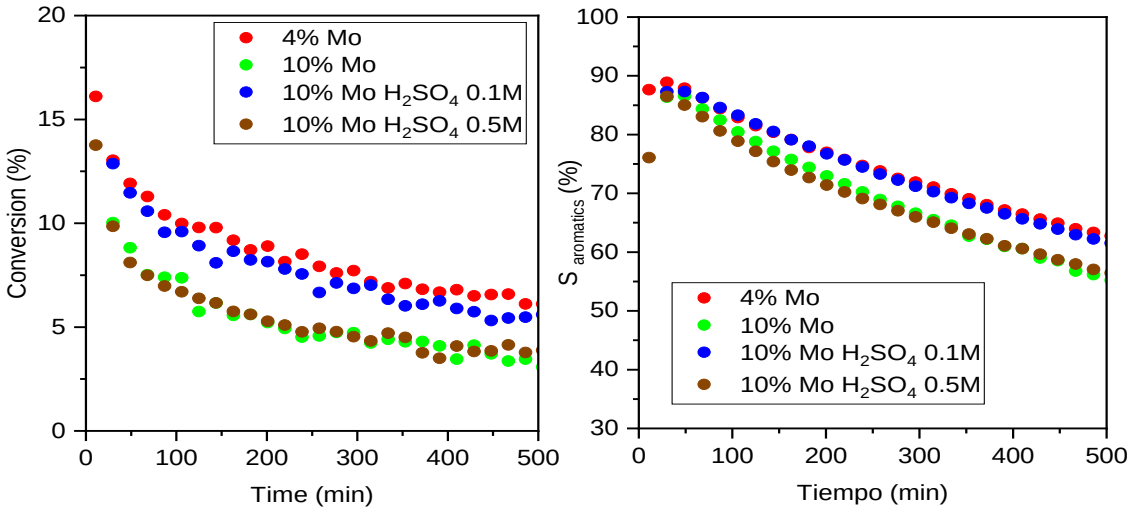

Figure 5. Conversion of methane and selectivity to benzene of 10%Mo/H-ZSM-5before and after acid treatment. Values of 4%Mo catalyst are also included for comparison.

4.3. Identifying and correlating Mo species with catalytic performances

From these results, it is evident that several Mo species coexist in the catalysts, playing different roles in the catalytic performance. But first, although we must consider the possibility that some of the reduction processes identified in **Figure 1** could correspond to the reduction of molybdenum to intermediate species (V, IV and/or II), a first set of interesting conclusions can be yielded from these results.

Thus, it can be assumed that the reduction processes *A* and *E*, the two appearing in the 2%Mo/H-ZSM-5 catalyst, would correspond to different Mo species, given that only *A* is eliminated from the zeolite support by the soft acid treatment.

Along with *A*, the *D* reduction process, which only appears in the 10%Mo sample, is also eliminated by this soft acid treatment. Therefore, it can also be assigned to a different Mo phase. Regarding the two remaining processes, *B* and *C*, they are also selectively extracted by respectively, the soft (*B*) and hard (*C*) acid treatment, also indicating that they should correspond to different Mo phases. Indeed, the absence of *C* species is one of the significant differences when compared the acid treated catalysts with the former 4%Mo sample, negatively affecting the catalytic performance of this acid treated 10%Mo.

In summary, these results even without being conclusive, seem to indicate the coexistence of up to 5 different Mo phases in the calcined Mo/H-ZSM5 catalytic system as a function of the metal loading. Moreover, these results suggest that the so named phase *C* clearly improves the catalytic performance of the Mo/H-ZSM-5 catalysts, while phase *D* seems to hinder the transformation process of methane in aromatics.

4.4. Locating the position of Mo in/on the zeolite support

A fundamental point in the characterization of these systems is to clarify where the metal entities are located, specifically on the external surface and/or the internal mesopores of the zeolite. For this, we have paid attention to the *in-situ* XPS study of the

reduction process of the 2, 4 and 10%Mo/H-ZSM-5 catalytic systems. Specifically, we have focused on the results obtained after hydrogen treatments at 650 °C. The Mo *3d* regions spectra obtained after calcination and reduction treatments, depicted in **Figure 6**, show Mo^{6+} as the only oxidation state present after the calcination treatment. In the same way the reduction treatment at 650 °C almost completely reduced the metal to Mo^{0}.

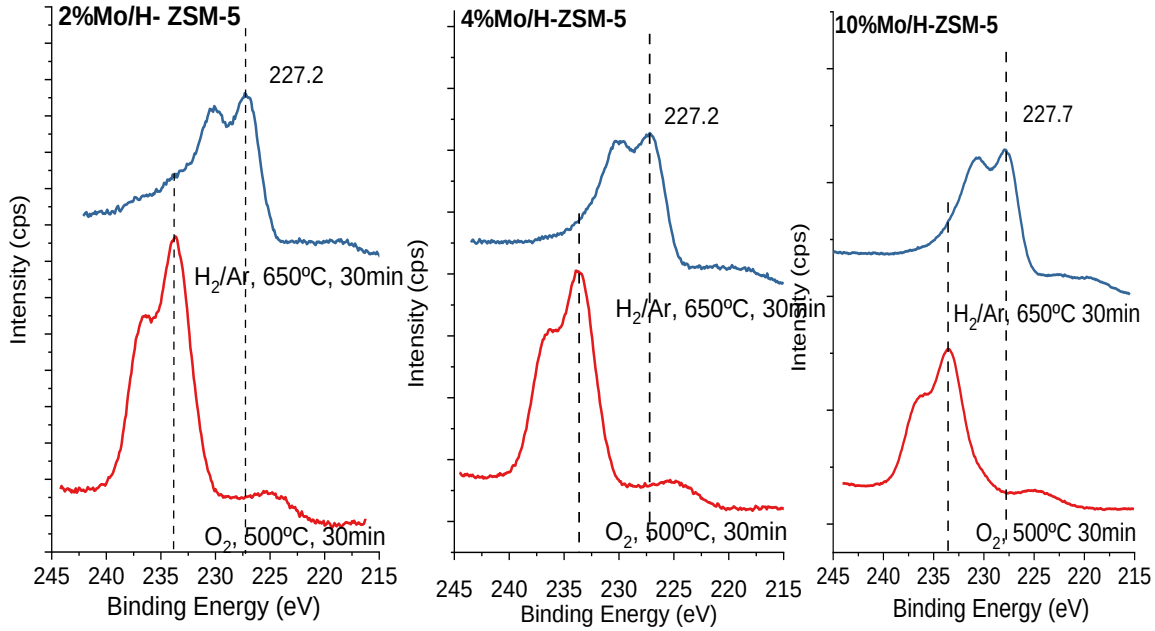

Figure 6. Mo *3d* region XPS spectra of Mo/H-ZSM-5catalysts calcined and after *in-situ* reduction.

In particular, the spectrum of the 2%Mo/H-ZSM-5 shows two contributions after the reduction treatment. A main peak centered at 227.2 eV, accounting for 79 % of total intensity and corresponding to Mo^{0} species, and a minor peak (17 % of total intensity) at 233.6 eV, the same position of the original Mo^{6+} species. Also, the remaining 4 % of intensity can be fitted with a small contribution Mo(IV). These results are quite interesting when compared and contrasted to the TPR in **Figure 1**. Taken in account that the reduction is kinetically driven,[24] from this profile it can be deduced that *A* species must be completely reduced at 650 °C, while the *E* species should remain oxidized. Even more, from the TPR the relative amount of *A*/*E* seems to be around 50/50, while the XPS

result shows a very different proportion, with the peak of the metallic molybdenum being more much intense. Thus, two important conclusions can be extracted. First of all, *A* and *E* are effectively two different Mo species, with *A* completely reduced at 650 °C while E remains oxidized. Secondly, taking into account that XPS is a surface sensitive technique, the very low intensity of *E* can be explained accepting that it is mainly located inside the microporous structure of zeolite and consequently, mostly invisible by this technique. This result is especially relevant as is generally assumed that at low metal loadings, all the molybdenum species are located in the microporous structure of zeolite.[6] The possibility that *E* is agglomerated, thus giving a low intensity peak in XPS can be discarded, as it will be shown later.[25]

Some additional conclusions can be also extracted from the XPS spectra of 4%Mo and 10%Mo/H-ZSM-5 catalysts. In both cases, the Mo appears completely reduced after the treatment in hydrogen at 650 °C. However, from the TPR profiles of **Figure 1** only species *A* and *B* must be effectively reduced, while *C*, *D* and *E* species should remain oxidized at this reduction temperature.

Once again, these results seem to prove that also the TPR peak assigned to *B* species should correspond to a different Mo phase that is reduced to Mo^0 at 650 °C, a phase that must be located on the external surface of the zeolite and detectable by XPS. Accordingly, the rest of species (*C* and *D*) which remain oxidized and undetected by XPS, should be located inside the micropores of the zeolite and/or agglomerated forming large particles. For this reason, it was decided to carry out the HAADF-STEM measurements shown below.

4.5. Visualizing the Mo particles: HAADF-STEM studies

To further characterize these Mo species, a HAADF-STEM and elemental analysis study has been accomplished. According to the images of 2%Mo/H-ZSM-5 presented in **Figure 7**, no individual metallic particles can be visualized, suggesting that Mo species are extremely well dispersed and distributed throughout the zeolite particles. The images also show that Mo species have the same distribution pattern as Al and Si. Thus, it can be concluded that both Mo phases *A*/*E* observed in the 2%Mo/H-ZSM-5 TPR profile of **Figure 1** are homogeneously distributed throughout the zeolite support and indistinguishable by TEM. Additionally, this result allows us to discard that the low intensity of XPS peak corresponding to the oxidized phase *E* is not due to the agglomeration of this phase in large particles (**Figure 6**), confirming that it must be located inside the micropores of the zeolite.

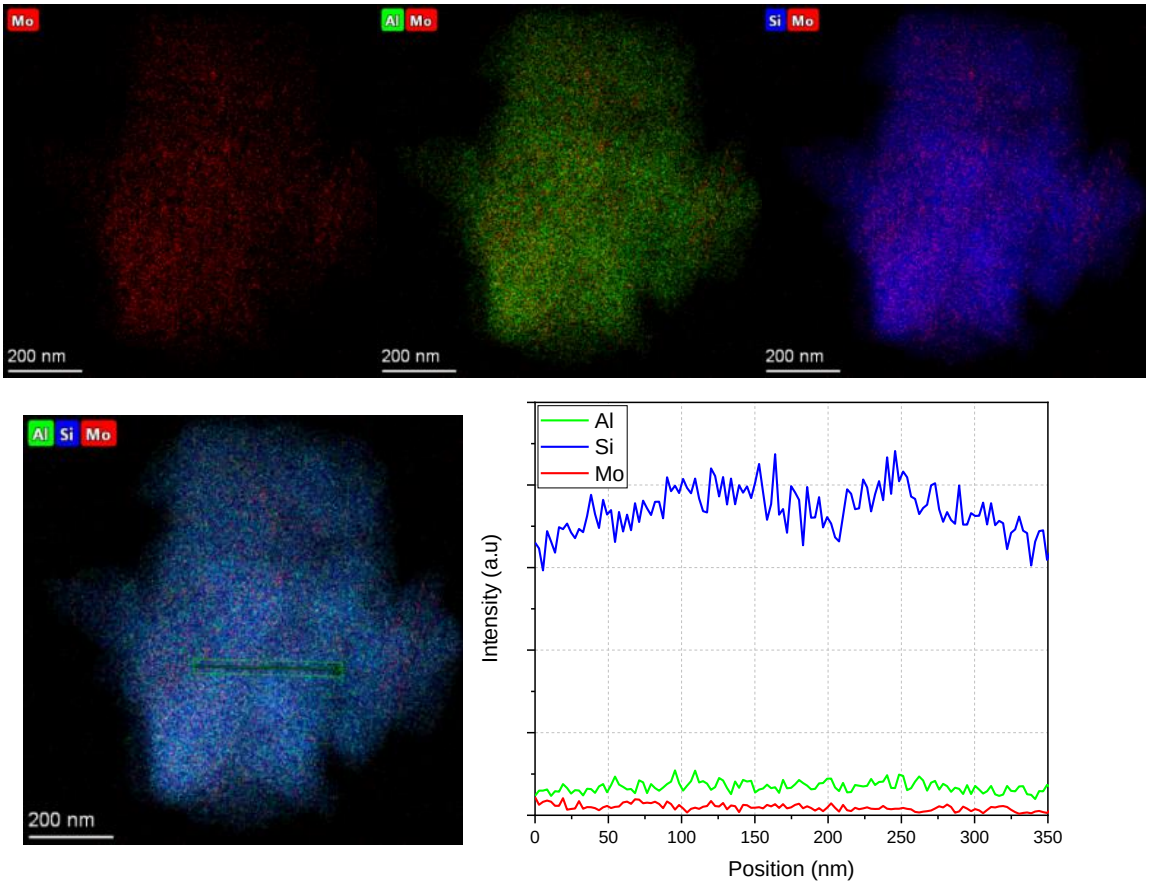

Figure 7. HAADF-STEM images of the 2%Mo/H-ZSM-5catalyst. Composition profile of the signaled line is also included.

In contrast, the images obtained for the 4%Mo/H-ZSM-5 sample (**Figure 8**) allow us to visually identify at least two different Mo phases. Thus, in addition to the homogeneously distributed Mo species (**Figure 8**, *upper panel),* it is detected the presence of larger Mo particles associated with Al-enriched areas of the zeolite support. (**Figure 8,** *bottom panel*) According to the dark field image it seems that such particles would be located on the external surface of the zeolite particles. This is especially relevant since neither the 2%Mo/H-ZSM-5 catalyst nor the original zeolite submitted to the same preparation treatment but without the addition of Molybdenum present any inhomogeneity in the Si/Al distribution (**Figures 8** and **9**).

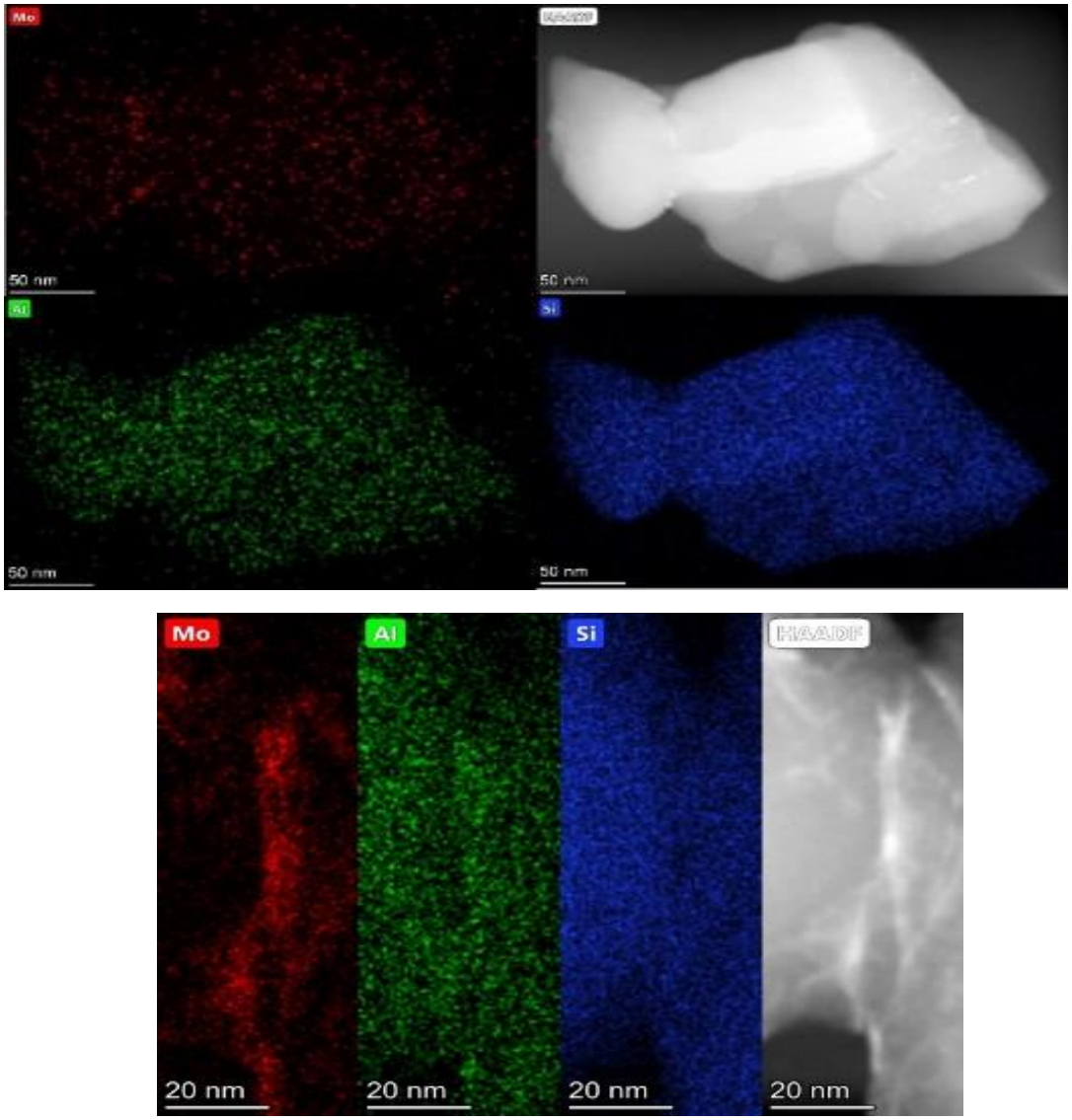

Figure 8. HAADF-STEM images of the 4%Mo/H-ZSM-5catalyst.

This result indicates that some Al have been partially segregated from the ZSM-5 network during the preparation method (impregnation and calcination). Thus, as previously discussed, this phase located on the external surface of zeolite can be associated with the *B* phase.

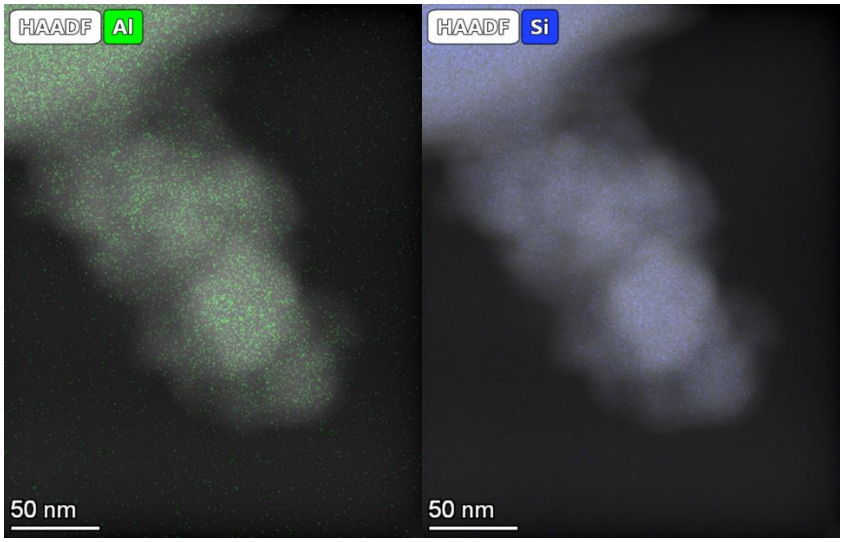

Figure 9. HAADF-STEM images of the ZSM-5 support.

Finally, the images in **Figure 10** corresponding to the 10%Mo/H-ZSM-5 sample show, together with the previous ones, the presence of a new phase consisting in large molybdenum particles (around 100 nm in diameter) clearly associated to aluminum. The composition profiles, also included in **Figure 10**, unambiguously confirms the formation of a Mo/Al_2O_3 phase, where Si cannot be detected. As it has been also incipiently observed in the 4%Mo/H-ZSM-5 catalyst, its formation seems to be due to some type of chemical etching of aluminum during the calcination treatment of the catalyst, maybe through the formation of a surface aluminum molybdate phase. In fact, the segregation of Al from zeolites induced by Mo has been previously observed by other authors, and identified as a $Al_2(MoO_4)_3$ phase which is assumed to be inactive for this reaction.[26,27] This etching process seems to be favored as the amount of Mo increases.

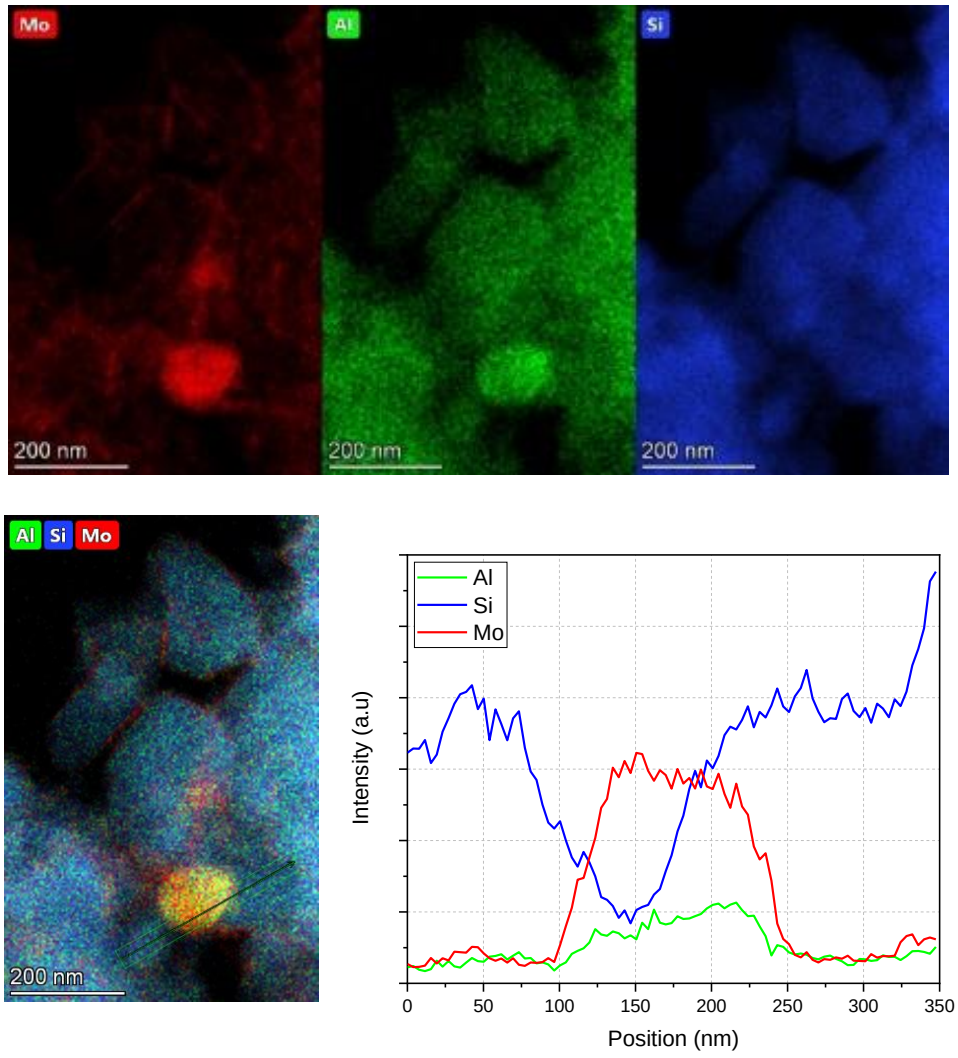

Figure 10. HAADF-STEM images of the 10% Mo/H-ZSM-5 catalyst. Composition profiles of the signaled round particle are also included.

In order to confirm the formation of a Mo/Alumina phase, we have used the same methodology to prepare a model 4%Mo/Al_2O_3 catalyst. The TPR profile of this sample, included as **Figure 11** shows a main peak centered between 800 and 900 °C, the same range as the phase *D*. Also, this catalyst does show no activity in the *MDA* reaction. Both features support the assumption that a Mo/Alumina phase is effectively formed in the 10%Mo/H-ZSM-5 catalyst.

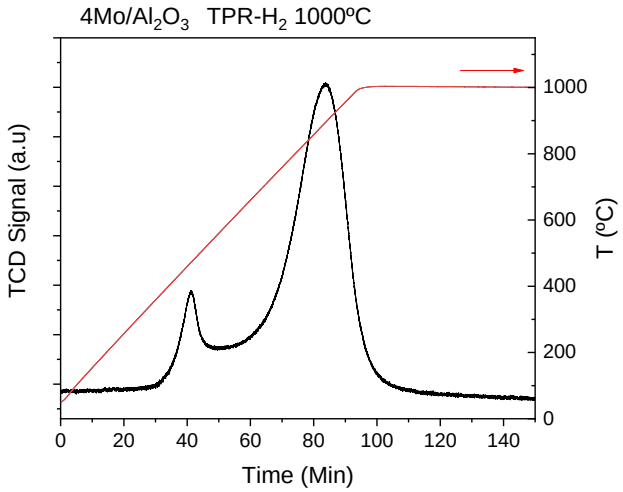

Figure 11. TPR profile of a 4%Mo/Al_2O_3 catalyst.

Therefore, all these findings strongly support that the new Mo/Alumina phase can be associated to the *D* peak detected in the TPR profile of the 10%Mo/H-ZSM-5 catalyst.

As a conclusion, by STEM/HAADF analysis we have identified different molybdenum phases, which seems to correspond to the previous *A*/*E*, *B*/*C* and *D* phases. Between them, phases *A*, *C* and *E* are undistinguishable by TEM, while phases *B* and *D* appear associated to aluminum, relatively dispersed in the case of *B* and as large particles in the case of *D*. As shown in a previous work, it is important to point out that no molybdenum phase can be detected by XRD in any of the catalysts, showing only peaks coming from the zeolite.[28] This can be clearly seen in **Figure 12**, where the three catalytic systems present similar profiles, showing basically the same XRD pattern, with no major changes from the zeolite support.

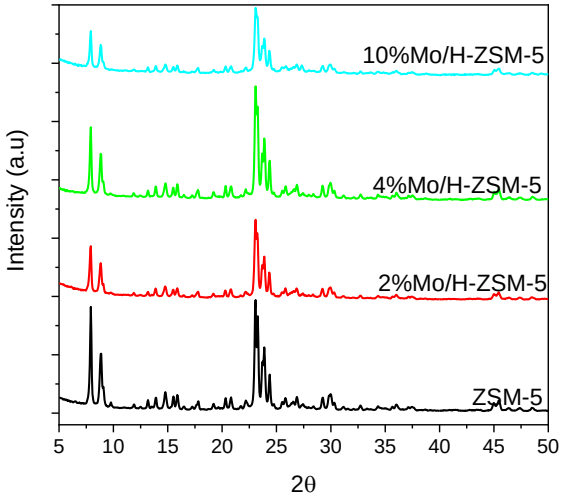

Figure 12. XRD patterns for ZSM-5 systems

4.6. Raman characterization

A further approximation on the nature of these molybdenum phases. For this, the results obtained by Raman spectroscopy (**Figure 13**) were analysed in greater depth with the aim of ascribing the species if possible.

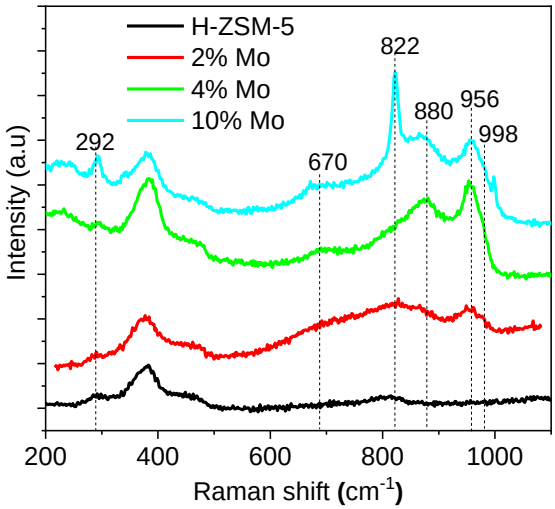

Figure 13. Raman spectra of calcined 2, 4 and 10%Mo/H-ZSM-5 catalysts.

As previously reported, ZSM-5 shows bands at 292 and 375 cm^{-1}, coming from the bending mode of six and five-membered rings of the zeolite, respectively.[29] The well-

known bands at 820 and 996 cm^{-1} ascribed respectively to Mo-O-Mo and Mo=O asymmetric and symmetric stretching of crystalline MoO_3 are also detected in the 10 %Mo/H-ZSM-5 catalyst,[30] indicating the presence of large MoO_3 entities in this catalyst.[31,32] The presence of these big particles must correspond to those previously detected by HAADF and associated to aluminum (**Figure 10**).

The assignment of well dispersed molybdenum species supported on oxide supports by Raman spectroscopy is still debatable, particularly between the spectra obtained under different hydrated conditions.[30] Nevertheless, although it is not possible to obtain analogous bulk species to compare with, some of these isolated Mo species, with different degrees of polymerization have been reported in the literature and could serve to elucidate the species present in our systems. Molybdate is usually considered to be in different forms from isolated monomers to dimers/olygomeric and polymeric species. Thus, the band at around 960 cm^{-1} could be attributed to terminal Mo=O groups of isolated tetrahedrally coordinated monomers, MoO_4^{2-}, while the weak and broad band at 870 cm^{-1} has been associated to bridge Mo-O-Mo entities of dimeric/oligomeric species.[30] As can be observed in the **Figure 13**, these bands are also present in the 10%Mo/H-ZSM-5 system, together with the MoO_3 bulk ones. In agreement with our previous findings, the presence of such different bands denotes the complexity of Mo speciation over zeolite support.[33]

In regards to 4%Mo/H-ZSM-5 catalyst, it exhibits two main bands centered at 870 and 960 cm^{-1}, previously described as typical for small 2D clusters of molybdenum oxide species forming both dimers and monomers, respectively.[30,34,35] Finally, the 2%Mo/H-ZSM-5 sample only present a well-defined band at ca. 960 cm^{-1}, coming from monomeric Mo species can be found. The band associated to dimeric species at around 870 cm^{-1} appears but as a very wide peak, almost undistinguishable from the background. Therefore, mainly monomeric and dimeric molybdenum species seem to be present at these low Mo loadings.[33]

Thus, according to these results, and assuming the presence of the previous characterized molybdenum phases (*A*-*E*), it seems plausible to assign the *A* and *E* species

to Mo monomers anchoring to the zeolite surface, *B* and *C* should mainly correspond to dimers and/or well dispersed phases, while the *D* specie comes from a bulk-like MoO_3 phase, which has been detected in the high loaded sample as a Mo associated to alumina particles segregated from the zeolite.

4.7. The role of the Mo/Alumina phase: Why higher Mo loading yields worse catalyst?

It is well known in the literature that the best catalytic performances are reached with intermediate Mo loading (3-5%), while higher metallic contents are deleterious.[1,2] Thus, it can be relevant to discuss the role of this bulk molybdenum/alumina phase in the low performance of the 10%Mo/H-ZSM-5 catalyst (**Figure 3**). For instance, it could be argued that it partially blocks the microporous channels of the zeolite, thus preventing the molecules of methane from reaching the active sites located inside these micropores. If this were the case, the microchannels could then be released by the soft acid treatment, which removes this bulk phase, opening the microstructure of the zeolite and improving the catalytic performance (**Figure 5**). This possibility can however be discarded in view of the surface area data collected in **Table 1.** Although the increasing loading of Mo causes a noticeable decline in the surface area of the catalysts, from 361 m^2/g in the original zeolite to 272 m^2/g in the 10%Mo/H-ZSM-5. After acid treatments the surface areas of the ex-10%Mo/H-ZSM-5 catalysts remain constant, in spite of the observed increase/decrease in the *MDA* performances attained for 0.1M/0.5M acid treated catalysts. Thus, as previously found by other authors, the initial loss of surface area compared to the zeolite support should be primarily initiated by the molybdenum precursors anchoring/linking inside the pores during the preparation step of the catalysts.[34]

The ultimate reason for the low performance of this catalyst could be found in the DTG profiles presented in **Figure 14.**

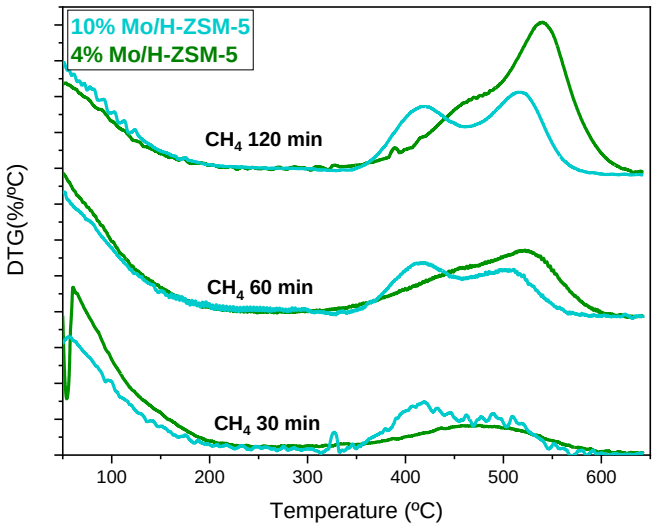

Figure 14. DTG profiles of spent 4% and 10%Mo/H-ZSM-5 catalysts after *MDA* reaction.

According to this, the key to understand the loss of performance in the 10%Mo/H-ZSM-5 would lay on the high activity of the phase *D* for production of coke. Thus, despite its lower activity converting methane, after only 30 minutes of TOS, the 10%Mo/H-ZSM-5 sample produces a significant amount of coke that is burned at 400 °C. The occurrence of such carbon species is absent in the 4%Mo/H-ZSM-5 catalyst after similar reaction time. This coke, presumably formed by the originally bulk MoO_3 phase, could account for a quick loss of catalytic performance in the 10%Mo catalyst. At longer reaction times and probably due to a side reaction, the 4%Mo system produces a significant amount of graphitic carbon, as indicated by the higher combustion temperature, which could explain the loss of activity at higher reaction time.

Thus, our results clearly show that the intermediate sample, namely 4%Mo/H-ZSM-5, exhibits the best performance in the *MDA* reaction. As presented in **Figure 15**, in this catalyst, in addition to species *E*, species *A*, *B* and *C* appear. Among these, *C Mo-species*, located inside the micropores of the support, would be the most active in the *MDA* reaction.

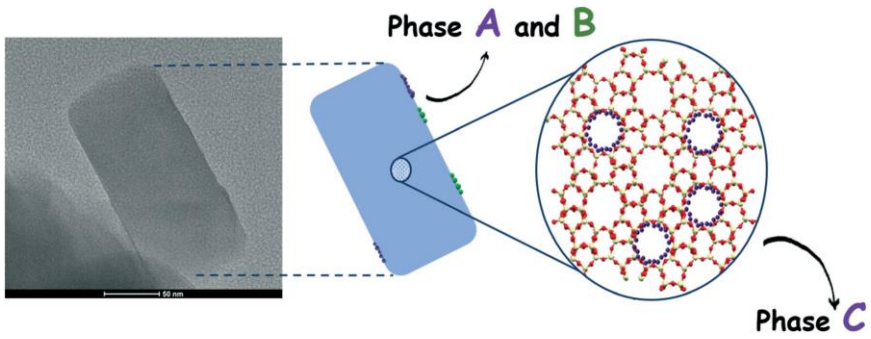

Figure 10. Schematic representation of species *A*, *B* and *C* in the 4%Mo/H-ZSM-5 catalyst.

4.8. Conclusions

The combination of characterization techniques has allowed us to identify the presence of at least five different Mo phases in calcined Mo/HZSM-5 catalysts, which are subsequently stabilized on the support as the loading of Mo increases from 2 wt% to 10 wt%. As a result, we have been able to know the location, the nature and the dispersion state of these phases. In addition, from the catalytic performances in the *MDA* reaction it has been possible to state the performance of some these phases, as follows:

- *Phase A*: small clusters of well-dispersed Mo monomers, reducing at 350-570 °C and located in the external surface of zeolite. It exhibits a certain activity in the *MDA* reaction.
- *Phase B*: small clusters of well-dispersed Mo dimers, reducing at 570-680 °C and located in the external surface of zeolite. In the HAADF images, it seems to be associated with Al-enriched areas of the zeolite. No direct evidence for its catalytic activity has been found. It seems to be a spectator as different amounts of it give rise to catalysts with similar performances (catalyst before and after acid treatments).
- *Phase C*: small clusters of well-dispersed Mo dimers/ polymers, reducing at 680-800 °C and located in the inner micropores of the ZSM-5 support. It is a very active phase and is mainly responsible for the high performance of the more active catalysts. When eliminated by a hard acid treatment, the catalytic performance

decreases. This phase seems to be similar to that previously found by other authors in a 4%Mo system, identified as isolated Mo-oxo species.[36]

- *Phase D*: the bulk-like phase of MoO_3, reducing at 800-915 °C and located in the external surface of the zeolite. The HAADF images unambiguously show that it is supported on aluminum oxide segregated from the zeolite network. It hinders the catalytic performance, prompting the formation of heavy coke deposits on the catalysts.
- *Phase E*: small clusters of well-dispersed Mo monomers, reducing at temperatures higher than 915 °C and located in the inner microporous channels of the zeolite. It is formed when small amount of Mo is added to the ZSM-5 and remains constant at Mo loadings higher than 2 wt%. This feature denotes a strong interaction with selected sites of the support. It is not affected even by a hard acid treatment. In this study, its role in the *MDA* reaction is similar to that of *A* phase.

In view of these previous conclusions, it is also worth noting that the phases totally or partially extracted by the soft 0.1 M sulfuric acid treatment (phases *A*, *B* and *D*) are all located on the external surface of the zeolite. However, with respect to the phases located in the microporous channels, one of them (phase *C*) is only extracted after a harder acid treatment (sulfuric acid, 0.5 M), while the phase *E* seems to be hardly affected, proving once again its strong interaction with the zeolite support.

4.9. References

1. Julian, I. *et al.* Supercritical solvothermal synthesis under reducing conditions to increase stability and durability of Mo/ZSM-5 catalysts in methane dehydroaromatization. *Appl. Catal. B Environ.* **263**, 118360 (2020).
2. Han, S. J. *et al.* Non-oxidative dehydroaromatization of methane over Mo/H-ZSM-5 catalysts: A detailed analysis of the reaction-regeneration cycle. *Appl. Catal. B Environ.* **241**, 305–318 (2019).
3. Tempelman, C. H. L. & Hensen, E. J. M. On the deactivation of Mo/HZSM-5 in the methane dehydroaromatization reaction. *Appl. Catal. B Environ.* **176**–**177**, 731–739 (2015).
4. Martínez, A. & Peris, E. Non-oxidative methane dehydroaromatization on Mo/HZSM-5 catalysts: Tuning the acidic and catalytic properties through partial exchange of zeolite

protons with alkali and alkaline-earth cations. *Appl. Catal. A Gen.* **515**, 32–44 (2016).

5. Tessonnier, J. P., Louis, B., Rigolet, S., Ledoux, M. J. & Pham-Huu, C. Methane dehydro-aromatization on Mo/ZSM-5: About the hidden role of Brønsted acid sites. *Appl. Catal. A Gen.* **336**, 79–88 (2008).
6. Kosinov, N. *et al.* Stable Mo/HZSM-5 methane dehydroaromatization catalysts optimized for high-temperature calcination-regeneration. *J. Catal.* **346**, 125–133 (2017).
7. Sobalík, Z., Tvarůžková, Z., Wichterlová, B., Fíla, V. & Špatenka, Š. Acidic and catalytic properties of Mo/MCM-22 in methane aromatization: An FTIR study. *Appl. Catal. A Gen.* **253**, 271–282 (2003).
8. Vollmer, I. *et al.* Relevance of the Mo-precursor state in H-ZSM-5 for methane dehydroaromatization. *Catal. Sci. Technol.* **8**, 916–922 (2018).
9. Tessonnier, J. P. *et al.* Quantitative measurement of the Brönsted acid sites in solid acids: Toward a single-site design of Mo-modified ZSM-5 zeolite. *J. Phys. Chem. B* **110**, 10390–10395 (2006).
10. Wang, D., Lunsford, J. H. & Rosynek, M. P. Characterization of a Mo/ZSM-5 catalyst for the conversion of methane to benzene. *J. Catal.* **169**, 347–358 (1997).
11. Tan, P. The catalytic performance of Mo-impregnated HZSM-5 zeolite in CH4aromatization: Strong influence of Mo loading and pretreatment conditions. *Catal. Commun.* **103**, 101–104 (2018).
12. Wang, L. *et al.* Dehydrogenation and aromatization of methane under non-oxidizing conditions. *Catal. Letters* **21**, 35–41 (1993).
13. Kosinov, N. *et al.* Methane Dehydroaromatization by Mo/HZSM-5: Mono- or Bifunctional Catalysis? *ACS Catal.* **7**, 520–529 (2017).
14. Kosinov, N. *et al.* Confined Carbon Mediating Dehydroaromatization of Methane over Mo/ZSM-5. *Angew. Chemie - Int. Ed.* **57**, 1016–1020 (2018).
15. Weckhuysen, B. M., Rosynek, M. P. & Lunsford, J. H. Characterization of surface carbon formed during the conversion of methane to benzene over Mo/H-ZSM-5 catalysts. *Catal. Letters* **52**, 31–36 (1998).
16. Kosinov, N. *et al.* Structure and Evolution of Confined Carbon Species during Methane Dehydroaromatization over Mo/ZSM-5. *ACS Catal.* **8**, 8459–8467 (2018).
17. Matus, E. V. *et al.* Study of methane dehydroaromatization on impregnated Mo/ZSM-5 catalysts and characterization of nanostructured molybdenum phases and carbonaceous deposits. *Ind. Eng. Chem. Res.* **46**, 4063–4074 (2007).
18. Ma, D., Shu, Y., Bao, X. & Xu, Y. Methane dehydro-aromatization under nonoxidative conditions over Mo/HZSM-5 catalysts: EPR study of the Mo species on/in the HZSM-5

zeolite. *J. Catal.* **189**, 314–325 (2000).

19. Julian, I., Ramirez, H., Hueso, J. L., Mallada, R. & Santamaria, J. Non-oxidative methane conversion in microwave-assisted structured reactors. *Chem. Eng. J.* **377**, 119764 (2019).
20. Liu, H. *et al.* The chemical nature of carbonaceous deposits and their role in methane dehydro-aromatization on Mo/MCM-22 catalysts. *Appl. Catal. A Gen.* **236**, 263–280 (2002).
21. Song, Y. *et al.* Coke accumulation and deactivation behavior of microzeolite-based Mo/HZSM-5 in the non-oxidative methane aromatization under cyclic CH_4-H_2 feed switch mode. *Appl. Catal. A Gen.* **530**, 12–20 (2017).
22. Vollmer, I., Yarulina, I., Kapteijn, F. & Gascon, J. Progress in Developing a Structure-Activity Relationship for the Direct Aromatization of Methane. *ChemCatChem* **11**, 39–52 (2019).
23. Xia, Y., Xiao, L., Xiao, C. & Zeng, L. Direct solvent extraction of molybdenum(VI) from sulfuric acid leach solutions using PC-88A. *Hydrometallurgy* **158**, 114–118 (2015).
24. Malet, P. & Caballero, A. The selection of experimental conditions in temperature-programmed reduction experiments. *J. Chem. Soc. Faraday Trans. 1 Phys. Chem. Condens. Phases* **84**, 2369–2375 (1988).
25. Rodriguez-Gomez, A. & Caballero, A. Identification of Outer and Inner Nickel Particles in a Mesoporous Support: How the Channels Modify the Reducibility of Ni/SBA-15 Catalysts. *ChemNanoMat* **3**, 94–97 (2017).
26. Liu, H., Shen, W., Bao, X. & Xu, Y. Methane dehydroaromatization over Mo/HZSM-5 catalysts : The reactivity of MoCx species formed from MoOx associated and non-associated Brönsted acid sites. **295**, 79–88 (2005).
27. Ma, D. *et al.* Towards guest - Zeolite interactions: An NMR spectroscopic approach. *Chem. - A Eur. J.* **8**, 4557–4561 (2002).
28. López-Martín, A., Caballero, A. & Colón, G. Structural and surface considerations on Mo/ZSM-5 systems for methane dehydroaromatization reaction. *Mol. Catal.* **486**, (2020).
29. Yu, Y., Xiong, G., Li, C. & Xiao, F. S. Characterization of aluminosilicate zeolites by UV Raman spectroscopy. *Microporous Mesoporous Mater.* **46**, 23–34 (2001).
30. Rzhevskii, A. M., Choi, P., Ribeiro, F. H., Gulotty, R. J. & Olken, M. M. Monitoring of molybdenum H-ZSM5 catalyst preparation by in situ ultraviolet Raman spectroscopy. *Catal. Letters* **73**, 187–191 (2001).
31. Windom, B. C., Sawyer, W. G. & Hahn, D. W. A raman spectroscopic study of MoS_2 and MoO_3: Applications to tribological systems. *Tribol. Lett.* **42**, 301–310 (2011).
32. Samantaray, S., Hota, G. & Mishra, B. G. Physicochemical characterization and catalytic

applications of MoO 3-ZrO2 composite oxides towards one pot synthesis of amidoalkyl naphthols. *Catal. Commun.* **12**, 1255–1259 (2011).

33. Hu, H. & Wachs, I. E. Surface structures of supported molybdenum oxide catalysts. Characterization by raman and Mo L3-edge XANES. *J. Phys. Chem.* **99**, 10897–10910 (1995).
34. Wei Li, George D. Meitzner, Richard W. Borry III, and E. I. Raman and X-Ray Absorption Studies of Mo Species in Mo/H-ZSM5 Catalysts for Non-Oxidative CH_4 Reactions. *J. Catal.* **191**, 373–383 (2000).
35. Chen, K., Xie, S., Bell, A. T. & Iglesia, E. Structure and properties of oxidative dehydrogenation catalysts based on MoO_3/Al_2O_3. *J. Catal.* **198**, 232–242 (2001).
36. Agote-Arán, M. *et al.* Determination of Molybdenum Species Evolution during Non-Oxidative Dehydroaromatization of Methane and its Implications for Catalytic Performance. *ChemCatChem* **11**, 473–480 (2019).

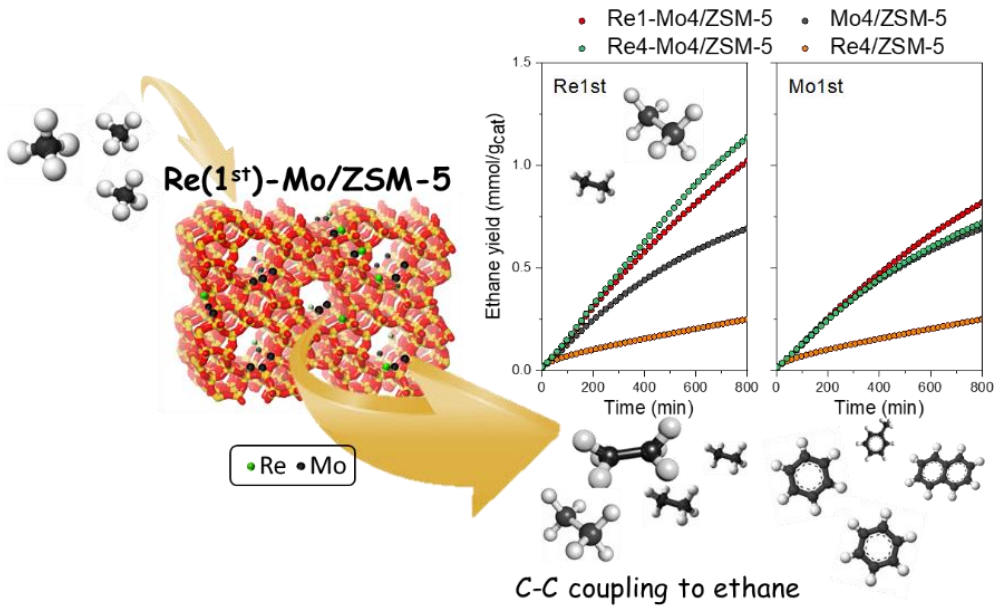

Chapter 5. Bimetallic Mo-Re supported ZSM-5 through sequential impregnation.

A. López-Martín, M.F. Sini, M.G. Cutrufello, A. Caballero, G. Colón

"Characterization of Re-Mo/ZSM-5 catalysts: How Re improves the performance of Mo in the methane dehydroaromatization reaction"

Applied Catalysis B: Environmental 304 (2022) 120960

In this chapter the promoting effect of rhenium addition on Mo/H-ZSM-5 catalysts system has been studied. Hence, bimetallic catalysts have been synthesized using a sequential impregnation methodology. The catalytic performance for direct aromatization of methane reaction has been determined and correlated with their physical and chemical state, combining chemical (TPR), spectroscopic (XPS), electron microscopy (TEM, HAADF) and other characterization techniques. An important synergy between Mo and Re, which it is strongly affected by the sequential impregnation, has been observed.

5.1. Introduction

As has been shown throughout this thesis, the challenges with the *MDA* reaction are two-fold: the reaction is thermodynamically limited with low one-pass methane conversion and even the best catalytic systems, Mo/zeolites, suffer rapid deactivation from coking.[1] Within this framework, several characteristics are yet unknown and how to prevent its deactivation caused by coke formation still remains an unsolved problem that hinders its industrial application.[2–4]

In order to improve the catalytic performance and to decrease the deactivation rate, multiple studies have focused on the addition of different metals as a co-dopant to the Mo catalysts for the *MDA* reaction. However, though reported results showed interesting effects, attained improvements appear always temporary and the stability of the catalysts was always a challenge.[5] For this sake, a catalyst design strategy is crucial to improve stability. So, the use of multifunctional Mo-X/zeolite systems where X is a co-dopant capable of modulating the stability has been widely reported. In this sense, the addition of metal dopants to would improve not only the catalytic performance but also the stability of Mo/H-ZSM-5 catalysts by influencing the catalyst deactivation step.

Thus, Scurrell and co-workers added platinum and/or tin on Mo/H-ZSM-5 zeolite catalyst for methane aromatization reaction.[6] They concluded that catalysts with additional tin led to lower methane conversion but higher aromatic products selectivity.

The incorporation of Fe modifying conventional Mo/H-ZSM-5 catalysts induces high stability and selectivity to aromatics [7]

Zhang *et a*l. studied the effect of indium on Mo/H-ZSM-5 in *MDA* concluding that although methane conversion decreases, the coke selectivity is reduced to 50 % that of Mo/H-ZSM-5.[8] Such stabilization seems to be related to the close proximity of In and Mo that would suppress coke formation.

More recently, Sridhar *et al.* reported the addition of different loadings of Co and Ni on Mo/H-ZSM-5 catalyst in order to evaluate the promoting effect of these metals on reactivity and stability of the Mo catalysts.[9] They observed a synergistic effect between Mo and the promoters, resulting in benzene yield and catalytic stability improvements.

Since it is proposed that Brönsted acid sites would play an important role in the reaction pathways, the modification of the zeolite acidity would be achieved through metal co-doping.[10] Thus, Cr, Ag and Ga were employed as additive that increased the catalyst acidity and resulted in improved methane conversion and benzene selectivity.[5]

Rhenium was discovered in 1925 and, in spite of the sparse distribution of rhenium and its low content in the earth's crust, the annual world mine production of rhenium from mining is about 50 tons.[11] During the past 30 years, the two most important uses of rhenium have been in high-temperature superalloys and platinum-rhenium catalysts for producing gasoline, where it can successfully replace the more expensive platinum group metals.[12,13]

Rhenium has many stable oxidation states: +3, +4, +6, +7, and its metallic form Re°, which allows its compounds to show a rich chemistry and a multifunctionality of Re catalysts. The most stable oxidation state is +7 state, unlike other group VII metals such as Mn^{+7}, which is a highly reactive and oxidizing species. It can also form numerous oxocations and oxyanions.[14]

This metal has certain similarities with the metals of group VIII in the periodic table in terms of its catalytic properties, which gives it the ability to catalyse both hydrogenation and dehydrogenation reactions, among others. In this way, we could say that rhenium has a combination of properties that makes it different from any other transition element with catalytic activity. Overall, among the catalytic properties of rhenium we could highlight its high selectivity and its high resistance to poisoning and deactivation by nitrogen, sulfur, etc, and thus, improves the yield of the process.[15] Therefore, rhenium is a very promising metal for its application in different catalytic processes, in

fact, rhenium-based catalysts have been extensively used in reforming, alkene metathesis and hydrodesulfurization of crude oil fractions. [15–17]

Some studies have used Re/H-ZSM-5 catalysts for the aromatization of ethane. Krogh *et al.* compared Re/H-ZSM-5 and Zn/H-ZSM-5 and found out that although Re exhibited lower activity initially, it was deactivated more slowly showing higher and stable ethane conversion values at long reaction times. The difference between both catalysts was attributed to the sublimation of Zn species that did not occur in the more stable case of Re/ZSM-5.[18] Solymosi *et al.* reported that Re in the Re/ZSM-5 catalysts was promoting the activation of the C-H bond that resulted in more ethane conversion and higher aromatics selectivity. Also, it was observed that the increase in the rhenium load in the catalysts caused less metal dispersion and made the catalyst less active. [19]

In this work we study the effect of rhenium addition as co-dopant to the classical Mo/H-ZSM-5 catalyst, and how it affects, on the one hand to the physicochemical properties, and on the other hand to the catalytic activity and stability during *MDA* reaction. We will study the important effect of the sequential addition of metals, preparing two different series of catalyst in which Mo has been loaded first in a case (Mo1st), and Re in the other (Re1st). Both catalyst series have been widely characterized by several techniques, in particular XPS and TPR, and also tested in order to evaluate its catalytic performance in the *MDA* reaction.

5.2. Bimetallic catalysts synthesis

The bimetallic catalysts were prepared using a commercial NH_4-ZSM-5 zeolite (Alfa Aesar, SiO_2/Al_2O_3=23/1) previously calcined at 550 °C for 3 hours to obtain the acid form. Mo and Re were sequentially added by impregnation procedure. Thus, for each series, one of the metal was firstly impregnated followed by calcination at 550 °C, 3h. After which, the second metal was subsequently introduced in a second step and further

calcined again at the same temperature. The obtained series were named as Mo1st and Re1st, respectively.

Molybdenum was loaded using ammonium heptamolybdate tetrahydrate of appropriate concentration ($(NH_4)_6Mo_7O_{24}{\cdot}4H_2O$, Sigma Aldrich) to obtain 4 wt% Mo, while rhenium was loaded using rhenium (VII) oxide (Re_2O_7, Sigma Aldrich) at the corresponding stoichiometric amount leading to 1 wt% and 4 wt%. As a result, the following bimetallic systems from both series were obtained: 1%Re-4%Mo and 4%Re-4%Mo.

5.3. Catalysts characterization and performance

5.3.1. Catalytic activity

Before reaction, catalysts were pretreated under O_2/N_2 (20% in O_2) flow of 15 mL/min at 250 °C for 1 h. Then the temperature was lowered to 150 °C under inert gas. Then, the methane dehydroaromatization reaction was performed as usual, with a CH_4/N_2 (85% in CH_4) flow of 5mL/min. Meanwhile, the temperature was ramped up with a rate of 10 °C/min from 150 °C until 700 °C, and held at this temperature for 18 h.

The first important issue to point out is that Re incorporation significantly improves the benzene/aromatic yield in both series with respect to Mo monometallic system. Moreover, a second point to be highlighted is that the catalytic activity for methane aromatization to benzene reveals that the addition sequence followed would have a marked effect (**Figure 1**). Thus, we may state that Re1st series shows better catalytic performance with respect to Mo1st one. Moreover, while for Re1st series the amount of Re seems not to affect to the aromatic yields, for Mo1st series the amount of Re appears to have certain influence.

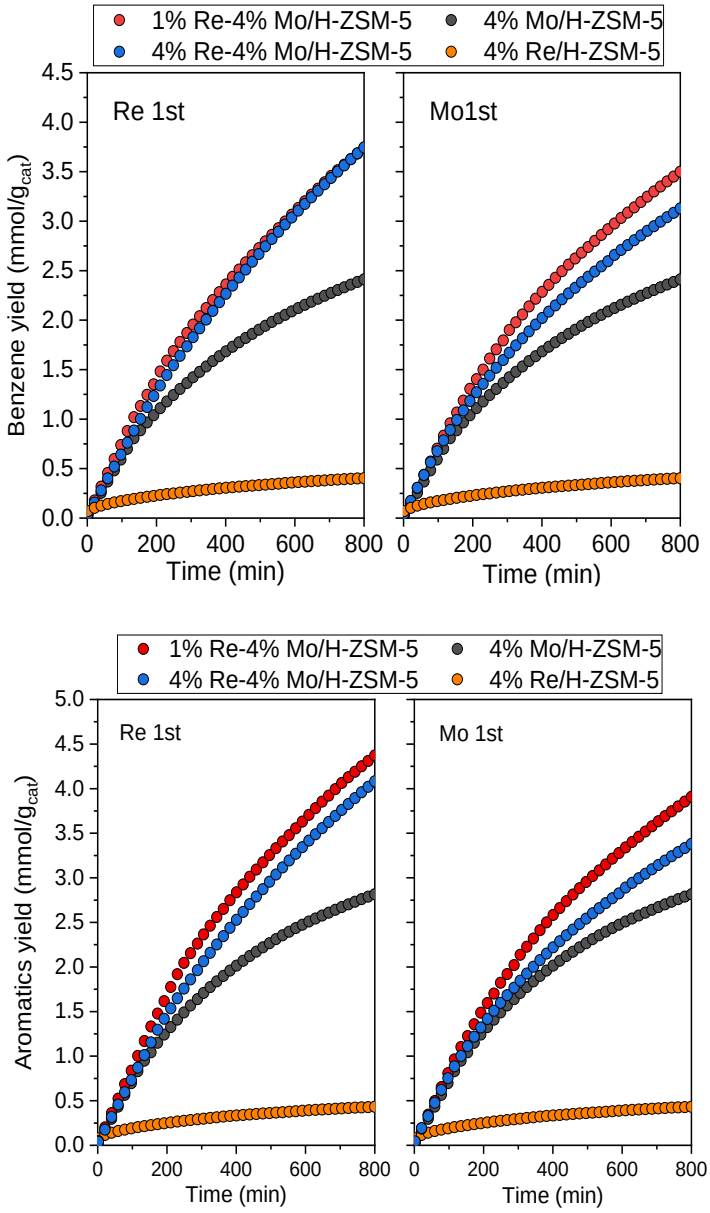

Figure 1. Accumulated benzene and aromatics yields for 4%Mo/H-ZSM-5, 4%Re/H-ZSM-5 and bimetallic catalysts for Mo1st and Re1st series.

The maximum activity is attained by 1%Re-4%Mo/H-ZSM-5 catalyst in the Re1st series, for which higher production of benzene and aromatics has been found (**Figure 1**). It is also worth of noting that the increasing amount of Re does not affect to the yield of benzene in the Re1st series. On the contrary, for Mo1st series increasing amount of Re seem to be detrimental. Moreover, in the case of aromatics production, irrespective of the sequence addition, higher Re content leads to a slightly lower yield. Thus, from both results it can be argued that 1%Re-4%Mo/H-ZSM-5 from Re1st series would favour the

naphthalene production with respect the other systems. Thus, from both results it can be argued that since benzene yield is similar for bimetallic systems in the Re1st series, the naphthalene production would be slightly favoured in the 1%Re-4%Mo/H-ZSM-5 within both series with respect to systems with higher Re content (**Figure 2**). Toluene is residually detected for 1%Re-4%Mo/H-ZSM-5 systems.

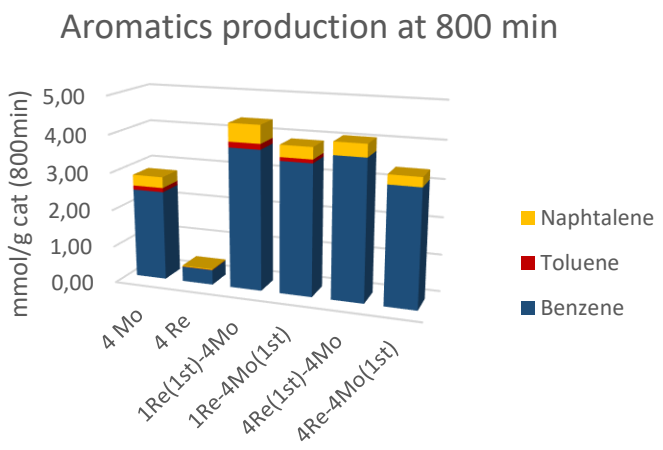

Figure 2. Aromatic accumulated production over different catalysts after 800 min reaction.

Specifically, after 800 min in stream the obtained aromatics yield was 4.4 mmol/g $_{cat}$ for the 1%Re-4%Mo/H-ZSM-5 within Re1st series, being significantly higher than the observed value using 4%Mo/H-ZSM-5 sample, for which 2.5 mmol/g_{cat} is obtained. The Re incorporation as promoter implies an enhancement of ca 50 % with respect to the monometallic system. This is an outstanding improvement if we compare with reported results by other promoters such as Fe, Co or Ni.[9,20]

Another interesting aspect concerns the evolution of intermediates. Early proposed mechanism argued that methane would react on the Mo sites to produce ethylene, which further proceeds on the acid sites of the catalysts to form aromatics (both benzene and coke precursors). In a first step, ethane could be formed from methane coupling reaction.[21] Then, in a second step, ethane would undergo dehydrogenation to ethylene.

However, a recent report questioned the bifunctional mechanism in which ethylene would be the primary intermediate.[22] Vollmer *et al.* proposed that ethylene would not be the major reaction intermediate since the hydrocarbon pool formed in the zeolite matrix during *MDA* is comprised of less dense and more hydrogenated species than the pool formed from ethylene. The hydrocarbon pool would be formed during the kinetic induction period and consist on compounds trapped within the voids. This mechanism based on the hydrocarbon pool contradicts the well stablished bifunctional mechanism. In this sense, Gu *et al.* argued that Brönsted acids sites predominantly serve as the anchoring points for the dispersion of Mo-species, but their participation in aromatization step is quite limited.[4] On this basis, aromatization is supposed to be the intrinsic property of (oxy-) carbidic Mo sites.

The production of these intermediates for both series have been represented in **Figure 3**. It is clear that while ethylene formation is not affected by the presence of Re nor the preparation sequence, in the case of ethane important differences can be observed. Furthermore, the enhanced formation of ethane in 1%Re-4%Mo/H-ZSM-5 catalyst is accompanied by the higher production of aromatics. Such different evolution would point out the fact that ethylene is not the primary but a side intermediate formed. Moreover, ethylene follows a growing evolution with time, pointing out that is not affected by catalyst deactivation. It is supposed that catalyst deactivation would take place over metal sites by coke deposition. Thus, the formation of ethylene would not be associated to these sites. Indeed, in a recent kinetic study Razdan *et al.* proposed that ethane is the initial product of C–C coupling.[23] Therefore, we may infer that the occurrence of Re and particularly when incorporated first, would be directly associated to the enhanced ethane evolution. Thus, it can be assumed that the differences in the aromatics production could be consequently associated in part to the best performance in C-C coupling step to ethane. Then, ethylene formation as a secondary intermediate, that is formed equally in all catalysts and therefore is not conditioned by Re presence, and seems not to be related with the final aromatics formation.

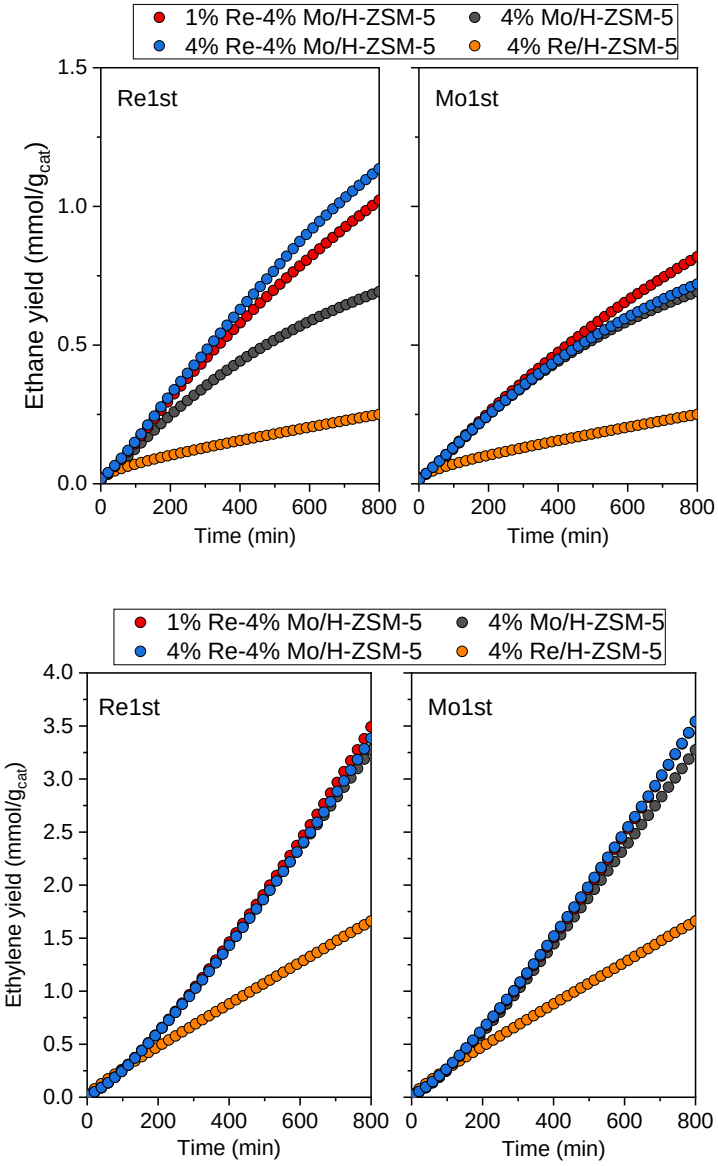

Figure 3. Evolution of accumulated ethane and ethylene formed during aromatization reaction over different catalysts from both series.

5.3.2. Surface area measurements

In order to delve into the origin of the observed differences in the catalytic behaviour of the Re-Mo bimetallic catalysts, the systems were widely structural, textural and electronic characterized. As showed from N_2 adsorption-desorption isotherms (**Figure 4)**, the introduction of metal in the zeolite certainly affects to surface features of the catalyst.

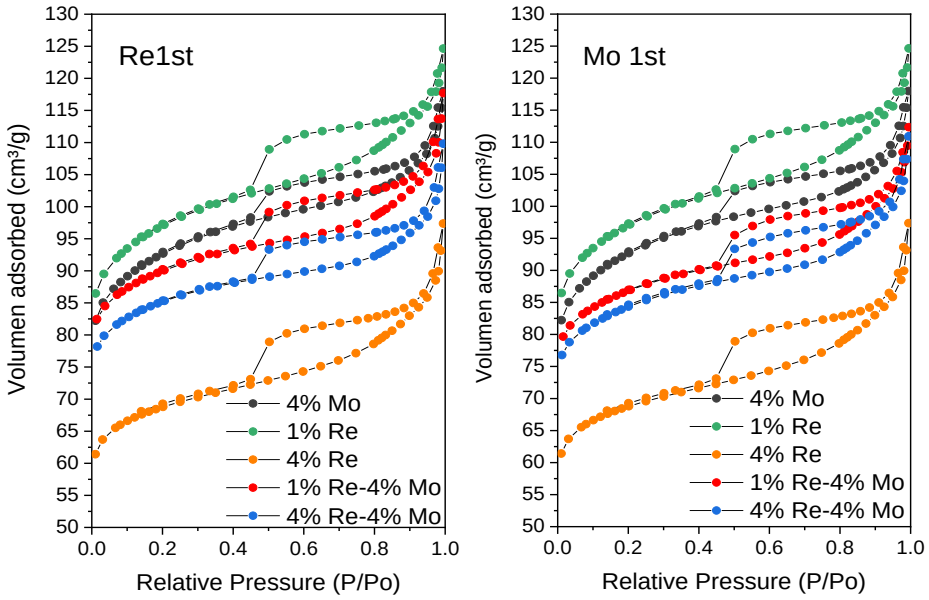

Figure 4. N_2 adsorption-desorption isotherms of: Re-Mo/H-ZSM-5 (Re1st) series (*left panel*); Re-Mo/H-ZSM-5 (Mo1st) series (*right panel*).

Thus, a slight decrease in the BET surface is observed for Mo and Re monometallic catalysts and occurs in both the micropore and the external surface areas in a similar way (**Figure 5**). Such decrease is largest in the case of 4% Re monometallic system, where BET change from 360 m^2/g for the ZSM-5 to 231 m^2/g for 4%Re/H-ZSM-5. This diminution in the BET value is significantly lower than that exhibited by 4%Mo sample. From this result it can be inferred that Re would percolate better than Mo inside the porous structure during calcination causing the pore blockage, particularly micropore ones.[4,24] This effect has been previously reported for Re-MFI system.[25] In this study, Lacheen *et al*. stated that through thermal treatment of Re_2O_7/H−MFI mixtures, the selective grafting of isolated and stable Re-oxo species via Re_2O_7 (g) reactions with OH groups to form Si−$O_f$$ReO_3$−Al (where O_f is framework O) is achieved. Moreover, grafting onto exchange sites would prevent the ubiquitous sublimation of ReO_x species.

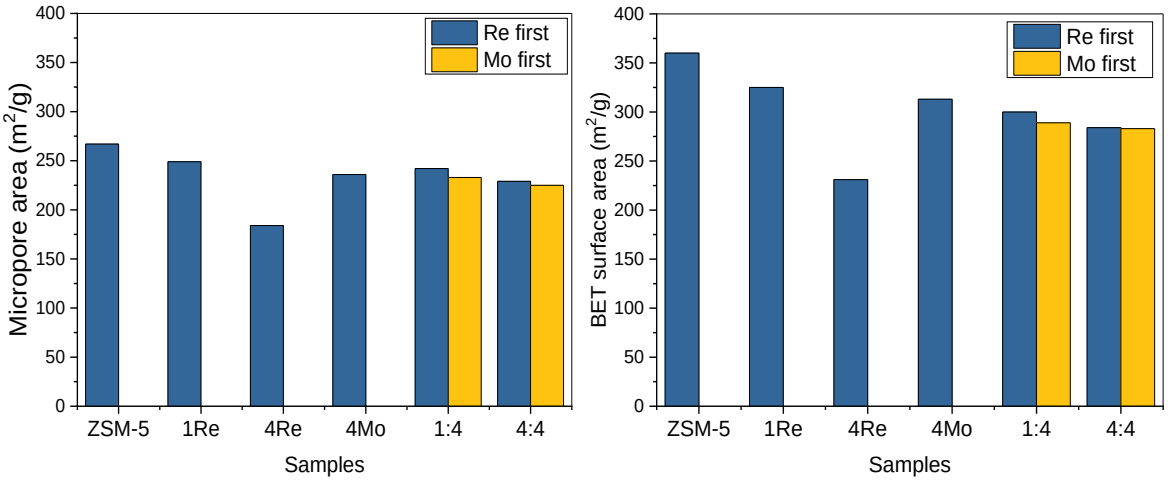

Figure 5. BET and micropore area results for the different catalysts prepared by both sequential methods.

It is surprising that bimetallic systems show similar surface features than monometallic 4%Mo/H-ZSM-5. Therefore, it appears that the changes in the surface area values are not related with the total metal loading. Moreover, the particular pore obstruction observed for monometallic Re seems not be present in these bimetallic samples. The surface area of 4%Re/H-ZSM-5 is smaller than 4%Re-4%Mo catalyst for which the metal loading is nearly double. Only a gradual decrease in the surface area with the total metal load increase is observed. In this sense, we have to consider that in the case of 4%Re-4%Mo/H-ZSM-5 (Re1st) the sample is submitted to a second calcination upon Mo impregnation that could help Re to diffuse. In the case of 4%Re-4%Mo/H-ZSM-5 (Mo1st), the inner pores would be firstly occupied by Mo, leading Re in the outer sites. On this basis, in neither case, the micropore surface area wouldn't exhibit a comparable situation as 4%Re/H-ZSM-5.

Comparing the Re-Mo systems between both series, it can be noticed that the introduction of Mo first (Mo1st series) led to a slightly lower surface area values than when Re is firstly impregnated (Re1st series). As a consequence of the observed evolution, we would may infer that initial drastic pore obstruction by Re ions is not taking place in Re1st series. Indeed, for these samples, once Re is impregnated the solid is submitted to a further calcination process upon Mo incorporation. If we consider the

high mobility of Re at moderate temperatures, it can be assumed that ions located at the inner micropore sites could be extracted and occupied the external surface or even partially sublimated.

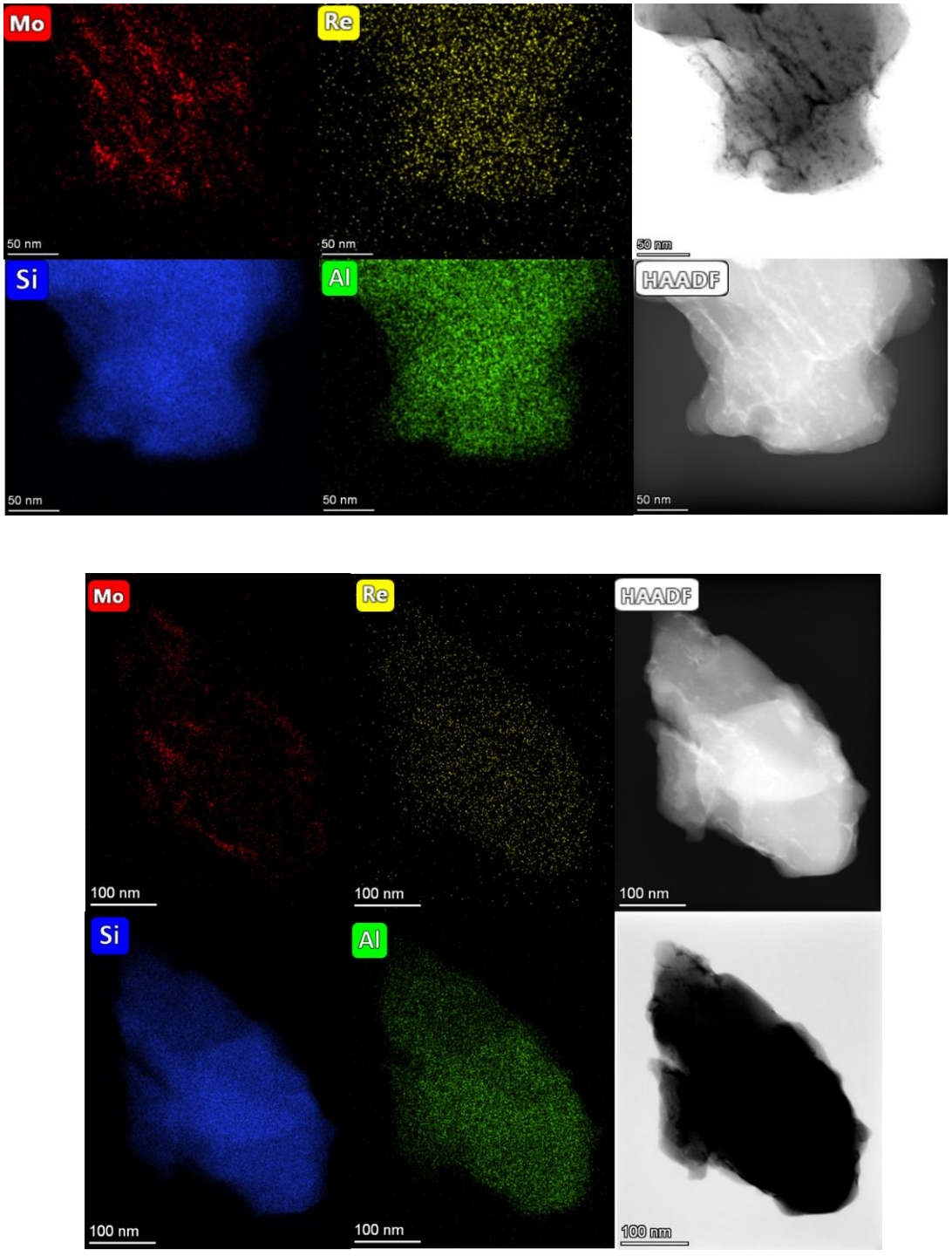

Figure 6. HAADF-STEM images of: 1%Re-4%Mo/H-ZSM-5 (Re1st) catalyst (*upper panel*); 1%Re-4%Mo/H-ZSM-5 (Mo1st) catalyst (*lower panel*).

Furthermore, when Re is incorporated in second place, it could be preferentially deposited close to Mo in close interaction as will be further discussed. This could explain that bimetallic samples do not show important diminution in the surface area. In spite of the different impregnation procedure, we have evidenced from HADDF a good dispersion of Re ions on the zeolite support (Figure 6). This fact denotes that Re would easily diffuse through zeolite pore structure upon different calcination treatments.

5.3.3. Ammonia adsorption microcalorimetry

Ammonia adsorption microcalorimetry experiments were carried out to determine the total number, strength and strength distribution of surface acid sites.

The differential heats of ammonia adsorption at 80 °C on selected catalysts are presented in **Figure 7** (*left panel*) with increasing surface coverage. The populations of the surface acid sites at various heat intervals of adsorption are shown in **Figure 7** (*right panel*)**.**

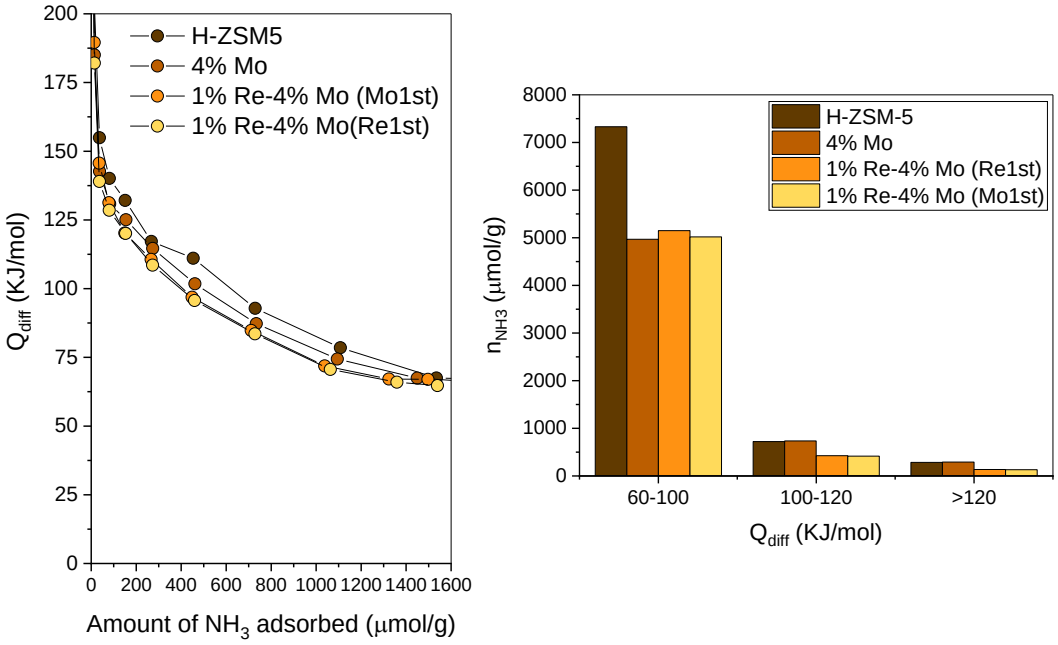

Figure 7. Differential heats of ammonia adsorption (left) and acid sites strength distribution obtained after ammonia adsorption for different catalysts (right).

For all samples, after outgassing at 80 °C, NH_3 readsorption occurred only to a limited extent and with low values of differential heat of adsorption (Q_{diff} from 100 kJ/mol down to 60 kJ/mol). This indicates that the sites characterized by $Q_{diff} \leq 100$ kJ/mol are weak enough to readily desorb ammonia molecules adsorbed during the first adsorption run. Therefore, they can be classified as weak.

By observing the different distribution of sites for weak, medium and strong acid sites it can noted that the incorporation of metals largely affects the weak acid sites. Moreover, it can be pointed out that Mo incorporation only affects these weak sites (60-100 kJ/mol). When Re is present, it is worthy to note that strongest sites (> 100 kJ/mol) are specifically affected.

In addition, it can be said that the sequence of metal incorporation in bimetallic systems would not have a clear effect on the number of these stronger acid sites. From these results, it can be argued that Re naturally trends to occupy the strongest sites while Mo the weakest ones. Such differential behaviour could be related with the different acid character of the Mo and Re ions.

In a recent work, Gao *et al.* described that the strong interaction between acidic proton and Mo sites correlates with the products formation and catalyst lifetime.[26] These authors argued that this issue would have an important implication in modulating the catalytic *MDA* performance by taking advantage of the proximity of the acidic proton-Mo sites at atomic-level. Furthermore, other authors stated that tuning the surface acidity of charged catalyst would balance the aromatization performance and coke resistance for stability enhancement.[27] Thus, the strong Lewis and Brönsted acidity of Ag/H-ZSM-5 would be closely related to its good catalytic performance towards aromatization

In our case, as stated from NH_3 microcalorimetry, such stronger acid sites would be occupied by Re ions that would condition Mo location and therefore favour the

interaction with these acid sites. This fact would be associated to the particular ethane evolution observed (**Figure 2**).

5.3.4. Temperature-programmed reduction

Figure 8 depicts the TPR profiles obtained for the samples. As we have extensively discussed above, 4%Mo/H-ZSM-5 sample showed a complex TPR profile.[28,29]

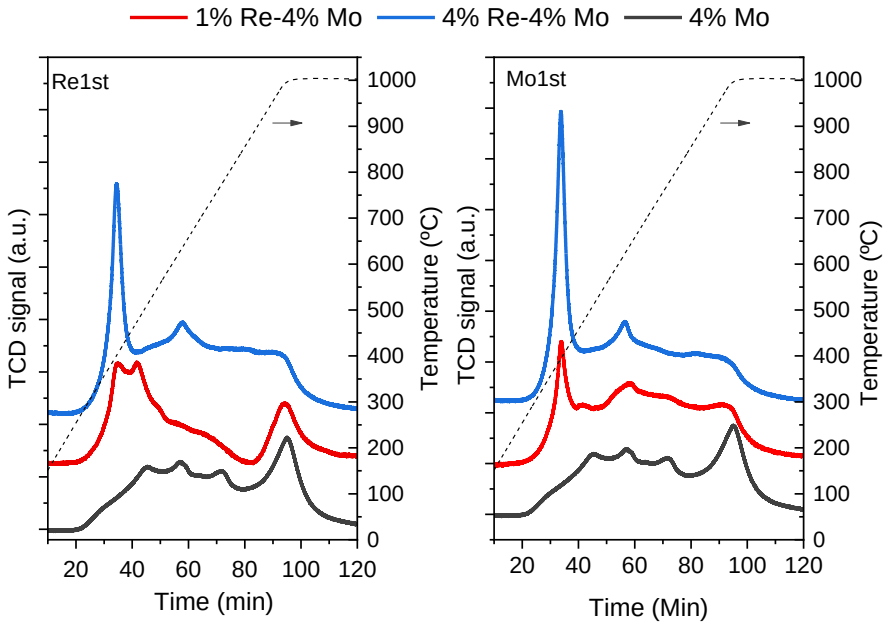

Figure 8. TPR profiles of monometallic 4%Mo/H-ZSM-5, and bimetallic Re-Mo/H-ZSM-5 catalysts from both series.

Such complexity that is denoted from TPR profile renders quite difficult the identification of the active site for this reaction.[30] In this sense, Kosinov *et al*. concluded that MoC_x species inside zeolite channels are the active sites, whereas MoC_x particles on the zeolite outer surface are "spectators" that only produce coke.[1] However, later they reassigned the active sites from MoC_x to single Mo atoms, which shows the intricacy of this question.[31]

Thus, we proposed the occurrence of different molybdenum oxides species, that changed as the metal loading increases. Essentially, we reported four main reduction

processes for this monometallic Mo sample (whose reducing processes peaked are at 510 °C, 615 °C, 755 °C and 1000 °C), showing the high heterogeneity of the chemical states of molybdenum supported on zeolite. However, Re reduction is much simpler and only one defined reduction peak is observed at ca. 400 °C (**Figure 9**).

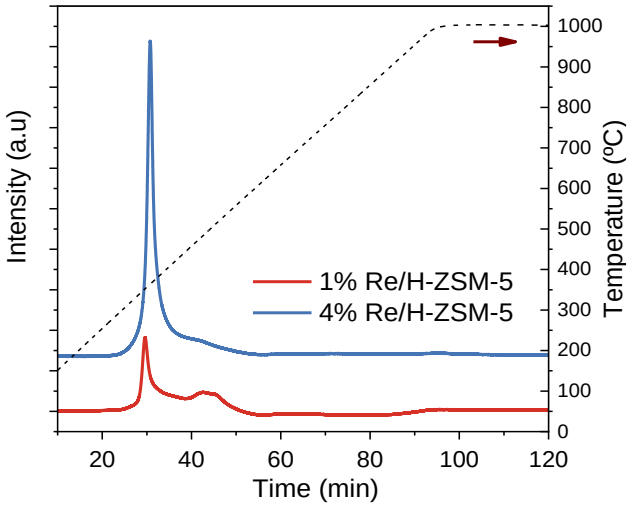

Figure 9. TPR profiles of monometallic 1%Re/H-ZSM-5 and 4%Re/H-ZSM-5 reference catalysts.

In the case of bimetallic catalysts, the reduction profile is quite different from monometallic references and cannot be represented as the sum of both profiles. This fact would point out that certain Mo-Re interaction is present. Such assumption would also be in agreement with the particular evolution of surface feature discussed above (**Figure 5**). Moreover, particularly for 1%Re-4%Mo systems, it appears that metal introduction sequence also affects to the reduction profile. Thus, this catalyst from Re1st series (**Figure 8**), the sharp peak associated to Re reduction appears shifted to a slightly higher temperature with lower intensity and showing a new notable shoulder. At the same time, most of the reduction peaks associated to Mo appeared in certain extent diminished. This change in the TPR profile would imply a different reorganization of Mo ions in the structure with respect to the monometallic system. As we have previously stated,[28] the highest reduction temperature (ca. 1000 °C) has been associated to small clusters of well-dispersed Mo monomers located at the inner microporous channels of the zeolite. As we have discussed, the role of these species would be similar

to those small clusters of well-dispersed Mo monomers located on the external surface of the zeolite and would show certain activity. Therefore, the diminution of this particular reduction peak would be associated to the presence of Re ions that could avoid in part the insertion and formation of Mo small clusters at these inner sites. However, the observed diminution of these Mo-species seems not to affect notably the catalytic performance for bimetallic systems.

Moreover, the new important reduction process at ca 450 °C together with the partial disappearance of Mo reduction peaks would indicate that Mo is reduced at lower temperatures in the presence of Re. It is worthy to mention that 1%Re-4%Mo/H-ZSM-5 sample from Re1st series showed a more marked different profile with respect to monometallic 4%Mo/H-ZSM-5. Thus, in addition to the identified Mo active sites, new active sites probably associated to Re-Mo entities are expected and would be responsible of the improved performance.

We could infer that main diminution in the TPR profile is attained in the region 800° - 920 °C (**Figure 8**). If we consider the different species described in a previous work, this reduction temperature range would be associated to external located bulk MoO_3. From HAADF images we unequivocally showed that these species would be supported on aluminium oxide segregated from the zeolite network and would be responsible of the heavy coke formation.[28] The particular modifications observed in this sample were not so marked for the same catalyst in the Mo1st series (**Figure 8**); so the different sequential deposition clearly induces a different structural situation. For this series, it seems that the TPR peak that appeared more affected was that at higher temperature. Thus, reduction peak has been associated to the well dispersed Mo-monomers located at the inner micropores with strong interaction with the support. The diminution of this reduction peak in this series would point out that upon Re incorporation these Mo species would diffuse to other positions, becoming easily reducible.

In the case of 4%Re-4%Mo catalysts, the TPR profiles do not show important differences between both series. It is worthy to note that in spite of the higher Re loading with respect to 1%Re-4%Mo catalysts the low temperature peak in principle associated to Re reduction appears with similar intensity as in the case of 1%Re-4%Mo catalysts. This fact would denote that the reduction would not be complete.

If we consider the metal content for both series (**Table 1**), it is worthy to note that while Mo content appears in all cases close to the nominal one, in the case of Re it can be noticed that for Re1st series the metal content is lower. This fact could be related with the high mobility of Re previously mentioned. Indeed, it has been reported that Re_2O_7 sublimation would occur at 250 °C.[32] This fact has been used for achieving stable Re-oxo species grafted on zeolite precursors via Re_2O_7 reactions with OH groups.[25] That issue has been pointed out from surface acidity discussion.

Catalysts	Re wt% *	Mo wt% *	µmol H_2/mg_{cat}	Average reduction %
4%Mo	---	4.2	1.16	88
1%Re	1.3	---	0.23	93
4%Re	3.6	---	0.66	97
1%Re-4%Mo (Re1st)	0.8	4.2	0.98	67
4%Re-4%Mo (Re1st)	2.3	3.8	1.43	91
1%Re-4%Mo (Mo1st)	1.2	3.8	1.25	99
4%Re-4%Mo (Mo1st)	3.0	3.8	1.36	81

* *Metal content from ICP analysis*.

Table 1. Metal content, H_2 consumption from TPR and oxidation state variation for Re-Mo/H-ZSM-5 from both series.

Indeed, for Re1st series the second calcination after Mo impregnation would provoke certain metal sublimation that lead to the slight metal loading diminution. Moreover, this process would explain that inner micropores that initially were blocked became free

after the second calcination due to the migration toward the external surface. Such high mobility of Re ions would play an important role in the explanation of TPR profiles above discussed.

From H_2 consumption and considering the metal content observed from ICP, we have also calculated the variation in the oxidation state for supported metals (**Table 1**). In the case of monometallic samples, the obtained reduction degree for each catalyst highlight that after TPR treatment, metal ions were fully reduced from 6+ and 7+ oxidation state for Mo and Re monometallic catalysts respectively.

Additionally, by observing the reduction degree for the bimetallic systems it is clear that 1%Re-4%Mo/H-ZSM-5 from Re1st series would show a particular behaviour. For this catalyst, a fraction of the metal content would remain partially oxidized (67 % of ions are reduced). This would clearly imply the coexistence of Re-Mo species that are stabilized in a partial oxidized state. Such behaviour is not observed in the similar catalyst from Mo1st series or even for 4%Re-4%Mo catalysts. Therefore, the order in the sequential incorporation notably condition the final structural and chemical situation of metals.

5.3.5. X-ray photoelectron spectroscopy

In **Figure 9** we show the XPS Mo *3d* and Re *4f* spectra for all samples after soft oxidation at 250°C. The binding energy for Mo $3d_{5/2}$ in 4%Mo/H-ZSM-5 is located at 233.3 eV, which has been reported for Mo^{6+} in MoO_3.[33,34]

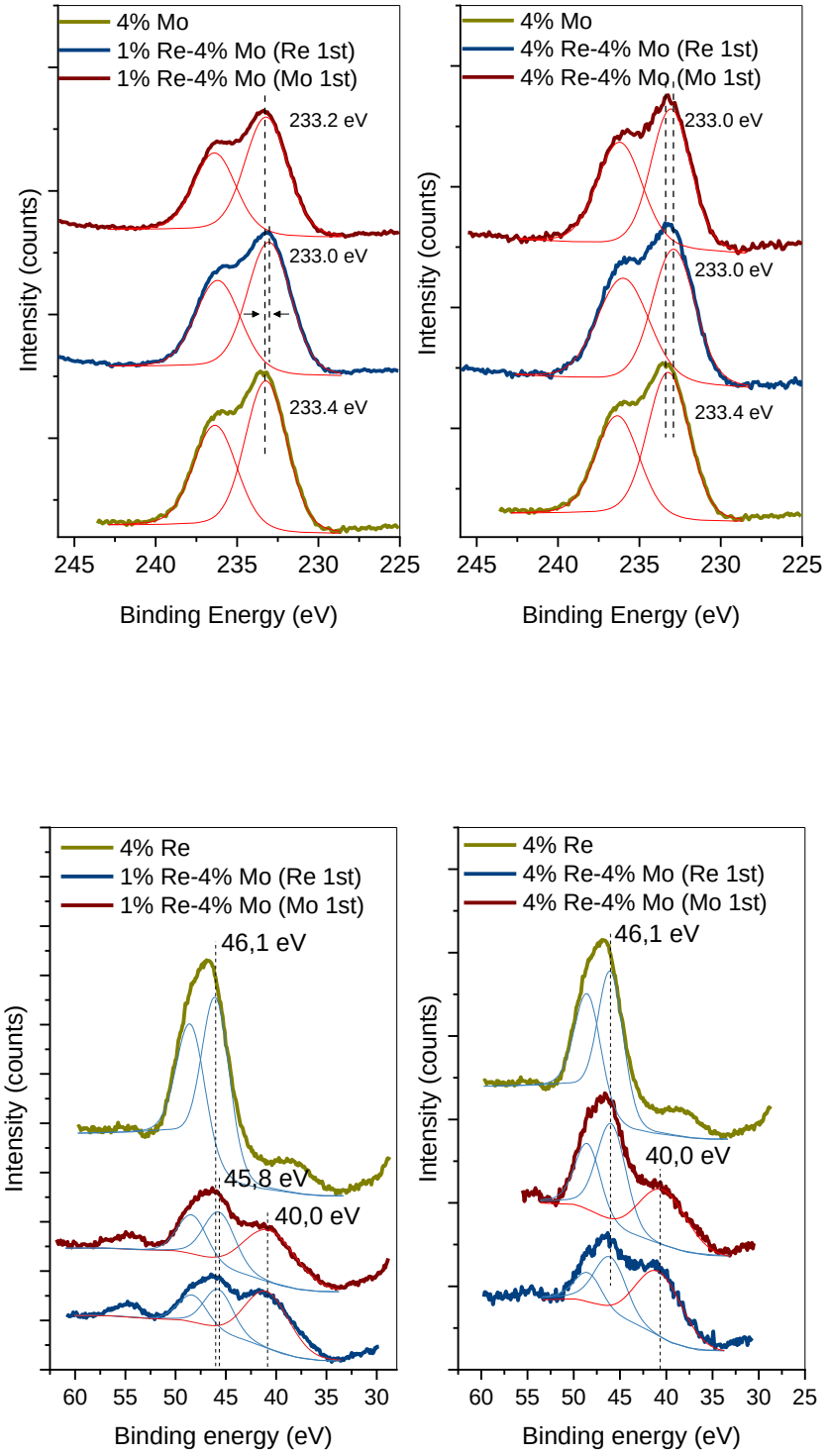

Figure 9. XPS Mo *3d* and Re *4f* core-level spectra for monometallic and bimetallic Mo-Re/H-ZSM-5 catalysts after soft oxidation at 250 °C.

For the 4%Re/H-ZSM-5 catalyst, the observed binding energy for Re $4f_{7/2}$ level was 46.1 eV, which is in accordance with values associated to Re^{7+}.[35] In the case of bimetallic 1%Re-4%Mo/H-ZSM-5catalysts, Mo *3d* and Re *4f* bands show a slight shift toward lower binding energy values. Such small shift would point out a strong interaction with Re. Indeed, as previously discussed above from TPR experiments we have denoted a different reduction profile and a lower reduction degree in the case of Re1st series. Additionally, from BET surface area and acidity measurements we also pointed out such possibility. Thus, when rhenium is present it can be assumed that Mo and Re form a new entity in close interaction.

Catalyst	Mo $3d_{5/2}$ (eV)	Re $4f_{7/2}$ (eV)	Mo/Si* ratio	Re/Si** ratio	Re/Mo ratio
4%Mo	233.3	---	0.061	---	---
4%Re	---	46.0	---	0.013	---
1%Re-4%Mo (Re1st)	233.0	46.0	0.050	0.004	0.08
4%Re-4%Mo (Re1st)	233.2	46.0	0.059	0.007	0.12
1%Re-4%Mo (Mo1st)	233.0	46.0	0.044	0.005	0.11
4%Re-4%Mo (Mo1st)	233.0	46.0	0.055	0.012	0.22

* *calculated from Mo 3d*

** *calculated from Re 4f*

Table 2. XPS binding energies for Mo $3d_{5/2}$ and Re $4f_{7/2}$ levels and surface atomic ratio for monometallic and bimetallic Re-Mo/H-ZSM-5 catalysts.

If we consider the surface composition (**Table 2**), it can be noticed that in the case of Mo similar Mo/Si ratios have obtained for all catalysts, being in all cases close to Mo content in the monometallic one. However, for rhenium the surface content for 4%Re-4%Mo in the Re1st series lies markedly below the reference value of monometallic one (0.013 vs 0.007 for 4%Re/H-ZSM-5 and 4%Re-4%Mo/H-ZSM-5 Re1st, respectively). The observed differences could be related in principle to a different surface content probably due to a certain loss of Re during second calcination but more importantly to a different distribution of rhenium ions due to the second calcination treatment.

In order to confirm the above behaviour, we have studied the evolution of the surface during reduction treatment. The results obtained by *in-situ* XPS study of the reduction process of the monometallic (4%Mo/H-ZSM-5 and 4%Re/H-ZSM-5) and bimetallic catalysts from both series are shown in **Figure 10.**

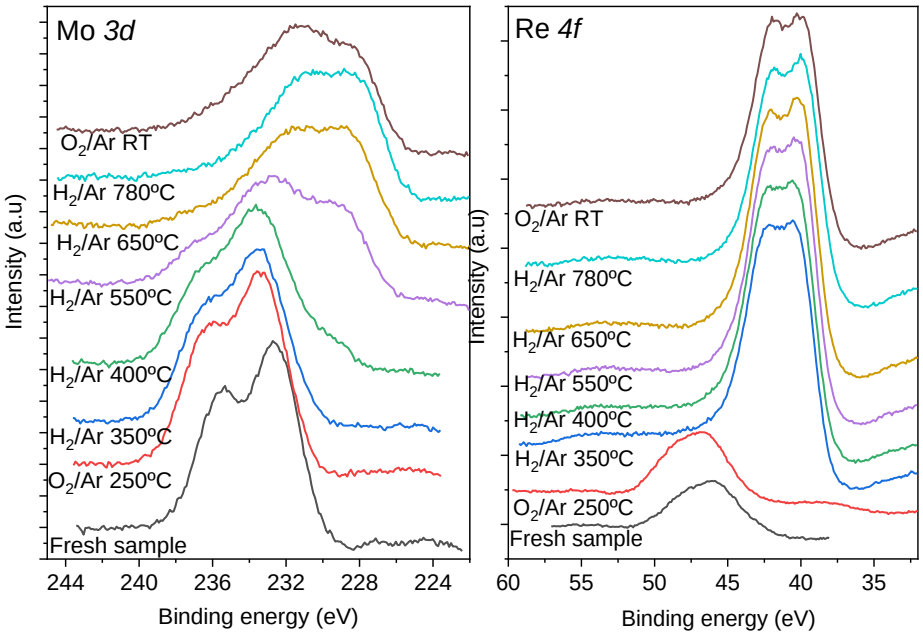

Figure 10. Mo *3d* and Re *4f* regions XPS spectra for the 4% Mo/H-ZSM-5 and 4% Re/H-ZSM-5 monometallic catalyst calcined and after *in-situ* reduction treatment.

The Mo *3d* and Re *4f* regions spectra obtained along different reduction treatments of the monometallic 4%Mo/H-ZSM-5and 4%Re/H-ZSM5 systems have been represented. As previously indicated, for Mo system the only oxidation state present after evacuation pretreatment in O_2 is Mo^{6+}. Upon reduction, the Mo *3d* peak doublet becomes less defined pointing out the co-existence of other species as it was stated from the complex TPR profile. Just after reduction at 650 °C, the Mo *3d* peak becomes wider and clearly shifted to lower binding energy (being Mo $3d_{5/2}$ at ca. 228.0 eV) denoting that surface Mo is almost reduced to Mo^0 (**Table 2**). Therefore, it can be said that at this temperature all Mo species at the surface got reduced. On the other hand, regarding to 4%Re/H-ZSM-5, after calcination the wide peak located at ca 46.1 eV would denote that the main oxidation state is 7+ (**Figure 9**). As observed from TPR, total reduction is achieved at a

significantly lower temperature. Indeed, after reduction treatment at 350 °C the Re $4f_{7/2}$ peak at 40 eV clearly points out the complete reduction of Re. It is also worthy to note that the intensity of this peak is notably higher than that for calcined sample. Thus, it is evidenced that upon reduction a notable Re surface enrichment is taking place (**Figure 10**).

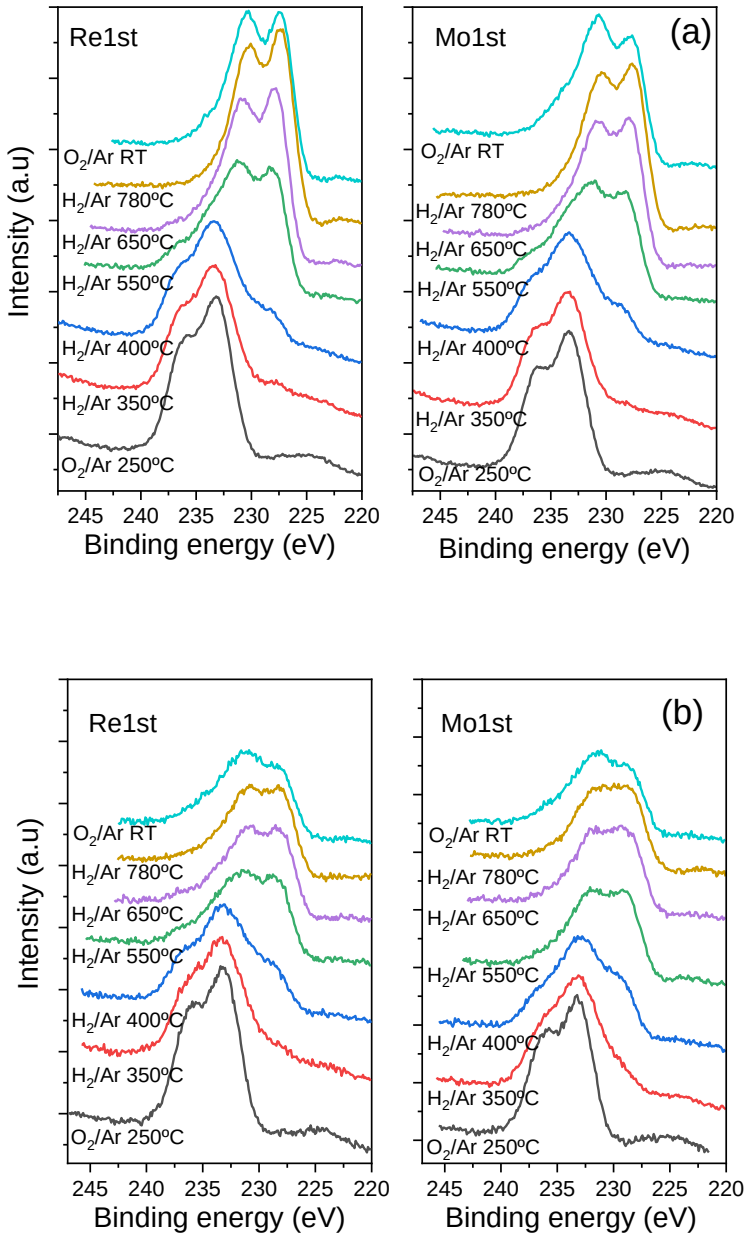

Figure 11. Mo *3d* region XPS spectra for 1%Re-4%Mo/H-ZSM-5catalysts (a) and 4%Re-4%Mo/H-ZSM-5 catalysts (b) from both series calcined and after *in-situ* reduction.

The evolution of Re-Mo bimetallic catalysts upon reduction is shown in **Figure 11** and **Figure 12**. In the case of molybdenum, 1%Re-4%Mo and 4%Re-4%Mo catalysts follow similar reduction evolution within each different series (**Figure 10** and **Figure 11**). Mo reduction is taking place in both series at lightly lower temperature with respect to that observed for Mo-monometallic catalyst. Irrespective of the Re amount or addition sequence, contributions of reduced Mo species can be seen at 400 °C. On the other hand, in the case of Re almost complete reduction is achieved upon treatment at 350 °C, which agrees with the behaviour observed for monometallic Re catalyst.

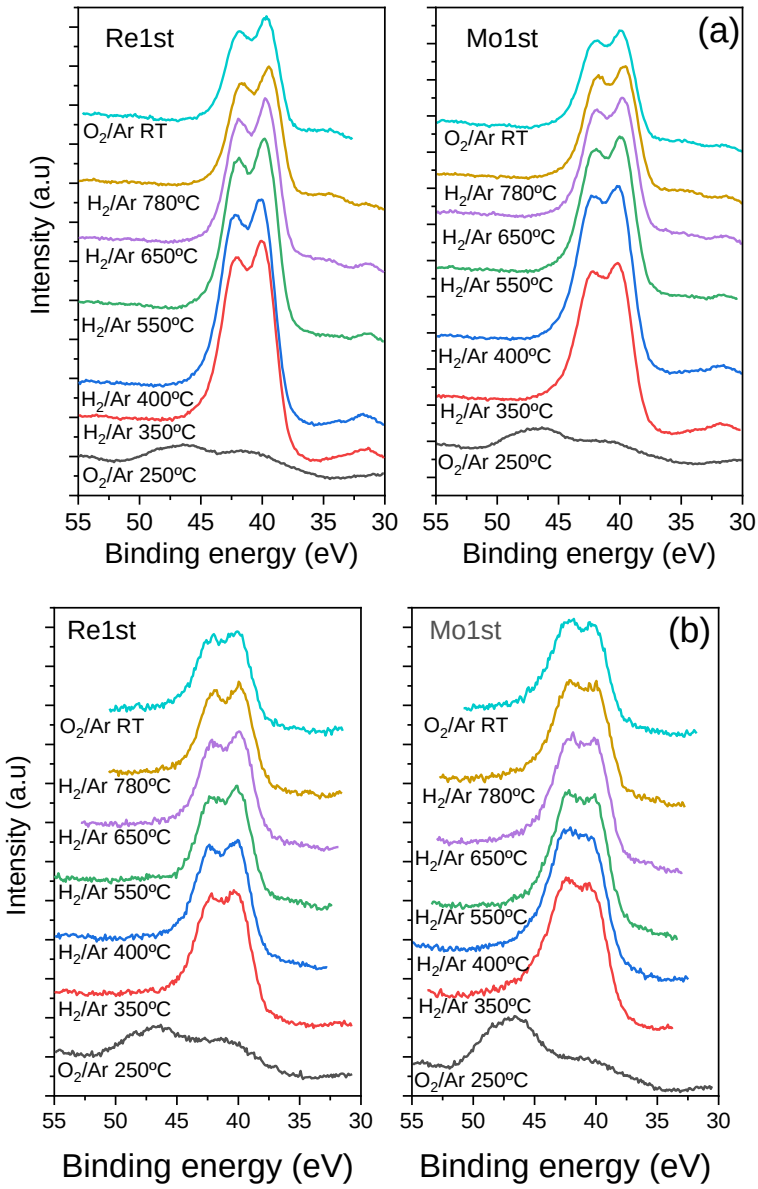

Figure 12. Re *4f* region XPS spectra for 1%Re-4%Mo/H-ZSM-5 catalyst (a) and 4%Re-4%Mo/H-ZSM-5 catalyst (b) from both series calcined and after *in-situ* reduction.

As previously pointed out for monometallic systems, an important Re enrichment can be also observed in these bimetallic systems. In **Figure 13** we have plotted the evolution of Re/Si and Mo/Si ratios for all catalyst along the reduction treatment.

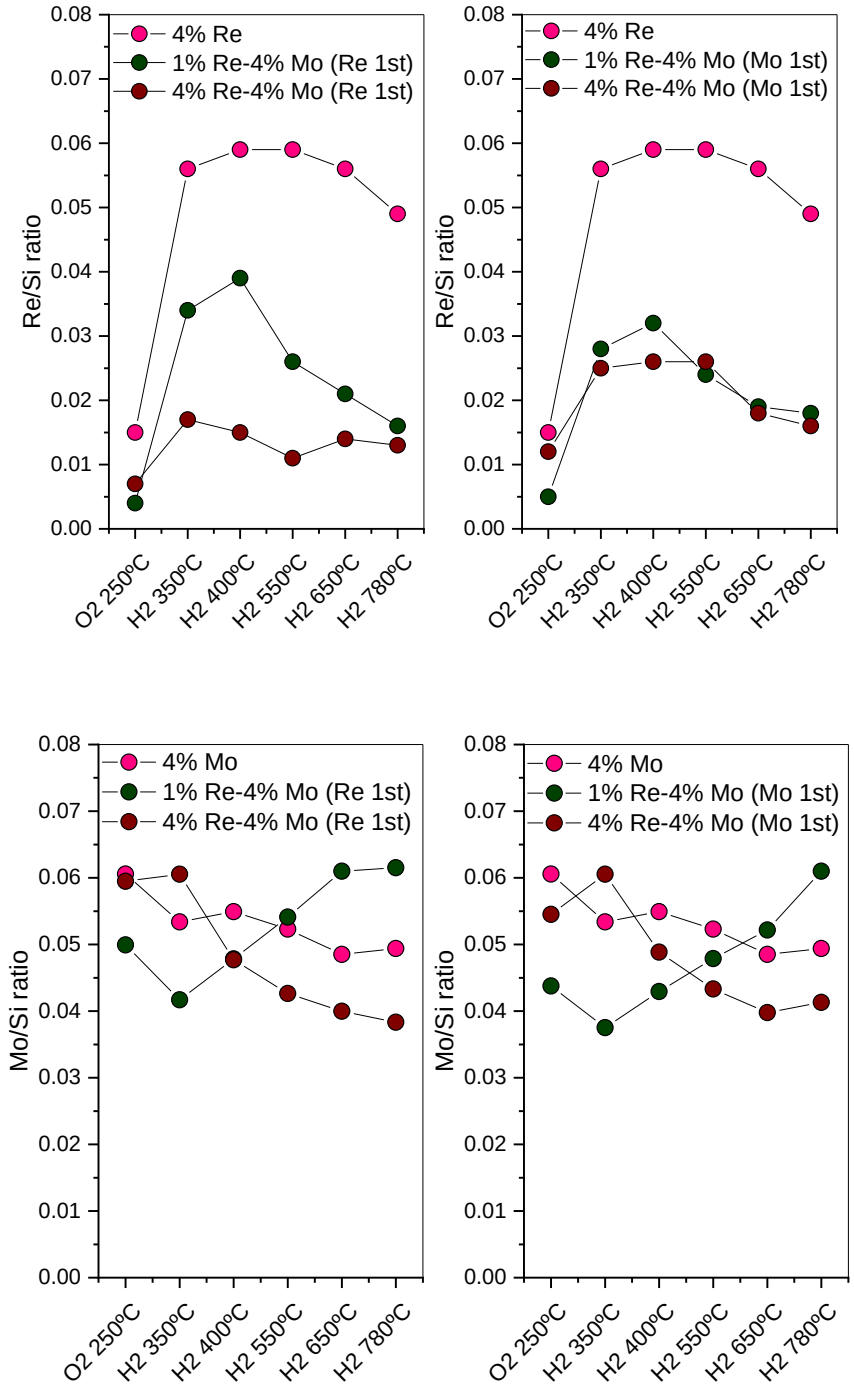

Figure 13. Evolution of the Re/Si and Mo/Si surface ratios upon reduction treatment.

As a general trend we can state that surface Re/Si ratio seems to increase in the first stage of reduction treatment, after which starts to decay. This would point out that after the first surface enrichment, a slight loss of Re by sublimation, or even certain aggregation forming higher size clusters, occurs.

On the contrary, for Mo/Si ratio more stable evolution is attained though certain slight decrease can be observable for monometallic catalyst and more markedly for 4%Re-4%Mo bimetallic catalyst. It is worthy to note that for 1%Re-4%Mo the evolution is the opposite, as Mo/Si surface ratio exhibits a progressive increase. This would indicate that Mo clusters could be dispersed upon reduction in the presence of Re. From these results it is clear that the surface follows a complex evolution during reduction at different temperatures and that the presence of Re would strongly affect to the behaviour of Mo upon reaction conditions denoting the observed strong interaction of both metals.

Thus, Mo would show certain dispersion/enrichment for 1%Re-4%Mo/H-ZSM-5 while would suffer aggregation as reduction temperature increases for 4%Re-4%Mo. This later aggregation would be associated to the formation of Mo-Re species as was discussed from TPR results.

All this particular structural surface and chemical features showed by bimetallic Re-Mo with respect to monometallic Mo system that has been widely discussed along this study could be correlated with the different catalytic behaviour observed for bimetallic catalysts, particularly with low Re content. Within this context, the sequential impregnation would also play an important role, unblocking inner micropores during second calcination and favouring a close Re-Mo interaction that would lead to Re-Mo stabilized against reduction.

5.4. Conclusions

The incorporation of rhenium as co-dopant to the Mo/H-ZSM-5 catalyst have showed a notable improvement in the *MDA* reaction, as it is shown in **Figure 14**. Benzene and aromatics yields for bimetallic systems appeared significantly enhanced. Moreover, the catalytic performance of bimetallic systems is clearly affected by the sequence addition of metals. Thus, best catalytic behaviour has been attained for 1%Re-4%Mo/H-ZSM-5in which Re has been firstly deposited (Re1st series).

Due to the high mobility of Re ions, for the Re1st series Re would undergo a particular evolution that conditions the further Mo incorporation. This fact has been stated through the wide surface and structural characterization of the systems. Based on these results, we evidenced that Re ions would be preferentially located at strong acid sites. This fact modifies also the state of Mo species, which showed a close interaction with Re entities. As a result, the C-C coupling step would be favoured which seems to be the responsible of the catalytic performance improvement. Indeed, as we have evidenced, the formation of ethylene is similar for all systems and therefore seems not to be related with the presence of Re. Thus, the higher aromatics yield would be directly related to the higher ethane formation.

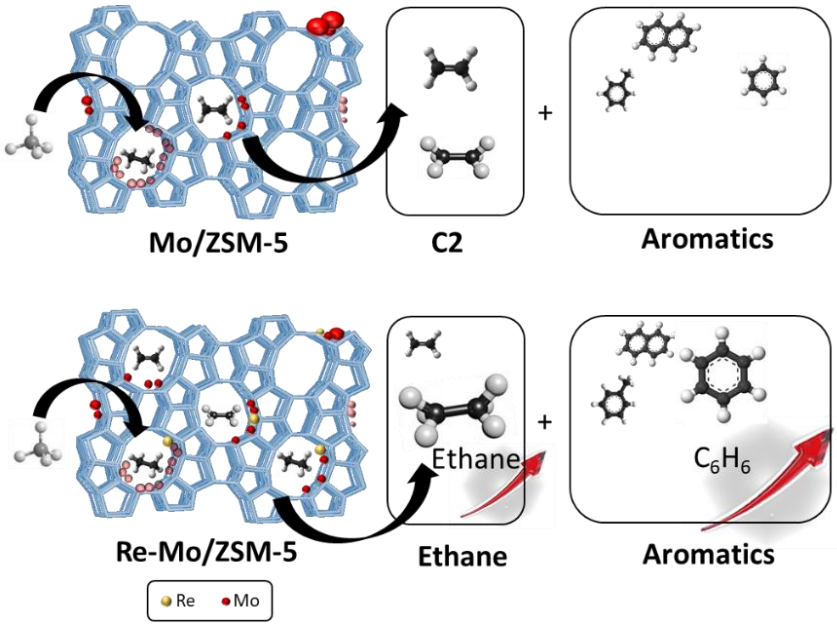

Figure 14. Representation of the Re-Mo/H-ZSM-5 catalytic activity improvement.

5.5. References

1. Kosinov, N. *et al.* Structure and Evolution of Confined Carbon Species during Methane Dehydroaromatization over Mo/ZSM-5. *ACS Catal.* **8**, 8459–8467 (2018).

2. Han, S. J. *et al.* Non-oxidative dehydroaromatization of methane over Mo/H-ZSM-5 catalysts: A detailed analysis of the reaction-regeneration cycle. *Appl. Catal. B Environ.* **241**, 305–318 (2019).

3. Tempelman, C. H. L. & Hensen, E. J. M. On the deactivation of Mo/HZSM-5 in the methane dehydroaromatization reaction. *Appl. Catal. B Environ.* **176–177**, 731–739 (2015).

4. Gu, Y. *et al.* Coking mechanism of Mo/ZSM-5 catalyst in methane dehydroaromatization. *Appl. Catal. A Gen.* **613**, (2021).

5. Menon, U., Rahman, M. & Khatib, S. J. A critical literature review of the advances in methane dehydroaromatization over multifunctional metal-promoted zeolite catalysts. *Appl. Catal. A Gen.* **608**, 117870 (2020).

6. Tshabalala, T. E., Coville, N. J. & Scurrell, M. S. Applied Catalysis A : General Dehydroaromatization of methane over doped Pt / Mo / H-ZSM-5 zeolite catalysts : The promotional effect of tin. *"Applied Catal. A, Gen.* **485**, 238–244 (2014).

7. Abdelsayed, V., Shekhawat, D. & Smith, M. W. Effect of Fe and Zn promoters on Mo/HZSM-5 catalyst for methane dehydroaromatization. *Fuel* **139**, 401–410 (2015).

8. Zhang, Y. *et al.* Promotional Effects of In on Non-Oxidative Methane Transformation Over Mo-ZSM-5. *Catal. Letters* **146**, 1903–1909 (2016).

9. Sridhar, A. *et al.* Bimetallic Mo-Co/ZSM-5 and Mo-Ni/ZSM-5 catalysts for methane dehydroaromatization: A study of the effect of pretreatment and metal loadings on the catalytic behavior. *Appl. Catal. A Gen.* **589**, 117247 (2020).

10. Schwach, P., Pan, X. & Bao, X. Direct Conversion of Methane to Value-Added Chemicals over Heterogeneous Catalysts: Challenges and Prospects. *Chem. Rev.* **117**, 8497–8520 (2017).

11. Shen, L., Tesfaye, F., Li, X., Lindberg, D. & Taskinen, P. Review of rhenium extraction and recycling technologies from primary and secondary resources. *Miner. Eng.* **161**, 106719 (2021).

12. Polyak, D. E. 2017 Minerals Yearbook - Rhenium. 62.1-62.6 (2020).

13. Argimbaev, K., Ligotsky, D. & Loginov, E. Current state of production and consumption of rhenium abroad. *E3S Web Conf.* **258**, (2021).

14. Ryashentseva, M. A. & Minachev, K. M. Catalytic Properties of Rhenium and Its Compounds. *Russ. Chem. Rev.* **38**, 944–956 (1969).

15. Davenport, W. H. Letters: Advances in Rhenium Catalysts. *Ind. Eng. Chem.* **61**, 9 (1969).

16. DS Kim, I. W. Surface rhenium oxide-support interaction for supported Re2O7 catalysts. *J. Catal.* **141**, 419–429 (1993).

17. Mol, J. C. & Moulijn, J. A. The Metathesis of Unsaturated H y d roca r b o n s Ca ta I yze d by Tra nsi ti on Metal Compounds. *Adv. Catal.* **24**, 131–175 (1975).

18. Krogh, A., Hagen, A., Hansen, T. W., Christensen, C. H. & Schmidt, I. Re/HZSM-5: A new catalyst for ethane aromatization with improved stability. *Catal. Commun.* **4**, 627–630 (2003).

19. Solymosi, F. & Tolmacsov, P. Conversion of Ethane into Benzene on Re/ZSM-5. *Catal. Letters* **93**, 7–11 (2004).

20. Sridhar, A., Rahman, M. & Khatib, S. J. Enhancement of Molybdenum/ZSM-5 Catalysts in Methane Aromatization by the Addition of Iron Promoters and by Reduction/Carburization Pretreatment. *ChemCatChem* **10**, 2571–2583 (2018).

21. Galadima, A. & Muraza, O. Advances in Catalyst Design for the Conversion of Methane to Aromatics: A Critical Review. *Catal. Surv. from Asia* **23**, 149–170 (2019).

22. Vollmer, I., Abou-Hamad, E., Gascon, J. & Kapteijn, F. Aromatization of Ethylene – Main Intermediate for MDA? *ChemCatChem* **12**, 544–549 (2020).

23. Razdan, N. K., Kumar, A., Foley, B. L. & Bhan, A. Influence of ethylene and acetylene on the rate and reversibility of methane dehydroaromatization on Mo/H-ZSM-5 catalysts. *J. Catal.* **381**, 261–270 (2020).

24. Kosinov, N. *et al.* Stable Mo/HZSM-5 methane dehydroaromatization catalysts optimized for high-temperature calcination-regeneration. *J. Catal.* **346**, 125–133 (2017).

25. Lacheen, H. S., Cordeiro, P. J. & Iglesia, E. Structure and catalytic function of Re-oxo species grafted onto H-MFI zeolite by sublimation of Re2O7. *J. Am. Chem. Soc.* **128**, 15082–15083 (2006).

26. Gao, W. *et al.* Dual Active Sites on Molybdenum/ZSM-5 Catalyst for Methane Dehydroaromatization: Insights from Solid-State NMR Spectroscopy. *Angew. Chemie - Int. Ed.* **60**, 10709–10715 (2021).

27. Wang, A. *et al.* Catalytic co-aromatization of ethanol and methane. *Appl. Catal. B Environ.* **198**, 480–492 (2016).

28. López-Martín, A., Caballero, A. & Colón, G. Structural and surface considerations on Mo/ZSM-5 systems for methane dehydroaromatization reaction. *Mol. Catal.* **486**, 110787 (2020).

29. López-Martín, Á., Platero, F., Colón, G. & Caballero, A. Elucidating the nature of Mo species on ZSM-5 and its role in the methane aromatization reaction. *React. Chem. Eng.* (2021). doi:10.1039/d1re00044f

30. Wang, N. *et al.* Probing the Catalytic Active Sites of Mo/HZSM-5 and Their Deactivation during Methane Dehydroaromatization. *Cell Reports Phys. Sci.* **2**, 100309 (2021).

31. Kosinov, N. *et al.* Confined Carbon Mediating Dehydroaromatization of Methane over Mo/ZSM-5. *Angew. Chemie - Int. Ed.* **57**, 1016–1020 (2018).

32. Otsuka, T. *et al.* Effects of rhenium contents on oxidation behaviors of tungsten-

rhenium alloys in the oxygen gas atmosphere at 873 K. *Nucl. Mater. Energy* **25**, 100791 (2020).

33. Choi, J. G. & Thompson, L. T. XPS study of as-prepared and reduced molybdenum oxides. *Appl. Surf. Sci.* **93**, 143–149 (1996).

34. Schroeder, T., Zegenhagen, J., Magg, N., Immaraporn, B. & Freund, H. J. Formation of a faceted MoO2 epilayer on Mo(1 1 2) studied by XPS, UPS and STM. *Surf. Sci.* **552**, 85–97 (2004).

35. Kuznetsov, V. V., Gamburg, Y. D., Zhulikov, V. V., Batalov, R. S. & Filatova, E. A. Re–Ni cathodes obtained by electrodeposition as a promising electrode material for hydrogen evolution reaction in alkaline solutions. *Electrochim. Acta* **317**, 358–366 (2019).

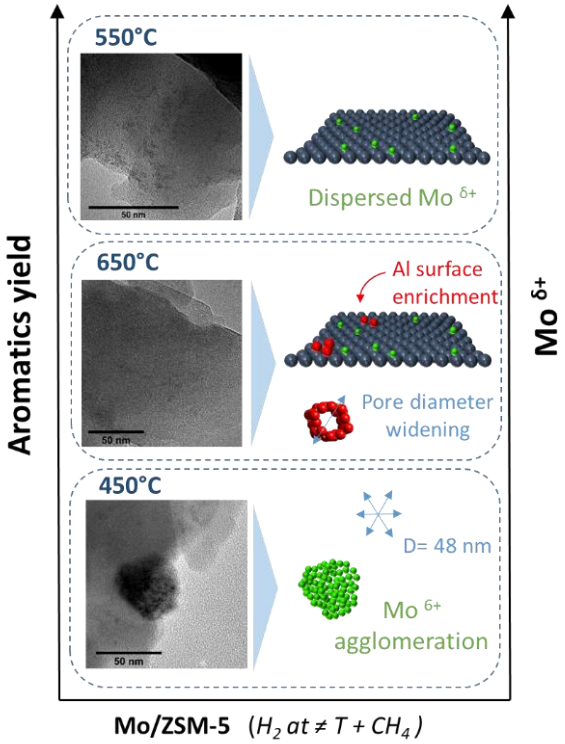

Chapter 6. On the effect of the catalyst reduction pre-treatment on *MDA* reaction

In this chapter a reduction pre-treatment was performed over 4%Mo/H-ZSM-5 system at different temperatures before methane dehydroaromatization reaction. We have stated the crucial effect of reduction temperature on the final catalytic performance. Outstanding improvement in the aromatics conversion has been attained. Thus, H_2 formation form methane cracking reaction seems to be hindered for pre-treated catalysts. As a consequence, the deposition of coke in these samples appeared also notably suppressed. The optimum performance has been achieved for reduction pretreatment at 550 ˚C. For this temperature, we have observed that the fraction of reduced Mo species is higher.

6.1. Introduction

Given the short lifetime of *MDA* catalysts, different strategies to decrease the coking rate have been investigated over the last few decades. In an attempt to achieve this, the effect that the incorporation of a pre-reaction stage has on catalytic behaviour has been studied.

The effect of pretreatment condition on the activity of Mo/H-ZSM-5 catalysts for *MDA* reaction to aromatics was first investigated in 1997 by Wang *et al*. They showed how catalyst pretreatment under air atmosphere at high temperature led to an increase in the pore size and a decrease in methane conversion and activity maintenance. However, stabilizing the catalysts under an atmosphere of methane it was possible to form a new Mo phase which promoted the production of aromatics.[1]

Three years later, Bouchy *et al*. identified two forms of molybdenum carbide: the stable hexagonally close packed (hcp) and the metastable face centered cubic (fcc). The last one could be prepared by controlled pre-activation in hydrogen of MoO_3 and showed superior performance.[2] According to these results, other groups tried to transform Mo species from hexagonally close packing (hcp) to face-centered cubic (fcc) structures by H_2 pre-treatments at 350 °C.[3]

In this sense, Tempelman *et al.* reported that the effect of pre-reduction of Mo/H-ZSM-5 at 700 ˚C under inert (He), oxidizing (artificial air), or carburizing (CH_4/He mixture) atmospheres.[4] Thus, they argued that precarburization in methane gave catalysts with the highest aromatic selectivities and the lowest rates of catalyst deactivation. The more rapid formation of molybdenum carbides during methane pretreatment decreased the amount of mobile molybdenum oxide species and their diffusion into the micropores.

Similarly, Portilla *et al.* showed that the optimum Mo speciation was achieved by pretreatment at increasing temperature under N_2 flow.[5,6]

Already in 2018, the influence of different types of pretreatment on Fe-Mo/ZSM-5 catalyst systems were studied for methane aromatization. The results showed that pre-carburized catalysts were more stable due to the formation of smaller amounts of carbon deposits, and consequently lower pore blockage.[7]

Recently, Tan *et al.* published a work where they probed how Mo/H-ZSM-5 catalyst with Mo loading higher than 10 wt% improved the catalytic activity and stability after pretreatment with a CH_4/Ar/He gas mixture.[8] These conclusions were corroborated for other studies, which showed how H_2 pretreatment prior to methane activation improved the catalyst activity with increase in Mo loading and reduced the induction time on benzene formation.[9] Sridhar *et al.* published a study about *MDA* reaction using Co and Ni as additives on Mo/ZSM-5 catalyst. They found how a synergy effect between Mo and the additives appeared when the catalyst was exposed to a reduction/carburization pretreatment. They suggested this effect was due to the reduction of the Al extraction from the ZSM-5 framework, and also because of the interaction Mo-additives prevented Mo aggregation in reaction and modified the reducibility of the Mo sites.[10]

In this chapter, we study the effect of the incorporation of a pre-reduction stage has on the final catalytic performance of 4%Mo/H-ZSM-5 on *MDA* reaction. We discuss in depth how the different reduction temperature affects to the catalyst structural, chemical and morphological features that drastically conditions the final performance.

6.2. Catalysts characterization and performance

6.2.1. Catalytic activity

As usual, the catalysts were tested in a fixed-bed stainless steel tube reactor with 0.1 g of different catalysts diluted in 0.1 g of SiC and located between two quartz wool plugs. Methane dehydroaromatization reaction was performed under pure CH_4 /N_2 (85 %, 5ml/min), from 50 ˚C to at 700 °C with a 10 °C temperature ramp. Obtained products were analysed by using online GC (Agilent, 7890B) equipped with 3 channels for separate analyses of light gases (HAYESEP Q precolumn, MolSieve 5Å column, thermal

conductivity detector, TCD), light hydrocarbons (GS-GASPRO column, flame ionization detector, FID) and aromatics (HP-88, flame ionization detector, FID).

Alternatively, pre-reduction treatment at different temperatures were performed before reaction. For reduction treatment, pure H_2 was flown at 25 mL/min for one hour at temperatures between 450 ˚C and 650 ˚C. After which, the temperature was lowered to 150 ˚C and the flow changed to CH_4/N_2 **(Scheme 1)**.

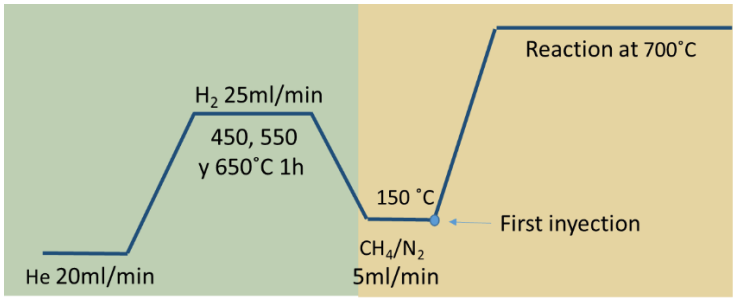

Scheme 1. Pretreatment and reaction scheme followed in this study.

The first important issue to highlight is that the reduction treatment on the catalytic performance strongly depends on the temperature. Obtained initial methane conversions laid in all cases around 10-12 %, which is in accordance to reported thermodynamic equilibrium conversion of methane in this reaction, as it was described in **Chapter 1**.

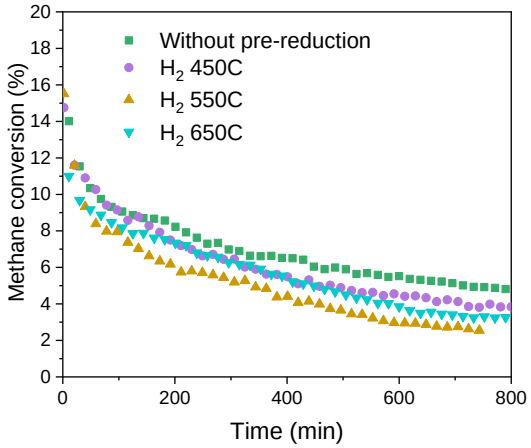

Figure 1. Methane conversion (*left*) and selectivity to C_6H_6 (*right*) for 4%Mo/HZSM-5 without pre-treatment and with reduction pre-treatments at 450, 550 and 650 °C.

Thus, by observing the evolution of conversion values, we evidenced that pre-reduction treatments seem to affect negatively with respect to not pre-treated sample (**Figure 1**). This is due to the contribution of methane cracking in that later sample. Therefore, in order to avoid the important contribution of methane cracking reaction in the methane conversion, we show the conversion to aromatics (**Figure 2**). As we can observe, while reduction at 450 ˚C surprisingly leads to a noteworthy detrimental effect, the reduction at 550 ˚C clearly induces an outstanding improvement. The higher reduction temperature at 650 ˚C does not infer any enhancement with respect to non-pre-treated catalyst.

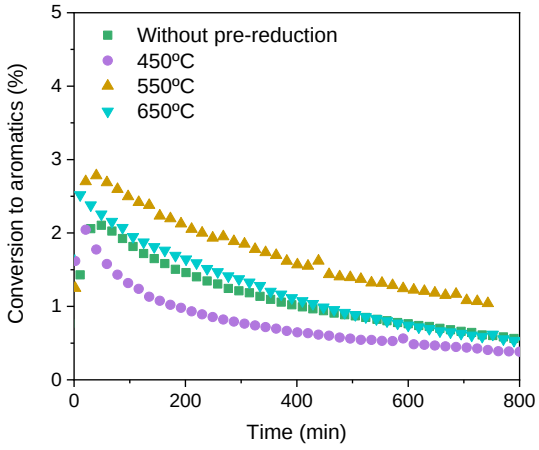

Figure 2. Aromatics conversion plot for 4%Mo/H-ZSM-5 catalysts during methane aromatization reaction.

In **Figure 3** we show the yields to different aromatic products (benzene, naphthalene, and toluene). In all cases, the higher yields are attained for pre-reduction treatment at 550 ˚C.

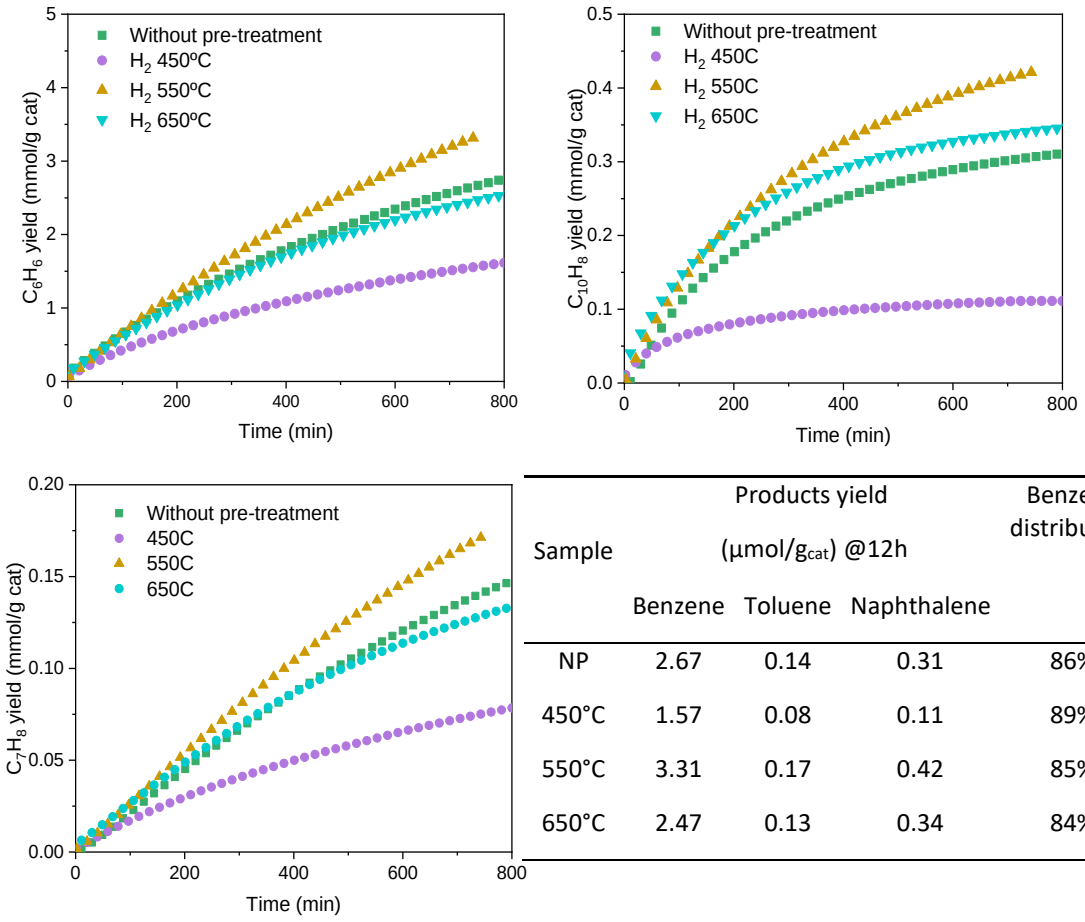

Sample	Products yield (µmol/g_{cat}) @12h			Benzene distribution
	Benzene	Toluene	Naphthalene	
NP	2.67	0.14	0.31	86%
450°C	1.57	0.08	0.11	89%
550°C	3.31	0.17	0.42	85%
650°C	2.47	0.13	0.34	84%

Figure 3. Aromatic products yield and product distribution table for 4% Mo/H-ZSM-5 catalysts during methane aromatization reaction.

Moreover, pre-reduction at 450 ˚C clearly favours the formation of benzene at the expense of naphthalene. In particular, the selectivity to benzene is more stable for 550 ˚C pre-treated catalyst, with values between 62 and 56 % of selectivity to C_6H_6 during the reaction (**Figure 4**).

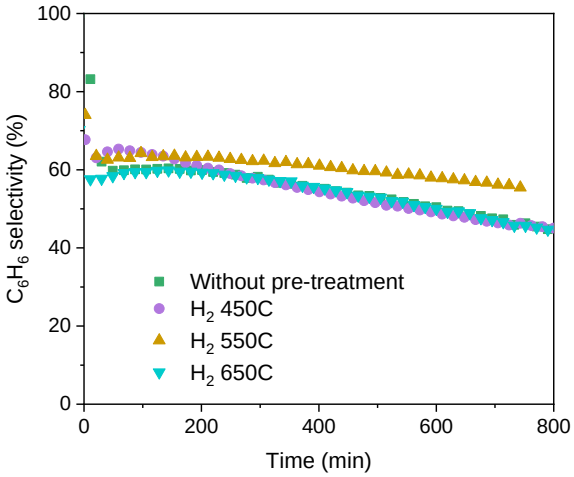

Figure 4. Selectivity to C_6H_6 for 4%Mo/H-ZSM-5without pre-treatment and with reduction pre-treatments at 450, 550 and 650 ˚C.

On the contrary, it is worthy to note the slightly higher formation of naphthalene upon reaction after 550 ˚C and 650 ˚C reduction treatment (**Figure 3**). So, larger conversion to aromatics and greater selectivity is clearly observed in the case of the sample reduced to 550 ˚C.

As it has been widely reported, H_2 and coke formation from methane cracking is an undesirable process that would compete with methane aromatization.[11] Thus, the observation of H_2 production would serve not only as an indication of the dehydrogenation process but also of cracking and therefore catalyst deactivation. Upon these considerations, we may notice that the higher H_2 production is observed for the non-pre-treated catalyst (**Figure 5** (*left*)). For all pre-reduced catalysts, the H_2 evolved is notably lower. As a general trend, the total conversion of methane reaches its maximum at the beginning of the reaction, obtaining values of ca. 16 % in non pre-treated 4%Mo/H-ZSM-5 and slightly smaller conversion values for the pre-treated catalysts. This fact can be understood by considering the lower methane consumption to form coke and hydrogen.

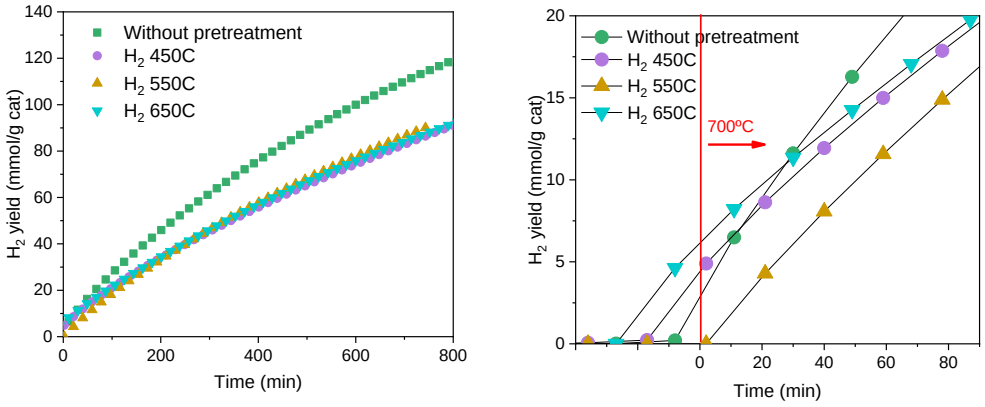

Figure 5. H_2 yields for 4%Mo/H-ZSM-5 catalysts during methane aromatization reaction.

In this sense, pre-reduction treatment clearly conditions the H_2 evolution at the first stage of the reaction pointing out the different reaction pathway during the carbide formation (**Figure 5** (*right*)). It is widely accepted that within the reaction induction period, Mo oxide species are firstly reduced and then carburized to Mo carbide species when exposed to the CH_4 reactant.[12,13] Such new Mo-species are proposed to be responsible for activating CH_4, and the initial C-C bond formation to C_2 species. In the case of pre-reduced catalysts methane would proceed directly to the carburization step leading to a lower H_2 evolution. Additionally, a lower H_2 formation would also indicate a lower contribution of coke formation reaction in the overall methane conversion. Indeed, DTG results obtained for the spent 4%Mo/H-ZSM-5 with and without pre-treatment are represented in **Figure 6**.

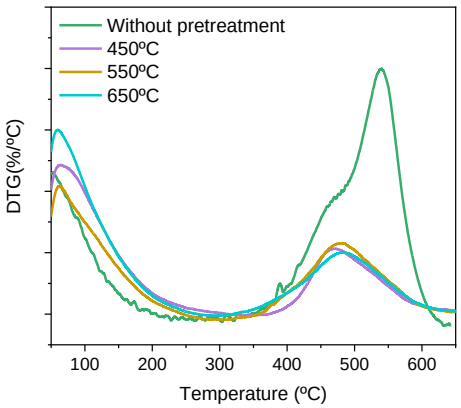

Figure 6. Thermogravimetric analysis of different pre-treated 4%Mo/H-ZSM-5 catalysts after 120 min reaction at 700 ˚C.

Indeed, DTG results obtained for the spent 4%Mo/HZSM-5 with and without pre-treatment confirmed that the amount of coke formed during the different stages are similar for the pre-treated samples, being much smaller than the amount obtained for the sample without pre-treatment. Thus, we could state that heating the catalysts in CH_4 results in the formation of higher amounts of carbon deposition. Finally, we should consider that the lower H_2 observed could also point out a higher participation of coke hydrogenolysis reaction.[14]

On this basis, it is clear that reduction pre-treatment at different temperatures strongly conditions the catalytic behaviour of Mo/H-ZSM-5 catalyst. The 550 ˚C reduction pre-treatment plainly has a different effect on the catalyst performance, which is reflected in a higher conversion, selectivity and production to aromatics. In addition, these catalysts produce a smaller amount of H_2 and coke than the pre-treated catalysts at different reduction temperatures as well as much smaller than the non-treated 4%Mo/H-ZSM-5 catalyst. This fact would do have a positive effect on the catalyst stability for *MDA* reaction.

6.2.2. X-ray powder diffraction.

In order to understand how the catalyst pre-reduction affects to the final catalytic performance we have studied the structural, morphological and chemical state of catalyst. By observing the XRD patterns, different reduction treatments do not affect to the crystalline structure of ZSM-5.

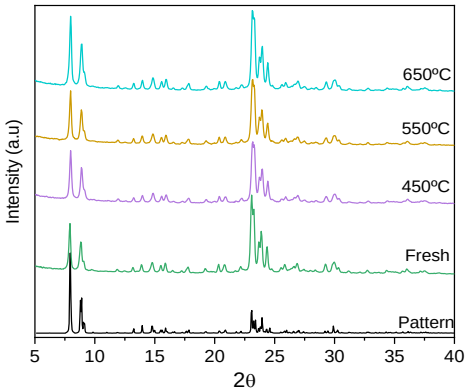

Figure 7. XRD patterns for different pre-treated 4%Mo/H-ZSM-5 catalysts after 120 min reaction at 700 ˚C.

6.2.3. Surface area measurements.

The surface features seem to be certainly affected by different reduction pre-treatments. Reduction at lower temperature show a drastic diminution in BET surface area (**Table 1**). On the contrary, after reduction at 650 ˚C a notable decrease is observed. Therefore, this feature could not be correlated with the lower catalytic performance discussed before. By comparing the not pre-treated spent catalyst with those from pre-reduced series, it is worthy to note that pre-reduction at 550 ˚C and 650 ˚C clearly induces a significant stress to the surface area, with outstanding diminution of the mesopore fraction, leaving the micropore fraction almost unaffected by the pre-treatment.

Treatment	T (°C)	Surface area (m^2/g)		V_{pore} (cm^3/g)	
		BET	micro	Total	Micro
Fresh	---	313	236	0.17	0.11
After 2h CH_4 700 °C (without pre-treatment)	---	245	207	0.14	0.10
After 1 h H_2 (T)	450	298	230	0.17	0.11
	550	296	229	0.16	0.11
	650	242	193	0.14	0.09
After 1 h H_2 (T) and 2h CH_4 700 °C	450	263	220	0.14	0.10
	550	227	199	0.12	0.09
	650	218	202	0.11	0.09

*****_Mesoporous diameter_.

Table 1. Surface area of fresh, pre-treated and post-reaction catalysts.

6.2.4. Transmission electron microscopy (TEM) and high angle annular dark field (HAADF).

After observing the samples by TEM and STEM (**Figure 8**), the formation of large agglomerates of molybdenum in the spent 450 ˚C pre-treated sample is striking. The fact that no peaks of MoO_3 appear on XRD would indicate that the particles formed are not

crystalline. Moreover, the micrographies showed the formation of ca. 50 nm molybdenum agglomerates composed by smaller particles and slightly Al-enriched.

The images obtained for the fresh 4%Mo/H-ZSM-5 were shown in our previous work,[15] and in addition to the homogeneously distributed Mo species, the presence of larger Mo particles associated with Al-enriched areas of the zeolite were detected. However, these particles were usually located on the edge of the zeolite, and the size was around 10 nm and more asymmetric. The agglomeration observed after reaction for 450 ˚C pre-reduced catalyst was circular, and the smaller particles inside the agglomeration can be distinguish.

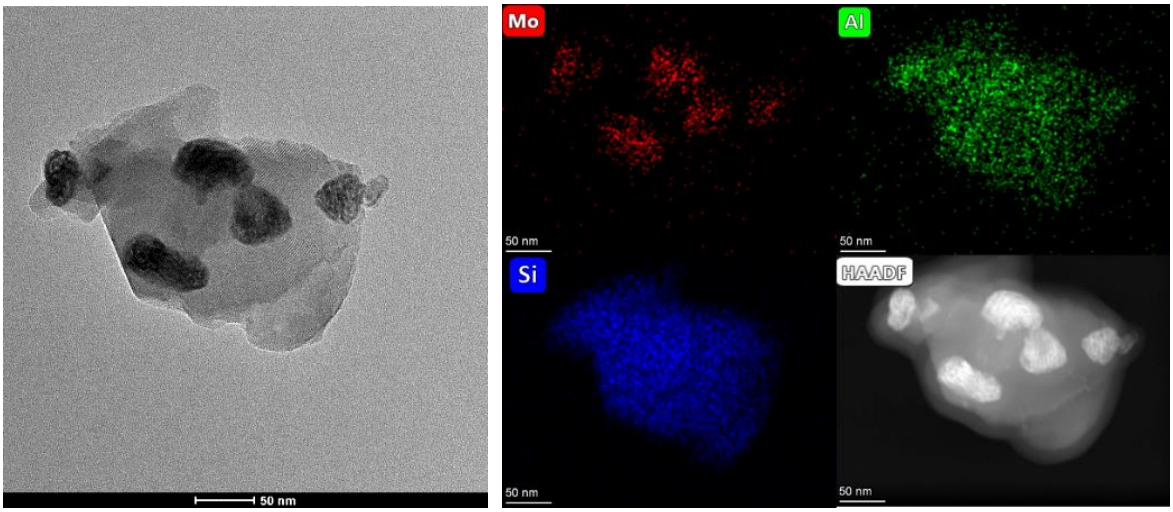

Figure 8. HAADF-STEM images of the spent 4%Mo/H-ZSM-5 catalyst after the 450 ˚C H_2 pre-reduction treatment.

The formation of such evident agglomerated Al-enriched Mo species could be explained by considering that upon reduction step at 450 ˚C, structural water is evolved from the zeolite. Thus, due to the kinetic limitation of water elimination during isothermal reduction process at 450 ˚C, water evolution would be limited and it would diffuse inside the pore structure. During this partial dehydration process Al and Mo would be partially segregated forming these large aggregates. Indeed, by observing the mass 18 in the mass spectrometer during TPR experiments after different pre-reduction processes, it is evident that for 450 ˚C water evolves outstandingly with respect to pre-reduced at

higher temperatures. This fact clearly denotes that at this pre-reduction temperature, structural water would remain in the pore structure creating a certain '*hydrothermal*' ambient (**Figure 9**). At such conditions, Al extraction and Mo aggregation would be favoured forming the observed Al-enriched Mo-aggregates.

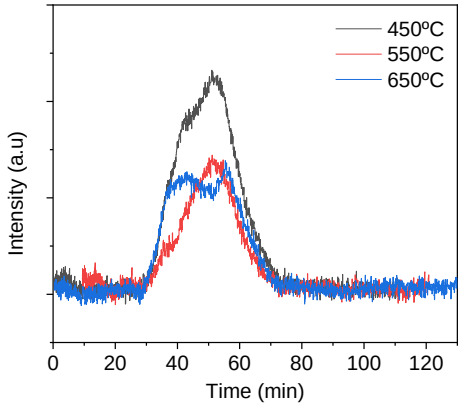

Figure 9. Mass spectrometer signals for mass 18 during different pre-reduction treatment over 4%Mo/H-ZSM-5 catalysts.

For the spent samples pre-reduced at 550 ˚C and 650 ˚C, these particles are not observed. On the contrary, molybdenum particles seem to be more dispersed, as can observed in **Figures 10-12**.

For the 550 ˚C pre-reduced catalyst molybdenum particles appear homogeneous in shape and size, with a diameter of 2-4 nm. It is more difficult to resolve the morphology of the particles in spent 650 ˚C pre-reduced catalyst. However, it is interesting how in both later samples the formation of carbon nanotubes can be observed. As was explained before, the pre-reduction treatment at 550 ˚C and 650 ˚C gives rise to a higher conversion to aromatics than pre-reduction treatment at 450 ˚C. The formation of these large amorphous Mo-Al agglomerates could be the reason for a smaller conversion and selectivity to aromatics.

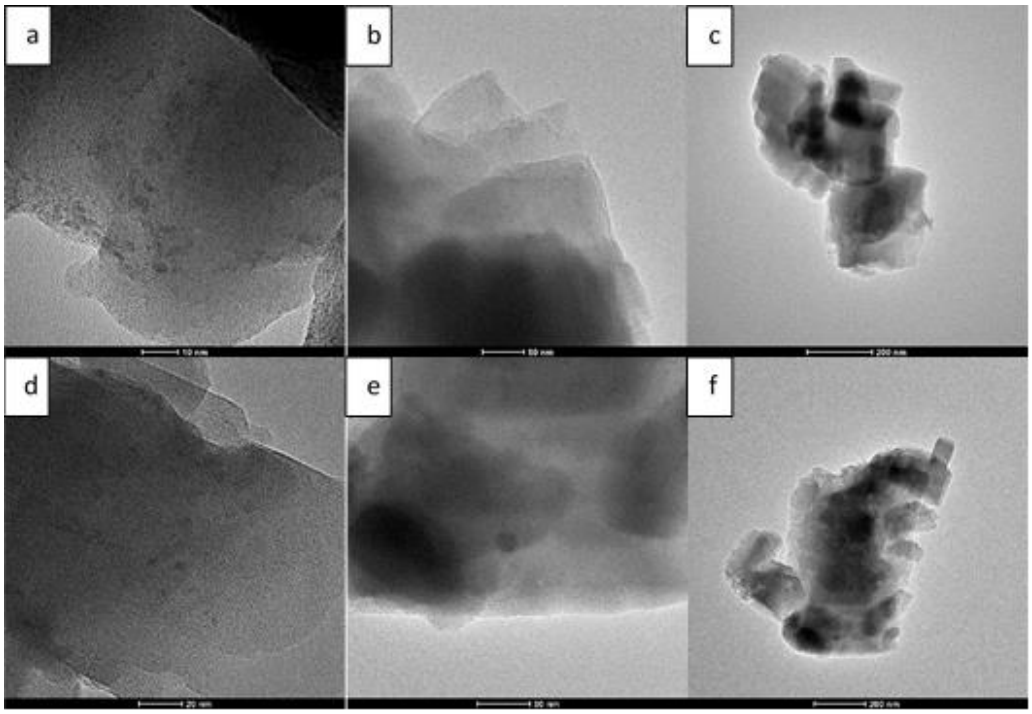

Figure 10. TEM of spent samples after 550 ˚C pre-reduction treatment (a, b, c) and 650 ˚C pre-reduction treatment (d, e, f).

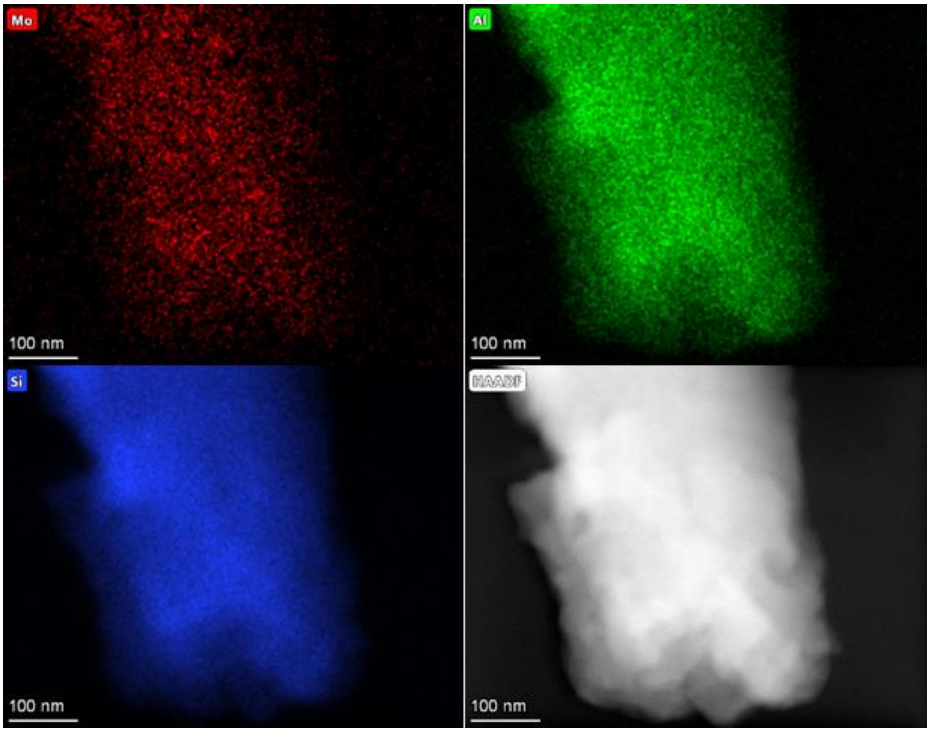

Figure 11. HAADF-STEM images of spent samples after 550 ˚C pre-reduction treatment.

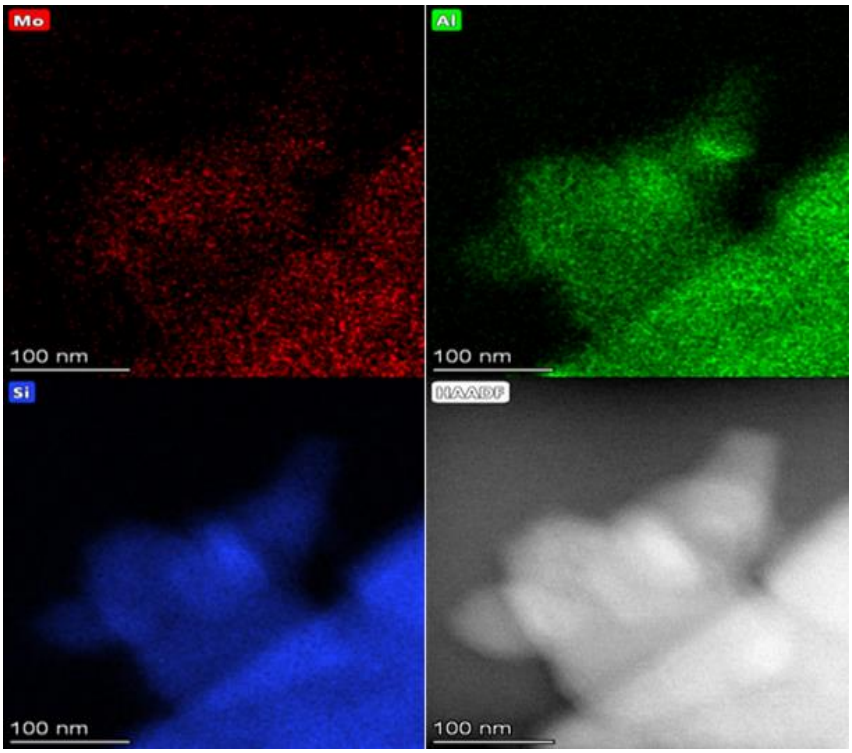

Figure 12. HAADF-STEM images of spent samples after 650 ˚C pre-reduction treatment.

In addition, the HAADF-STEM images of the spent 4% Mo/H-ZSM-5catalyst after the 650 ˚C pre-reduction treatment it can be detected some Al-enriched areas. However, unlike in the case of 450 ˚C pre-treated catalyst, within these areas molybdenum did not appear aggregated, remaining homogeneously dispersed.

6.2.5. Temperature-programmed reduction

The reducibility of the calcined systems has been followed by temperature programmed reduction measurements. As we have shown in previous works, 4%Mo/H-ZSM-5 catalyst showed a complex TPR profile, with the presence of at least five different Mo phases, with different location, dispersion and catalytic performances in the *MDA*.[15] In this case, two successive TPR-H_2 have been carried out, the first up to 450 ˚C, 550 ˚C or 650˚C for 1h (that would be equivalent to the pre-reduction treatment carried out on the samples), and the second from 250 ˚C to 1000 ˚C that could help to assess the situation of the catalyst after reduction pre-treatment (**Figure 13**).

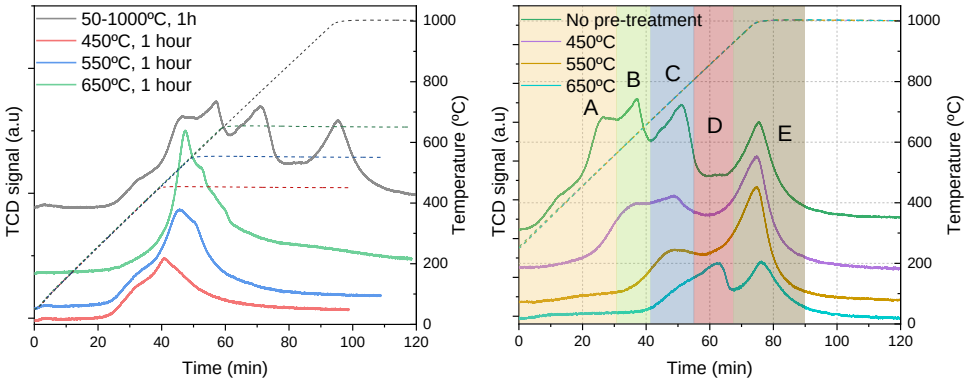

Figure 13. TPR profiles for 4%Mo/H-ZSM-5 catalysts: Reduction pre-treatment profile *(left)*; Reduction profile for pre-reduced catalysts(*right*). [15]

By comparing with the TPR profile of fresh catalysts, pre-reduction treatment induces important modifications in the Mo-species identified in our previous study (**Figure 13.** *right*).[¡Error! Marcador no definido.] The first important issue that might be highlighted is that upon reduction treatment, the Mo species reducing between 350 °C – 570 °C (*A* Mo-species, ascribed as small clusters of well-dispersed Mo monomers, located on the external surface of the zeolite) disappear almost completely. Furthermore, the reduction regions at 570 °C –680 °C (*B* family, small clusters of well-dispersed Mo dimers/polymers associated with Al-enriched areas of the zeolite) and 680 °C – 800 °C (*C* family small clusters of well-dispersed Mo dimers/polymers located in the inner micropores) gradually decrease with the pre-reduction treatment temperature, indicating that they are already reduced during pre-treatment.

It should be remembered that the Mo-species reducing at 680 °C – 800 °C, were identified as the highly active species for the reaction.[¡Error! Marcador no definido.] On this basis, it could be expected that pre-reduction would progressively improve the catalytic performance as reduction temperature increases. However, as already stated, water evolution during reduction pre-treatment appears at ca. 250 °C - 300 °C and ends at 600 °C. We have shown that reduction at 450 ˚C contributes to the extraction of molybdenum and aluminium to the surface, which under reaction conditions would

agglomerate, forming the particles observed by TEM and HAADF. This leads to a strong decrease in the catalytic activity of the catalyst. On the other hand, pre-reduction at 650 ˚C would affect importantly to the surface and structural features of the support. Even more, we have denoted certain surface Al clustering from STEM images. Therefore, in spite of the presence of a higher fraction of Mo-reduced species such structural and surface detrimental features would lead to a lower catalytic performance. In addition, the catalytic promoting effect of a larger amount of reduced species *C* at 650 ˚C pre-reduced catalyst could be reduced by a smaller amount of species *E* (small clusters of well-dispersed Mo monomers, reducing at temperatures higher than 915 °C and located in the inner microporous channels of the zeolite*)*.

As reported in the literature, a reduction treatment of Mo catalyst in H_2 flow resulted in an improvement on the stability.[13] However, it is necessary to add that there is an optimal temperature at which to reduce the catalyst in order to obtain a better performance. As we have demonstrated here, the different reduction temperatures could lead to agglomeration (low conversion and rapid deactivation) or surface/structure deterioration that would negatively affect the catalytic performance and increase at the same time the selectivity to naphthalene.

6.2.6. X-ray photoelectron spectroscopy

The study of physicochemical state of the external surface region is crucial to determine how different reduction pre-treatment could tune the surface Mo-species. Thus, in **Figure 14** we plot the recorded signals of the Mo *3d* and C *1s* regions of the different reduction pre-treatment and after 2 h of reaction.

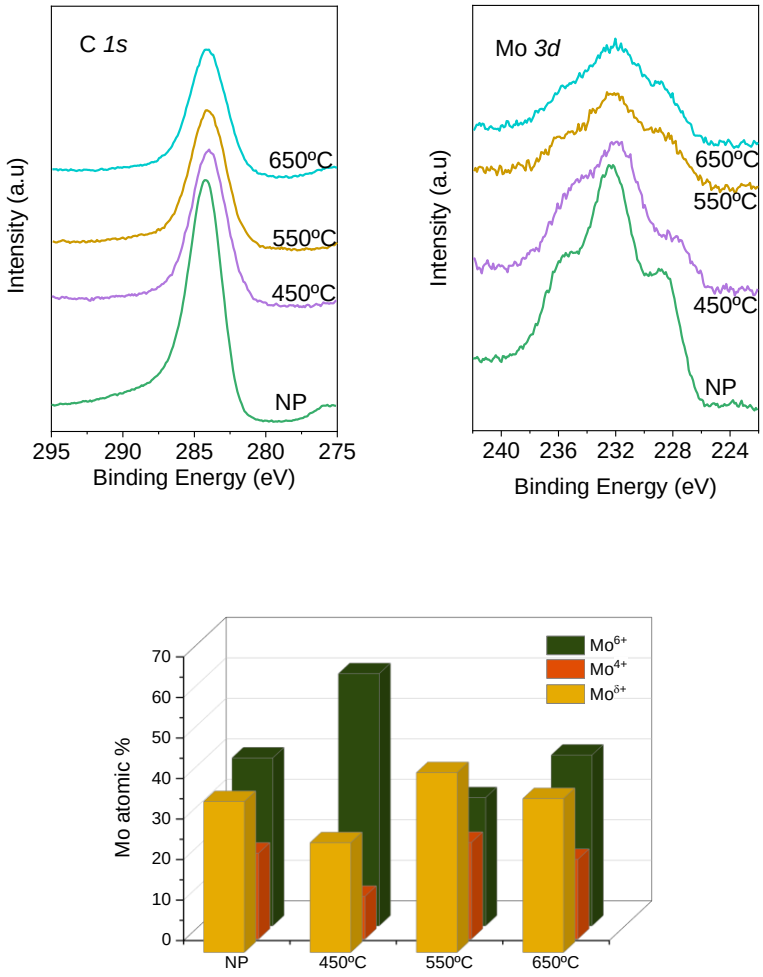

Figure 14. *Upper panel*: Normalized Mo *3d* and C *1s* spectra of the spent 4%Mo/H-ZSM-5catalysts with and without reduction pre-treatment. *Lower panel*: Atomic % for different Mo oxidation states from Mo *3d* deconvolution.

By observing the Mo *3d* signals of different spent catalysts it is evident the important influence of reduction pre-treatment in the final situation of Mo species. Even more, the chemical composition of the surface seems to be also strongly conditioned by the pre-treatment temperature. Indeed, the suggested aggregation is plainly observed from the higher Mo/Si ratio obtained for this catalyst with respect to the rest of pre-treated catalysts (**Figure 15**). We have to say the for all pre-treated catalysts, the Mo/Si ratios observed are always below the attained one for non pre-treated catalyst. This could be indicating the pre-reduction induces a certain redispersion of Mo-species. Additionally,

the Al/Si ratio also suffers a particular variation depending on the reduction temperature, being significantly lower in the case of the catalyst pre-reduced at 550 ˚C. In fact, we have stated from HAADF mapping images clear Al aggregation after pre-reduction at 450 ˚C and 650 ˚C.

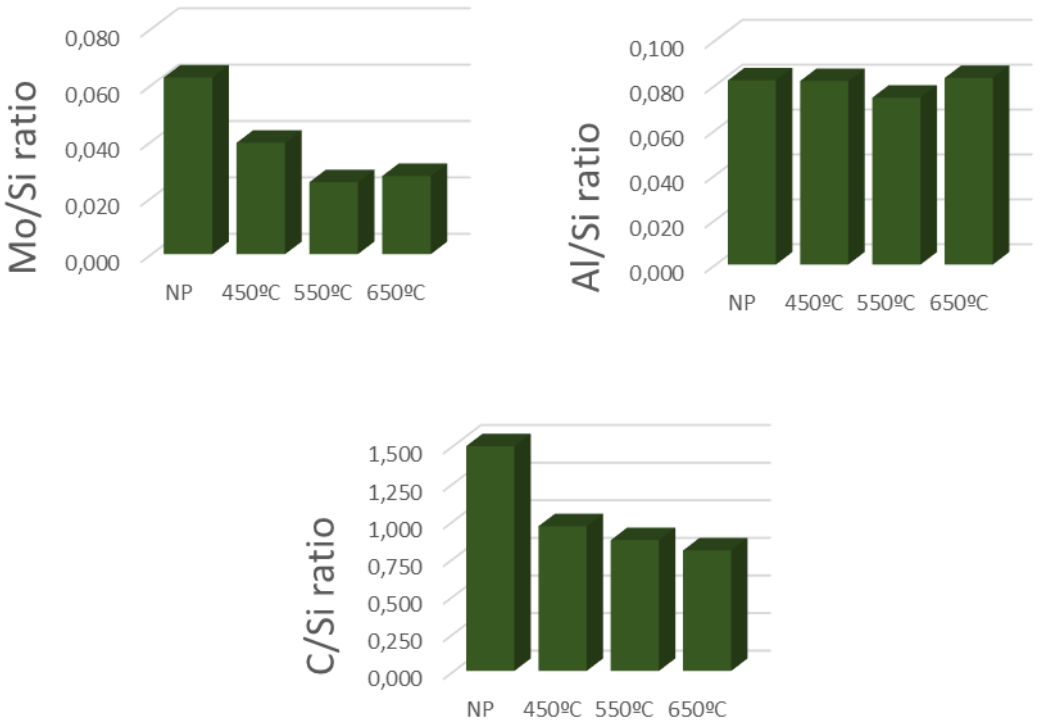

Figure 15. Surface Mo/Si, Al/Si and C/Si atomic ratios from XPS analysis for different pre-reduction treated 4%Mo/H-ZSM-5 catalysts.

Moreover, by deconvoluting the Mo *3d* spectra (**Figure 16**) we have found interesting differences in the Mo chemical state after different processes (**Figure 14**, *lower panel*). Thus, it is worthy to mention the high fraction of Mo^{6+} found in the catalyst pre-reduced at 450 ˚C. The occurrence of this oxidised species could be correlated with the observed Mo extraction/aggregation due to the important water evolution during reduction pre-treatment. Similarly, but at less extent, the pre-reduction at 650 ˚C also favours the presence of Mo^{6+}. On the contrary, Mo $^{\delta+}$ species appear prominently in the catalyst pre-reduced at 550 ˚C.

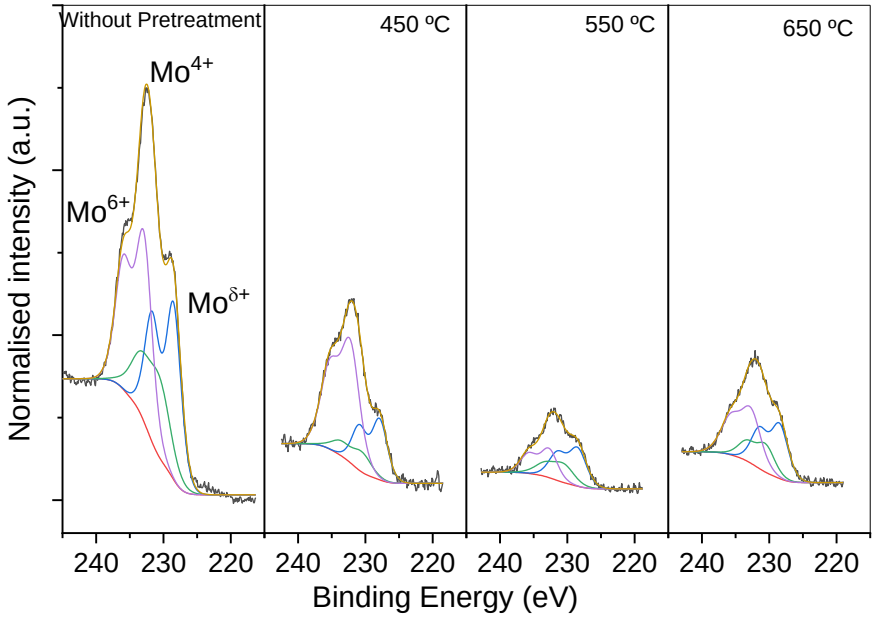

Figure 16. Deconvolution of the Mo 3d XPS spectra for different pre-reduction treated 4%Mo/H-ZSM-5 catalysts.

Another important issue concerns to the C *1s* signal (**Figure 14** and **15**). In all pre-reduced catalysts, the surface carbon content appears significantly lower confirming the observation from DTG analysis of spent samples.

From these results, we may argue that reduction at different temperatures induces particular effects on surface Mo that could strongly condition the final catalytic performance. In this sense, the more active catalysts, obtained after pre-reduction at 550 ˚C, shows a higher fraction of Mo $^{\delta+}$ with a lower fraction of Al. On the contrary, reduction pre-treatment at 450 ˚C or 650 ˚C would favour Mo^{6+} and/or Al extraction.

6.3. Conclusions

The results showed that a reduction pre-treatment could help to improve the catalytic performance of 4%Mo/H-ZSM-5 on *MDA* reaction. Moreover, we have stated that the temperature at which the reduction is carried out has a strong influence on both, the position and the state of the molybdenum species, as is represented on **Scheme 2**.

Thus, from TPR experiments and STEM images we have shown that reduction of the samples revealed that the pre-treatment of hydrogen at different temperatures causes the redistribution of molybdenum species in the zeolite. Such reorganization was corroborated from XPS analysis. A clear correlation between the amount of $Mo^{\delta+}$ species and the catalytic performance (conversion and selectivity to aromatics) on the 4%Mo/H-ZSM-5 catalysts was proved.

The H_2 pre-treatment at 450 ˚C resulted in the formation of large agglomerates of aluminium and molybdenum as a consequence of the extraction of structural water from the zeolite, as well as a low reduction degree of the molybdenum species present on the surface. That led to a decrease in reactivity with respect to the rest of the samples tested for the methane aromatization reaction.

In the case of pre-treatment at 650 °C of the 4%Mo/H-ZSM-5catalyst, this resulted in a widening of the pore diameter, which acquired a size close to twice the size of the fresh sample. In addition, there was an aluminium enrichment of the surface, this time without molybdenum agglomerations. Both processes seem to be related to the re-oxidation produced after the formation of water as a consequence of the greater carburization of the sample. As a result, catalysts are obtained after reaction with a degree of reduction less than expected but greater than that obtained in the sample at 450 °C. The catalytic activity values are similar to those obtained for the sample without pre-treatment (although with a higher selectivity to naphthalene given its increased pore diameter and the change in shape selectivity).

The catalyst subjected to a pre-treatment at 550 °C showed great improvements in catalytic activity over the catalyst without pre-treatment and pre-treated at 450 ˚C and 650 ˚C. The fact that the total methane conversion was lower contributed to the lower obtainment of coke in the sample after pre-treatment. The greater selectivity to aromatics and the greater formation of these could be due to the greater degree of reduction of the alkalized surface molybdenum species in the sample reduced to this temperature, and to the fact that the molybdenum seems to be found inside the structure, whereby it can be detected by TPR but not by XPS.

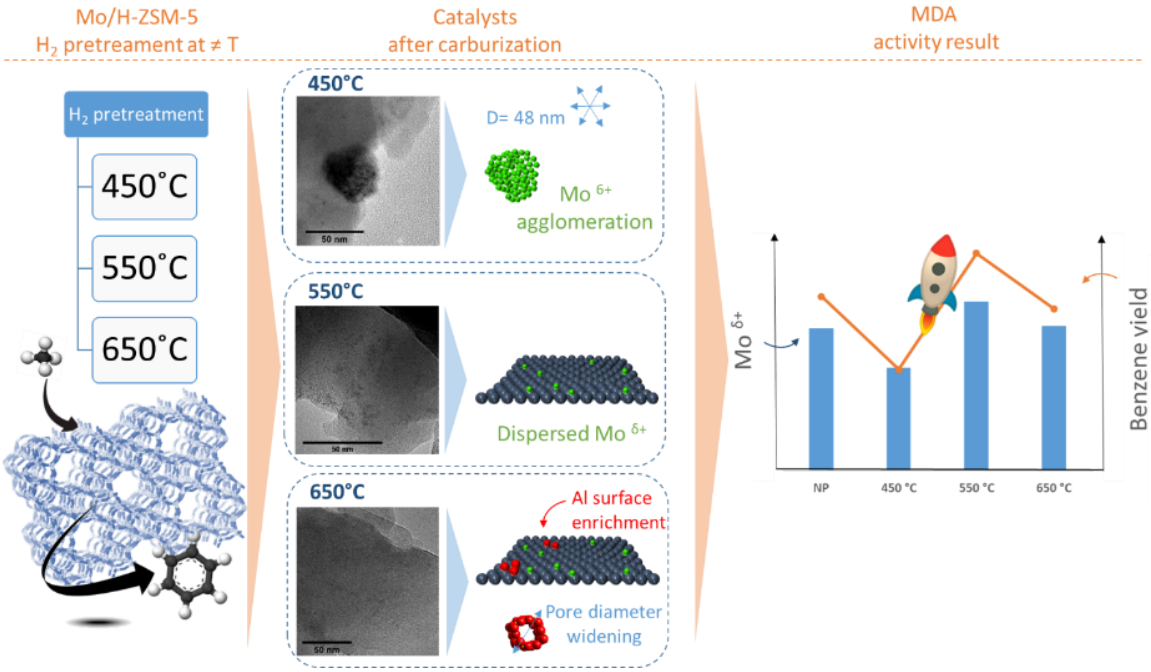

Scheme 2. Pretreatment, reaction samples and Mo $^{\delta+}$ species vs *MDA* activity result scheme for 4%Mo/H-ZSM-5.

6.4. References.

1. Wang, L., Xu, Y., Wong, S. T., Cui, W. & Guo, X. Activity and stability enhancement of Mo/HZSM-5-based catalysts for methane non-oxidative transformation to aromatics and C2 hydrocarbons: Effect of additives and pretreatment conditions. *Appl. Catal. A Gen.* **152**, 173–182 (1997).
2. Bouchy, C. *et al.* Metastable fcc α-MoC(1-x) supported on HZSM5: Preparation and catalytic performance for the non-oxidative conversion of methane to aromatic compounds. *J. Mol. Catal. A Chem.* **163**, 283–296 (2000).
3. Liu, H., Bao, X. & Xu, Y. Methane dehydroaromatization under nonoxidative conditions over Mo / HZSM-5 catalysts : Identification and preparation of the Mo active species. **239**, 441–450 (2006).
4. Tempelman, C. H. L., Zhu, X. & Hensen, E. J. M. Activation of Mo/HZSM-5 for methane aromatization. *Cuihua Xuebao/Chinese J. Catal.* **36**, 829–837 (2015).
5. Portilla, M. T., Llopis, F. J., Moliner, M. & Martinez, C. Influence of preparation conditions on the catalytic performance of Mo/H-ZSM5 for methane

dehydroaromatization. *Appl. Sci.* **11**, (2021).

6. Portilla, M. T., Llopis, F. J. & Martínez, C. Non-oxidative dehydroaromatization of methane: An effective reaction-regeneration cyclic operation for catalyst life extension. *Catal. Sci. Technol.* **5**, 3806–3821 (2015).
7. Sridhar, A., Rahman, M. & Khatib, S. J. Enhancement of Molybdenum/ZSM-5 Catalysts in Methane Aromatization by the Addition of Iron Promoters and by Reduction/Carburization Pretreatment. *ChemCatChem* **10**, 2571–2583 (2018).
8. Tan, P. The catalytic performance of Mo-impregnated HZSM-5 zeolite in CH4aromatization: Strong influence of Mo loading and pretreatment conditions. *Catal. Commun.* **103**, 101–104 (2018).
9. Ramasubramanian, V., Ramsurn, H. & Price, G. L. Methane dehydroaromatization – A study on hydrogen use for catalyst reduction, role of molybdenum, the nature of catalyst support and significance of Bronsted acid sites. *J. Energy Chem.* **34**, 20–32 (2019).
10. Sridhar, A. *et al.* Bimetallic Mo-Co/ZSM-5 and Mo-Ni/ZSM-5 catalysts for methane dehydroaromatization: A study of the effect of pretreatment and metal loadings on the catalytic behavior. *Appl. Catal. A Gen.* **589**, 117247 (2020).
11. Gu, Y. *et al.* Coking mechanism of Mo/ZSM-5 catalyst in methane dehydroaromatization. *Appl. Catal. A Gen.* **613**, (2021).
12. Vollmer, I. *et al.* Activity Descriptors Derived from Comparison of Mo and Fe as Active Metal for Methane Conversion to Aromatics. *J. Am. Chem. Soc.* **141**, 18814–18824 (2019).
13. Rahman, M. *et al.* Increasing the catalytic stability by optimizing the formation of zeolite-supported Mo carbide species ex situ for methane dehydroaromatization. *J. Catal.* **375**, 314–328 (2019).
14. Samanta, A., Bai, X., Robinson, B., Chen, H. & Hu, J. Conversion of light alkane to value-added chemicals over ZSM-5/metal promoted catalysts. *Ind. Eng. Chem. Res.* **56**, 11006–11012 (2017).
15. López-Martín, Á., Platero, F., Colón, G. & Caballero, A. Elucidating the nature of Mo species on ZSM-5 and its role in the methane aromatization reaction. *React. Chem. Eng.* (2021). doi:10.1039/d1re00044f

Chapter 7. Synthesis and characterization of Mo/MCM-22 systems for *MDA* reaction

We have prepared a series of 4%Mo/MCM-22 systems following the different zeolite synthesis methods. The obtained catalysts have been widely structural and surface characterized. Factors as the metal loading or metal doping have been studied during this thesis for the Mo/H-ZSM-5. In this chapter it is shown how these factors affect to the molybdenum supported on MCM-22 catalyst. The influence on the catalytic activity of factors as the MCM-22 synthesis, Mo metal loading, SiC dilution, and Re addition are depict.

7.1. Introduction.

MCM-22 zeolite (IZA code MWW), first synthesized by Mobil researchers,[1] belongs to the MWW-type family of materials, which also includes MCM-36,[2] MCM-49,[3] MCM-56 [4] and ITQ-2.[5] The differences between them are mainly due to the degree of packing of the layers, and it is a consequence of the differences in the synthesis. In all cases, synthesis is carried out from the laminar zeolitic precursor MWW (P), a material formed by individual sheets of 2.5 nm thickness with a single sinusoidal channel of 10-membered rings, separated from each other by organic cations and solvation molecules. During the calcination stage, if the MWW (P) laminar precursor is directly calcined without any type of previous treatment, the silanol groups present on the surface of each sheet react with their equivalents in the adjacent sheets, condensing and forming a three-dimensional crystalline structure that corresponds to the MCM-22 zeolite. This zeolite has two non-intersecting pore systems which are both accessed through 10-membered rings. One of these is a two-dimensional, sinusoidal channel, defined by 10-membered rings with dimensions 4.1x5.1 Å. The other is composed of large cavities defined by 12-membered rings with a diameter of 7.1 Å. and a height of 18.2 Å. [6]

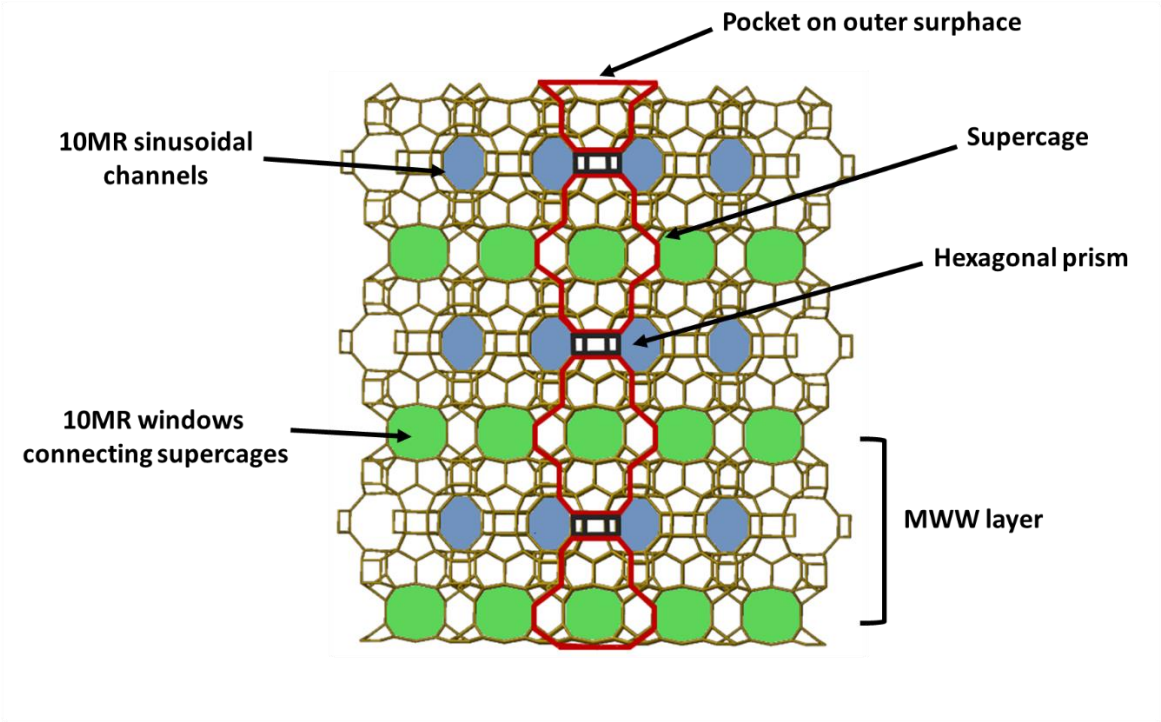

Scheme 1. MCM-22 structure illustration.

The unusual framework topology, large surface area, mild acid property and high thermal stability render MCM-22 zeolite a variety of applications in adsorption and catalysis, such as benzene alkylation, [7,8] p-xylene production,[9] n-butane aromatization,[10] and as additive in FCC catalysts.[11,12] Because of that, the MCM-22 zeolite is one of the very few zeolites that are currently in commercial application.[13]

The first study of MCM-22 based catalysts used in *MDA* reactions was published in 2000 by Bao *et al.* They compared the Mo/H-ZSM-5 and Mo/H-MCM-22 catalysts and showed how MCM-22 based catalysts presented a higher yield of benzene, which was explained by the difference in the pore size of the channels between both zeolites.[14] They also explained how the molybdenum migrates to the Brönsted acid sites into the internal channels of the zeolite, reacting with hydroxyls groups and modifying the acidic properties of the zeolite. The formation of both octahedral non framework aluminium and $Al_2(MoO_4)_3$ crystallites could occur if this interaction Mo-BAS becomes stronger, expelling the aluminium from the lattice.[15] They also suggested that only the 12 MR supercage channel system keeps functioning after introduction of Mo while the 10 MR channel is instead blocked and claimed that the 4%Mo/H-MCM-22 catalyst exhibited the best catalytic performance for the *MDA* reaction.[16] In addition, in another study they distinguished three types of carbon: carbidic carbon in molybdenum carbide, molybdenum-associated coke, and aromatic-type cokes on acid sites. It is suggested that the aromatic-type cokes on Brönsted acid sites are responsible for catalyst deactivation.[17,18]

The study of the acidity was also the aim of Špatenka *et a*l. They characterised fresh and used Mo/MCM-22 catalyst for methane aromatization using the FTIR technique. They found that both bridged hydroxyls and the content of Lewis sites decrease with the introduction of molybdenum and with the time of stream. Also that regeneration in oxygen produced only a very limited restoration of the OH groups restoring the catalytic activity partly, not to its original value.[19]

Huang, L. Q. *et al*. proposed a variation in the SiO_2/Al_2O_3 ratio in MCM-22 based catalysts.[20] Results showed that methane conversion and benzene selectivity increase with the decrease of SiO_2/Al_2O_3 ratio, and reach maximum on Mo/MCM-22 catalyst with SiO_2/Al_2O_3 ratio of 25.

Recently, other authors have also studied the effect of varying SiO_2/Al_2O_3 ratios on MCM-22 systems, therefore, the effect of framework Brönsted acidity:

In 2018, Kim *et al*. verified that Brönsted acid site facilitate that Mo oxides migrate into the microchannel of zeolite influencing the distribution of Mo oxide species. They also found that a high temperature type coke was composed of polyaromatics such as naphthalene and anthracene, and its formation was mainly affected by the amount of Mo oxides present on the external surface of zeolite. So, an increment in BAS enhances the dispersion of Mo oxides, improves benzene formation rate while suppressing the formation of high temperature type coke.[21]

Last year, Pant and his group published that the maximum transformation of MoO_x species into active molybdenum carbide over MCM-22 (SiO_2/Al_2O_3 ratio = 30) during carburization results in higher activity of the 5% Mo catalyst with lower coke content.[22]

Others publications to take into consideration in the study of catalysts for the MDA reaction based on MCM-22 zeolite are the work of the Ichiwaka group. They dealuminated a MCM-22 and found that this catalyst exhibits highly selective and coking-resistant catalytic performance for *MDA* reaction, compared with conventional catalysts [23]

The incorporation of additives to the methane feed,[24] or the use of other metals supported in MCM-22[25] as catalyst have been also studied. Several promoted W-Zn-Ga

or Mo-Co/MCM-22 based catalysts have been developed and used for *MDA*, reaching values of 70% selectivity of benzene at 14-17% conversion of methane at 800°C

The importance of small particles to the performance of catalysts has stimulated the studies for preparation of nanosized MCM-22 zeolites,[26] or nano-MoO_3-modified H-MCM-22.[27] Mo/H-MCM-22-nanosized showed better methane conversion, higher benzene yield and considerably more durability of the catalyst as compared to the conventional microsized catalyst, while nano-MoO_3-modified H-MCM-22 showed higher methane conversion and aromatics yield than commercial MoO_3-modified H-MCM-22.

Other types of strategies to improve the results obtained for *MDA* reaction using MCM-22 based catalysts include the use of hydrogen-selective membranes, [28] or molecular polyoxomolybdate (POM) anions as alternative Mo precursors to conventional Mo salts for the preparation of catalysts.[29]

7.2. Synthesis.

7.2.1. MCM-22.

For the synthesis of this zeolite silicic acid ($SiO_2 \cdot H_2O$, 100-200 mesh, Sigma-Aldrich), sodium hydroxide (NaOH, Merck), sodium aluminate ($NaAlO_2 \cdot 2H_2O$, Al_2O_3:50-56% Na_2O: 7-45%, Sigma-Aldrich) and hexamethyleneimine (HMI, 99%, Sigma-Aldrich) were used in the indicated proportions: SiO_2/Al_2O_3= 30, Na/SiO_2= 0.18, HMI/SiO_2=0.35 and H_2O/SiO_2=19.5 5 for the synthesis mixtures [30], except the last one where a smaller amount of NaOH was used. In this way, the correct amount of sodium hydroxide and sodium aluminate were dissolved in the required volume of deionized water, after which the silicic acid and hexamethyleneimine were added. The resulting mixture was stirred until it was visually homogeneous. After that, the slurry was reacted using three different procedures. The first involved heating the mixture by microwave radiation in a Teflon coated autoclave at 150 ˚C for 60 hr while stirring. Previously, the mixture was aging one hour at 60 ˚C in rotation. The second procedure involved heating the reaction

mixture in a hydrothermal reactor at 150 °C for 10 days in static. The third procedure also involved heating in an autoclave at 150 °C, but under stirring and for a period of 7 days. Finally, for preparation 4, the synthesis with a lower amount of NaOH, the same procedure was used as in the first synthesis, heating this mixture in the microwave for 60 h at 150 ˚C, with stirring, and after a previous aging of one hour at 60 ˚C in which the solution is homogenized.

	RECIPE	PROCEDURE
P1	0,39g NaOH, 0,47g $NaAlO_2 \cdot 2H_2O$, 5,85 g $SiO_2 \cdot H_2O$, 30ml H_2O, 2,97 g HMI	Synthesis in the microwave at 150˚C for 60h, with 1 h prior aging at 60 ˚C
P2	0,78g NaOH, 0,94g $NaAlO_2 \cdot 2H_2O$, 11,69 g $SiO_2 \cdot H_2O$, 60ml H_2O y 5,90 g HMI	Synthesis in an autoclave at 150˚C, for 10 days in static.
P3	0,78g NaOH, 0,94g $NaAlO_2 \cdot 2H_2O$, 11,69 g $SiO_2 \cdot H_2O$, 60ml H_2O y 5,90 g HMI	Synthesis in an autoclave at 150˚C, for 7 days under stirring.
P4	0,28g NaOH, 0,47g $NaAlO_2 \cdot 2H_2O$, 5,85 g $SiO_2 \cdot H_2O$, 30ml H_2O, 2,97 g HMI	Synthesis in the microwave at 150˚C for 60h, with 1 h prior aging at 60˚C

Table 1. Different synthesis procedures for MCM-22

The solid obtained was filtered, washed several times and dried overnight at 110 ˚C. The organics were removed from the as-synthesized materials using calcination in air at 550 ˚C for 8 h using a heating rate of 2 ˚C·min^{-1}. After that, zeolites were ion-exchanged three times using 1 M aqueous ammonium nitrate (NH_4NO_3, 95% min, Alfa Aesar. Weight ratio of zeolite to NH_4NO_3 solution = 1:10) for 12 h, filtrated, washed and dried at 110˚C overnight. In order to obtain the acid form of the MCM-22, the zeolites were calcined again at 550˚C in air, for 3h and using a heating rate of 5 ˚C·min^{-1}. During calcination organic surfactants were removed from MCM-22(P) and condensation of zeolite layers and the formation of 3D microporous structure of MCM-22 took place.

7.2.2. Metal loading.

Molybdenum monometallic catalyst was synthesis as it was described in **Chapter 2** for the synthesis of Mo/H-ZSM-5 catalysts.

Bimetallic system synthesis followed this process: molybdenum was first loaded using ammonium heptamolybdate tetrahydrate ($(NH_4)_6Mo_7O_{24}{\cdot}4H_2O$, Sigma Aldrich) of appropriate concentration to obtain 4w.t%. Mo. After air calcination at 550 ˚C for 3h using a heating rate of 5 ˚C min^{-1} rhenium was loaded. For this purpose, rhenium (VII) oxide (Re_2O_7, Sigma Aldrich) at the corresponding stoichiometric amount was used. As a result, 1%Re-4%Mo/MCM-22 bimetallic systems were obtained.

7.3. Results and discussion

7.3.1. Synthesis of MCM-22 zeolites

The XRD patterns of the MCM-22 zeolites are shown in **Figure 1**.

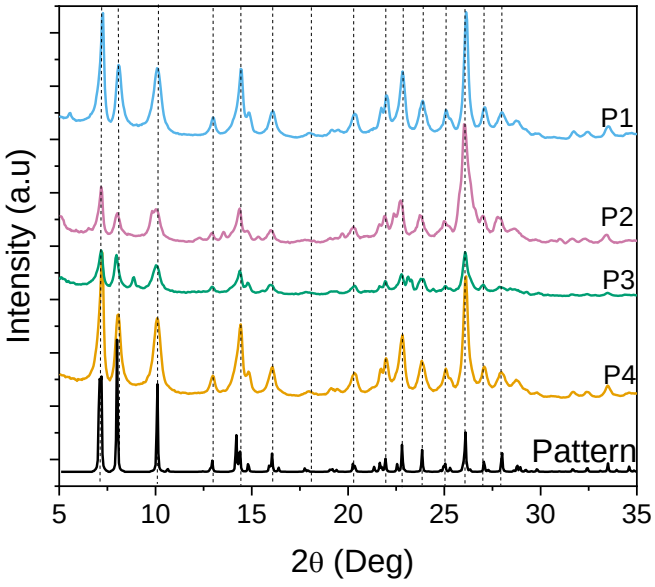

Figure 1. X- ray powder diffraction patterns of the H-MCM-22 zeolites.

By comparing the line positions of the XRD obtained from our samples with the reference pattern, the materials can be identified as crystalline MCM-22 samples. However, we can distinguish the P2 diffractogram from the rest, due to its complete broadening in all 2 theta values which is attributable to structural "mistakes" or concentration gradients. In order to obtain more information, the textural characterization analysis was carried out. The results are shown in **Table 2**, where it is clear that P2 zeolite has a lower surface area (355 m^2/g while MCM-22 (P1) has a value of 474 m^2/g) and the pore diameter value it is exactly a half (7.7 nm while MCM-22 (P1) has a value of 15 nm).

	SURFACE AREA (m^2/g)		PORE VOLUME (cm^3/g		PORE DIAMETER (nm)
	BET	Micro	Total	Micro	BJH Desorption
P1	474	333	0,48	0,16	14,99
P2	355	269	0,25	0,13	7,69
P3	398	303	0,32	0,14	14,85
P4	453	328	0,41	0,15	14,73

Table 2. Textural properties of the different support synthesis determined using N_2 adsorption–desorption isotherms

It has to be pointed out that the MCM-22(P2) synthesis was carried out in static conditions. In the literature is indicated that this type of synthesis fails to produce MCM-22 with a high percentage crystallinity.[30] It can be concluded that P2 zeolite has not been well crystallized.

7.3.2. Effects of different synthesis procedures for MCM-22 on the activity, selectivity, and stability of Mo/MCM-22 catalysts

To compare the effect of the different synthesis procedures on the catalytic activity, the zeolites were loaded using ammonium heptamolybdate tetrahydrate to obtain 4%Mo/MCM-22 (P1), 4%Mo/MCM-22 (P2), 4%Mo/MCM-22 (P3) and 4%Mo/MCM-22 (P4).

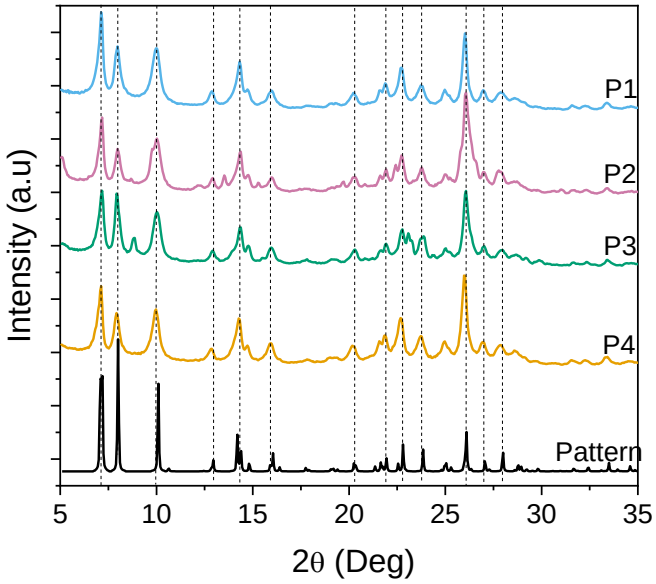

Figure 2. X- ray powder diffraction pattern of the 4%Mo/MCM-22 catalysts.

Figure 2 shows how loading of Mo and calcination do not produce apparent changes in the structure of the zeolites. The XRD of fresh samples does not exhibit indications of the presence of large MoO_3 crystallites in the diffractograms. The reducibility of the calcined systems has been followed by temperature programmed reduction measurements (**Figure 3**).

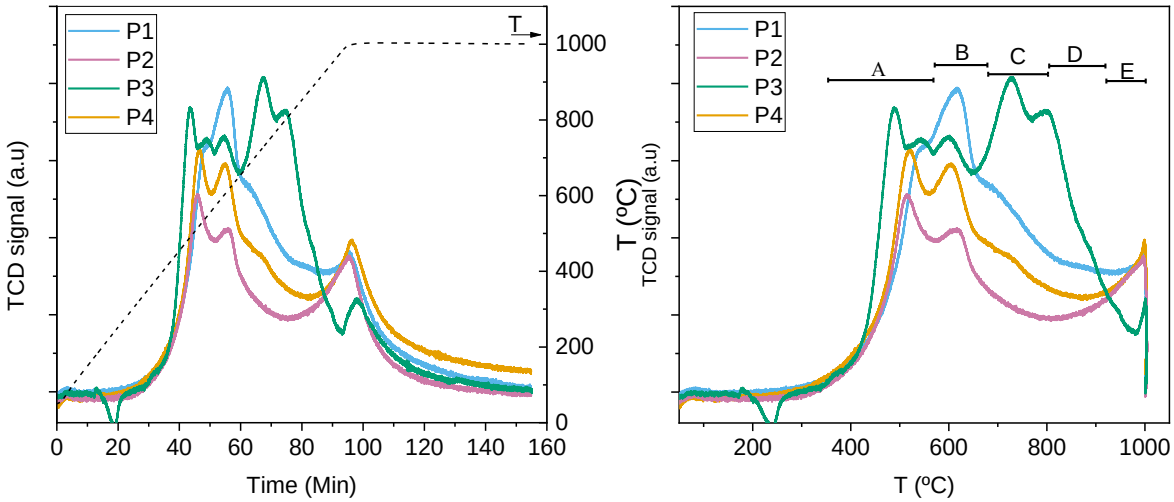

Figure 3.- TPR profiles of Mo/MCM-22 catalysts vs. time (*left*) and temperature (*right*).

According to the results obtained in the previous work for 4%Mo/H-ZSM-5 catalysts, the presence of at least four different Mo phases was identified. Those phases were named as phase A, B, C and E, with reducing processes peaking at 510, 615, 755 and 1000 °C respectively.[31] It is interesting that Mo catalyst supported on MCM-22 show similar TPR profiles. Three reduction processes with peaks centered at 490–550 °C (A), 600-614°C (B) and 1000 °C (E) can be observed in all the samples. In addition, small amounts of Mo reducing at 727 °C can be noticed for 4%Mo/MCM-22 P1, P3 and P4. This phase could be the identified as "phase C" presents in the 4%Mo/H-ZSM-5. The P3 sample differs from the rest. It shows a larger reducing process at ca. 727 °C and a shoulder at 800 °C.

Furthermore, H_2 consumption can be estimated by assuming the total transformation of MoO_3 into metallic molybdenum along the TPR experiment. As shown in **Table 3**, a consumption of 1.08, 0.79, 1.21 and 1.06 mmol / g of H_2 is found for 4% Mo/MCM-22 P1, P2, P3 and P4 respectively. According to the following reaction:

$$MoO_3 + 3H_2 \rightarrow Mo^\circ + 3H_2O,$$

these values represent a reduction of 86, 63, 97 and 85% of the total MoO_3 phase in each case.

4%Mo/MCM-22	A total	mmol H_2 / g cat	%Mo	Δn^+
P1	7,84	1,08	3,45	5,18
P2	5,74	0,79	2,53	3,79
P3	8,82	1,21	3,88	5,83
P4	7,72	1,06	3,4	5,1

Table 3. H2 consumption in the partial reduction of 4%Mo/MCM-22 catalysts

Again sample 2 draws attention, showing a lower value. The smallest H_2 consumption could be caused by a low dispersion of molybdenum species in this sample. The increment in size of the Mo particles on the 4%Mo/MCM-22 (P2) sample was confirmed by TEM. It is shown in **Figure 4**:

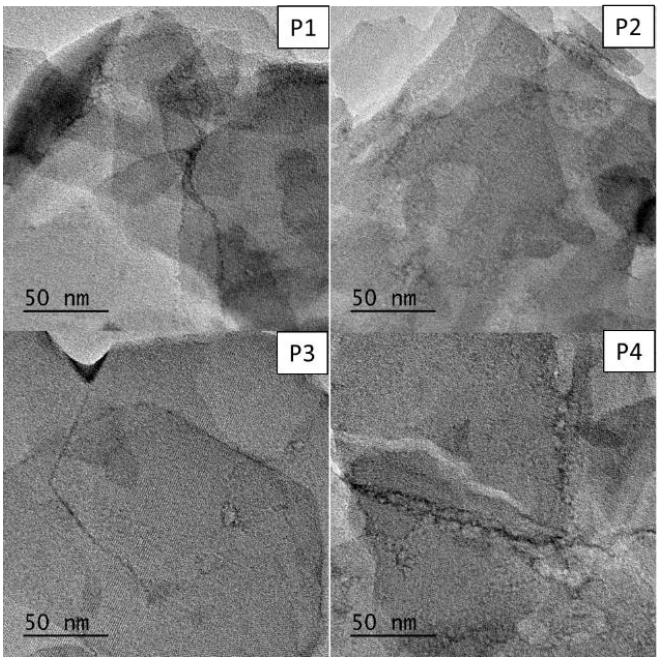

Figure 4. TEM images of calcined 4%Mo/MCM-22.

The use of the different procedures for zeolite synthesis described above may have some effect on methane aromatization. The differences observed in parameters such as crystallinity, surface area, or sample reducibility are critical factors in any process. For

this reason, a series of catalytic tests were carried out. 200 mg of catalyst were introduced into the equipment described in **Chapter 2.** The catalytic performance was followed for approximately 16 h. The results are depicted in **Figure 5:**

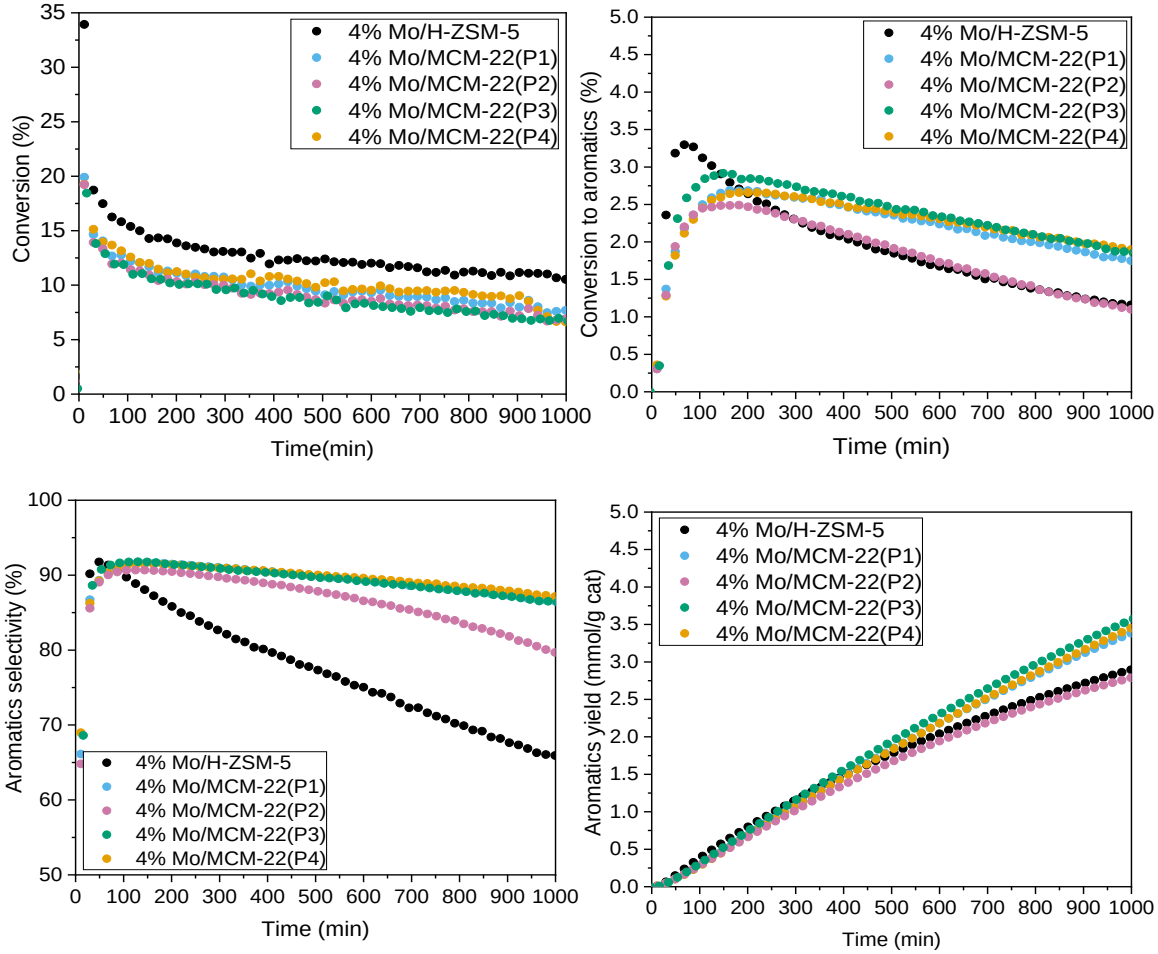

Figure 5. Effect of the MCM-22 synthesis on the catalytic activity for *MDA* reaction over 4%Mo/MCM-22 catalysts.

For all the samples, the methane conversion usually decreases rapidly in the first 100 min of reaction. This coincides temporarily with the induction period of the reaction where the Mo(VI)-oxo phases are transformed into the active Mo species. The catalytic activity for this amount of 4%Mo/H-ZSM-5 has been added to the graphs in order to compare the results. Looking at the ZSM-5 catalyst, the initial methane conversion is 33 %, decreasing in the first 100 minutes by 54 %. In the case of MCM-22 systems, all of

them have initial conversions around 20 %, producing a decrease of around 35 - 40 % in the first 100 min of reaction. Methane conversion is relatively stable at the later stage of the reaction.

The conversion to aromatics has been also represented. In that graph H_2 formation has been suppressed and different trends are observed. On the one hand, during the induction period, it is observed that 4%Mo/ZSM-5 presents a steeper curve, with a maximum of 3.3 % conversion to aromatics at 70 min of reaction, and a rapid deactivation. However, in the case of MCM-22 catalysts, the maximum conversion is lower (2.5 - 2.9 %) and it appears at longer reaction times (150 - 180 min). The deactivation in this case is slower, except for the catalyst 4%Mo/MCM-22 (P2), which deactivates faster.

Regarding aromatic selectivity, all the catalysts have maximum values greater than 90 %. However, for 4%Mo/H-ZSM-5, again the maximum appears at a shorter reaction time, decreasing drastically until reaching values of 66 % selectivity at 16 h of reaction. In the case of the systems supported in MCM-22, the aromatic selectivity values are more stable. At 16 h of reaction, the selectivity is still 86%, except again for the 4%Mo/MCM-22 (P2) catalyst, whose selectivity to aromatics is slightly lower.

The aromatics yields are also shown in **Figure 5.** Among four Mo/MCM-22 catalysts, 4%Mo/MCM-22 (P1), 4%Mo/MCM-22 (P3), 4%Mo/MCM-22 (P4) gives a similar stable catalytic performance. These are the systems synthesized using a dynamic procedure, including the one with different NaOH amount. Aromatics formation is between 3.3 - 3.5 mmol / g cat after 16 hours of reaction. On the other hand, the 4%Mo/MCM-22 (P2) shows an activity similar to the values obtained for the 4%Mo/ZSM-5 catalyst. Aromatics formation after 16 h of reaction is 2.7 and 2.8 mmol/g cat respectively.

From **Figure 5**, it is clear that methane dehydrogenation on Mo catalysts depends substantially on the zeolite supports. As stated by many authors,[14] the catalytic performance obtained for *MDA* is higher for Mo/MCM-22 than for Mo/H-ZSM-5 catalysts. In addition, the aromatics yield changes with the MCM-22 synthesis procedure. Smaller crystallinity of the support could lead to a smaller Mo dispersion, and consequently, to a smaller aromatic production. However, it is necessary to indicate that smalls differences in the characterisation parameters of the MCM-22 don't seem to have an effect on *MDA* performance. Both the syntheses carried out in a dynamic oven as well as those carried out by microwave radiation present similar values of catalytic activity even though they present different values of textural properties. In addition, the synthesis called P4 had a lower amount of NaOH, indicating that this factor is not decisive in the formation of aromatics either. Clearly, the 4%Mo/MCM-22 (P2) catalyst shows abnormal behaviour. The static synthesis of this zeolite for 10 days seems to have not been sufficient to obtain the MWW-type structure. As a result, micropores with a smaller size developed, which eventually lead to the blockage of the channels of the P2 zeolite and it makes the active sites inaccessible for the reactant and other reaction intermediates.

7.3.3. Effect of Mo loading and SiC dilution.

After observing that the synthesis of MCM-22 by procedures 1, 3 and 4 gave similar catalytic results for the systems with 4% molybdenum, one of the procedures was selected to continue with the study. In this case, given its greater speed in obtaining large amounts of zeolite, we opted for procedure 3. In order to determine the optimal load of molybdenum for the reaction, different catalysts were prepared following the described procedure. The series of 2, 4 and 10% Mo/MCM-22 was obtained for its characterization.

Figure 6 reveals a crystallinity lost after the introduction of the 10 % of metal, which is confirmed in **Table 4** where a surface area and micropore volume drop is seen.

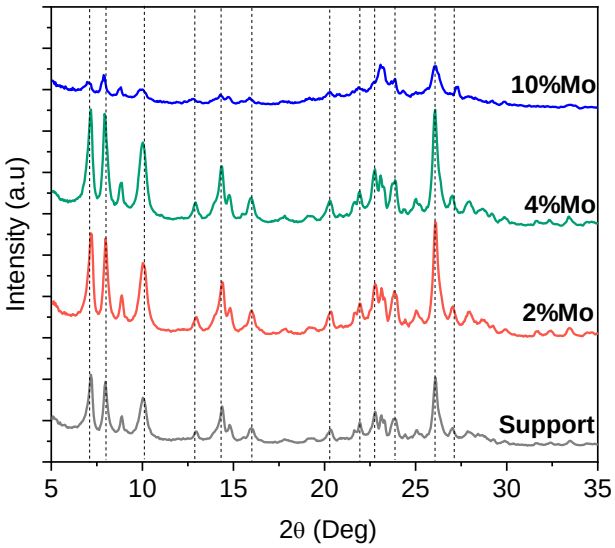

Figure 6. X- ray powder diffraction pattern of the Mo/MCM-22 (P3). serie.

	SURFACE AREA (m^2/g)		PORE VOLUME (cm^3/g)	
	BET	Micro	Total	Micro
Support	398	303	0.32	0.14
2%Mo	367	259	0.29	0.12
4%Mo	337	246	0.29	0.12
10%Mo	197	137	0.19	0.06

Table 4. Textural properties of the Mo/MCM-22 (P3) serie determined using N_2 adsorption–desorption isotherms.

The electron microscopy analysis obtained for this set of samples and the differences between the 3 catalysts can be observed in **Figure 7**. While the 2% Mo sample micrograph reveals a zeolite with a very well dispersed metallic phase, with even the channels of the MCM-22 appreciated, for the 10%Mo/MCM-22 sample the metallic phase appears aggregated and the zeolite presents some holes that appear to be lack of

matter or changes in the support composition. This could be the result of the damage caused by Al extraction from the zeolite framework, previously observed on ZSM-5 catalysts with high Mo loading.[31] That Al extraction would explain also the results obtained for XRD, area surface and micropore volume for the 10%Mo/MCM-22 sample.

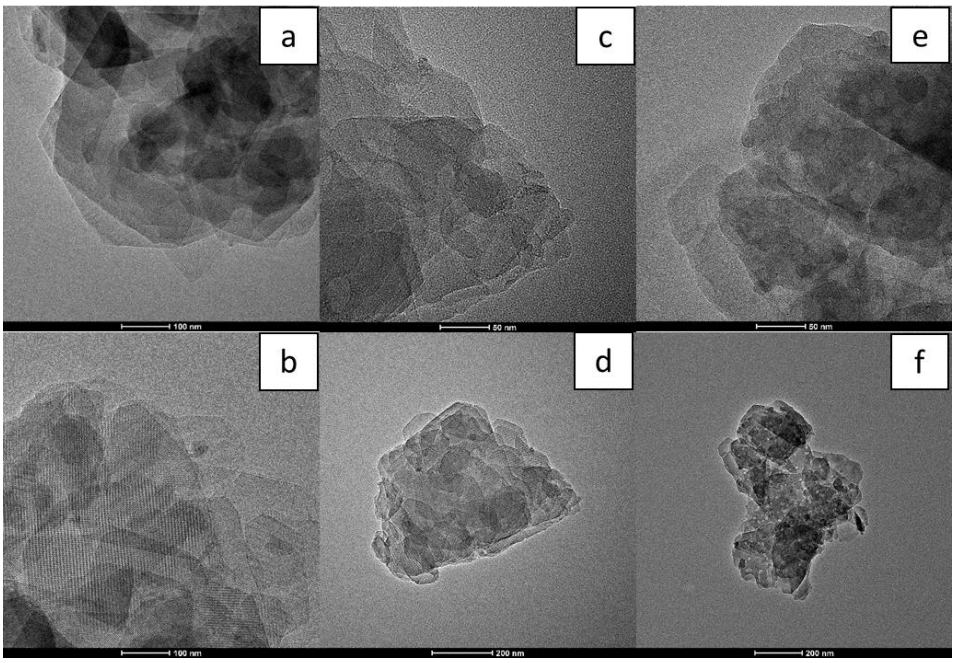

Figure 7. TEM images of calcined 2% Mo/MCM-22 (a, b), 4% Mo/MCM-22 (c, d), and 10% Mo/MCM-22 (e,f).

In order to obtain more information about the molybdenum phases present in this new set of samples a TPR study was carried out (**Figure 8**). The results for 2%Mo/MCM-22 reveals that the phases named as *phase A, B*, and *E*, with reducing processes peaked at 524, 613, and 1000 °C respectively are present. For 10% Mo/MCM-22 large amounts of Mo species reducing at 590 °C (*B*) appears and there is also a reduction peak centered at 830 °C This one is similar to one present on the ZSM-5 catalysts and reduced at 825 °C which also appears on samples with higher Mo loading (10% Mo) and that was identified as a *phase D*, a bulk-like phase of MoO_3, located in the external surface of the zeolite and supported on aluminum oxide segregated from the zeolite network. A

previous work revealed that this phase hinders the catalytic performance for Mo/ZSM-5 catalysts. The same effect was confirmed on MCM-22 supported catalysts after the study of catalytic activity **(Figure 9**).

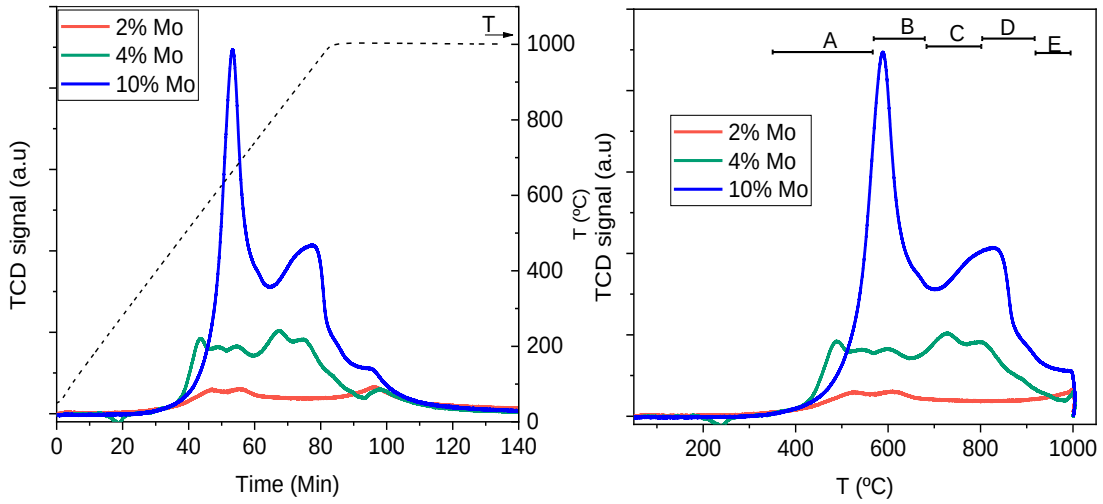

Figure 8. TPR profiles of 2, 4 and 10% Mo/MCM-22 catalysts vs. time (*left*) and temperature (*right*).

The study of the catalytic activity is represented in **Figure 9.** The results obtained for 4%Mo/H-ZSM-5 catalyst were also represented in order to compare. Again we can see how among the studied systems, 4 wt% molybdenum loading had the maximum CH_4 conversion rate and aromatics yield. If the Mo content is bigger or smaller than 4 % the catalytic performance decreases.

If the conversion to aromatics graph is observed, it is revealed how the 10% Mo/MCM-22 presents a maximum of 2.5 % of conversion to aromatics at 120 min, while the 2% Mo catalyst shows a 2 % of conversion to aromatics at 140 min of reaction. However, the deactivation of the 10%Mo is faster.

Regarding aromatic selectivity, 4%Mo/MCM-22 sample has good and constant values greater than 90 %. On the contrary, the rest of the catalysts show a decrease in aromatic selectivity, values below 70 % at the end of the reaction were observed.

The aromatics yields graph indicates how 4%Mo/MCM-22 catalyst obtains the best results in the catalytic performance for this set of catalysts, while the 10% Mo and 2%Mo/MCM-22 present lower aromatics yield than the Mo/H-ZSM-5 used as a reference.

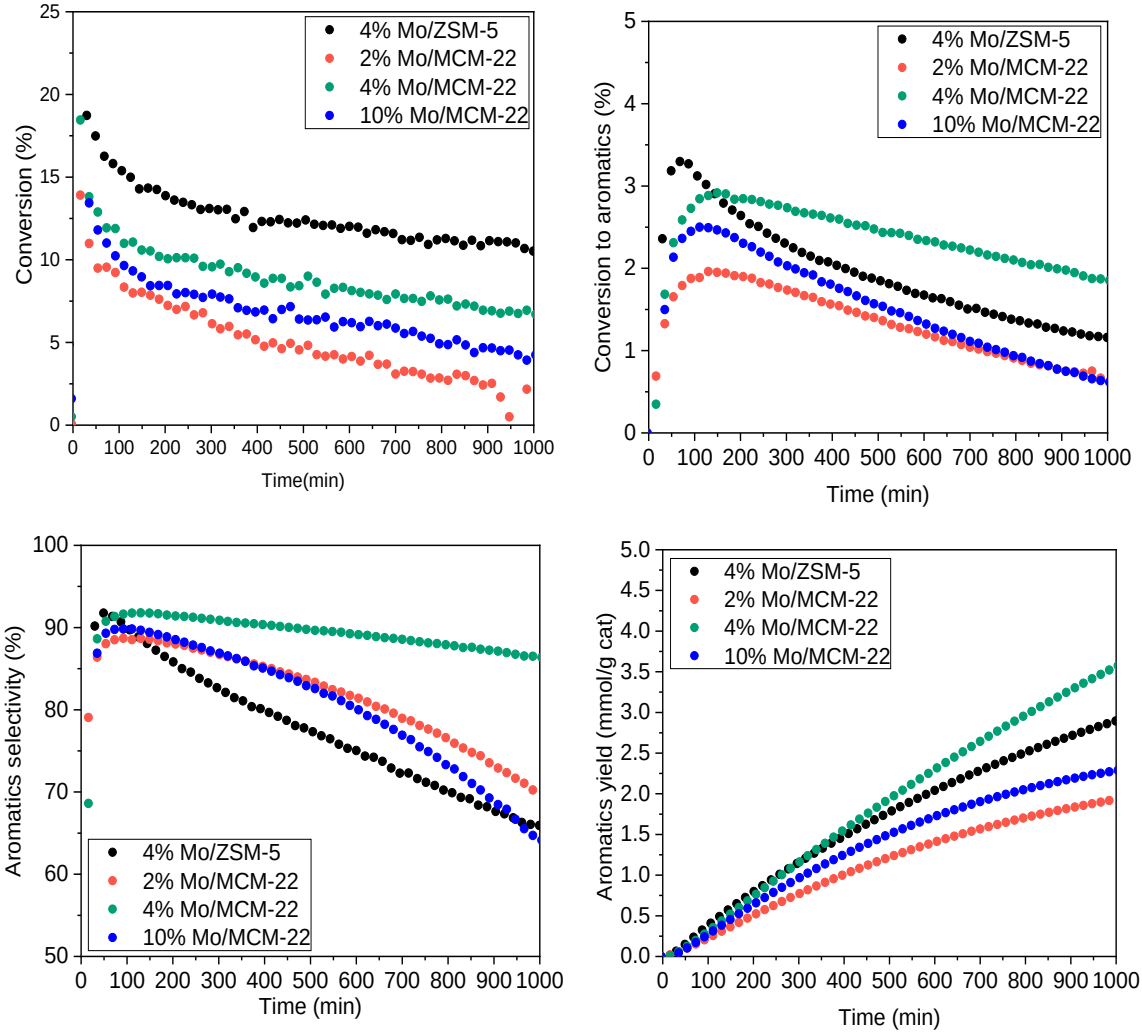

Figure 9. Effect of the Mo loading on the catalytic activity for MDA reaction over Mo/MCM-22 catalysts.

Thermogravimetric analysis (TGA) is frequently used to characterize the carbonaceous deposit. The results for the spent catalysts after 16 h of the *MDA* reaction are represented on **Figure 10** and are quite dependent on the Mo loading.

TG profiles (*top*) show a weight loss before 200 °C for all the samples, which is attributed to the desorption of the adsorbed water. Furthermore, the different combustion features shift to a lower temperature as the Mo loading increases.

According to the literature, the type of coke could be distinguished relative to the weight loss temperature. The slight weight increase below 400 °C is caused by oxidation of carbidic coke. From the DTG analysis (**Figure 10,** *bottom*), two more types more of coke present in 2, 4 and 10% Mo/MCM-22 in the range of 450 °C – 550 °C and 550 °C – 600 °C can be distinguished. The amounts of each of the carbonaceous types are different on the samples, increasing the peak at 450 °C –550 °C with the Mo loading while the peak at 550 °C –600 °C decreases. These two types were commonly designated to molybdenum-associated coke, and aromatic-type coke on acid sites, respectively. It was shown that these type of carbon deposits differ in their chemical nature and formed respectively on Mo and Brönsted acid sites.[17]

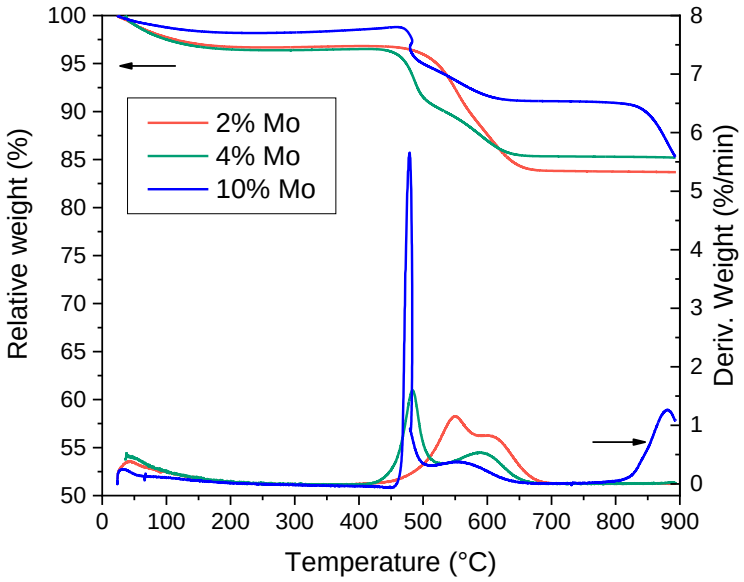

Figure 10. TGA and DTG profiles of 2%, 4% and 10%Mo/MCM-22 catalysts after reaction.

However, later research indicates that the chemical specificity of these methods is questionable and the coke combustion in these type of experiments is limited by the

diffusion through the zeolite which would be affected by the size of zeolite crystals and the nature and location of metal species.[32] Still, we can observe in the graph that the 10%Mo/MCM-22 sample produces a significant amount of coke that is burned at 480 °C, while the amount is considerably less in the 4% Mo/MCM-22 catalyst. Also it is clear how the molybdenum species sublimate at 880 °C for the 10%Mo/MCM-22, while the samples with lower Mo load don't show any weight losses at high temperatures. This high coke formation and the lower thermal stability could account for the loss of catalytic performance in the 10% Mo catalyst.

Considering the importance of diffusion through the catalyst systems, the effect of the SiC dilution in the catalytic activity was also studied. With this purpose, the *MDA* reaction was performed using 50, 100 and 200 mg of 4%Mo/MCM-22 catalyst diluted with 150, 100 and 0 mg of SiC respectively. The same experiment was carried out using the 4%Mo/ZSM-5 catalyst. The results are represented in the **Figure 11** where the aromatics yield for the different dilutions are shown.

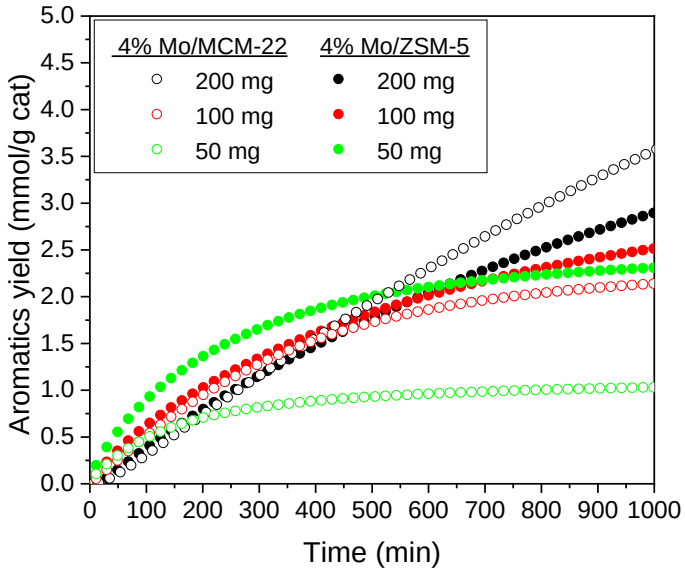

Figure 11. Effect of SiC dilution on the catalytic activity for *MDA* reaction over 4%Mo/zeolite catalysts.

From the results it is clear that the dilution effect is more pronounced for ZSM-5 catalysts than for MCM-22 catalysts. For the latter, the best performance is obtained by the test carried out with 200 mg of catalyst and without SiC. This could indicate that the presence of cages benefits the diffusion through the MCM-22. Furthermore, it is interesting how for Mo/H-ZSM-5 systems the MDA performance for cycles shorter than 500 min is favoured in the case of 50 mg of catalyst diluted with 150 mg of SiC.

7.3.4. Effect of the Re incorporation to the 4% wt. Mo/MCM-22 catalyst.

For the bimetallic synthesis metals were sequentially added by impregnation and the systems were calcined between steps and at the end of the preparation. **Figure 12** shows how the addition of rhenium and the additional calcination step does not produce apparent changes in the 1%Re-4%Mo/MCM-22 diffractogram.

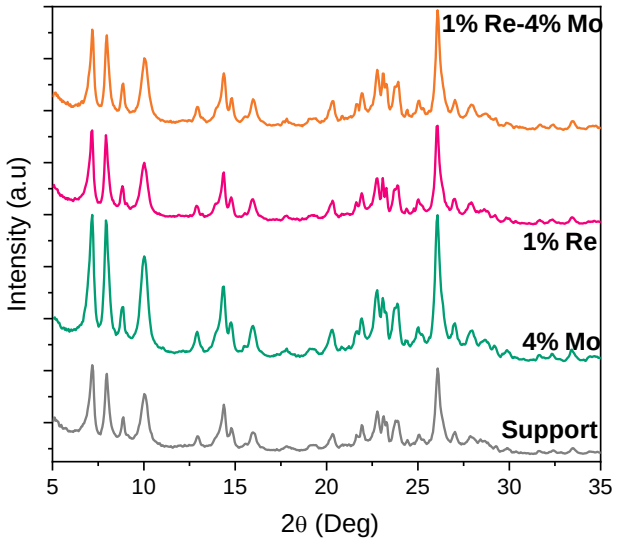

Figure 12. X- ray powder diffraction pattern of the Re-Mo/MCM-22(P3) system.

However, as shown in **Table 4**, the introduction of metal in the zeolite affects the surface features of the catalyst and a slight decrease in the BET surface is observed after the Re addition to the 4% Mo catalysts. Such a decrease is larger than that observed for the

ZSM-5 systems, showing a change from 398 m^2/g for the MCM-22 to 301 m^2/g for 1%Re-4%Mo/MCM-22 (24 %), while the decrease for the ZSM-5 catalyst goes from 361 to 289 m^2/g (20 %). The surface decrease on MCM-22 supported catalyst occurs in a different way than for the ZSM-5 systems, and the decrease is more pronounced in the micropore surfaces. However, this diminution in the BET value and in the micropore surface after the rhenium introduction (11 and 13%, respectively) is significantly lower than that exhibited by Mo incorporation (15 and 19%, respectively).

SAMPLES		SURFACE AREA (m^2/g)		PORE VOLUME (cm^3/g)	
		BET	Micro	Total	Micro
ZSM-5	Support	361	267	0.2	0.12
	4%Mo	313	236	0.17	0.11
	1%Re	325	249	0.18	0.12
	1%Re-4%Mo	289	233	0.16	0.11
MCM-22	Support	398	303	0.32	0.14
	4%Mo	337	246	0.29	0.12
	1%Re	388	291	0.31	0.14
	1%Re-4%Mo	301	213	0.3	0.11

Table 5. Textural properties of the MCM-22 (P3), 4%Mo/MCM-22 (P3), 1%Re/MCM-22 (P3) and 1%Re-4%Mo/MCM-22 (P3) and the comparable ZSM-5 catalysts.

Summarising, both metals are differently distributed in the two zeolites, occupying predominantly the micropore sites in the case of the MCM-22. For this zeolite, it is the Mo incorporation which produces the biggest surface decrease, with the rhenium better dispersed on the surface. Such good dispersion of Re ions on the MCM-22 has been confirmed by HADDF (**Figure 13**)**.** This denotes that Re would easily diffuse through zeolite pore structure upon different calcination treatments, as it was the case for bimetallic ZSM-5 catalyst.[33]

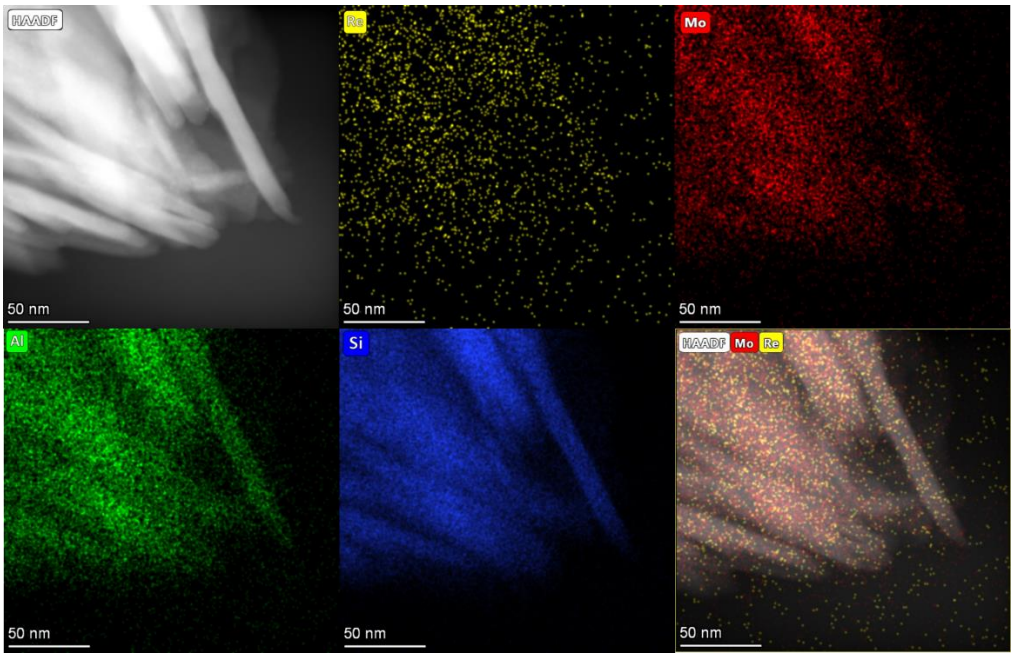

Figure 13. HAADF-STEM images of 1%Re-4% Mo/MCM-22 catalyst.

The reducibility of the bimetallic system has been followed by temperature programmed reduction measurements. Both monometallic catalysts are represented as a reference. According to the profiles shown in **Figure 14**, the Re monometallic system presents the main reduction process with a peak centered at 375 °C. It is also shown that Re proactively facilitates the reduction of Mo in the Re-Mo/MCM-22 catalyst and the reduction process shifted to a lower temperature. As observed by HAADF, Re species are dispersed on the support and are not always close to Mo particles, however, the Mo reduction is enhanced by Re. This result suggests a hydrogen spillover mechanism, where Re produces active hydrogen species, and they spill over the support to reduce Mo species distant from Re.[34,35] As it was observed for Re-Mo/ZSM-5 catalyst,[33] there is a diminution of the region at 800°C in the TPR profile after Re introduction, which would indicate a decrease on the bulk MoO_3 phase located on the external surface. However, a rising of the reduction process with a peak at 1000 °C, associated with the well dispersed Mo-monomers located at the inner micropores with strong interaction with the support is shown. The increase of this reduction peak in this series would point out that Re would facilitate the Mo dispertion and its introduction into the microporous channels allowing the small Mo cluster deposition.

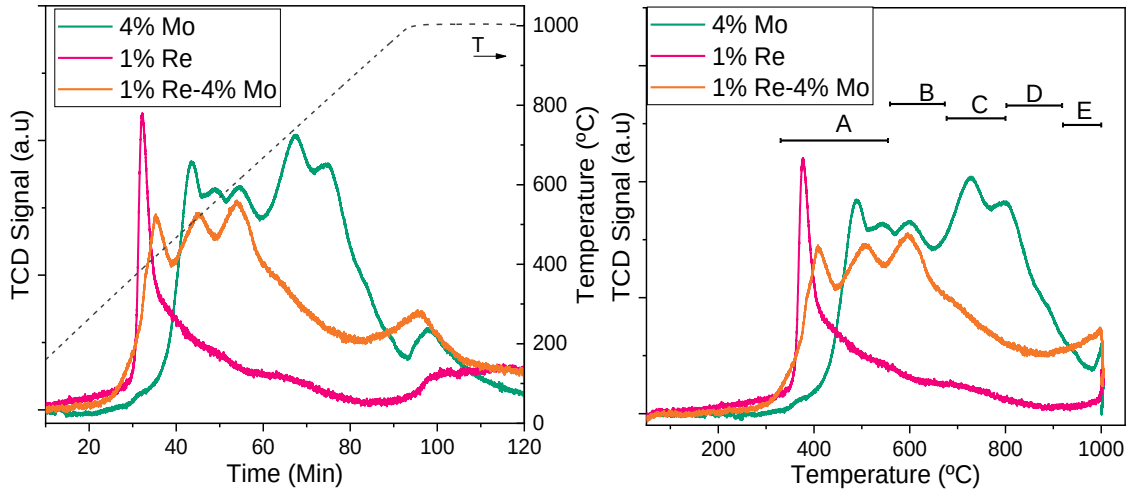

Figure 14. TPR profiles of of the 4%Mo, 1%Re and 1%Re-4%Mo/MCM-22 (P3) catalysts vs. time (*left*) and temperature (*right*).

The H_2 consumption in the different catalyst could be estimated by assuming the total transformation of MoO_3 and Re_2O_7 into metallic molybdenum and rhenium throughout the TPR experiment. A consumption of 1.2, 0.2 and 0.9 mmol/g of H_2 is found for 4% Mo, 1% Re and 1%Re-4%Mo/MCM-22, respectively. According to the following reaction:

$$MoO_3 + 3\ H_2 \rightarrow Mo^\circ + 3\ H_2O,$$

$$Re_2O_7 + 7\ H_2 \rightarrow 2\ Re^\circ + 7\ H_2O,$$

these values for the Mo and Re monometallic catalyst represent a reduction of 97 and 100 % respectively, and the bimetallic would show a loss of a 36 % compared with the monometallic reduction value, implying the coexistence of Re-Mo species that are stabilized in a partial oxidized state.

The catalytic activity results of the calcined samples are shown in **Figure 15**. While the rhenium monometallic catalyst does not show any aromatics production, the addition of Re to the 4%Mo/MCM-22 system improves the aromatic yield with respect to Mo monometallic system. Specifically, after 1000 min in stream the aromatics yield was 5

mmol/g cat for the 1%Re-4%Mo/MCM-22, higher than the value obtained using 4%Mo/MCM-22 and 1%Re/MCM-22 samples (3.5 and 0.4 mmol/g cat, respectively).

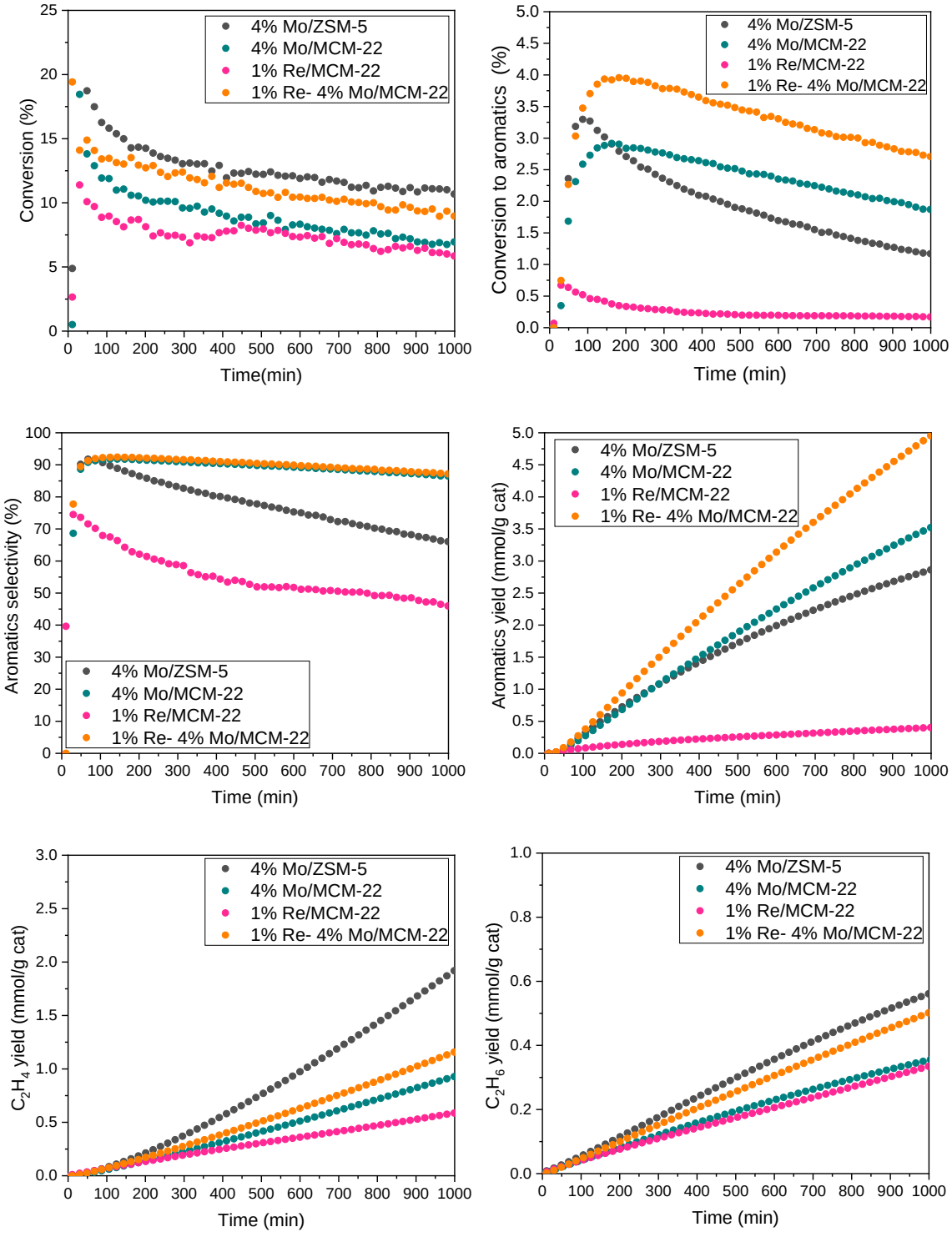

Figure 15. Effect of the rhenium addition over 4%Mo/MCM-22 catalysts on the catalytic activity for *MDA* reaction.

This is the result of a higher aromatic conversion of the bimetallic catalyst, even when the selectivity to aromatics is identical to the showed for the 4%Mo/MCM-22. Observing the production to C2, ethane and ethylene, the graphs showed that in both cases the maximum yields are reached for 4%Mo/ZSM-5 (0.6 and 1.9 mmol/g cat for ethane and ethylene after 1000 min of reaction, respectively), while the catalysts supported on MCM-22 showed lower values. Among then, it is the bimetallic the one showing a higher formation of both C2 products (0.5 and 1.2 mmol/g cat for ethane and ethylene respectively), decreasing for 4%Mo/MCM-22. Meanwhile, the Re/MCM-22 catalyst is basically inactive, with a conversion to aromatics maximum of 0.7 % after 30 min of reaction that decrease until 0.2 % at ca. 500 min.

The external surface of Re-Mo bimetallic catalyst was examined using X-ray photoelectron spectroscopy (XPS). **Figure 16** plots the recorded signals of Mo *3d* and Re *4f* regions of the fresh samples.

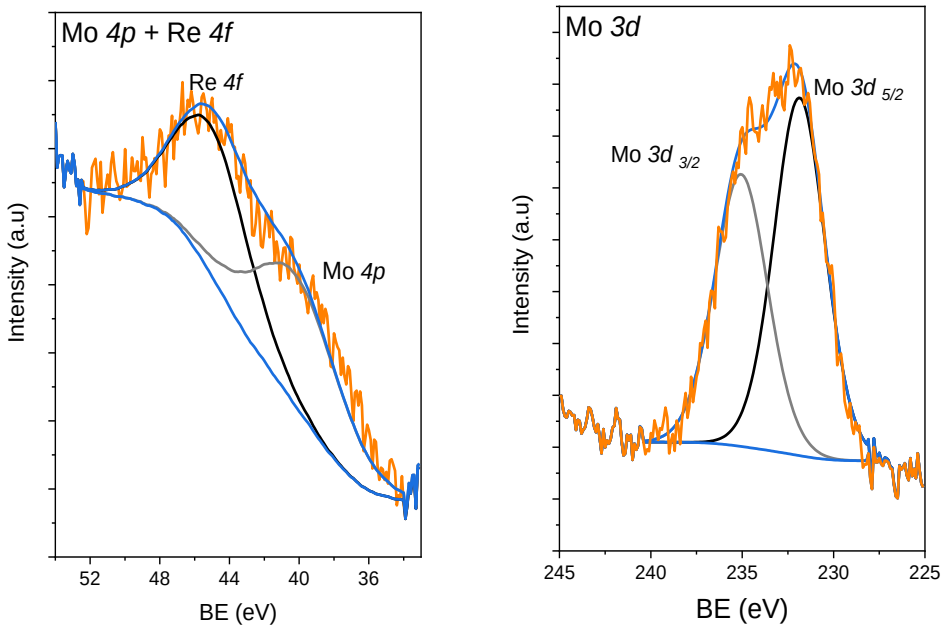

Figure 16. Mo *3d* and Re *4f* regions. XPS spectra of calcined 1%Re-4%Mo/MCM-22 catalysts.

The study showed that Mo and Re species on the bimetallic catalyst surfaces existed as Mo^{4+},[36] and Re^{6+}.[37]

Despite the coupling between the Mo *4p* and Re *4f* signals, XPS results demonstrate that the concentration of Mo and Re on the external surface of 1%Re-4%Mo catalyst is very low, ca. 0.7 and 0.06 % respectively. Considering the surface sensitivity of the XPS technique, this result indicates that the majority of molybdenum and rhenium species would be located inside the MCM-22 structure, being not detectable for XPS. The Si/Al ratio calculated suggest that the surface of the catalyst in enriched on Si (**Table 6**.).

Sample	% at Mo /% at Si	%at Re/% at Si	% at C /% at Si	% at Al /% at Si
1%Re-4%Mo/MCM-22	0.016	0.002	0.280	0.050
1%Re-4%Mo/ZSM-5	0.045	0.006	0.1601	0.088

Table 6. Surface composition measured by XPS of the fresh bimetallic catalysts.

The metal introduction and the successive calcinations led to a smaller Al extraction in the case of MCM-22 catalysts. This could be another reason for the better stability in long MDA reactions for MCM-22 catalyst.

7.4. Conclusions

To summarize, a series of Mo/MCM-22 type catalyst systems have been prepared following different zeolite synthesis methods. The catalysts obtained have been extensively characterized structurally and superficially. The influence on the catalytic activity with factors such as the synthesis of MCM-22, the Mo metal load, the dilution of the SiC catalyst and the addition of Re has been studied.

The activity results have shown how the MCM-22 catalyst has a slower deactivation rate than the ZSM-5 catalyst in the same reaction condition. Furthermore, Mo/MCM-22 has

shown more stable aromatic selectivity values and higher aromatic yield for all the MCM-22 dynamic synthesis procedure. In relation to the synthesis of the support, it can be seen how the variation of different factors, such as aging, time for the synthesis, radiation used for heating or NaOH amount affects some of the sample properties, such as the surface area. However, just the structural factors alone seem to influence the activity performance. Only the sample prepared under static conditions, and which shows a broadening of the peaks in its diffractogram, has shown a diminished catalytic activity result.

There appear to be several similarities between these samples and their homologous Mo/ZSM-5 catalysts. On the one hand, the catalysts with the best catalytic properties appear to be those with 4% Mo. As in the case of the Mo/ZSM-5 catalysts, an increase or decrease in this percentage leads to a decrease in aromatics production. In fact, for the 10%Mo/MCM-22 catalysts, Al extraction from the zeolite frameworkhas been observed, which had previously been observed on ZSM-5 catalysts with high Mo loading. DTG results have shown how the high coke formation and the lower thermal stability could account for the loss of catalytic performance in the 10% Mo catalyst. On the other hand, the results of this study have shown that Mo/MCM-22 samples have similar TPR profiles to the profiles observed for Mo/H-ZSM-5. An extension of the results obtained for ZSM-5-based catalysts can be made to the MCM-22 systems, identifying the same Mo precursors stabilized in both zeolites.

Regarding the effect of dilution on SiC of the catalyst, it does not have a strong effect on the Mo/MCM-22 systems. The presence of cages in the MWW-type structure benefits the diffusion through the support. However, the dilution effect is important in the case of molybdenum supported on ZSM-5, which does not have these cavities and it shows a more difficult diffusion.

Finally, regarding the effect of the addition of rhenium as a second metal in MCM-22-based catalysts, surface area measurements and TPR results have shown how both

metals are differently distributed in the two zeolites, occupying predominantly the micropore sites in the case of the MCM-22. Although in both ZSM-5 and MCM-22 catalysts the rhenium is homogeneously distributed, the presence of cages in the MWW structure facilitates the entry of Mo into the micropores. This is reflected in the appearance of reduction peaks at 1000°C in the TPR. Furthermore, TPR profiles also shows that Re proactively facilitates the reduction of Mo in the Re-Mo/MCM-22. Regarding the catalytic activity, the addition of Re to the 4%Mo/MCM-22 system improves the aromatic yield with respect to Mo monometallic system.

The stability of the catalyst also appears to improve with the introduction of rhenium, and is also higher than Re-Mo/H-ZSM-5 catalysts. XPS results showed that for Re-Mo/MCM-22 catalysts the Al concentration on the surface was lower than for ZSM-5 supported catalysts. Which seems to indicate that there is a lower Al extraction on these catalysts. This could be another reason for the better stability in long *MDA* reactions for the MCM-22 catalyst.

7.5.References

1. Rubin, M. K. & Chu, P. Composition of Synthetic porous Crystalline material, Its Synthesis and Use. PATENT US4954325A. (1990).

2. Roth, W. J. *et al.* MCM-36: The first pillared molecular sieve with zeolite properties. *Stud. Surf. Sci. Catal.* **94**, 301–308 (1995).

3. Lawton, S. L. *et al.* Zeolite MCM-49: A three-dimensional MCM-22 analogue synthesized by in situ crystallization. *J. Phys. Chem.* **100**, 3788–3798 (1996).

4. Roth, W. J. MCM-22 zeolite family and the delaminated zeolite MCM-56 obtained in one-step synthesis. *Stud. Surf. Sci. Catal.* **158 A**, 19–26 (2005).

5. Corma, A., Fornes, V., Pergher, S. B., Maesen, T. L. M. & Buglass, J. G. Delaminated zeolite precursors as selective acidic catalysts. *Nature* **396**, 353–356 (1998).

6. Leonowicz, M. E., Lawton, J. A., Lawton, S. L. & Rubin, M. K. MCM-22: A Molecular

Sieve with Two Independent Multidimensional Channel Systems. *Science.* **264**, 1910–1913 (1994).

7. Perego, C. *et al.* Experimental and computational study of beta, ZSM-12, Y, mordenite and ERB-1 in cumene synthesis. *Microporous Mater.* **6**, 395–404 (1996).

8. Corma, A., Martínez-Soria, V. & Schnoeveld, E. Alkylation of benzene with short-chain olefins over MCM-22 zeolite: Catalytic behaviour and kinetic mechanism. *J. Catal.* **192**, 163–173 (2000).

9. Wu, P., Komatsu, T. & Yashima, T. Selective formation of p-xylene with disproportionation of toluene over MCM-22 catalysts. *Microporous Mesoporous Mater.* **22**, 343–356 (1998).

10. Kumar, N. & Lindfors, L. E. Synthesis, characterization and application of H-MCM-22, Ga-MCM-22 and Zn-MCM-22 zeolite catalysts in the aromatization of n-butane. *Appl. Catal. A Gen.* **147**, 175–187 (1996).

11. Leite, R. C. N., Sousa, B. V. & Rodrigues, M. G. F. Static Synthesis and Characterization of Mcm-22 Zeolite Applied As Additive in Fluid Catalytic Cracking Operations. *Brazilian J. Pet. gas* **3**, 75–82 (2009).

12. Ahmad, A., Naqvi, S. R., Rafique, M., Nasir, H. & Sarosh, A. Synthesis, characterization and catalytic testing of MCM-22 derived catalysts for n-hexane cracking. *Sci. Rep.* **10**, 1–11 (2020).

13. Zones, S. I. Translating new materials discoveries in zeolite research to commercial manufacture. *Microporous Mesoporous Mater.* **144**, 1–8 (2011).

14. Shu, Y., Ma, D., Xu, L., Xu, Y. & Bao, X. Methane dehydro-aromatization over Mo/MCM-22 catalysts: A highly selective catalyst for the formation of benzene. *Catal. Letters* **70**, 67–73 (2000).

15. Ma, D. *et al.* Mo/HMCM-22 catalysts for methane dehydroaromatization: A multinuclear MAS NMR study. *J. Phys. Chem. B* **105**, 1786–1793 (2001).

16. Ma, D. *et al.* The synergic effect between Mo species and acid sites in Mo/HMCM-

22 catalysts for methane aromatization. *Phys. Chem. Chem. Phys.* **7**, 3102–3109 (2005).

17. Ma, D. *et al.* Carbonaceous deposition on Mo/HMCM-22 catalysts for methane aromatization: A TP technique investigation. *J. Catal.* **208**, 260–269 (2002).

18. Liu, H. *et al.* The chemical nature of carbonaceous deposits and their role in methane dehydro-aromatization on Mo/MCM-22 catalysts. *Appl. Catal. A Gen.* **236**, 263–280 (2002).

19. Sobalík, Z., Tvarůžková, Z., Wichterlová, B., Fíla, V. & Špatenka, Š. Acidic and catalytic properties of Mo/MCM-22 in methane aromatization: An FTIR study. *Appl. Catal. A Gen.* **253**, 271–282 (2003).

20. Liu, L. *et al.* Methane dehydroaromatization on Mo/HMCM-22 catalysts: Effect of SiO 2/Al2O3 ratio of HMCM-22 zeolite supports. *Catal. Letters* **108**, 25–30 (2006).

21. Lim, T. H., Nam, K., Song, I. K., Lee, K. Y. & Kim, D. H. Effect of Si/Al2 ratios in Mo/H-MCM-22 on methane dehydroaromatization. *Appl. Catal. A Gen.* **552**, 11–20 (2018).

22. Mishra, S., Ali Haider, M. & Pant, K. K. Controlling the Evolution of Active Molybdenum Carbide by Moderating the Acidity of Mo/HMCM-22 Catalyst in Methane Dehydroaromatization. *Catal. Letters* **150**, 3653–3666 (2020).

23. Shu, Y., Ohnishi, R. & Ichikawa, M. A highly selective and coking-resistant catalyst for methane dehydrocondensation. *Chem. Lett.* 418–419 (2002). doi:10.1246/cl.2002.418

24. Bai, J., Liu, S., Xie, S., Xu, L. & Lin, L. The role of coke in the deactivation of Mo/MCM-22 catalyst for methane dehydroaromatization with CO2. *Stud. Surf. Sci. Catal.* **147**, 715–720 (2004).

25. Huang, L. Q. *et al.* Dehydro-aromatization of CH4 over W-Mn(or Zn, Ga, Mo, Co)/HZSM-5(or MCM-22) catalysts. *Stud. Surf. Sci. Catal.* **147**, 565–570 (2004).

26. Yin, X., Chu, N., Yang, J., Wang, J. & Li, Z. Synthesis of the nanosized MCM-22 zeolite and its catalytic performance in methane dehydro-aromatization reaction.

Catal. Commun. **43**, 218–222 (2014).

27. Hu, J. *et al.* Nano-MoO_3-modified MCM-22 for methane dehydroaromatization. *Appl. Organomet. Chem.* **29**, 638–645 (2015).

28. Gao, K., Yang, J., Seidel-Morgenstern, A. & Hamel, C. Methane Dehydro-Aromatization: Potential of a Mo/MCM-22 Catalyst and Hydrogene-Selective Membranes. *Chemie-Ingenieur-Technik* **88**, 168–176 (2016).

29. Julian, I. *et al.* Polyoxometalates as alternative Mo precursors for methane dehydroaromatization on Mo/ZSM-5 and Mo/MCM-22 catalysts. *Catal. Sci. Technol.* **9**, 5927–5942 (2019).

30. Güray, I., Warzywoda, J., Baç, N. & Sacco, A. Synthesis of zeolite MCM-22 under rotating and static conditions. *Microporous Mesoporous Mater.* **31**, 241–251 (1999).

31. López-Martín, Á., Platero, F., Colón, G. & Caballero, A. Elucidating the nature of Mo species on ZSM-5 and its role in the methane aromatization reaction. *React. Chem. Eng.* (2021). doi:10.1039/d1re00044f

32. Kosinov, N. *et al.* Structure and Evolution of Confined Carbon Species during Methane Dehydroaromatization over Mo/ZSM-5. *ACS Catal.* **8**, 8459–8467 (2018).

33. López-Martín, A., Sini, M. F., Cutrufello, M. G., Caballero, A. & Colón, G. Characterization of Re-Mo/ZSM-5 catalysts: How Re improves the performance of Mo in the methane dehydroaromatization reaction. *Appl. Catal. B Environ.* **304**, (2022).

34. Hilmen, A. M., Schanke, D. & Holmen, A. TPR study of the mechanism of rhenium promotion of alumina-supported cobalt Fischer-Tropsch catalysts. *Catal. Letters* **38**, 143–147 (1996).

35. Kumar, N., Payzant, E. A., Jothimurugesan, K. & Spivey, J. J. Combined in situ XRD and in situ XANES studies on the reduction behavior of a rhenium promoted cobalt catalyst. *Phys. Chem. Chem. Phys.* **13**, 14735–14741 (2011).

36. Grim, S. O. & Matienzo, L. J. X-Ray Photoelectron Spectroscopy of Inorganic and Organometallic Compounds of Molybdenum. *Inorg. Chem.* **14**, 1014–1018 (1975).

37. Komiyama, M., Ogino, Y., Akai, Y. & Goto, M. X-ray photoelectron spectroscopic studies of unsupported and supported rhenium using argon-ion bombardment. *J. Chem. Soc. Faraday Trans. 2 Mol. Chem. Phys.* **79**, 1719–1728 (1983).

.

Chapter 8. General conclusions, future work and outlook.

8.1. General conclusions

The findings presented in this thesis have been summarized at the end of each chapter. A summary of the conclusions is shown below:

Firstly, the different nature and reactivity of the molybdenum species in the Mo/H-ZSM-5 systems was observed, as well as its great complexity. In the study described in **Chapter 3** we compared the catalytic performance of Mo/H-ZSM-5 catalysts where the nominal load of Mo was in the range of 1 to 10% Mo. In all cases, the species of Mo exhibited high dispersion, so they were not detected by XRD even at high loadings. The results obtained in the catalytic test showed that the optimal Mo loading was 4%, while the performance decreased at a higher Mo load. This could be due to the higher formation of coke in these cases (greater cracking of methane), which would lead to the blocking of the pores, making the active sites inaccessible to methane. Reduction studies of these systems were carried out, both by TPR and XPS. These showed how the complexity and diversity of the Mo species presented in the catalysts increased as the molybdenum loading increased. In addition, *in-situ* carburization study was carried out in which it was observed how the formation of Mo-carbide took place at different temperatures, again conditioned by the metal load.

Secondly, the presence of at least five different Mo phases were identified in the Mo/H-ZSM-5 systems previously studied. Thus, in **Chapter 4** it was shown how the combination of techniques such as TPR and XPS allowed us to obtain information about the location, nature and state of dispersion of these phases. This information was complemented with the catalytic studies of some additional samples that were subjected to acid treatments. This study allowed us to deduce that the main species responsible for the high performance of the most active catalysts are the small clusters of well-dispersed Mo dimers/ polymers, reducing at 680 °C - 800 °C and located in the inner micropores of the ZSM-5 support. In addition to this species, two other species were found that exhibit a certain activity in the *MDA* reaction and both were identified as small groups of well-dispersed Mo monomers. The difference between these is the location, one

being on the external surface of the zeolite and reducing to 350 °C - 570 °C, and the other in the internal microporous channels of the zeolite and reducing at temperatures above 915 °C.

It was also possible to determine that the species responsible for the detriment on the catalytic activity is a bulk phase of MoO_3 located in the external surface of the zeolite and reducing at 800 °C - 915 °C. The HAADF images unambiguously show that it is supported on aluminium oxide segregated from the zeolite network. It hinders the catalytic performance, prompting the formation of heavy coke deposits on the catalysts.

Thirdly, the incorporation of other metals to the Mo/H-ZSM-5 catalyst was evaluated. During this thesis, these systems were tested using different metals as a dopant. Among them, rhenium and iron stood out, but the latter was discarded due to the low reproducibility of the results (the large amount of carbon generated caused the reactor pressure to increase, which hampered the control of the catalytic activity tests). For that reason, **Chapter 5** focused on the study of the addition of rhenium to Mo/H-ZSM-5 system. The results showed a remarkable improvement in the *MDA* reaction, increasing the aromatic yield. It could be concluded that the catalytic performance of these bimetallic systems was also affected by the sequence addition of metals, obtaining the best catalytic behaviour for 1%Re-4%Mo/H-ZSM-5 (Re1st series). The study developed in this chapter also showed how the higher aromatics yield would be directly related to the higher ethane formation.

The optimization of the reaction conditions of the different systems is a requirement to take into account. After the variation or modification of these, the optimal conditions for the methane dehydroaromatization must be determined. That is why a large part of this thesis has been devoted to this as part of the routine. Adding a pre-reaction step increases the complexity of the process. This is why a lot of time had to be spent studying and optimizing pre-treatment methods. The results obtained after reduction pretreatments of the 4%Mo/H-ZSM-5 catalyst has been described in **Chapter 6**. In this work we corroborate that, effectively, a reduction pre-treatment could help to improve

the catalytic performance on *MDA* reaction. However, we stated that the temperature at which the reduction is carried out has a strong influence on both, the position and the state of the molybdenum species and this influences the catalytic activity. In this chapter it was shown how a H_2 pretreatment at 450 ˚C resulted in the formation of large agglomerates of aluminium and molybdenum and a low reduction degree of the molybdenum species. However, if the temperature was increased to 650 °C, the data showed a widening of the pore diameter and an aluminium enrichment of the surface. It was after the analysis of the H_2 pretreatment at 550 °C that a great improvement in catalytic activity were observed. It was concluded that there is a correlation between the amount of $Mo^{\delta+}$ species and the catalytic performance.

The results obtained for the catalysts supported on ZSM-5 were extended to the new catalysts supported on MCM-22 in **Chapter 7**. However, further studies of these systems are necessary. The results obtained so far showed a higher stability of the systems based on MCM-22. As expected, the existence of cages in these structures would facilitate diffusion and prevent blockage of the pores, thus making the catalysts have a longer life.

8.2. Future work

The work carried out in this thesis provides valuable information on the nature of the Mo species active for *MDA* and the effect of the addition of promoters such as Rhenium, or the effect of the pretreatment of the catalysts with H_2 at different temperatures. The findings shown throughout these chapters could be useful for the development of efficient and stable catalysts in the *MDA* reaction that favour its implementation on an industrial scale. In order to continue with the lines of these studies and obtain a deeper understanding of the results found, some extra experiments are proposed:

A deeper understanding of the structure-catalytic activity relationship could be derived from the study developed in **Chapter 6** if XPS experiments were performed *in-situ*. In them, the pretreatment phases at different temperatures and reaction would be emulated, without the need to remove the catalyst to the atmosphere. The control of

the atmosphere and the time would allow us to see the evolution of the species present on the surface of the zeolite. Although this experiment would not provide the same information as an *in operando* experiment, it is also true that both performance and data processing are simpler. This could serve as the basis for future visits to the synchrotron to carry out for example AP-XPS in operando experiments.

Completion of the catalyst regeneration study started during the thesis period would be a good achievement. In this, the reaction-regeneration cycles carried out were at least 5-6 h. The assessment of such cycles affects the catalytic activity and the stability of the catalyst, performing cycles of 40 min or 60 min maximum instead. The formation of coke will be smaller so the regeneration cycle should be less drastic, allowing the elimination of the coke deposits that block the pores, preventing the diffusion of methane and reaction products, which ends up deactivating the catalyst. The study of H_2 pretreatment at different temperatures described in **Chapter 6** could be the beginning of a study of the regeneration of 4%Mo/H-ZSM-5 with short cycles.

The evaluation of the regeneration of bimetallic catalysts 1%Re-4%Mo/H-ZSM-5 (Re First) described in **Chapter 5** is also presented as a study to be carried out in the near future. It would be necessary to burnt off the coke at lower temperatures to avoid the sublimation of the species, as well as damage to the structure.

Finally, determining how the Mo loading, the addition of rhenium as co-dopant, or the pretreatment with H_2 at different temperatures affect other types of systems such as Mo/MCM-22 and comparing the results. The presence of cages in this type of zeolite should improve the stability of the catalyst as well as improve the diffusion of the products.

8.3. Outlook

Over the last three decades, there have been many studies and publications on this reaction in general and on Mo/H-ZSM-5 systems in particular. However, despite the advances made in understanding the process and the development of new and more

efficient catalysts, a deeper understanding of the *MDA* reaction for its industrial application is still necessary. Therefore, the knowledge of the structure-catalytic activity relationship, as well as the mechanism and the species involved in the *MDA* reaction, must be expanded.

For this purpose, the *operando* spectroscopic studies are of great help, since they provide information about the catalyst in real conditions. However, it is important to be careful with the technique and sample selected, data analysis, etc. The reaction is carried out at such a high temperature due to thermodynamic limitations, that the evolution of the active species is very quick and the appearance of many parallel reactions is favoured. These techniques are in constant and rapid evolution thanks to the great work carried out by many research groups, which will allow us to solve some of the problems we encounter in the very near future.

Engineering the synthesis of molybdenum catalysts (among others) would also be a good strategy. Simplifying and choosing the Mo species on the catalyst would help to understand the nature and location of the active sites generated on reaction conditions which would allow us to understand some of the key aspects of this reaction.

The development and innovation of the technical characteristics of the process, such as the use of hydrogen permeable reactors, multi-bed reactors, high pressure operation, etc. could also be of great help. Uniting this technology, with the development of spectroscopic techniques, and the recent advances obtained, it could be possible in the future to improve the stability and catalytic activity of the process.